Robust real-time control of a parallel hybrid electric vehicle

Enang, Wisdom

Award date:
2017

Awarding institution:
University of Bath

ROBUST REAL-TIME CONTROL OF A PARALLEL HYBRID ELECTRIC VEHICLE

Wisdom Patrick Enang

A thesis submitted for the degree of Doctor of Philosophy

University of Bath

Department of Mechanical Engineering

December 2016

ABSTRACT

The gradual decline in global oil reserves and the presence of ever so stringent emissions rules around the world have created an urgent need for the production of automobiles with improved fuel economy. HEVs (hybrid electric vehicles) have proved a viable option to guaranteeing improved fuel economy and reduced emissions. The fuel consumption benefits which can be realised when utilising HEV architecture are dependent on how much braking energy is regenerated, and how well the regenerated energy is utilised. The challenge in developing a real-time HEV control strategy lies in the satisfaction of often conflicting control constraints involving fuel consumption, emissions and driveability without over-depleting the battery state of charge at the end of the defined driving cycle.

Reviewed literature indicates some research gaps and hence exploitable study areas for which this thesis intends to address. For example, despite the research advances made, HEV energy management is still lacking in several key areas: optimisation of braking energy regeneration; real-time sub-optimal control of HEV for robustness, charge sustenance and fuel reduction; and real-time vehicle speed control. Consequently, this thesis aims to primarily develop novel real-time near-optimal control strategies for a parallel HEV, with a view to achieving robustness, fuel savings and charge sustenance simultaneously, under various levels of obtainable driving information (no route preview information, partial route preview information).

Using a validated HEV dynamic simulation model, the following novel formulations are proposed in this thesis and subsequently evaluated in real time:

1. A simple grouping system useful for classifying standard and real-world driving cycles on the basis of aggressivity and road type.
2. A simple and effective near-optimal heuristic control strategy with no access to route preview information.
3. A dynamic programming-inspired real-time near-optimal control strategy with no access to route preview information.
4. An ECMS (Equivalent Consumption Minimisation Strategy) inspired real-time near-optimal control strategy with no access to route preview information.
5. An ECMS-inspired real-time near-optimal control strategy with partial access to route preview information.
6. A dynamic programming based route-optimal vehicle speed control strategy which accounts for real-time dynamic effects like engine braking, while solving an optimisation problem involving the maximisation of fuel savings with little or no penalty to trip time.
7. A real-time vehicle speed control approach, which is based on smoothing the speed trajectory of the lead vehicle, consequently reducing the acceleration and deceleration events that the intelligent vehicle (follower vehicle) will undergo. This smoothing effect translates into reduced fuel consumption, which tends to increase with increasing traffic preview window.

Among other studies performed in this thesis, the fuel savings potential of the proposed near-optimal controllers was investigated in real time over standard driving cycles and real-world driving profiles. Results from these analyses show that, over standard driving cycles, properly formulated near-optimal real-time controllers are able to achieve a fuel savings potential within 0.03% to 3.71% of the global optimal performance, without requiring any access to route preview

information. It was also shown that as much as 2.44% extra fuel savings could be achieved over a driving route, through the incorporation of route preview information into a real-time controller.

Investigations were also made into the real-time fuel savings that could be realised over a driving route, through vehicle speed control. Results from these analyses show that, compared to an HEV technology which comes at a bigger cost, far higher fuel savings, as much as 45.96%, could be achieved through a simple real-time vehicle speed control approach.

Dedicated to my mother, **Mrs Sarah Patrick Enang**, whose unconditional love and support was instrumental to the successful completion of my PhD research studies

ACKNOWLEDGEMENTS

The realisation of my doctoral research studies was made possible by the grace of God Almighty, and contributions from a number of people, who I wish to especially thank.

First, I am grateful to my supervisors, specifically Dr Chris Bannister, for his enormous support, ardent encouragement and valuable feedback on my research work. Throughout my PhD research, Dr Bannister doubled both as a supervisor and as a friend. He made several valuable inputs to my research and was very encouraging through the challenging times. With his continuous strive for excellence, Dr Bannister was always able to bring out the very best in me.

This research work was supported with engine test data from Ashwoods Automotive UK, electric motor test data from Perm Motor Germany, and a generic dynamic programming tool from Dr Olle Sundstrom of the Cognitive Computing and Industry Solutions Department at IBM Research - Zurich. This support is gratefully acknowledged.

I would also like to thank my colleagues in the University of Bath, Powertrain and Vehicle Research Centre (PVRC) research group and other members of the Department of Mechanical Engineering, for creating such a positive, pleasant and enabling research environment for me.

I forever owe a debt of gratitude to my parents (Chief and Mrs Patrick Enang), sisters (Sylvia, Favour and Ofonime) and wife (Idorenyin) for their constant support and encouragement through the challenging years of my studies. I feel my family deserves a PhD as well, as it would have been impossible to successfully go through all the challenging moments I faced during my studies, without their love.

Ofonime, it is sad you passed away before I could finish my studies. I am sure you are proud of me wherever you are.

TABLE OF CONTENTS

LIST OF FIGURES

LIST OF TABLES

1 INTRODUCTION

1.1 Background of study

Increasing concerns about fossil fuels availability in the long term and environmental pollution have focused considerable attention on the problem of efficient energy utilisation in automobiles [1-5]. In response to these concerns, regulators around the world have set out various stringent emissions targets to curb regulated emissions (hydrocarbons, nitrogen oxides, carbon monoxide and particulate matter). Figure 1-1 provides a comparison of the EU CO_2 passenger car standards with similar regulations around the world. This chart converts all regulatory programs to the European test cycle (NEDC – New European Driving Cycle) for comparison.

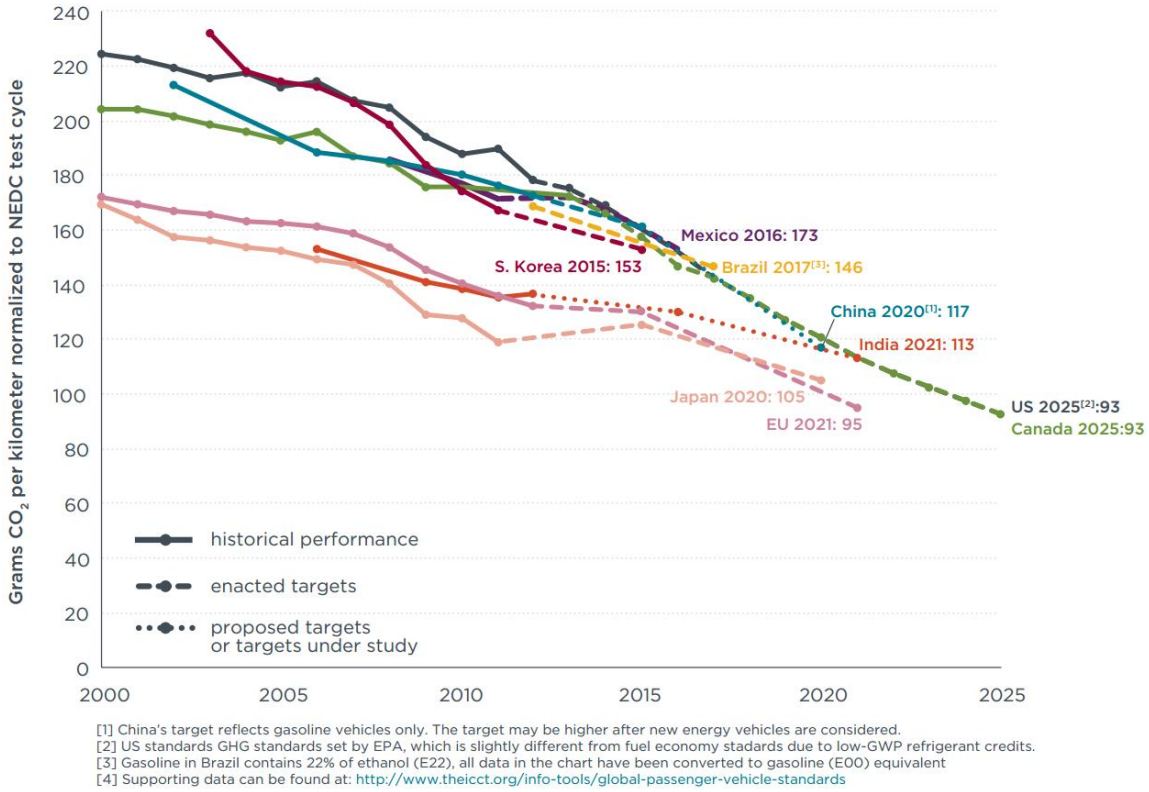

Figure 1-1: Comparison of global CO_2 regulations for passenger cars, in terms of NEDC gCO_2/km (source [6])

According to Figure 1-1, Europe has the most progressive emissions legislation to date with an intended target of 95 grams of CO_2 per km in 2021. This figure represents a 27% reduction from the 2015 level and a 50% reduction from the 2010 level. In the US, a CO_2 target of 109 grams per km is intended for 2020 (~ 50% of the level in 2010). Similar targets have also been set in Asian countries: Japan (105 g/km by 2020), China (117 g/km by 2020) and India (113 g/km by 2021).

Meeting these standards is non-trivial, and requires the adoption of new technologies to reduce energy loss and increase efficiency within the internal combustion engine and vehicle powertrain. Over the last 20 years, the scientific

community and industries alike have proposed a variety of innovations to face this challenge, developing solutions such as Turbochargers to improve fuel efficiency and catalytic converters to remove harmful gases. Although these technologies have directly contributed to huge improvements in automotive technology, the ever-rising emissions levels (due to the increasing number of cars on the road) necessitates a new and drastic technology, with the potential to:

1. Optimise existing internal combustion engines without compromising on the performance of the vehicle [7].
2. Optimise energy demand for operation of the vehicle accessory system (42-volt electric system, low energy lighting, etc.) [8].
3. Reduce losses due to aerodynamic drag, rolling resistance and braking losses due to vehicle inertia [7].

1.2 Limitations in baseline vehicles

Conventional vehicles powered by internal combustion engines have dominated ground transport due to their long driving range, fuelling ease, ease of extraction and low cost compared to other vehicular technologies [9]. In recent years, internal combustion engines have achieved thermal efficiencies up to 25% for spark-ignition engines and 30% for compression-ignition engines [10]. However, internal combustion engines seldom operate at their peak efficiencies (located in the low engine speed, high engine torque area), for the following reasons:

1. Energy losses within the engine itself: The theoretical peak efficiency of a heat engine is limited by the air standard cycle, which employs the Otto cycle for reciprocating the engine. Attaining the theoretical peak efficiency

is practically impossible for at least two reasons; the first being the loss of heat through the walls of the cylinder and the second being the compression of fuel at limited compression ratios due to knock.

2. Highly dynamic utilisation which is typical of road cycles, where vehicle speed and torque request vary continuously and rapidly.
3. Working gas is air.
4. Inertia effects.

The resultant effect of these shortcomings results in less than optimal fuel consumption and increased emissions, which is harmful to health.

HEVs are able to compensate for some of these shortcomings and simultaneously meet the requirements for vehicle performance and environmental protection mentioned in section 1.1, by introducing a powertrain with an additional propulsion system, constituted in its simplest form by an electric energy storage unit (electric battery), an electric torque actuator (electric motor) and a device which couples together the electric and thermal drivelines. It is a culmination of mechanical, electrical, electronic and power engineering technologies embracing the best of both conventional ICE vehicles and electric vehicles (EVs). The additional driveline allows for greater flexibility in engine use, while ensuring the fulfilment of the power request at the wheels.

1.3 Industrial evolution of hybrid electric vehicles

The development of the first hybrid car was reported to be in 1899 by the Pieper establishment of Liege, Belgium [11]. In 1900, Dr Ferdinand Porsche developed the world's first series hybrid electric vehicle where two water-cooled combustion engines with a cumulative capacity of 5 hp were used to generate electricity to run the wheel hub motors. The main aim of these motors was to assist the weakly powered gasoline engines. This concept was however short-lived due to the associated cost. In 1995, hybrid electric vehicles experienced a renewed interest from competing manufacturers, owing to its potential for fuel and emissions reduction. As a result, several variations to the hybrid electric vehicle technology, as explained below, were developed: micro HEVs, mild HEVs, full HEVs and plug-in HEVs [12].

1. **Micro HEVs:** In micro HEVs, the electric motor, in the form of a small integrated alternator/starter, is used to shut down the engine when the vehicle comes to a complete stop, and start it up when the driver releases the brake pedal. Once in motion, the vehicle is propelled by the internal combustion engine (ICE). Examples of micro HEVs on the road today are the BMW 1 and 3 series, Fiat 500, SMART car, Peugeot Citroen C3, Ford Focus and Transit, and Mercedes-Benz A-class [13].

2. **Mild HEVs:** The mild HEV is very similar to a micro HEV, but with an increased size of the integrated alternator/starter motor and a battery which permits power assist during vehicle propulsion. Typical fuel efficiency increase for mild HEVs are around 20 - 25% for real-world driving compared

to a non-hybrid. Examples of mild HEVs on the market include the BMW 7 Series ActiveHybrid, Buick LaCrosse with eAssist, Chevrolet Malibu with eAssist, Honda Civic and Insight Hybrid, and the Mercedes-Benz S400 BlueHybrid [13].

3. **Full HEVs:** In full HEVs, the electric motor and batteries are significantly bigger than that of the micro HEVs and mild HEVs. As such, depending on the vehicle power demand, the electric motor can be used as the sole power source. Compared to micro HEVs and mild HEVs, full HEVs have much smaller engines and require more sophisticated energy management systems. Typical fuel efficiency increase for full HEVs are around 40 - 45% for real-world driving compared to a non-hybrid. Examples of full HEVs on the road today are the Chevrolet Tahoe Hybrid, Toyota Prius and Camry Hybrid, Ford C-Max, Honda CR-Z, and Kia Optima Hybrid.

4. **Plug-in HEVs (PHEVs):** PHEVs essentially possess the same configuration as full HEVs but with the addition of an external electric grid charging plug, much bigger electrical components (electric motor and battery) and a downsized engine. Owing to the high capacity electrical components, PHEVs are able to run on electric power for long periods of time. Examples of PHEVs on the road today are the Chevy Volt, Ford C-Max Energi and Fusion Energi, Fisker Karma, Porsche Panamera S E-Hybrid, and Toyota Prius Plug-in.

In December 1997, the Toyota Prius became the first mass-produced hybrid electric passenger vehicle in the world [14]. Being one of the most successful HEVs

in the market, Toyota Prius uses a complex hybrid powertrain called the Toyota hybrid system. Since its original introduction, the Toyota Prius has undergone several improvements in engine and powertrain. For example, in 2004, the highly efficient THS II Prius was introduced with an efficient gasoline engine which runs on the Atkinson cycle as well as a powerful permanent magnet AC synchronous motor. With a combined parallel and series hybrid configuration, the Toyota Prius utilises the advantages of both the series and parallel systems [15]. In 2010, the Toyota Prius was equipped with an improved drivetrain called the Toyota hybrid synergy drivetrain, which showed better fuel economy and driving performance as compared to its predecessors [14]. In the Toyota hybrid synergy drivetrain, the primary motor acts as a mechanical assist to the ICE and also as a generator to recharge the batteries during regenerative braking. The secondary motor acts as a generator that extracts power from the engine to trickle charge the batteries. The resultant power split system is known as the electronic continuously variable transmission because of its ability to shift gears and drive wheels without the use of clutches or hydraulic systems.

1.4 Advantages of hybrid electric vehicles

In comparison to conventional vehicles, HEVs offer a number of advantages. One of such advantage is the possibility of downsizing the original internal combustion engine whilst still meeting the power demand at the wheels. This advantage is brought about by the capability of the hybrid powertrain to deliver power to the wheels from both the internal combustion engine and the electric motor at the same time, thus resulting in reduced fuel consumption [10, 16]. The introduction of an electric driveline in an HEV also allows for:

1. The regeneration of kinetic braking energy, which would otherwise be lost as heat to mechanical brakes in conventional vehicles [17-19].
2. The possibility of powering the wheels through the electric propulsion system alone when the torque request at the wheels is low.

In full HEVs, fuel consumption during idling can be eliminated by use of the engine shut off/start up feature [20].

Aside from fuel consumption related advantages, HEVs also present the possibility of cranking the engine with the electric motor, which allows for the removal of the starter motor from the powertrain. This new cranking procedure allows for a faster, smoother and a more improved cranking technique, as in the case of inertia cranking [21].

Crucial to achieving the aforementioned advantages is a real-time control strategy capable of coordinating the on-board power sources in order to maximise fuel economy and reduce emissions.

1.5 Motivation

To date, several HEV control strategies have been proposed and developed (non-causal methods, causal methods [22-24] and those with future information [25, 26]), with a view to reducing vehicle fuel consumption and emissions. Despite the research advances made, the following key issues are yet to be fully addressed and thus form the motivation for the work contained in this thesis:

1. Optimisation of braking energy regeneration.
2. Real-time near-optimal control of HEV for robustness, charge sustenance and fuel reduction with:
   (a) Partial route preview information.
   (b) No route preview information.
3. Real-time vehicle speed control.

1.6 Aim and objectives

This thesis aims to develop novel real-time near-optimal control strategies for a parallel HEV, with a view to achieving robustness, fuel savings and charge sustenance simultaneously under various levels of driving information (no route preview information, partial route preview information).

This will be achieved through the completion of the following objectives:

1. Conducting a detailed review of existing literature.
2. The development of a novel and simple grouping system useful for classifying standard driving cycles on the basis of aggressivity and road type.
3. Development and validation of a quasi-static vehicle model.

4. Investigation of the impact of gear up-shift RPM on baseline fuel consumption.
5. Investigation of the impact of braking patterns on kinetic energy recovery.
6. Development of a novel, simple and effective near-optimal heuristic control strategy with no access to route preview information.
7. Development of a dynamic programming-inspired real-time near-optimal control strategy with no access to route preview information.
8. Development of an ECMS (Equivalent Consumption Minimisation Strategy) inspired real-time near-optimal control strategy with no access to route preview information.
9. Development of an ECMS-inspired real-time near-optimal control strategy with access to partial route preview information.
10. Development of a dynamic programming based route-optimal vehicle speed control strategy which accounts for real-time dynamic effects like engine braking, while solving an optimisation problem involving the maximisation of fuel savings with little or no penalty to trip time.
11. Development of a real-time vehicle speed control approach, which is based on smoothing the speed trajectory of the lead vehicle, consequently reducing the acceleration and deceleration events that the intelligent vehicle will undergo.
12. Investigation of the fuel savings potential of the proposed controllers over real-world driving profiles.

1.7 Organisation of thesis

This dissertation consists of eight chapters whose contributions are described below:

Chapter 1

A general introduction is given to energy problems facing the automotive industry. As a viable solution to these problems, HEVs are briefly discussed in light of the research advances made to date, and the existing research gaps, which this dissertation intends to address. The resulting research motivation, aim and objectives are also defined.

Chapter 2

A review of relevant existing literature on HEV architectures is carried out. Previously proposed HEV control strategies are also rigorously reviewed, with their advantages and disadvantages presented to identify existing research gaps, and contextualise the innovative contents of this thesis.

Chapter 3

The research vehicle in question is introduced (a full parallel HEV) and a detailed quasi-static simulation model is developed for it, with much emphasis on the most relevant subsystems that affect fuel consumption (driver, vehicle dynamics, internal combustion engine, electric motor and electric battery). Using the validated baseline model of this vehicle (without the hybrid subsystem), a simple but effective gear shift strategy is proposed and used to investigate the impact of early gear upshift on cumulative fuel consumption over the NEDC driving cycle.

Next, a simple and novel heuristic control strategy is developed and analysed over different driving scenarios (urban driving, neighbourhood driving and highway driving) with a view to identifying and understanding the dynamic characteristics of the hybrid subsystem (electric motor and electric battery). The resulting inferences from this simulation study are then used to reformulate the proposed heuristic control framework towards achieving near-optimal charge-sustaining control results across different driving conditions. Finally, the impact of braking patterns on kinetic energy recovery is quantitatively analysed.

Chapter 4

The energy management problem of the research vehicle is optimally formulated and solved using dynamic programming. Though non-causal in nature (requires complete knowledge of future driving conditions), the obtained results are useful in establishing the ultimate performance benchmark for the vehicle, as well as providing various inferences and inputs for creating real-time sub-optimal controllers. The optimal energy management trajectories obtained from dynamic programming are subsequently modelled using Markov chains, where probabilities are assigned to govern the transition between energy states. Under the assumption of no access to route preview information, the resulting transition probability matrix is used to estimate future energy variations within a defined prediction horizon. The estimated energy variations are used subsequently, to adjust real-time control policies near-optimally, such that charge sustenance and optimisation of energy utilisation are simultaneously achieved. The performance of the proposed controller over different driving conditions (standard driving cycles) is also evaluated in comparison to another literature-based dynamic programing inspired real-time sub-optimal controller.

Chapter 5

An ECMS approach rooted in variational calculus (based on Pontryagin's minimum principle) is introduced as an instantaneous optimal control approach to solve the global optimisation problem defined in Chapter 4. The ECMS approach typically employs a cycle dependent equivalence factor, which physically represents the equivalent conversion ratio between the thermal energy from fuel and electrical energy. Under the assumption of no access to route preview information, an ad hoc, novel and simple approach is proposed to dynamically adjust the equivalence factor online, using optimised adaptation factors (initial equivalence factor and the proportional controller gain). These factors contrast the battery SOC (state of charge) variation, thus maintaining its value around a constant SOC reference. Consequently, the resulting real-time ECMS controller is optimised for robustness, fuel savings and charge sustenance. Using real-time simulation analysis, the fuel savings potential of the proposed ECMS controller is investigated and compared to the fuel savings potential of other ECMS controllers published in literature.

Chapter 6

The ECMS energy management problem formulated in Chapter 5 is remodelled to employ some readily available partial route preview information in the form of road grade variation and average route driving speed. Using this information, the constant reference SOC in Chapter 5 is replaced with one that is route-optimised for maximum energy regeneration, fuel savings and charge sustenance. For simplicity, the adaptation factors estimated in Chapter 5 are applied to the problem formulated in this chapter. The performance of the resulting controller is assessed over different urban driving conditions, with a view to investigating the additional fuel economy benefits of HEV predictive control. Two novel methods of

achieving significant fuel savings through vehicle speed control are also investigated. The first approach is an optimal but non-causal vehicle speed control approach, which is formulated through the use of dynamic programming, and accounts for real-world dynamic effects like engine braking. The second approach is a real-time vehicle speed control method, which is formulated using past speed trajectories of the vehicle immediately in front of the controlled vehicle (lead vehicle). Using real-time simulation studies, the fuel savings potential of both methods are investigated over real-world driving profiles. The additional benefits of using a hybrid system alongside the proposed vehicle speed control methods are also investigated.

Chapter 7

The fuel savings potential of three causal controllers are investigated over 1,197 real-world driving profiles, representing 28,903 km and 667 hours of real-world driving patterns.

Chapter 8

Chapter 8 summarises the main conclusions of this thesis and identifies opportunities for further research work.

1.8 Publications

1. ***Modelling and heuristic control of a parallel hybrid electric vehicle*****.** ***Wisdom Enang,*** Chris Bannister, Chris Brace, and Chris Vagg. Proceedings of the Institution of Mechanical Engineers, Part D: Journal of Automobile Engineering 0954407014565633, first published on January 19, 2015. doi:10.1177/0954407014565633

2. ***Robust proportional ECMS control of a parallel hybrid electric vehicle*****.** ***Wisdom Enang*** and Chris Bannister. Proceedings of the Institution of Mechanical Engineers, Part D: Journal of Automobile Engineering 0954407016659198, first published on August 25, 2016. doi:10.1177/0954407016659198

3. ***Modelling and control of hybrid electric vehicles (A comprehensive review)*****.** ***Wisdom Enang*** and Chris Bannister. Renewable and Sustainable Energy Reviews. http://dx.doi.org/10.1016/j.rser.2017.01.075

2 LITERATURE REVIEW

2.1 Introduction

To date, a number of energy management strategies have been proposed in literature. This chapter aims to present a comprehensive review of these literatures, focusing primarily on contributions to parallel hybrid electric vehicle modelling and control. As part of this treatise, exploitable research gaps are also identified.

The review will focus on HEV configurations in light of their characteristics and applications, along with an examination of modelling techniques and the relative importance of each approach. HEV control strategies will be reviewed at depth on two main tiers: offline and online control strategies. This detailed appraisal will be aimed at highlighting the control structure of the reviewed techniques, their novelty, as well as contributions towards the satisfaction of several optimisation objectives, which include but are not limited to: reduction of fuel consumption and emissions, charge sustenance, optimisation of braking energy regeneration, and improvement of vehicle driveability. Finally, exploitable research gaps which form the main inspiration for the studies contained in this thesis will be identified and discussed.

2.2 HEV configurations

Today, there are two types of hybrid electric system configurations ("series hybrid" and "parallel hybrid") currently in use by automotive engineers [27, 28]. The dissimilarities that separate HEVs into these categories lie in the design of the power flow from the sources of energy. Power flow in the series HEV is passed down to the transmission over a single path (electrical path) [29]. Parallel HEVs allow power flow through two paths (electrical and mechanical path) from the energy sources to the transmission [29].

2.2.1 Series hybrid electric vehicle

The series hybrid electric system is a classification given to vehicles where an energy transformer is placed in series with one or more electric motors for traction of the vehicle. The main function of the internal combustion engine (ICE) in this case is to generate electricity for the battery, which in turn feeds power to the traction motor either directly or via an electric generator. This HEV configuration permits no direct mechanical connection between the internal combustion engine and the propelling wheels. Consequently, the internal combustion engine can be controlled independently of the vehicle power demand and close to its peak-efficiency region. The series HEV could thus be described as being powered primarily by the electric motor and secondarily by the ICE. Detailed in Figure 2-1 is a schematic of the series HEV configuration.

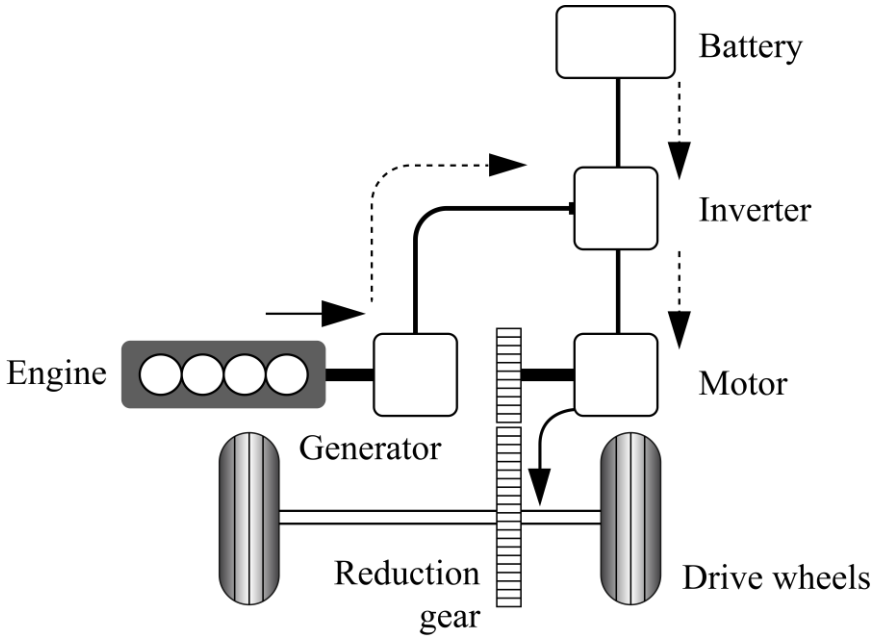

Figure 2-1: Series hybrid electric vehicle

Internal combustion engines used in series HEVs are generally small compared to those used in conventional vehicles and only account for less than 50% of the maximum power needed to propel the vehicle. Several automotive companies, e.g. Mitsubishi, Volvo and BMW, have explored the possibility of series HEV development. Despite this in-depth research, commercial application of the series HEV development is still very limited to heavy duty vehicles. Although series HEVs tend to have highly efficient engine operation, this benefit is quickly outweighed by the fact that they often require very powerful and expensive batteries, with a high energy density to operate. The powerful batteries are needed because in most cases, the motor may have to produce 50% of the required total power demand on its own [29, 30].

2.2.2 Parallel hybrid electric vehicle

In the parallel HEV configuration, both the engine and the electric motor are able to work independently or co-operatively to provide traction. In this configuration, the engine is mechanically connected to the driving wheels via a gearbox, while the electric motor is used to support the engine during accelerations. Depending on the power of the motor, it could also be used as the sole power source of the vehicle while idling and during start-ups. The engine used in the parallel HEV configuration is usually bigger than those used in the series configuration, while the electric motor is comparatively smaller and less powerful. The possibility for direct energy flow from the ICE to the wheels enables the parallel HEV to switch to the most efficient operating point by using the ICE, whenever it can operate around the peak-efficiency region. This is due to the parallel connection between the electric motor and the internal combustion engine, which implies that the capacities of the ICE and the electric motor can be varied, without changing the total driving capacity of the vehicle [30]. Detailed in Figure 2-2 is a schematic of the parallel HEV configuration. Parallel HEVs come in two sub configurations: the pre-transmission parallel and the post-transmission parallel.

In the pre-transmission parallel HEV configuration, the gearbox is located on the main drive shaft, which implies that the gear speed ratios do apply to both the engine and the electric motor. In this configuration, the power summation occurs at the gear box. Consequently, torque from the electric motor is added to the engine torque at the input shaft of the gearbox. In the post-transmission parallel HEV configuration, the gearbox is situated on the engine shaft before the torque splitter and the electric motor. This implies that the gear speed ratios only apply to the engine. In this configuration, the electric motor torque is usually added to the

engine torque at the output shaft of the gearbox. If a motor only transmission is required on a parallel HEV configuration, the use of a disconnecting device such as a clutch can be employed to disengage the gear, while running the electric motor independently.

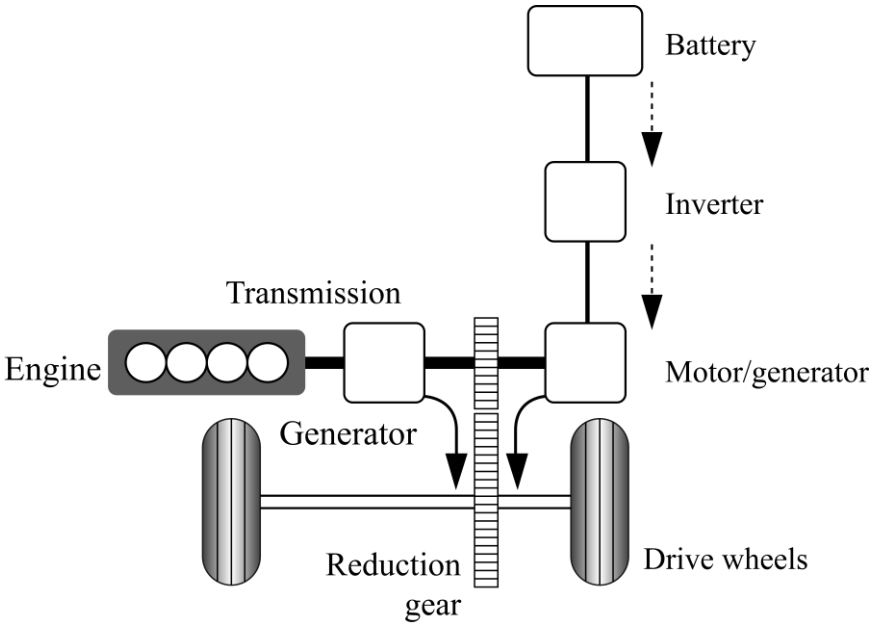

Figure 2-2: Parallel hybrid electric vehicle

2.2.3 Recent developments in hybrid powertrains

HEV development today is mostly aimed towards the use of series hybrid electric systems in heavy-duty vehicles, primarily in buses, and the use of parallel hybrid electric systems for light-duty vehicles. Specifically, the development of parallel HEVs have focused on implementation of optimal and sub-optimal control algorithms which enable the internal combustion engine to run only in areas of high efficiency, thus mitigating the lack of ICE speed controllability, due to its mechanical connection with the wheels.

In a comparative sense, parallel HEVs have received more research attention compared to series HEVs and this is as a result of the flexibility in its powertrain design as well as the elimination of the need for a large traction motor in the parallel HEV configuration. One of such development has been the implementation of the parallel hybrid technology on an all-wheel drive vehicle, as shown in Figure 2-3. This sort of application is most beneficial if the internal combustion engine is used to power the rear wheels, while the electric motor is used to power the front wheels. Configuring the setup this way means that the high vehicle weight borne by the front wheels of the vehicle is used advantageously during regenerative braking, thus leading to high braking energy recapture.

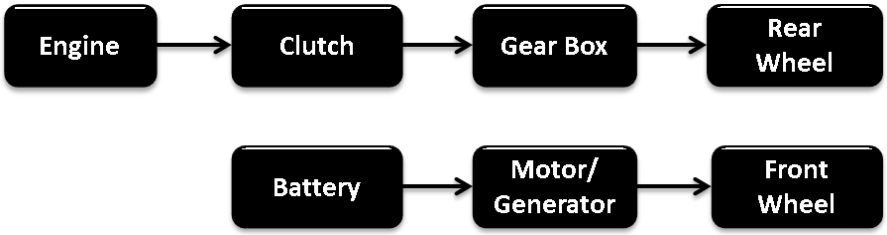

Figure 2-3: All-wheel drive parallel hybrid electric vehicle

The all-wheel drive parallel HEV configuration also offers an advantage with respect to vehicle longitudinal stability control in slippery conditions. Another recent product of parallel HEV research and development is the series-parallel HEV configuration. This design depends primarily on the presence of two electric motors and a connection between both, which can be either mechanical or electrical. Where mechanical connections are used between the electric motors, this is done using a planetary gear power splitting device. The series-parallel configuration offers the advantage and possibility of having the engine completely

decoupled from the vehicle, thus making it possible for the vehicle to be powered using just the electric motors [31]. It also offers the possibility of operating the ICE around its peak-efficiency region due to flexibility in both torque and speed changeability at the ICE output. These advantages becomes partially offset when energy losses during conversion of mechanical energy to electrical energy is taken into account. Although there exist a number of series-parallel hybrid electric vehicle configurations, it is worth highlighting the Toyota THS design, which was first pioneered on the Toyota Prius, as shown in Figure 2-4.

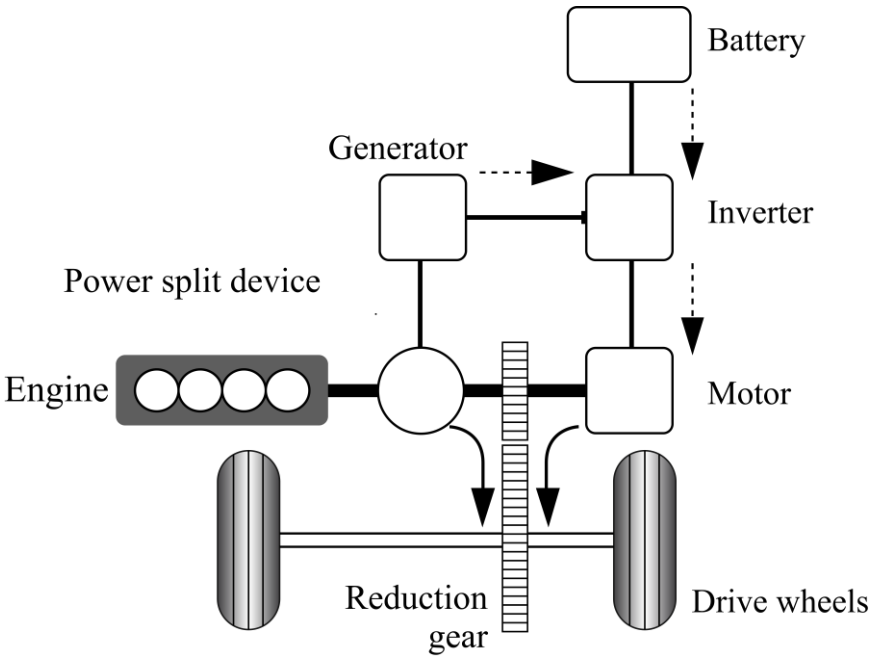

Figure 2-4: Series-parallel hybrid electric vehicle

2.3 HEV modelling approaches

There exist at least three main stages of computational modelling currently employed in the development of HEVs. These stages are:

- Detailed modelling, which is performed during the research and early development stages of the HEV. This sort of modelling centres mainly on single powertrain components such as internal combustion engine and electric motor. This type of modelling is aimed at providing detailed information about specific characteristics of the component being modelled.
- Software in the loop (SIL) modelling, which is carried out at a later stage of the HEV development cycle, but usually before any hardware production is made. The employment of SIL today has become popular in HEV control system development.
- Hardware in the loop (HIL) modelling, which is carried out once the production of controllers has been completed and validated.

Three typical approaches exist for HEV modelling at the detailed modelling stage of the development process: the kinematic or backward approach, the quasi static or forward approach, and the dynamic approach [28].

2.3.1 Kinematic approach

The kinematic approach, as shown in Figure 2-5, is a backward methodology where the input variables are the speed of the vehicle and the grade angle of the road. In this method, the engine speed is determined using simple kinematic relationships starting from the wheel revolution speed and the total transmission ratio of the

driveline. The tractive torque that should be provided to the wheels to drive the vehicle according to the chosen speed profile can be calculated from the main vehicle characteristics (e.g. vehicle mass, aerodynamic drag and rolling resistance).

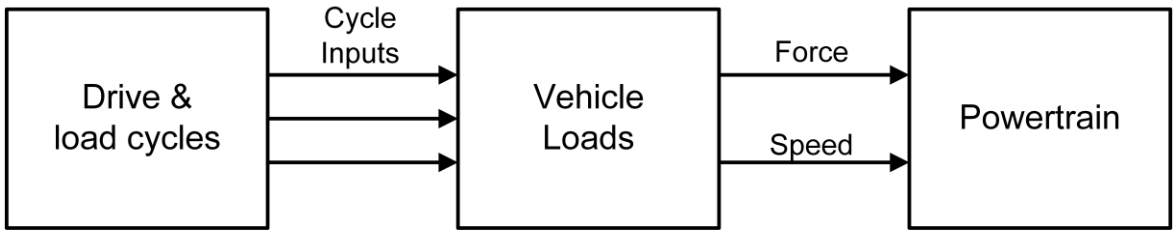

Figure 2-5: Information flow in a kinematic or backward HEV model (source [32])

The calculated engine torque and speed is then used alongside a statistical fuel consumption model to produce an instantaneous fuel consumption or emissions rate prediction [33]. The kinematic approach assumes that the vehicle meets the target performance, so that the vehicle speed is supposedly known a priori; thus enjoying the advantage of simplicity and low computational cost [32]. The backward or kinematic modelling method ensures that the driving speed profile will be exactly followed. However, there exist no guarantees that the given vehicle will actually be able to meet the desired speed trace, since the power request is directly computed from the speed and not checked against the actual powertrain capabilities. Typically, in simulation, the kinematic approach includes a “fail-safe” feature which stops the simulation run if the required torque exceeds the maximum torque available (from the electric motor and engine). Another flaw of this modelling technique is its negligence of thermal transient behaviour of engines which are noticeable after an engine cold start.

The simplification of transient conditions as a sequence of stationary states limits this modelling method to an option considered mainly for preliminary estimation of vehicle fuel consumption and emissions [28].

2.3.2 Quasi-static approach

The quasi-static approach of HEV modelling as shown in Figure 2-6 makes use of a driver model, typically a PID which compares the target vehicle speed (driving cycle speed), with the actual speed profile of the vehicle and then generates a power demand profile needed to follow the target vehicle speed profile. This power demand profile is generated by solving the differential motion equation of the vehicle [32]. Once the propulsion torque and speed of the engine have been determined, instantaneous fuel consumption can be estimated using a statistical engine model as already explained in the kinematic or backward approach.

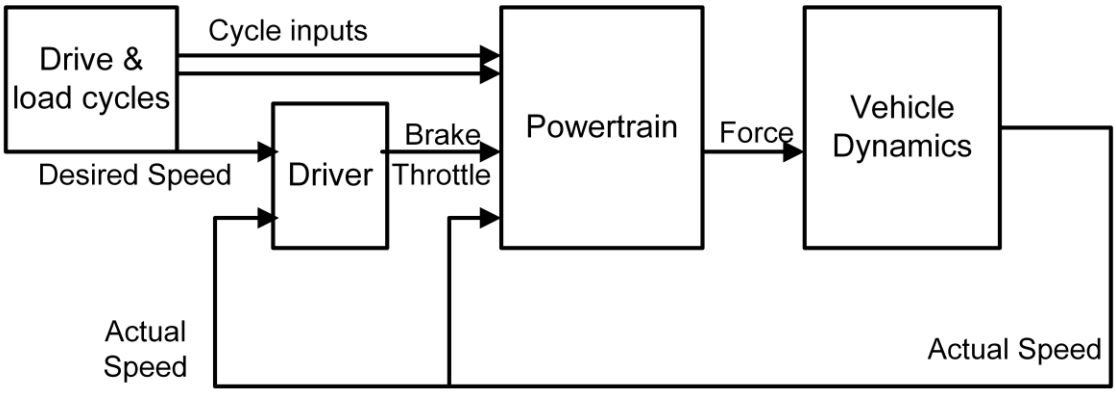

Figure 2-6: Information flow in a quasi-static powertrain model (source [32])

The suitability and accuracy of the quasi-static modelling approach depends very much on the nature of simulation studies to be conducted. The quasi-static modelling approach provides reasonable accuracy when it comes to the evaluation of the fuel consumption and NOx of a vehicle equipped with conventional

powertrain. For pollutants like soot, the acceleration transients and related “turbo-lag” phenomena significantly contribute to the cycle cumulative emissions, thus necessitating a more detailed engine simulation model which is capable of properly capturing engine transient behaviour in more detail [34].

2.3.3 Dynamic modelling approach

In the dynamic modelling approach, the internal combustion engine behaviour during transients is also modelled in addition to the longitudinal vehicle dynamics. The engine transient behaviour is modelled by means of a detailed one-dimensional fluid dynamic model. For example, the intake and exhaust systems of the internal combustion engine in the dynamic modelling approach are represented as a network of ducts connected by the junctions that represent either physical joints between the ducts, such as area changes or volumes, or subsystems such as the engine cylinder. Solutions to the equations governing the conservation of mass, momentum and energy flow for each element of the network can then be obtained using a finite difference technique. This makes it possible for highly dynamic events such as abrupt vehicle accelerations to be properly and reliably simulated with reasonable accuracy. The implementation of dynamic modelling comes with a huge time and computational burden and as such its application is often limited to research areas that deal with internal combustion engine development [35-37].

From a control development stand point, the quasi-static approach is preferred since it maintains the physical causality of the vehicle system, and allows for the possibility of using the same controller inputs/outputs in the simulator as well as on the real vehicle.

2.4 HEV control strategies

HEVs have been shown to significantly improve automotive fuel economy and reduce emissions whilst still meeting the vehicle power demand and, maintaining satisfactory vehicle performance and driver-feel [38]. Regardless of the HEV configuration in question, employing the right power split between the energy sources (ICE and electric motor) is crucial to the achievement of an improved fuel economy and reduced emissions. On this basis, several power split control strategies have been proposed, evaluated and employed on different HEV configurations. Typically, inputs to the power-split controller of HEVs often include vehicle power demand, vehicle speed or acceleration, battery state of charge, present road load, and on occasion, ”intelligent” future traffic conditions from the Global Positioning System (GPS). The controller outputs signal contains a set of control decisions which specify whether the HEV should operate in any of the following modes:

1. Engine only mode (ICE operates alone).
2. Assist mode (ICE and electric motor operates).
3. Electric motor only mode (Electric motor operates alone).
4. Regenerative mode (Electric motor is used for kinetic energy recovery).
5. Trickle charge mode (Engine produces power used in charging the battery).

Minimisation of fuel consumption and emissions without compromising vehicle performance, and battery state of charge are often the main control objectives of most HEV control strategies. HEV control strategies can be broadly classified into online control strategies and offline control strategies as shown in the control strategy classification chart in Figure 2-7.

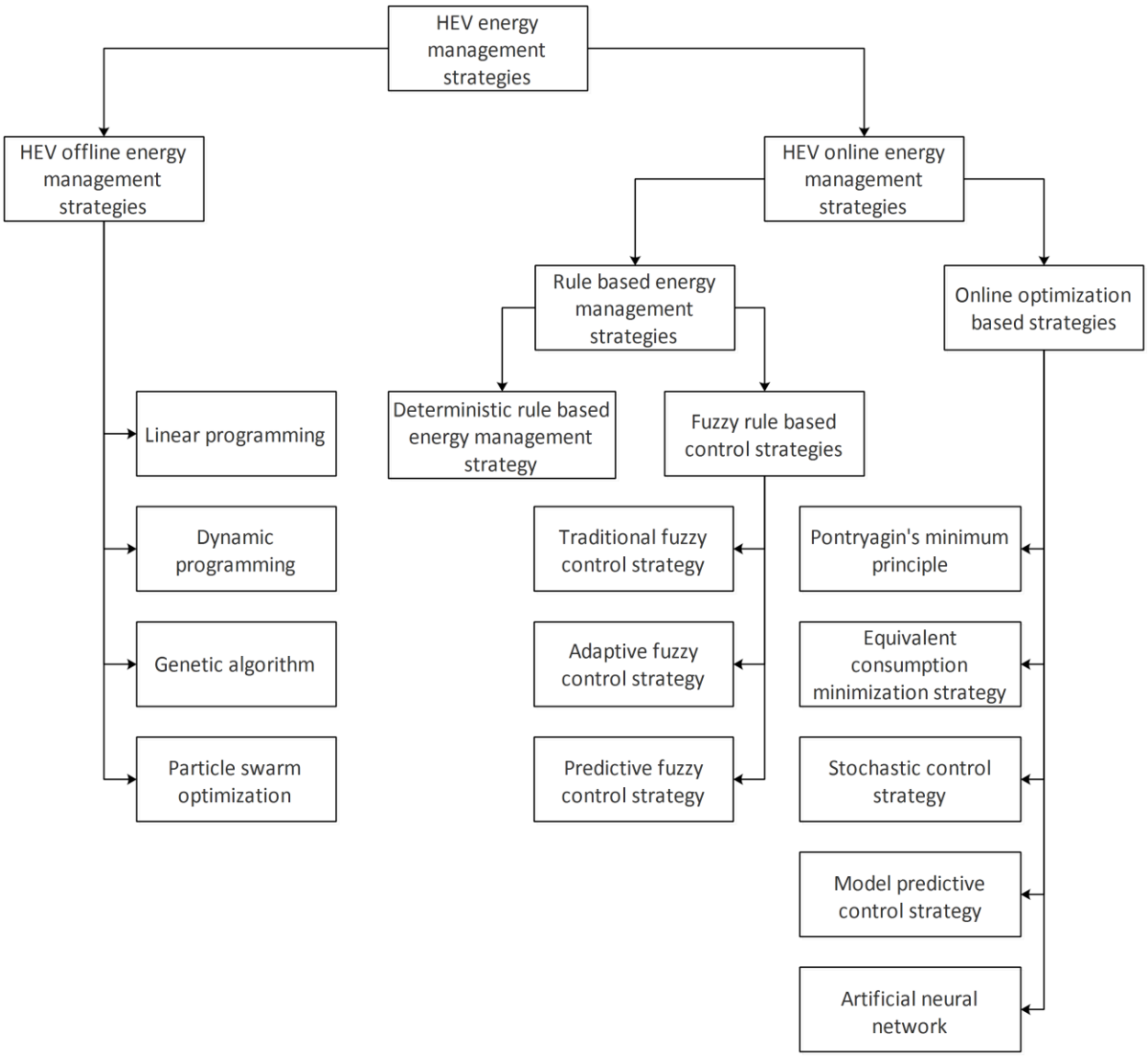

Figure 2-7: HEV control strategy classification

Although there have been several papers and research publications which have contributed to the compilation of reviews on HEV control strategies, this area of research is continuously advancing and with the introduction of newer techniques, there is need for an up-to-date review. The main objective of this section is not

only to contribute to the growing list of review discussions, but also to identify relevant research gaps in the field.

2.4.1 HEV offline control strategies

Optimisation-based control strategies decide the control signals either by minimising the sum of the objective function over time (global optimisation) or by instantaneously minimising the objective function (local optimisation).

The effectiveness of a global optimal control technique relies solely on the knowledge of the entire driving cycle a priori, and since this is usually difficult to determine in real time, global optimal techniques are usually referred to as "non-causal", which cannot be applied in real time, but are useful as a control benchmark to which all other causal real-time controllers can be compared. Linear programming, dynamic programming, genetic algorithms, etc., have been applied as global optimisation techniques for optimal energy management of HEVs.

2.4.1.1 Linear programming

Using linear programming, the non-linear fuel consumption model of an HEV is approximated and solved for a global optimal solution [39]. Linear programming has been applied successfully to automotive energy management problems. For example in the study of Kleimaier *et al.* [40], a convex optimisation technique for the analysis of propulsion capabilities using linear programming was proposed as shown in Figure 2-8. Pisu *et al.* [41] designed a stable and robust controller using linear matrix inequalities, to minimise fuel consumption.

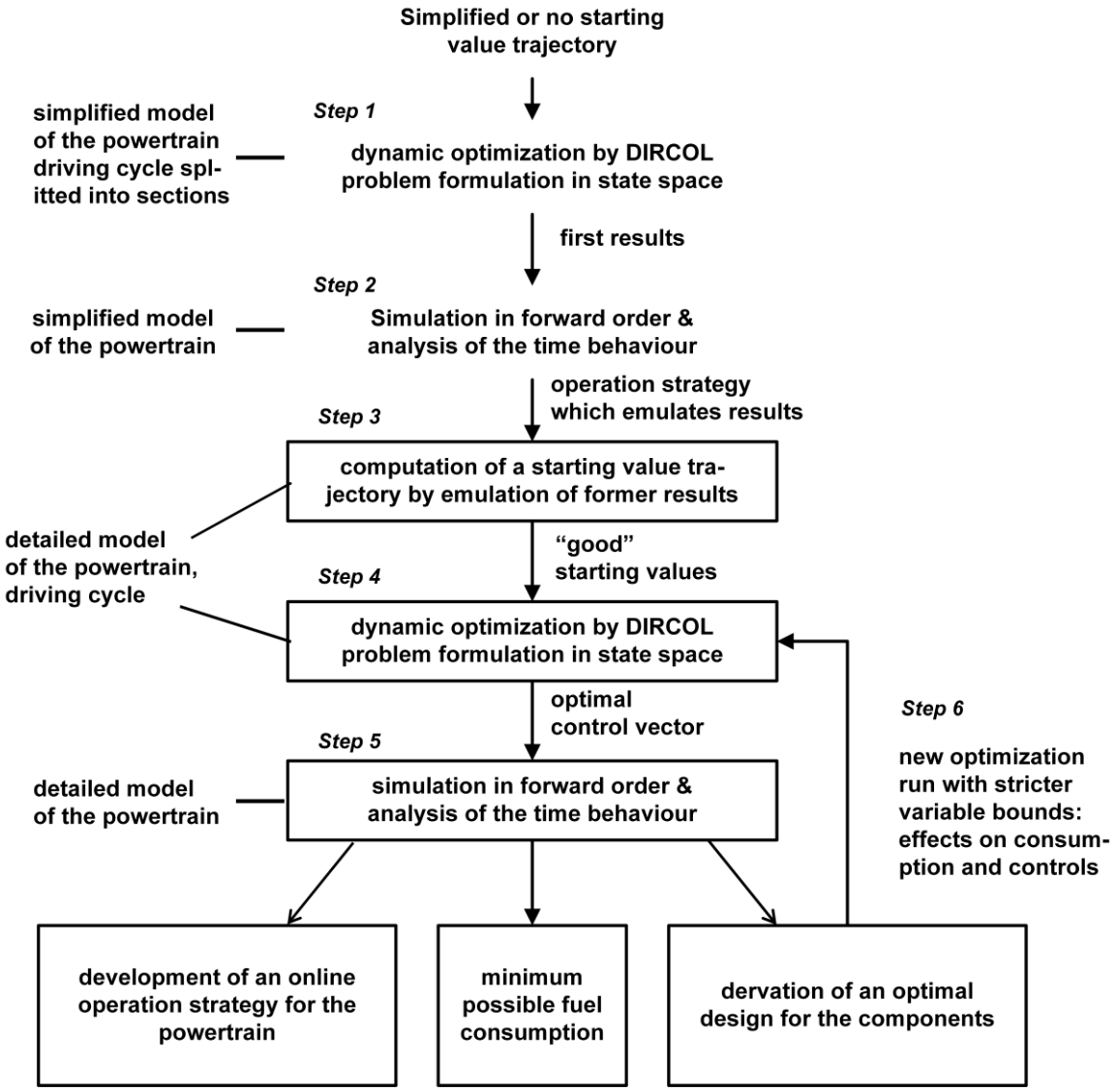

Figure 2-8: Structure of linear optimisation method (redrawn from [40])

2.4.1.2 Dynamic programming

The dynamic programming technique is a technique originally developed by Richard Bellman, which aims to find optimal control policies using a multi-stage decision process. As defined by Bellman:

> *An optimal control policy has the property that no matter what the previous decision (i.e., controls) have been, the remaining decisions must constitute an optimal policy with regard to the state resulting from those previous decisions* [42].

Dynamic programming algorithm is a discrete multi-stage optimisation problem in which a decision based on the optimisation criterion is chosen from a finite number of decision variables at each time step. Bellman's dynamic programming algorithm can be applied using two methods: the backward recursive method and the forward dynamic programming technique. In the backward recursive method, the optimal sequence of control variables is obtained proceeding backwards from the final state and choosing at each time step the path that minimises the cost-to-go (integral cost from that time step until the final state). By symmetry, most dynamic programming problems solved using the backward recursive method could also be solved using the forward dynamic programming technique. Although both techniques do lead to the same set of optimal control policies for the entire problem, their "by-products" are different. When solving a problem using the backward dynamic programming technique, the by-products obtained are the optimal values from every state in every stage to the end; whereas in solving a problem using forward dynamic programming, the corresponding by-products would be the optimal values from the initial state(s) in the first stage to every state in the remaining stages.

Dynamic programming has the advantage of being applied to both linear and non-linear systems as well as constrained and unconstrained problems. It also suffers two setbacks: its reliance on prior knowledge of the full driving cycle, and the curse of dimensionality which amplifies the computational burden. Consequently, control results from dynamic programming are only useful as optimal benchmarks for other controllers, or as a basis for the development and improvement of other sub-optimal controllers. In Shen *et al.* [43], an effort was made to reduce the computation time of the dynamic programming approach, through the use of a forward search algorithm.

Dynamic programming features prominently in HEV energy management studies [26, 43-63]. In this section, some notable examples of its application on HEVs are reviewed. Brahma *et al.* [44], applied dynamic programming to achieve a real-time optimal split between the ICE and electric motor of a series HEV. They suggested that by using the discrete state formulation approach of dynamic programming, computational efficiency can be further improved. Similarly, Lin *et al.* [48] found that optimal control rules could be extracted from dynamic programming, and used to near-optimally adapt a rule-based controller. The resulting improvement in fuel economy for different levels of heuristic controller modification is detailed in Table 2-1, for the UDDSHDV cycle.

	Fuel Economy (MPG)
Conventional	10.63
Preliminary Rule-Based	12.56
New Shift Control	13.02
New Power Split Control	13.17
New Recharging Control	13.24
Dynamic Programming	13.63

Table 2-1: Fuel economy comparison over UDDSHDV cycle (source [48])

In another study by Lin *et al.* [46], a simple approach for extracting heuristic control rules from dynamic programming (based on the ratio of power request to transmission speed) was formulated. Simulation results from this study showed that, by properly analysing control results from dynamic programming, an improved rule-based control strategy could be developed. In this study, heuristic control rules were extracted from one driving cycle and used to near-optimally control 7 other driving cycles. Obtained simulation results (Table 2-2) showed a 50 – 70% reduction in performance gap between the optimal controller (DP controller) and the improved rule-based controller. The combination of dynamic programming and rule-based control strategies for real-time charge-sustaining control of HEVs, have also been considered in Lin *et al.* [46, 48] and Kum *et al.* [61]. In Kum *et al.* [61], the control steps are articulated as follows: dynamic programming is first used to obtain a global optimal solution to the formulated energy management problem. Next, battery SOC for the remaining trip distance is estimated using the energy-to-distance ratio (EDR). An adaptive supervisory powertrain controller is applied subsequently, to reduce fuel consumption and emissions based on results from the EDR and catalyst temperature system.

In Perez *et al.* [24], a finite horizon dynamical optimisation problem is formulated and solved using dynamic programming, with the objective of maintaining battery energy levels within the prescribed range without affecting the battery state of health.

	FE (mi/gal)	NOx (g/mi)	PM (g/mi)	Performance Measure	
				g/mi	Improvement %
Preliminary Rule-Based	15.31	4.43	0.36	671.23	0%
New Rule-Based	14.61	3.02	0.30	582.18	13.27%
DP (Fuel Economy & Emissions)	15.41	2.78	0.26	526.67	21.54%

a. Results over the WVUSUB cycle (Suburban driving)

	FE (mi/gal)	NOx (g/mi)	PM (g/mi)	Performance Measure	
				g/mi	Improvement %
Preliminary Rule-Based	12.84	7.29	0.51	948.83	0%
New Rule-Based	12.72	6.31	0.49	896.00	5.57%
DP (Fuel Economy & Emissions)	12.97	6.17	0.44	847.67	10.66%

b. Results over the WVUNITER driving cycles (Interstate driving)

	FE (mi/gal)	NOx (g/mi)	PM (g/mi)	Performance Measure	
				g/mi	Improvement %
Preliminary Rule-Based	16.18	3.87	0.33	621.22	0%
New Rule-Based	15.09	2.49	0.23	494.12	20.46%
DP (Fuel Economy & Emissions)	16.63	2.04	0.16	403.58	35.03%

c. Results over the WVUCITY driving cycles (City driving)

Table 2-2: Fuel economy and emissions evaluation for a dynamic programming-inspired rule-based controller (source [46])

Gong *et al.* [64], investigated two variations of the dynamic programming algorithm (conventional dynamic programming and two-scale dynamic programming) on a charge-depleting plug-in HEV. In the two-scale dynamic programming algorithm, the electric mode of the operation is used first for the known trip distance. The rest of the distance is divided into different segments of known length and for each segment; fuel consumption and SOC level (Figure 2-9) are calculated. Finally, spatial domain optimisation is performed to find the optimal solution. Results from this study show that compared to the conventional dynamic programming algorithm which is very computationally expensive, a near-optimal fuel economy (3.7% less than optimal fuel economy) could be achieved using the two-scale dynamic programming algorithm. The two-scale dynamic programming algorithm was further used to develop an efficient on-board control strategy in another study by Gong *et al.* [26].

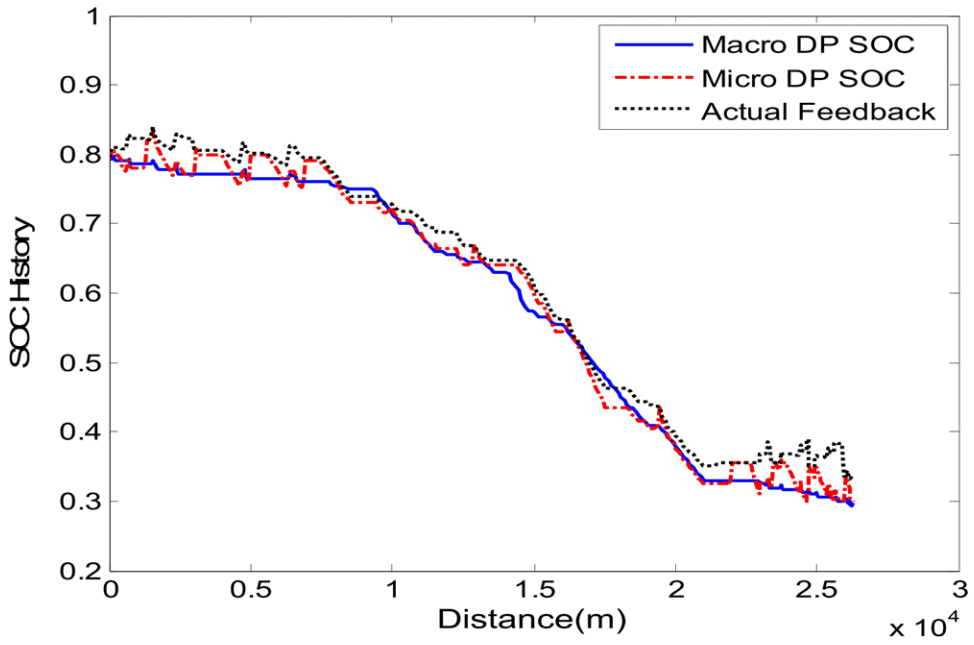

Figure 2-9: Trip segmentation on road segment (source [64])

2.4.1.3 Stochastic control strategy

Stochastic control is a framework developed to model and solve optimisation problems involving uncertainties. In this strategy, an infinite-horizon stochastic dynamic optimisation problem is formulated. The vehicular power demand is modelled as a random Markov process. Using the Markov driver, future power demand is predicted based on current transition probabilities. The optimal control strategy is then obtained using stochastic dynamic programming (SDP) [25, 65-67]. The obtained control policy is in the form of a stationary full-state feedback, optimised over a family of driving patterns; that can be directly implemented in a vehicle. In contrast to dynamic programming which optimises the control policy over a given driving cycle, stochastic dynamic programming optimises the control policy over a family of diverse driving patterns. Though relatively new, the concept of stochastic energy management in HEVs has attracted considerable attention worth reviewing. Using stochastic dynamic programming, Liu *et al.* [68] successfully formulated a hybrid power optimal control strategy which uses an engine-in-loop (EIL) system to instantly analyse the impact of transients on engine emissions. In a study by Tate *et al.* [69], two variations of the stochastic control strategy (infinite horizon SDP and shortest path SDP) were developed and implemented on a parallel HEV. As shown in Figure 2-10 and summarised in Table 2-3, the shortest path SDP controller was found to yield better results, as it offers better battery state of charge control and fewer parameters to be tuned.

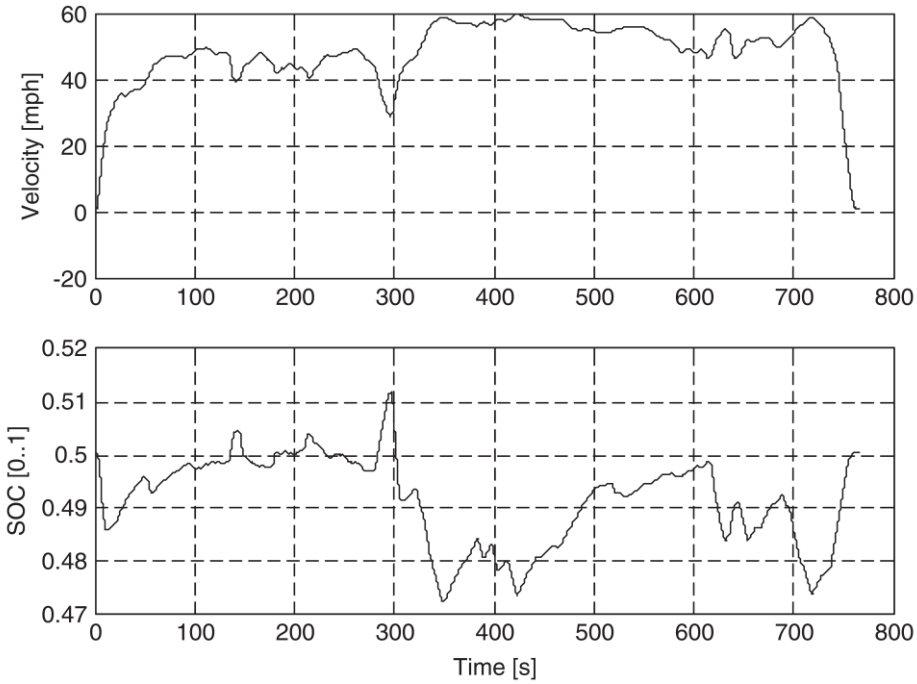

Figure 2-10: SOC on the HWFET using the SP-SDP controller (source [69])

	SP-SDP		SDP		SP-SDP improvement	
Cycle	**Performance**	**Final SOC**	**Performance**	**Final SOC**	**Performance (%)**	**Reduction in Final SOC error (%)**
UDDS HDV	833.58	0.4982	850.46	0.5128	2.03	85.94
WVU suburban	627.05	0.5058	654.44	0.5103	4.37	43.7
WVU city	509.46	0.4997	536.82	0.5095	5.37	96.84
FET highway	944.14	0.5004	972.93	0.5214	3.05	98.13

Table 2-3: Comparison of performance in control laws for the SP-SDP and SDP controller (source [69])

Using the shortest-path SDP method, the optimal trade-off between fuel consumption and tailpipe emissions was investigated on an HEV facilitated with a dual mode EVT [70]. Results from this study showed that even with the much simplified shortest-path SDP, 8000 simulation hours was required to obtain an optimal solution to the formulated energy management problem. The shortest-path SDP was further developed in a study by Opila *et al.* [71] to account for HEV energy management problems involving fuel economy and driveability. Results from this study showed that for the same level of driveability, the SP-SDP-based controllers were 11% more fuel efficient than a baseline controller over the FTP driving cycle (Table 2-4).

Controller Descriptions	**Fuel Economy (Corrected)**	**Engine Events**	**Gear Events**	**Final SOC**	**Fuel Economy (Uncorrected)**
Baseline Controller	1.000	88	93	0.505	0.997
SP-SDP #1- Best Fuel Economy	1.119	88	106	0.504	1.117
SP-SDP #2 Similar Drivetrain Activity	1.114	88	93	0.506	1.110
SP-SDP #3 Similar Fuel Economy	1.010	34	36	0.561	0.977

Table 2-4: SP-SDP controller performance over the FTP driving cycle

SP-SDP #1 is the controller with the best corrected fuel economy without regard to driveability. SP-SDP #2 has the closest driveability metrics to the baseline controller, and is closely related to SP-SDP #1. SP-SDP #3 is selected by finding a controller with similar fuel economy to the baseline controller and about half the number of driveability events.

Wang *et al.* [72] proposed an SDP-extremum seeking algorithm with feedback control as shown in Figure 2-11. By definition, this approach leverages the global optimality and SOC sustainability characteristics of the SDP controller, and compensates its optimal control errors by introducing a real-time extremum seeking output feedback. The resulting effect is a real-time near-optimal and charge-sustaining performance, as shown in Figure 2-12.

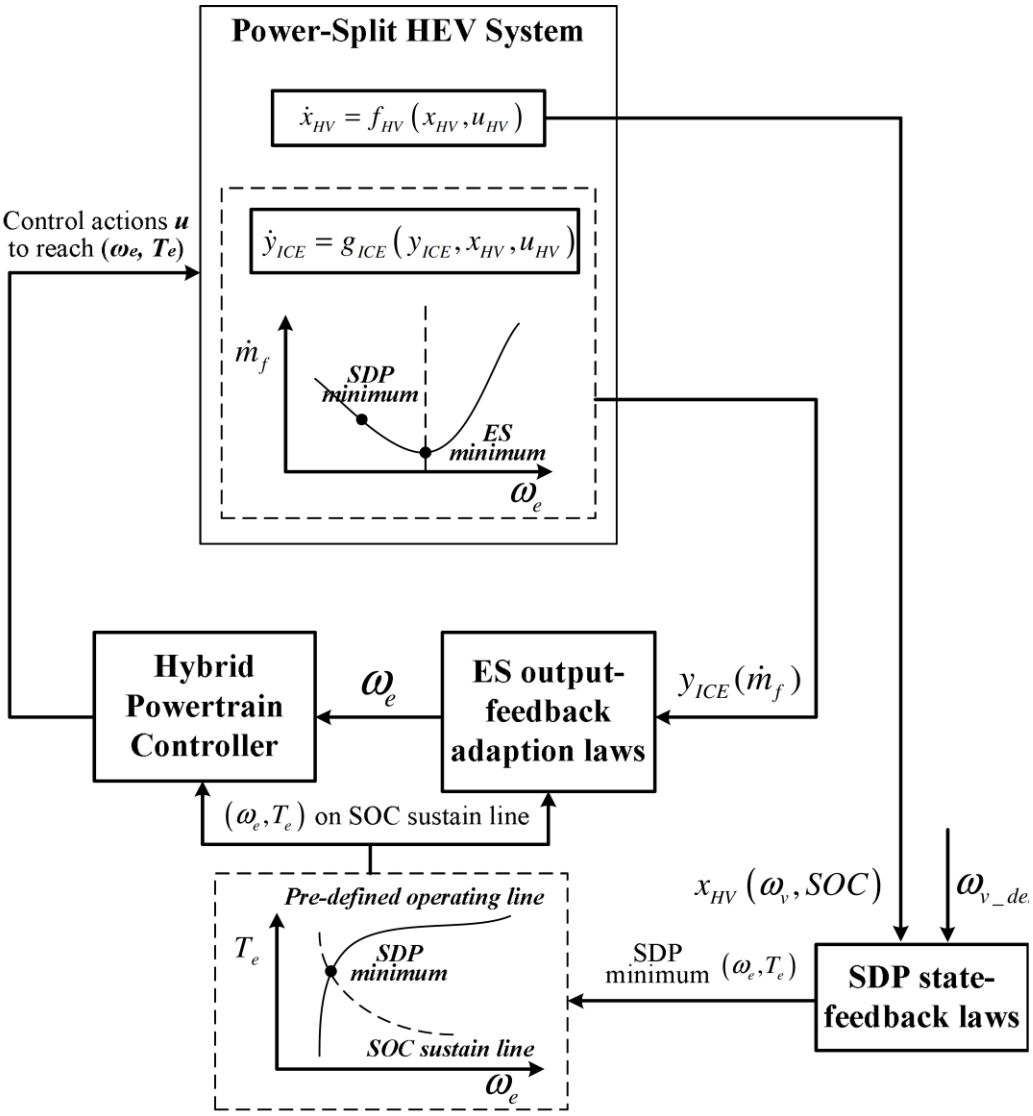

Figure 2-11: The schematic diagram of the SDP-ES optimisation algorithm (source [72])

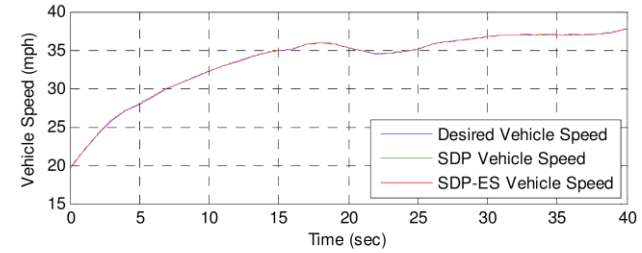

(a) vehicle speed

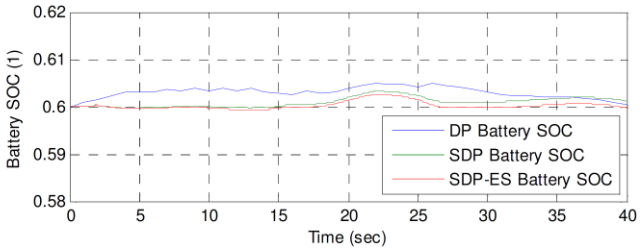

(b) battery SOC

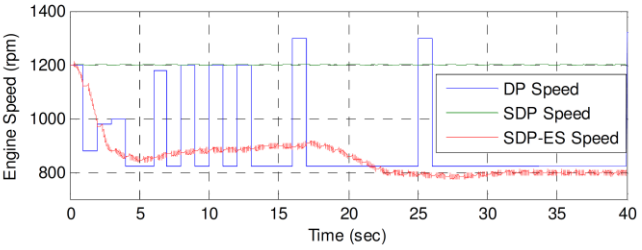

(c) engine speed

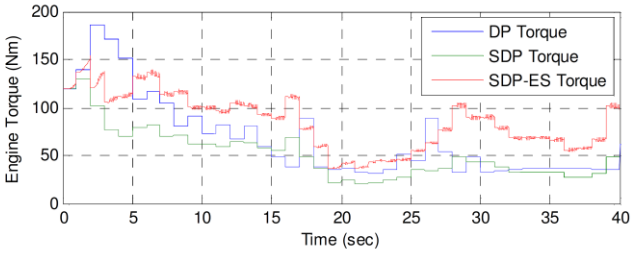

(d) engine torque

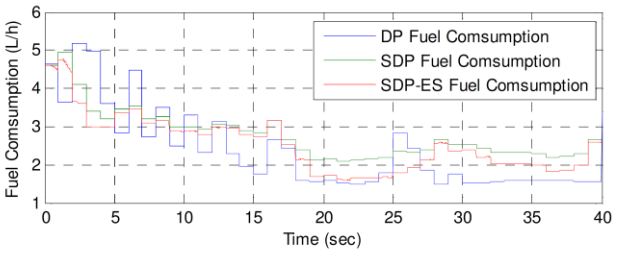

(e) fuel consumption

Figure 2-12: Comparison between the optimised results by SDP and SDP-ES (source [72])

2.4.1.4 Genetic algorithm

Genetic algorithm (GA) is a heuristic search algorithm for generating solutions to optimisation problems. This branch of artificial intelligence is inspired by Darwin's theory of evolution. In order to procure an optimal solution to a problem, GA begins with a set of preliminary solutions (chromosomes) called population. The solutions from each population are chosen according to their suitability to form new and improved versions. Consequently, the most suitable solutions have a better chance of growth than weaker solutions. The process is continuously repeated until the desired optimisation conditions are satisfied. Genetic algorithm is a robust and feasible global optimisation approach with a wide range of search space, useful for solving complex engineering optimisation problems characterised by non-linear, multimodal, non-convex objective functions.

A number of studies have considered genetic algorithm for energy management in HEVs [73-81]. Piccolo *et al.* [82] applied genetic algorithm to an on-road vehicle with the objective of optimising an objective function involving fuel consumption and emissions terms. They compared their genetic-based approach with a conventional gradient-based approach, and found that the genetic optimisation approach achieved a better reduction in CO emissions, while the HC and NOx emissions remained roughly the same (Table 2-5).

	Genetic Based	Gradient-based	Deviation %
CO (g/km)	4.53	5.18	-12.5
NOx (g/km)	0.25	0.25	0
HC (g/km)	0.45	0.44	+2.2
Fuel consumption (1/100km)	6.9	6.8	+1.4

Table 2-5: Genetic algorithm results over an urban driving cycle (source [82])

Ippolito *et al.* [83], combined a fuzzy clustering criterion with genetic algorithm to compensate for the performance of the proposed energy controller in dynamic and unpredictable driving conditions. Results from this study as detailed in Table 2-6 show that the combination of both strategies yield significant reduction in computational effort and improvement in fuel efficiency when compared to the multi-objective optimisation approach.

Wang *et al.* [84], Poursamad *et al.* [85] and Yi *et al.* [86], used genetic algorithm to tune and optimise a robust real-time implementable fuzzy-logic based HEV control strategy. The application of genetic algorithm for multi-objective energy management is considered by Huang *et al.* [80]. In this study, a multi-objective genetic algorithm (MOGA) is used to solve an optimisation problem for a series HEV. Their results show that genetic algorithm is flexible and effectively handles multi-objective optimisation problems. By comparing the multi-objective genetic algorithm (MOGA) to a single-objective genetic algorithm (SOGA) and a thermostatic algorithm over different driving cycles as shown in Figure 2-13, the authors conclude that if the performance of fuel economy and emissions are taken into account, the strategy based on multi-objective genetic algorithm is always better than the thermostatic and single-objective genetic algorithm. The MOGA

approach is further developed in a study by Desai *et al.* [87] to also optimise powertrain component sizing. The ICE, motor and battery sizes, as well as the control strategy parameters, were optimised. The results of the trade-off solutions (Table 2-7) demonstrated significant improvements in vehicle performance over the UDDS driving cycle. In Fang *et al.* [81], the MOGA approach is used to simultaneously optimise the control system and powertrain parameters. Genetic algorithm has also been used to solve an HEV control problem involving the optimisation of component sizes and the minimisation of fuel consumption and emissions [73-78, 88]. In *Hu et al.* [88], the proposed approach is a non-dominated sorting genetic algorithm (NSGA). The NSGA varies from GA only in the way the selection operator works. Crossover and mutation operations remain the same.

In a study by Montazeri-Gh *et al.* [89], a genetic-fuzzy approach is formulated to find an optimal region for engine operation. First, a hidden Markov model was developed to classify and recognise driving patterns from previous driving experiences. Afterwards, predicted driving patterns were utilised for the optimisation of HEV control parameters using a genetic-fuzzy approach. Simulation results from this study show that adaptation to traffic conditions using intelligent genetic-fuzzy approach is very effective in reducing fuel consumption (Figure 2-14).

Driving Cycle no.	Monitored Parameters	MOS	DB	Dev%
NEDC	HC (g/km)	0.247	0.2485	+0.63%
	CO (g/km)	1.469	1.4642	-0.36%
	NO (g/km)	0.134	0.1337	-0.59%
	Fuel Consumption (Litres/km*100)	3.593	3.5992	+0.17%
	Final SOC	0.557	0.5584	-0.16%
	CPU Time consumption during the cycle (s) (N=184)	965.86	70.09	-92.74%
FTP	HC (g/km)	0.173	0.1713	-0.75%
	CO (g/km)	0.996	0.8444	-15.2%
	NO (g/km)	0.151	0.1501	-0.6%
	Fuel Consumption (litres/km*100)	3.963	3.6926	-6.82%
	Final SOC	0.547	0.5219	-4.65%
	CPU Time consumption during the cycle (s) (N=465)	2018.3	287.45	-85.75%
US06	HC (g/km)	0.216	0.217	0.49%
	CO (g/km)	2.048	2.054	0.31%
	NO (g/km)	0.251	0.247	-1.69%
	Fuel Consumption (Liters/km*100)	5.127	5.165	0.006%
	Final SOC	0.0508	0.5077	0.75%
	CPU Time consumption during the cycle (s) (N=131)	747.75	35.5	-95.23%
HWFET	HC (g/km)	0.163	0.1603	-1.4%
	CO (g/km)	0.913	0.8853	-3.0%
	NO (g/km)	0.143	0.1381	-3.7%
	Fuel Consumption (Liters/km*100)	3.446	3.142	-0.99%
	Final SOC	0.357	0.5523	-0.86%
	CPU Time consumption during the cycle (s) (N=156)	833.39	52.24	-93.73%

Table 2-6: Simulation results: MOS (Multi-objective solutions), DB (Database), DEV% (Deviation in Percentile) (source [83])

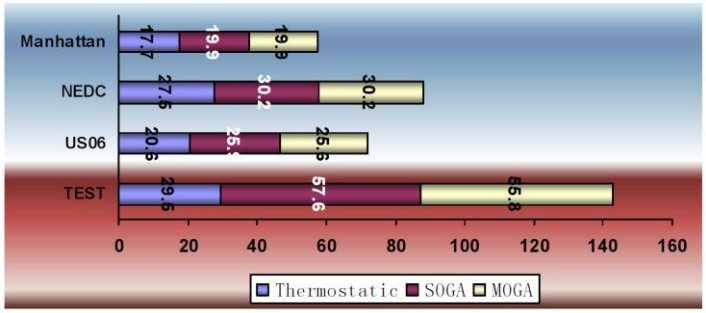

a. Fuel economy performance

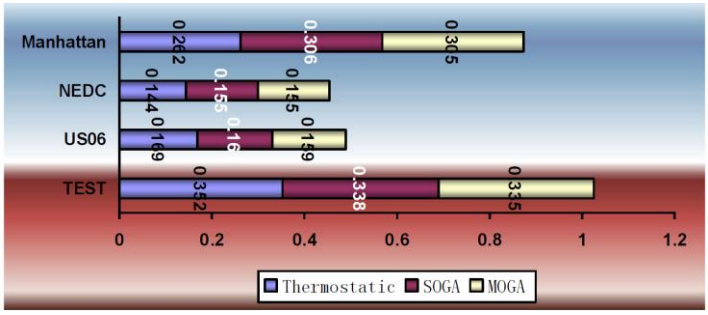

b. HC emissions

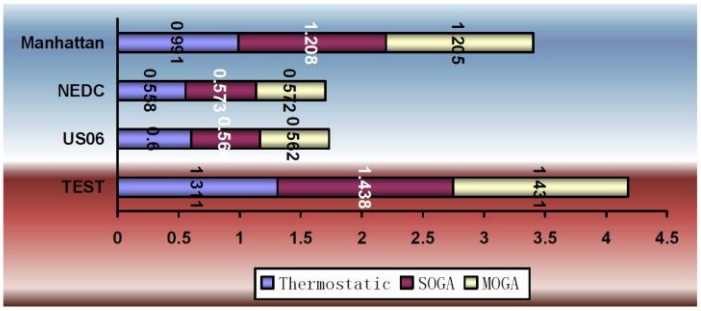

c. CO emissions

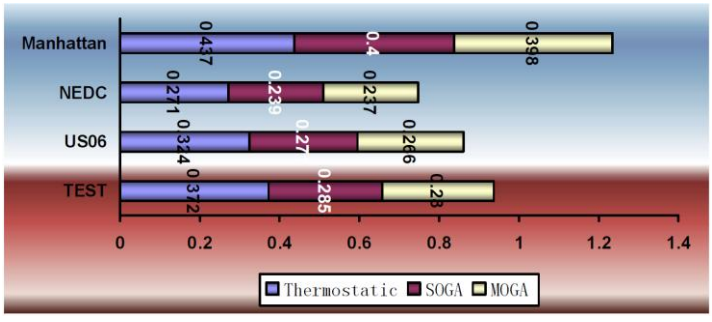

d. NOx emissions

Figure 2-13: Performance evaluation of the SOGA, MOGA and Thermostatic controller (source [80])

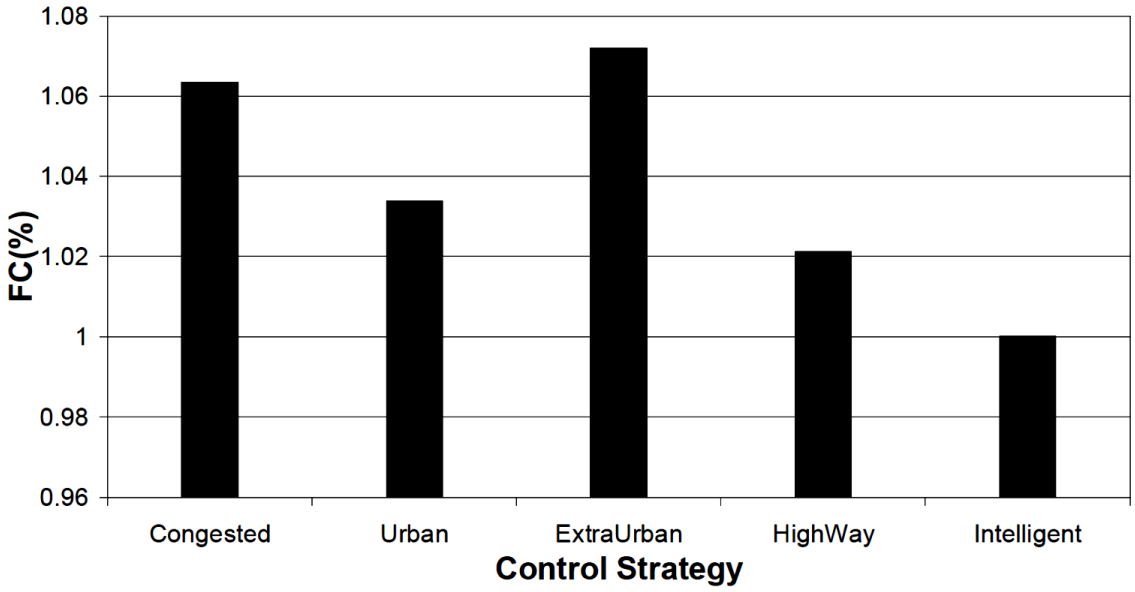

Figure 2-14: Fuel consumption obtained from simulation HEV over TEH-CAR driving cycle (source [89])

Design Variables							Objectives		Constraint
X1 ICE Power (kW)	X2 Motor Power (kW)	X3 Battery Power (kWh)	X4	X5	X6	X7 (km/h)	Fuel Cons. (L/100 km)	Emission (grams/ km)	Acceleration t1 (sec)
186.3	90.12	54.86	0.5	0.8	0.8	6.2	44.45	19.47	24.47
179.9	122.4	56.41	0.4	0.9	0.9	5.71	45.33	18.84	24.11
185.6	95.1	54.85	0.5	0.9	0.9	5.46	44.8	19.35	23.84
195.4	127.4	54.83	0.4	0.9	0.9	3.42	43.51	19.83	23.19
179.3	99.96	53.19	0.4	0.8	0.8	5.77	44.8	18.96	24.19
205.7	138.0	52.92	0.5	0.9	0.9	2.01	43.15	22.49	22.63
188.4	132.0	53.19	0.6	0.9	0.9	4.1	44.38	19.54	23.58
186.3	90.12	54.86	0.5	0.8	0.8	6.2	44.45	19.47	24.47
195.3	123.6	55	0.6	0.8	0.8	5.59	43.34	21.38	23.19
195.0	128.8	54.26	0.5	0.9	0.9	4.4	43.4	20.92	23.22
181.2	122.4	56.64	0.4	0.9	0.9	5.72	45.15	18.88	24.02
205.7	138.0	52.92	0.5	09	0.9	2.01	43.15	22.49	22.63

Table 2-7: Multi-objective genetic algorithm parameters over the UDDS driving cycle (source [87])

2.4.1.5 Particle swarm optimisation

Particle swarm optimisation (PSO) is a computational method developed by Dr. Eberhart and Dr. Kenedy in 1995 [90, 91]. This technique is inspired by the social behaviour of bird-flocking, which optimises a problem by iteratively trying to improve a candidate solution with regard to a given measure of quality. In PSO, particles move around a search space and are guided by best known positions in the search space, as well as the best known position of the entire swarm. Movement of the swarm particles occurs when improved positions are discovered.

PSO is a meta-heuristic approach, and can search very large spaces of candidate solutions. Though non-causal in nature, PSO does not require the optimisation problem to be differentiable and as such is very suitable for optimisation problems with some degree of noise or irregularity. Particle swarm optimisation has successfully been applied in HEVs.

In a study by Huang *et al.* [92], an improved particle swarm optimisation approach was used to optimise a multilevel hierarchical control strategy for a parallel HEV (Figure 2-15). Results from this study show that compared to a baseline control strategy (PSAT built-in control strategy), the optimal multilevel hierarchical control strategy is able to articulate the engine, electric motor and battery towards operating efficiently in an optimal state. In this way, fuel consumption and emissions are simultaneously minimised (Table 2-8). In Junhong [93], PSO was also successfully applied to solve an HEV energy management problem involving the simultaneous minimisation of fuel consumption and emissions.

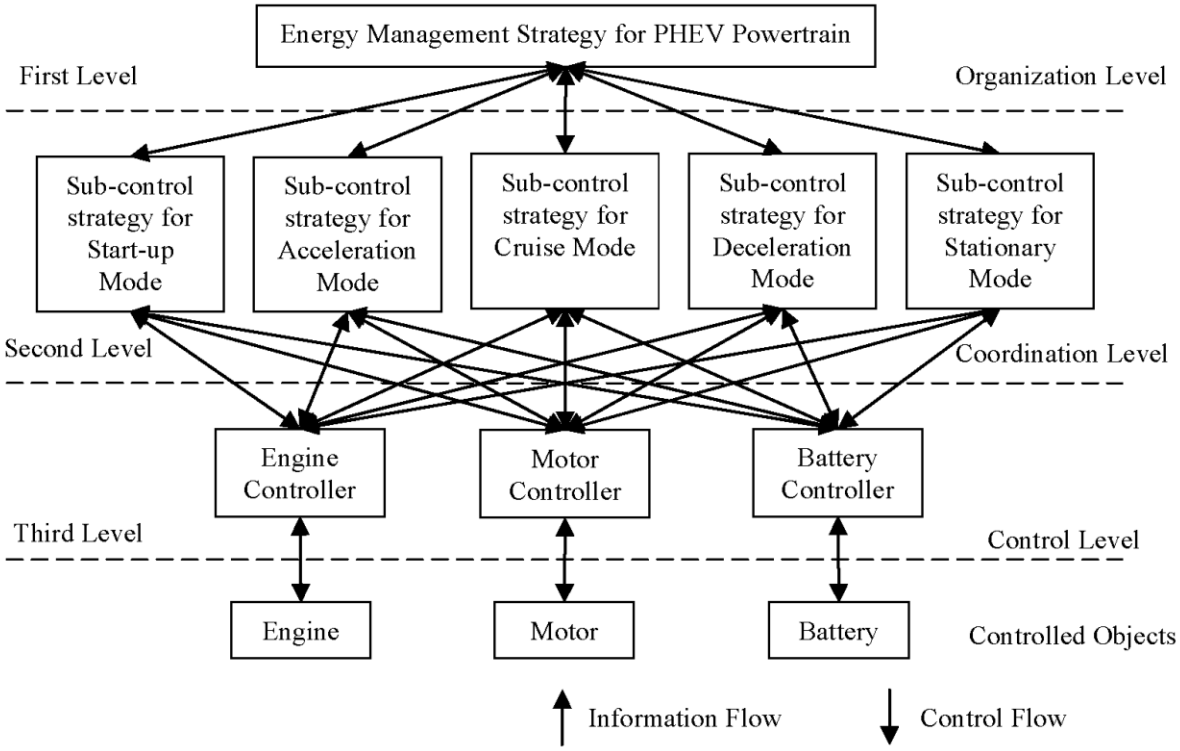

Figure 2-15: Structure of multilevel hierarchical control system of PHEV powertrain (source [92])

Control strategy	**Fuel Consumption (L/100km)**	**Final SOC (initial SOC-0.7)**
Optimal multilevel hierarchical control strategy	6.0921	0.6929
PSAT built-in control strategy	7.1597	0.7557

Table 2-8: Comparison of a baseline control strategy (PSAT built-in control strategy), with an optimal multilevel hierarchical control strategy (source [92, 94])

Wang *et al.* [95] proposed a control strategy to optimise fuel consumption and emissions in HEVs using PSO. Through simulation, the proposed PSO strategy is

shown to significantly improve fuel economy in high-speed driving cycles (US06), and emissions in middle or low-speed driving cycles (NEDC and Manhattan cycle) as detailed in Table 2-9.

Control Strategy	Fuel Economy (mpg)	HC Emission (g/mi)	CO Emission (g/mi)	NOx Emission (g/mi)
Before Opt	28.8	0.722	3.422	1.003
Direct	35.4902	0.7026	3.5538	0.9757
PSO	44.9723	0.6680	3.4383	0.8892

a. US06 driving cycle

Control Strategy	Fuel Economy (mpg)	HC Emission (g/mi)	CO Emission (g/mi)	NOx Emission (g/mi)
Before Opt	39.9	0.756	3.726	0.959
Direct	30.4926	0.6937	1.7738	0.5324
PSO	38.1694	0.6834	2.3926	0.6984

b. NEDC driving cycle

Control Strategy	Fuel Economy (mpg)	HC Emission (g/mi)	CO Emission (g/mi)	NOx Emission (g/mi)
Before Opt	32.7	2.256	11.497	2.613
Direct	34.8820	0.7056	3.5636	0.9829
PSO	32.5624	0.7304	1.9575	0.7098

c. MANHATTAN driving cycle

Table 2-9: PSO simulation results over different driving cycles (source [95])

Wu *et al.* [96] applied PSO to optimise the membership function and rules of a fuzzy logic HEV controller. The resulting strategy was simulated over different driving conditions, and found to yield near-optimal control signals in charge-sustaining operations. In Al-Aawar *et al.* [97] and Wu *et al.* [98], PSO is used for

sizing electromechanical components for higher efficiency and reduced fuel consumption. In Al-Aawar *et al.* [97, 99], the design optimisation environment consists mainly of a PSO module and an electromagnetic-team fuzzy logic (EM-TFL) module. As shown in Figure 2-16, the PSO optimiser searches the database of the EM-TFL algorithm to obtain the best population. The best population sets are then matched to the objective functions. If the degree of match is higher than the present tolerance, the PSO is considered as a successful candidate. The successful candidates of all components are subsequently gathered and a PSO algorithm is used to compute the global optimal sizing for all component combinations. In Wu *et al.* [98], the component sizing optimisation problem is solved using a multi-objective self-adaptive differential evolution algorithm (MOSADE). The proposed MOSADE (Figure 2-17) approach adopts an external elitist archive to retain non-dominated solutions that are found during the evolutionary process. To preserve the diversity of Pareto optimal solutions, the MOSADE approach consists of a progressive comparison truncation operator, based on the normalised nearest neighbour distance. Simulation results from both studies, demonstrate the capability of PSO to generate well-distributed Pareto optimal solutions to HEV multi-objective optimisation design problems.

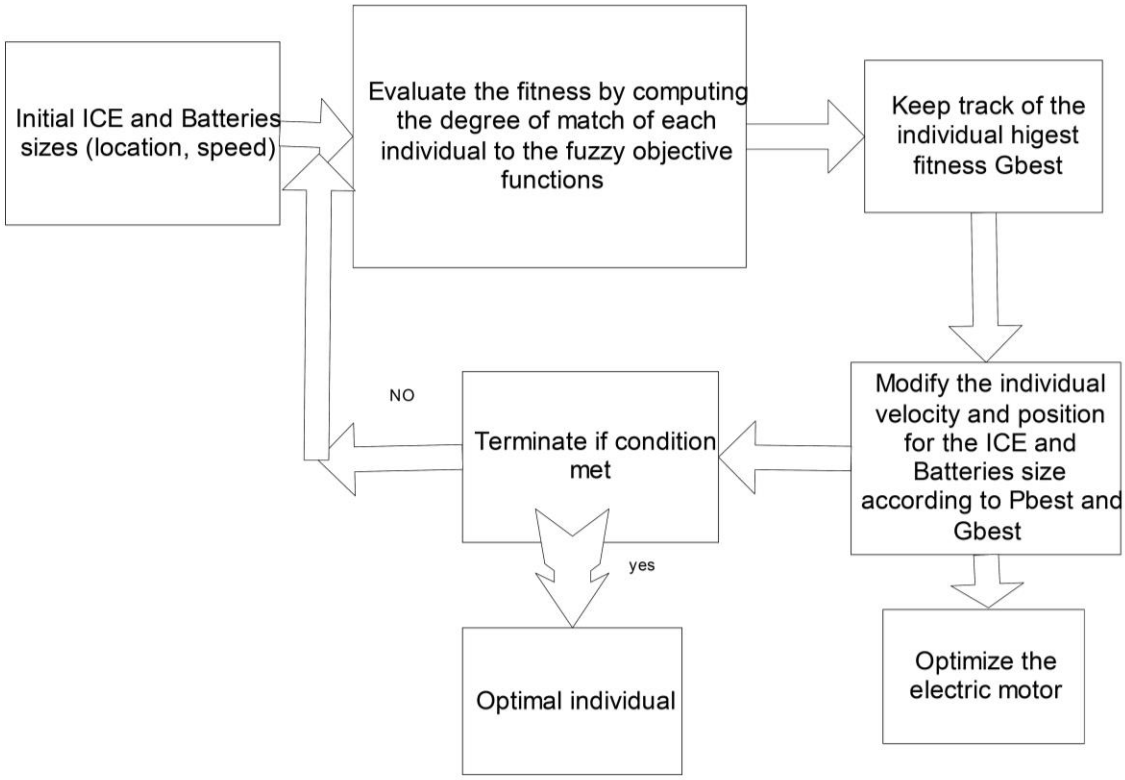

Figure 2-16: Electromagnetic-team fuzz logic PSO optimisation process for an HEV (source [97])

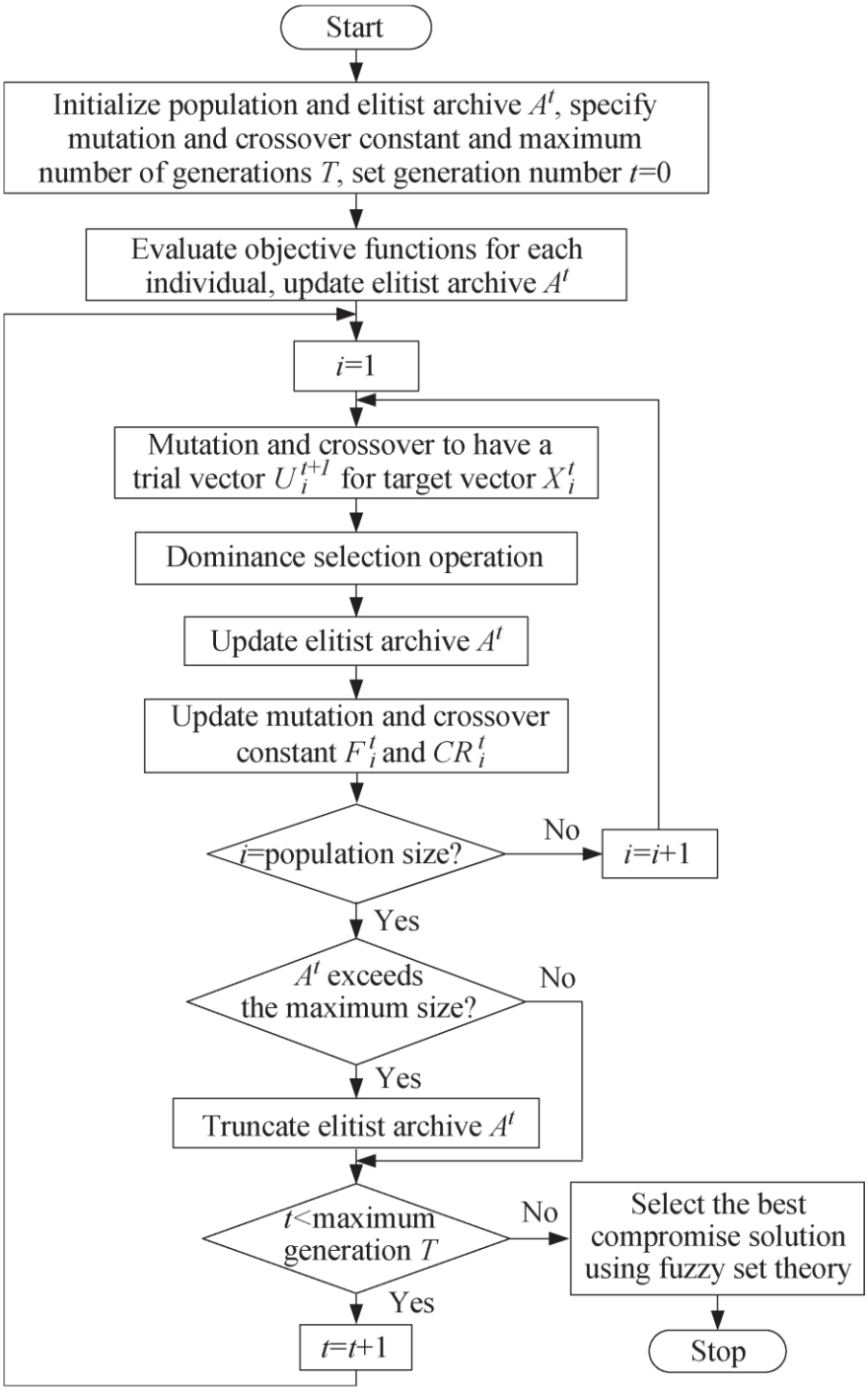

Figure 2-17: Flow chart describing the MOSADE approach (source [98])

Desai *et al.* [100], applied PSO to optimise both the powertrain and control strategy for reduced fuel consumption, improved efficiency and reduced emissions. As detailed in Figure 2-18, simulation results show an improvement in the fuel economy, emissions, and overall drivetrain efficiency. In Varesi *et al.* [101], PSO is used as shown in Figure 2-19 to find the optimal degree of hybridisation in a series-parallel HEV, to optimise vehicle performance, as well as reduce fuel consumption and emissions. By analysing real-time simulation results, the authors conclude that the PSO algorithm is a fast and efficient optimisation technique for component sizing.

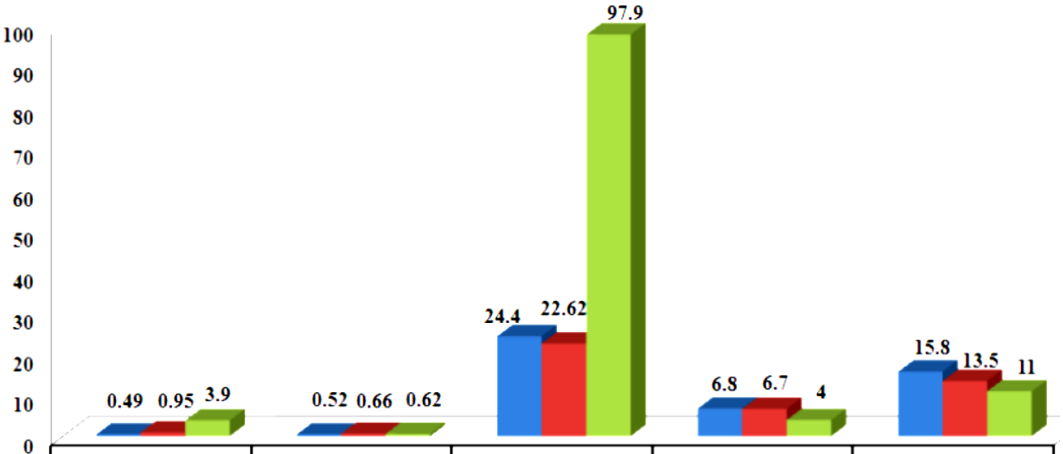

	HC (g/mile)	CO (g/mile)	Nox (g/mile)	Fuel Economy (mpg)	Drivetrain Efficiency (%)
UDDS	0.49	0.52	24.4	6.8	15.8
Montreal PI-IX 139	0.95	0.66	22.62	6.7	13.5
Conventional	3.9	0.62	97.9	4	11

Figure 2-18: Comparative plot of fuel economy, emissions and drivetrain efficiency for a particle swarm optimisation process (source [100])

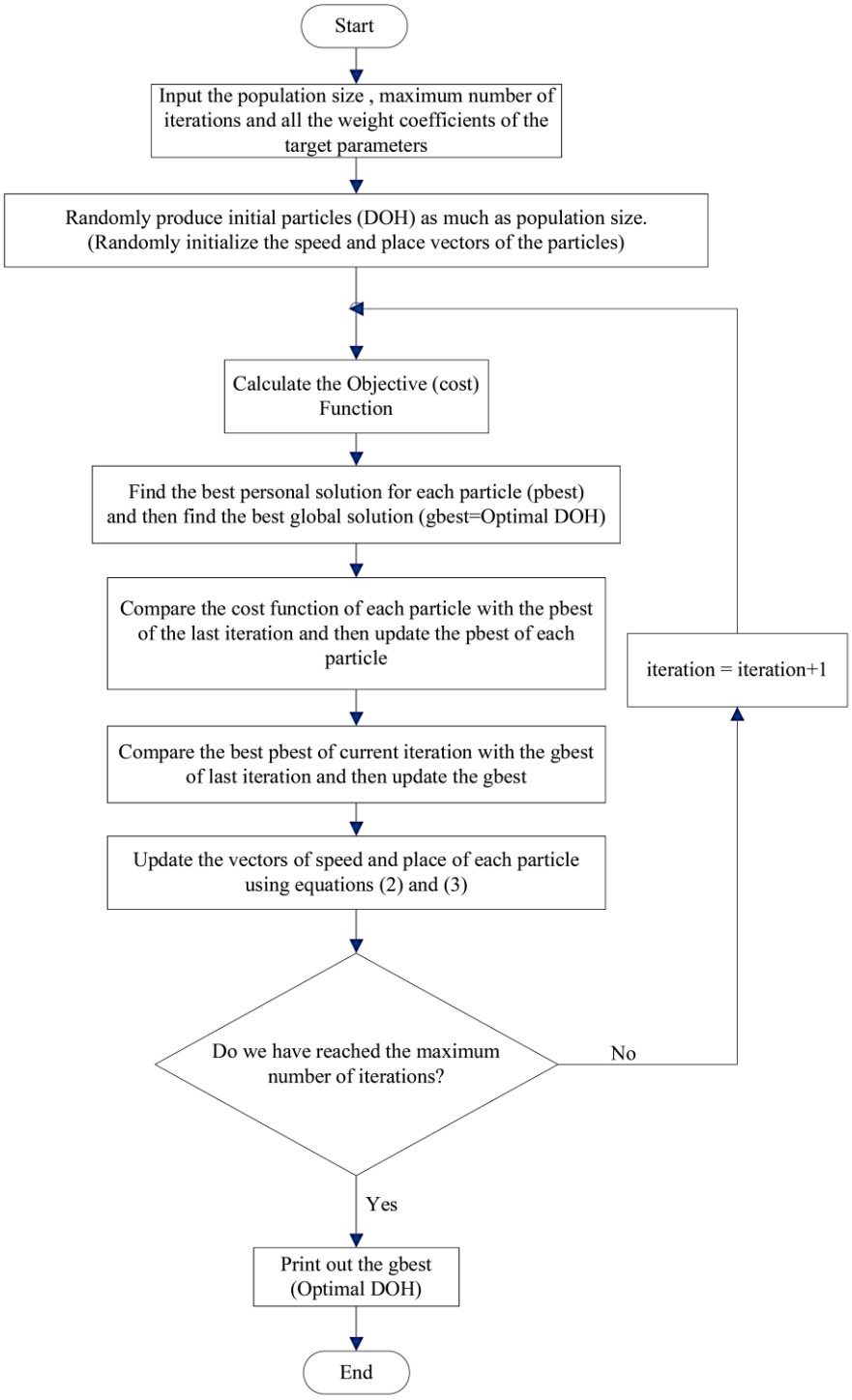

Figure 2-19: Optimal degree of hybridisation solution process using particle swarm optimisation algorithm (source [101])

2.4.2 HEV online control strategies

In contrast to HEV offline control strategies, HEV online control strategies are causal and can be implemented in real time. HEV online control strategies can either be formulated in the form of heuristic control rules (rule-based control strategies), or as an instantaneous optimisation of a defined objective function (online optimisation based strategies).

2.4.2.1 Rule-based control strategy

Rule-based control strategy is the most common way of implementing a real-time supervisory control in an HEV. The control rules are often based on heuristics, engineering intelligence, or mathematical models and are aimed at enabling the ICE to operate at high efficiency points, as well as enabling energy recuperation via regenerative braking [102-105].

The development of rule-based HEV control methods is generally articulated in two steps: the definition of the relevant rules for the powertrain control, and the calibration of the strategy, which is typically carried out by means of simulations on a vehicle model. Rule-based control methods are generally unable to guarantee the optimality of the solution found, or satisfy the desired final integral constraint (charge sustainability). To remedy this, the control rules must make sure that the integral constraint (SOC) remains between its prescribed lower and upper bounds. With rule-based control strategies, there is no standard approach to the control rules formation, and no way to determine a priori that the given set of rules is appropriate for the given application. However, there is a possibility that the control rules can be made detailed and complex enough to take care of any special event that may affect the vehicle [28, 106-111].

The main advantage of rule-based HEV control methods lie in their simplicity, which makes them fairly easy to understand and implement on actual vehicles [28, 106-111]. Owing to their low computational demand, natural adaptability to online-applications, good reliability and satisfactory fuel consumption results, rule-based control strategies have monopolised the production vehicle market. Despite widespread utilisation, rule-based HEV control methods, still present some significant challenges. Typically, in a rule-based HEV control strategy, a huge amount of time and investment in qualified work force is required to develop the strategy, owing to the long rules definition and calibration process. This situation is further worsened by the fact that the rules need to be redefined for every new driving condition and powertrain, thus posing some questions about the robustness of rule-based HEV control strategies [112]. In addition to this, recent research studies show that in comparison to optimisation methods, rule-based HEV control methods produce inferior but satisfactory fuel consumption results [113]. Rule-based controllers could further be subcategorised into deterministic rule-based control strategy [114] and fuzzy rule-based control strategy [105].

2.4.2.1.1 Deterministic rule-based control strategy

In the deterministic rule-based control strategy, rules are decided with the aid of a fuel economy or emissions map of the engine in question. Implementation of the rules, are often performed via pre-computed look up tables. Deterministic rule-based control strategy features notably in the study of Kim *et al.* [115], where the concept of hybrid optimal line was proposed for a parallel HEV, with continuous varying transmission (CVT). Using this concept, optimal values of CVT gear ratio,

motor torque and engine throttle were determined successfully and applied in real time.

One of the most successfully applied deterministic rule-based HEV control strategies is the electric assist control strategy. In this strategy, the ICE works as the sole source of power supply and the electric motor is only used to supply additional power when demanded by the vehicle. Thermostat control strategy is another variation of deterministic rule-based control. In this approach, the electric motor and ICE are used to generate the electrical energy which powers the vehicle. The battery state of charge is always maintained between predefined high and low levels, by simply turning on/off the internal combustion engine. Jalil *et al.* [104] used the thermostatic control strategy to turn the engine on/off based on the battery state of charge profile. Obtained results were found to be highly sub-optimal, compared to that of a deterministic rule-based control strategy.

In many of the widely employed rule-based control strategies, the following rules apply [116-118]:-

1. Below a certain vehicle power demand, the vehicle works purely as an electric vehicle (EV) and only the electric motor is used to supply the total power demand. This rule is generally set to avoid the engine operating in low engine efficiency points. The applicability of this rule, however, depends on the size of the electric motor and batteries employed on the HEV.
2. The electric motor is used for power-assist, when the vehicle power request exceeds the maximum engine power.
3. The electric motor charges the battery during regenerative braking.

4. The ICE is used to produce an extra torque to sustain the battery SOC, when it goes below the set minimum value.

2.4.2.1.2 Fuzzy rule-based control strategy

Fuzzy rule controllers in general originate from rule-based controllers. However, in a fuzzy rule controller, the linguistic representation of the control inputs is converted into numerical representation with membership function, in the fuzzification and defuzzification process. The underlying logic in the fuzzy rule-based control strategy is a form of multivalued logic derived from fuzzy set theory, to deal with reasoning that is approximate rather than precise. The relative simplicity associated with fuzzy rule controllers allows for tuning and adaptation where necessary, thus enhancing the degree of freedom of control. Its non-linear structure makes it even more useful in complex systems such as advanced powertrain. Fuzzy rule controllers typically accept as inputs, the battery state of charge, desired ICE torque and intended mode and outputs the ICE operating point. In Schouten *et al.* [106], Zeng *et al.* [119] and Khoucha *et al.* [120], driver command, battery SOC and motor/generator speeds were considered as fuzzy sets for the design of a fuzzy rule-based control strategy. In Liu *et al.* [121], the fuzzy control framework was extended to include a power notification system, which enables the engine to operate in its high efficiency region.

Typically, the electric motor makes up for the difference between the power demand and the ICE power. Currently, there are several variations to the fuzzy rule-based control in the form of: traditional fuzzy control strategy, adaptive fuzzy control strategy and predictive fuzzy control strategy.

2.4.2.1.2.1 Traditional fuzzy control strategy

Traditional fuzzy control is typically implemented to optimise fuzzy efficiency, thus enabling the ICE to operate more efficiently. This is achieved by means of load balancing, where the electric motor is used to force the engine towards operating in its most efficient region (low engine speed, high engine torque region), while sustaining the battery state of charge. Schouten *et al.* [106] proposed a fuzzy logic controller to optimise fuel consumption in a parallel HEV. The proposed method is based on the efficiency optimisation of the essential parts of the vehicle including the internal combustion engine, electric motor and battery. An efficiency map for a generic compression ignition direct injection (CIDI) engine is used. Taking into account the battery state of charge, the fuzzy controller is used to track the individual components so that they operate close to the optimal curve, as shown in Figure 2-20. The entire solution process can be articulated using the following steps: First, the power controller is used to convert the accelerator and brake pedal inputs to driver power command. The driver power command, battery SOC and electric motor speed are then used by a fuzzy logic controller, to compute the optimal generator power and scaling factor for the electric motor, as detailed in Table 2-10. The driver power command, optimal generator power, and scaling factor are then used to compute the optimal power for the ICE and electric motor.

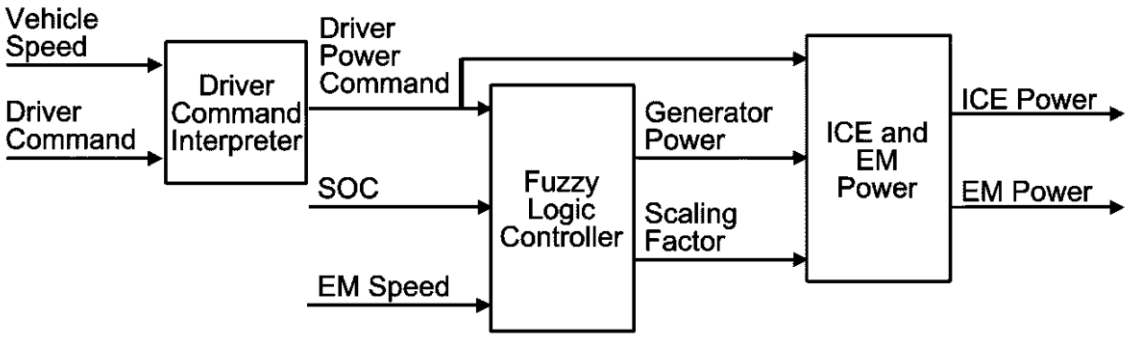

Figure 2-20: Simplified block diagram of the fuzzy logic controller (source [106])

1	**If** SOC is too high **then** P_{gen} is 0 kW
2	**If** SOC is normal **and** P_{driver} is normal **and** ω_{EM} is optimal **then** P_{gen} is 10 kW
3	**If** SOC is normal **and** ω_{EM} is **not** optimal **then** P_{gen} is 0 kW
4	**If** SOC is low **and** P_{driver} is normal **and** ω_{EM} is low **then** P_{gen} is 5 kW
5	**If** SOC is low **and** P_{driver} is normal **and** ω_{EM} is **not** low **then** P_{gen} is 15 kW
6	**If** SOC is too low **then** P_{gen} is $P_{gen,max}$
7	**If** SOC is too low **then** scale factor is 0
8	**If** SOC is **not** too low **and** P_{driver} is high **then** P_{gen} is 0 kW
9	**If** SOC is **not** too low **then** scale factor is 1

Table 2-10: Rule base of the fuzzy logic controller (source [106])

Simulation results show that compared to a default controller on the PSAT (PNGV systems analysis tool kit) simulation model, the fuzzy logic controller achieves on overall, a 6.8% improvement over an urban driving cycle, and a 9.6% improvement over a highway driving cycle as detailed in Table 2-11.

	Highway cycle		Urban cycle	
Normalised losses	**Default**	**FLC**	**Default**	**FLC**
Internal Combustion Engine (ICE)	62.7	59.4	66.5	64.5
Electric Motor EM	3.2	2.2	5.2	3.2
Battery	0.85	0.53	0.6	0.3
Drivetrain	12.3	7.3	12.3	9.4
Vehicle	19.3	19.3	10.8	10.9
Friction braking	0.35	0.35	2.5	2.8
Accessories	1.3	1.3	2.1	2.1
Total	**100**	**90.4**	**100**	**93.2**

Table 2-11: Comparison of normalised losses for a default PSAT controller and a fuzzy logic controller (source [106])

2.4.2.1.2.2 Adaptive fuzzy control strategy

Adaptive fuzzy control strategy is becoming increasingly popular in automotive applications on HEV, because it potentiates simultaneous optimisation of fuel efficiency and emissions. Fuel efficiency and emissions are often conflicting objectives and as such an optimal solution cannot be achieved to the satisfaction of each individual objective. However, a sub-optimal solution is achievable using the weighted-sum approach, where appropriate weights are tuned over different driving conditions, for fuel efficiency and emissions. The weights assigned are relative, and thus reflect the importance of the individual objectives to which they are assigned (fuel consumption, NOx, CO and HC emissions) [122]. Consequently, with adaptive fuzzy controllers it is possible to control individual objectives by changing the value of the weights assigned. An application of adaptive fuzzy logic controllers in solving conflicting objective control problems involving NOx, CO and HC emissions, have been reported in literature [85, 122].

2.4.2.1.2.3 Predictive fuzzy control strategy

Predictive fuzzy controller utilises prior information about a planned driving trip. This information is often acquired with the aid of a Global Positioning System (GPS), which provides knowledge about the type of obstacles that the vehicle is bound to encounter e.g. heavy traffic, steep grade etc. Typical inputs to the predictive controller are vehicle speed, speed state in the look-ahead window and the elevation of the sampled points along a predetermined route.

Based on the available history of vehicle motion, and the speculation of its possible motion in future, the predictive fuzzy controller calculates the optimal ICE torque contribution for each vehicle speed and outputs a normalised signal in the order of -1 to +1, which prescribes whether the battery should be charged or discharged respectively.

Owing to simplicity and robustness, fuzzy controllers have attracted a lot of attention from heuristic control experts within the research and automotive industry. Arsie *et al.* [123] for example, implemented a fuzzy controller to control the parameters related to driver-vehicle interaction, torque management, and battery recharge. The proposed driver model uses fuzzy control rules (Table 2-12), to formulate a realistic representation of the cognitive process of a human driver. Consequently, in a situation where the vehicle speed is greater than the reference speed and the vehicle is already decelerating, the fuzzy driver would not brake hard, but would either keep the throttle closed or brake gently. As shown in Figure 2-21, simulation results show an excellent agreement between the target and the instantaneous vehicle speed.

Acc.	A	O	ST	C	MC	MC	HC	HC
	LA	MO	O	ST	C	MC	MC	HC
	ST	HO	MO	O	ST	C	MC	HC
Dec.	LD	HO	MO	MO	O	ST	C	MC
	D	HO	HO	MO	MO	O	ST	C
		HS	MS	S	ST	F	MF	HF
		Slow				Fast		

Membership functions legend			
HS	High Slow	A	Acceleration
MS	Medium Slow	LA	Low Acc.
S	Slow	C	Close
F	Fast	HC	High Close
MF	Medium Fast	MC	Medium Close
HF	High Fast	O	Open
LD	Low Deceleration	MO	Medium Open
D	Deceleration	HO	High Open
ST	Steady		

Table 2-12: Rule-base for driver model fuzzy controller (source [123])

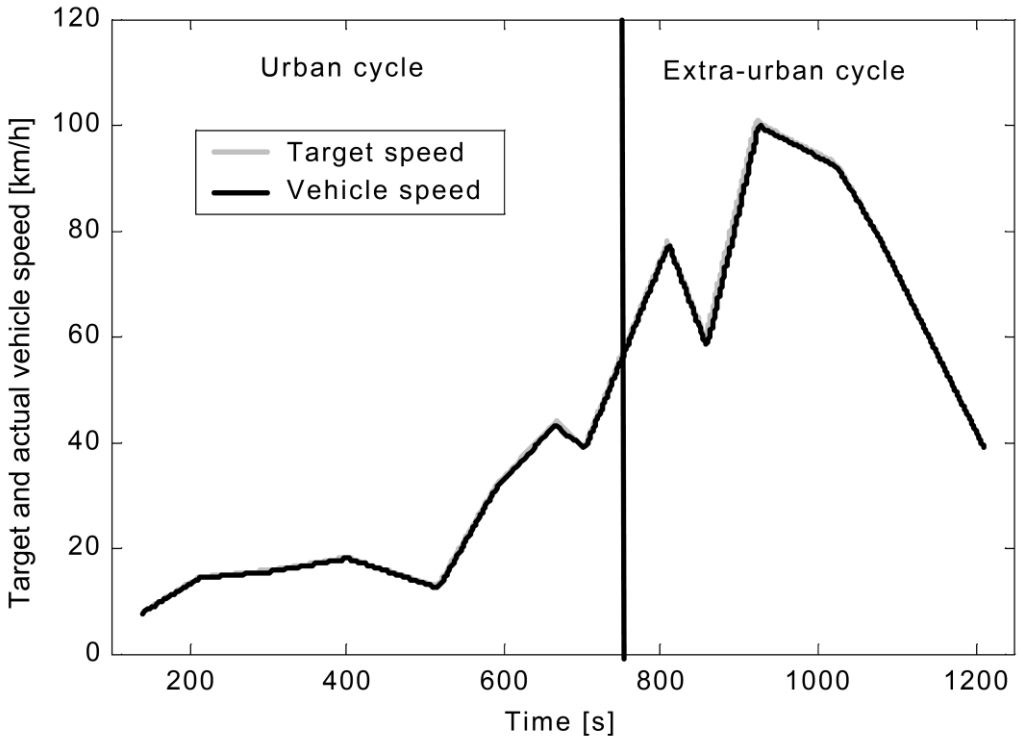

Figure 2-21: Target and actual vehicle speed for a fuzzy driver model (source [123])

Lee *et al.* [124] proposed a fuzzy controller that is robust and unaffected by vehicle load variation and road pattern. The proposed fuzzy logic controller is mainly composed of two parts: the driver's intention predictor (DIP) and the power balance controller (PBC), as shown in Figure 2-22. The difference between the two fuzzy logics is that the DIP generates the torque reference responding to the rapid acceleration or deceleration of the vehicle regardless of the battery's state, while the PBC generates the torque reference responsible for keeping the battery charge balanced.

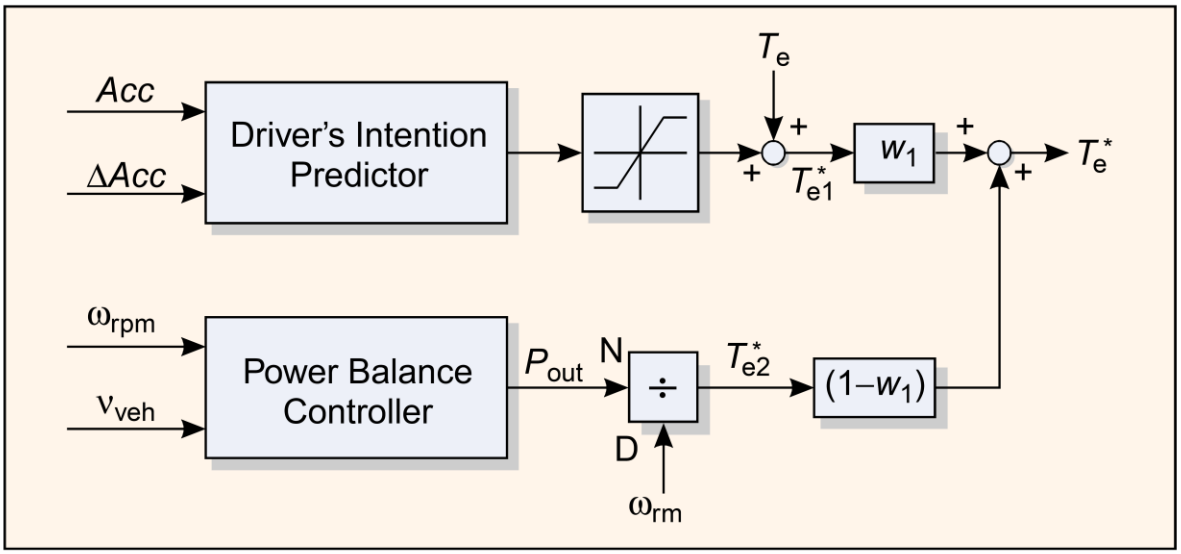

Figure 2-22: Block diagram of the DIP and PBC fuzzy controller (source [124])

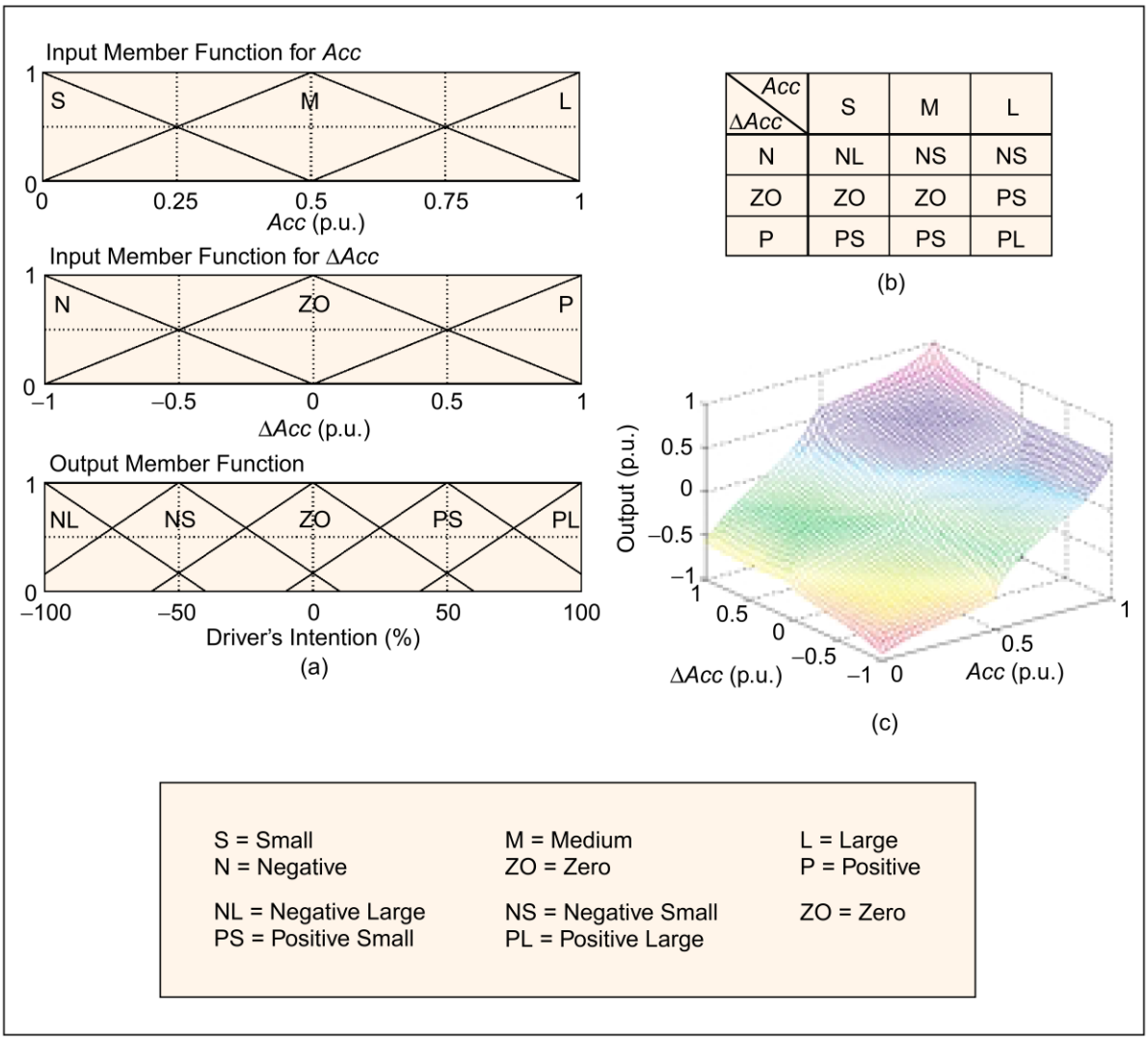

Figure 2-23: Fuzzy logic based driver's intention predictor (DIP). (a) Input and output membership functions (b) Rule-base (c) Output (source [124])

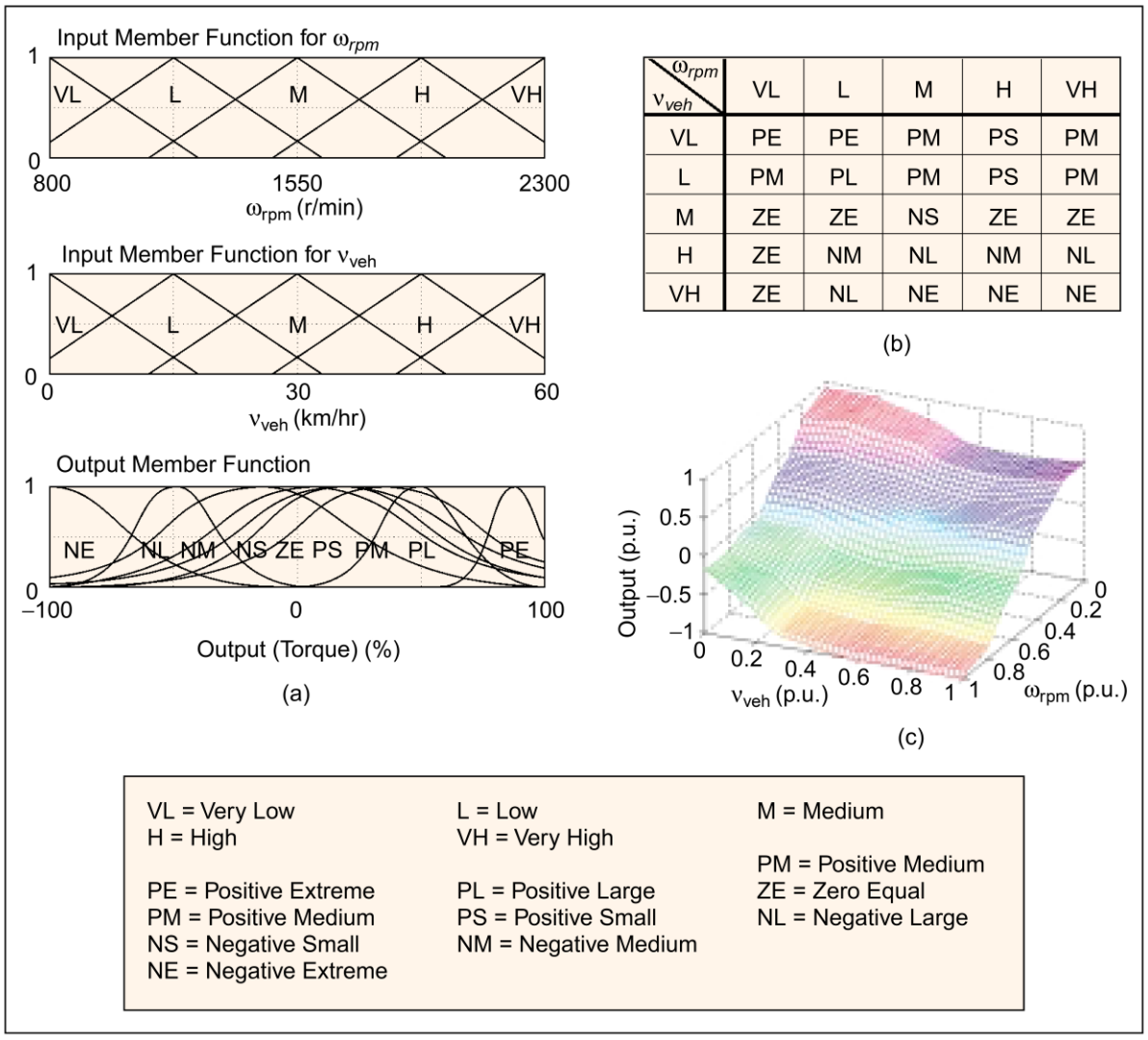

ω_{rpm} / v_{veh}	VL	L	M	H	VH
VL	PE	PE	PM	PS	PM
L	PM	PL	PM	PS	PM
M	ZE	ZE	NS	ZE	ZE
H	ZE	NM	NL	NM	NL
VH	ZE	NL	NE	NE	NE

Figure 2-24: Fuzzy logic based power balance controller (a) Input and output membership functions. (b) Rule base (c) Output (source [124])

Simulation results show that over a 20 days testing period, the proposed controller is able to preserve the battery voltage between its nominal voltage (120% fully charged voltage) without any extra charge (Figure 2-25).

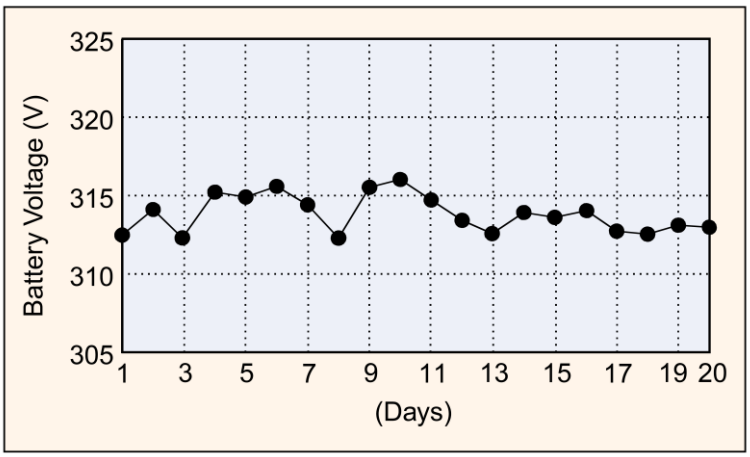

Figure 2-25: Battery voltage variations for the DIP and PBC fuzzy controller (source [124])

Baumann *et al.* [107], demonstrated the effectiveness of fuzzy controllers to increase fuel economy and showed that it works well for non-linear, multi-domain and time varying systems. The proposed control scheme forces the majority of operating points to be in the vicinity of the highest point of efficiency. The resulting effect is an increase in average efficiency from 23% to 35.4% over the federal urban driving schedule as shown in Figure 2-26.

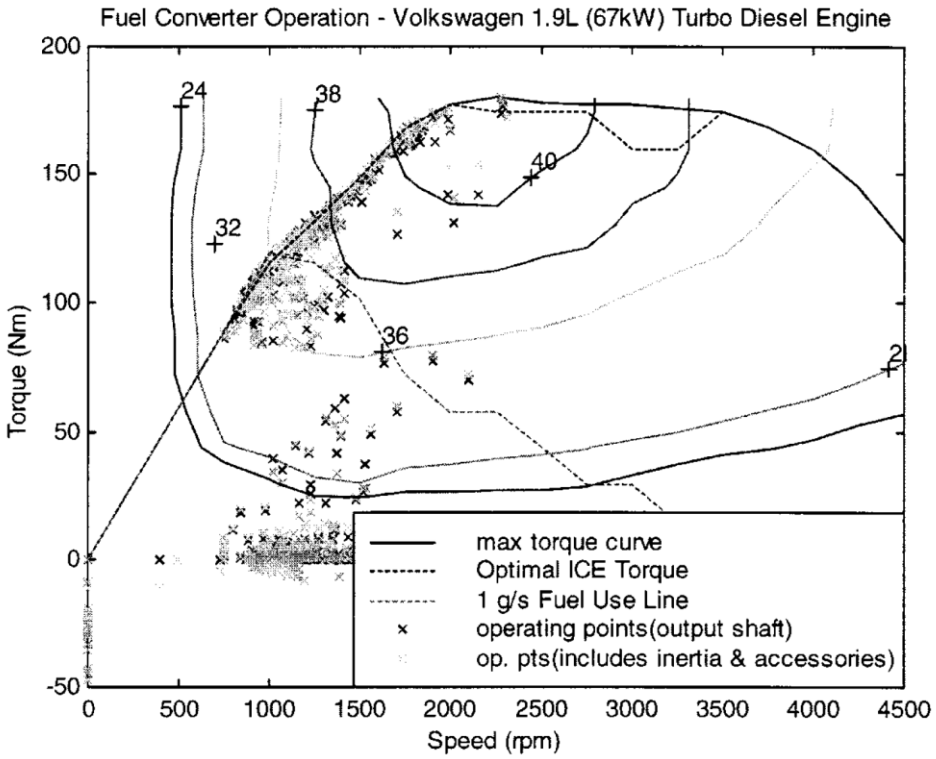

Figure 2-26: Efficiency map for HEV using efficiency strategy (source [107])

Tao *et al.* [125] designed a PID-like fuzzy controller with heuristic functional scaling which is easy to adjust even in the absence of a mathematical model for the vehicle. The proposed controller dubbed "FPIDF" (flexible complexity reduced PID-like fuzzy controller) (Figure 2-27) was simulated against a normal PID-like fuzzy controller and a PD controller. Simulation results show that compared to the other controllers, the FPIDF controller performs the best with the shortest rise and settling time. Proportional-integral (PI) controllers have also been shown to be effective in the control of non-linear plants [16, 126-128]. In Syed *et al.* [126] for example, a PI controller is designed and optimally scheduled using a fuzzy-gain scheduling system, to control engine power and speed in an HEV.

In Jianlong *et al.* [129], an attempt is made to formulate a computationally efficient fuzzy control strategy, using a network structure of 2 inputs and 1 output. In Zhou *et al.* [130], particle swarm optimisation is used to improve the accuracy, adaptability and robustness of a fuzzy control strategy.

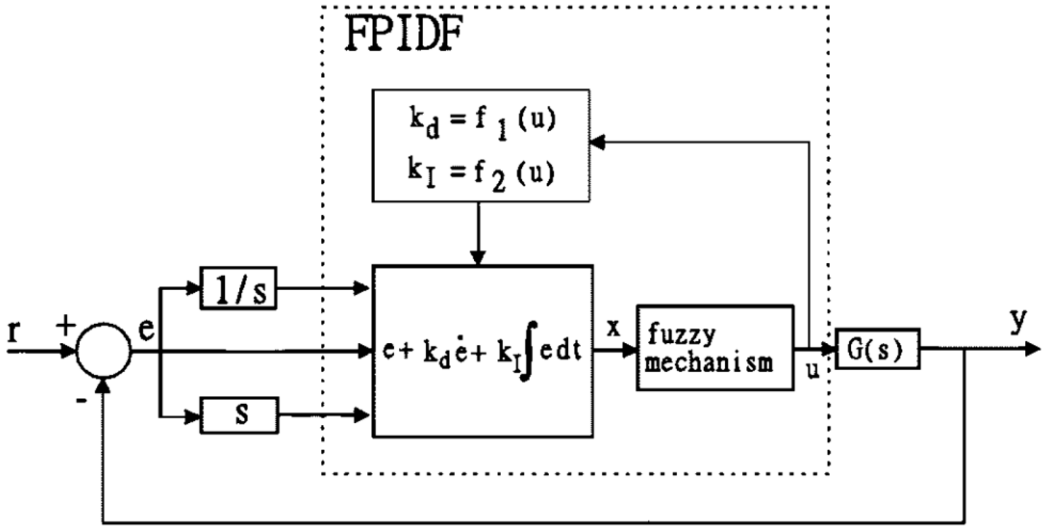

Figure 2-27: Block diagram of the fuzzy control system with FPIDF (source [125])

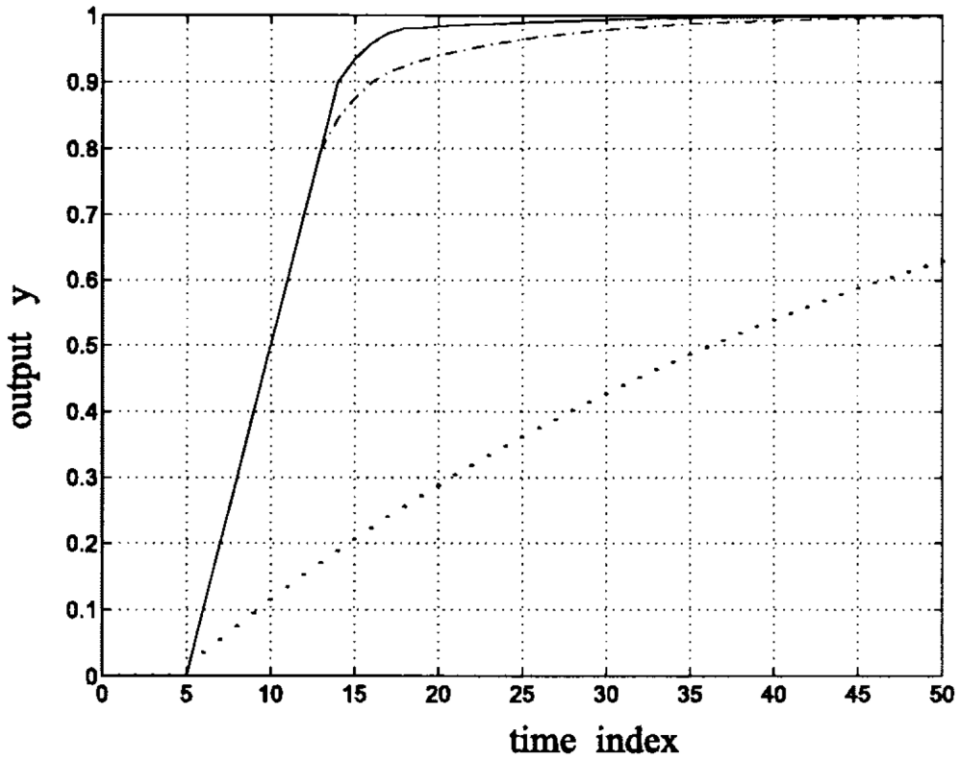

Figure 2-28: Performances of fuzzy controllers FPIDF (solid line), PIDF (dash-dot line), and PD (dotted line) for delayed plant (source [125])

In Hajimiri *et al.* [131], a predictive fuzzy logic controller which uses inputs such as present elevation, future elevation, present speed and predictive speed is proposed to manage the power flow in a series HEV. Based on the future state of the vehicle, related to traffic and elevation positions, the rules are defined accordingly as detailed in Table 2-13.

Future state	Increasing elevation	Constant elevation	Decreasing elevation
Increasing traffic flow	Nothing	Normal discharging	High discharging
Constant traffic flow	Normal discharging	Nothing	Normal discharging
Decreasing traffic flow	High charging	Normal discharging	Nothing

Table 2-13: Fuzzy rule base of a predictive control strategy (source [131])

The foregoing rules imply that, when the GPS indicates “decreasing elevation” and “increasing traffic flow” for the future state, the output command is “high discharging”. In this case, more battery energy is consumed in slower traffic and higher elevation; while the future state of the vehicle, i.e. decreasing elevation and increasing traffic flow, will compensate for the high rate of discharging at present. The comparison results of the predictive fuzzy controller and a power follower algorithm are detailed in Table 2-14.

	Predictive algorithm	Power follower algorithm
Fuel consumption [Lit/mile]	0.189	0.202
CO [g/mile]	4.293	5.08
HC [g/mile]	0.656	0.676
NOx [g/mile]	0.878	0.894

Table 2-14: Fuel consumption and emissions of a fuzzy predictive controller and a power follower controller (source [131])

These results show that the predictive fuzzy controller outperforms the power follower algorithm on the basis of fuel consumption reduction and emissions reduction.

In Langari *et al.* [132], the concept of fuzzy intelligent energy management agent (IEMA) is proposed and implemented for vehicle torque distribution and charge sustenance, on the basis of current vehicle state, vehicle power demand and available online driving cycle data. Simulation results show that the IEMA is able to manage the torque distribution of a parallel HEV in a charge-sustaining manner.

In Golkar *et al.* [133], an online adaptive intelligent fuzzy controller (Figure 2-29) is proposed, and used to optimally control the ICE torque such that conflicting objectives involving fuel consumption and emissions are simultaneously minimised.

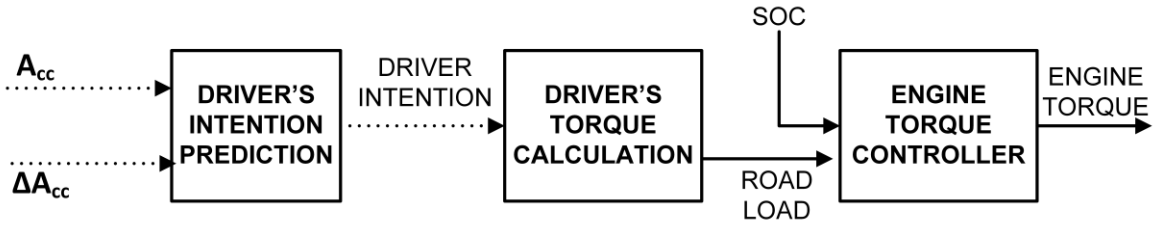

Figure 2-29: Layout of fuzzy controller with driver intention predictor and driver torque computation (source [133])

Using different variations of the predictive fuzzy control strategy, similar results were observed in Lu *et al.* [134] (Table 2-15) and Fu *et al.* [135].

Drive cycle	Control strategy	NOx Emissions g/km	HC Emissions g/km	CO Emissions g/km	Fuel Economy L/(100km)
NEDC	Electric assist control strategy	0.195	0.344	1.795	7.7
	Fuzzy logic control	0.108	0.295	1.361	5
	Improve (%)	44.62%	14.24%	24.18%	35.06%
UDDS	Electric assist control strategy	0.253	0.323	1.467	7.7
	Fuzzy logic control	0.132	0.269	1.282	4.4
	Improve (%)	47.83%	16.72%	12.61%	42.86%
China	Electric assist control strategy	0.244	0.398	1.869	8.6
	Fuzzy logic control	0.132	0.346	1.62	4.6
	Improve (%)	45.90%	13.07%	13.32%	46.51%

Table 2-15: Comparison between electric assist control and fuzzy logic control (source [134])

	Fuzzy logic energy management strategy	
	After optimisation	Before optimisation
HC (grams/miles)	0.34	0.421
CO (grams/miles)	1.713	2.071
NO_X (grams/miles)	0.159	0.169
Fuel economy (mpg)	63.6	62.4

Table 2-16: Simulation results from a fuzzy logic energy management strategy (source [135])

Poursamad *et al.* [85] proposed an adaptive genetic-fuzzy control strategy to determine how to distribute vehicle power demand between the internal combustion engine and the electric motor of a parallel HEV. First, a fuzzy logic controller is designed, and then the rules are determined and optimised using genetic algorithm. The resulting controller is used to optimise an objective function whose target values are minimised fuel consumption and exhaust emissions (HC, CO, and NOx). Simulation results show that over the TEH-CAR driving cycle, the genetic-fuzzy controller is able to simultaneously achieve reduced fuel consumption, improved vehicle performance and battery charge sustenance (Figure 2-30).

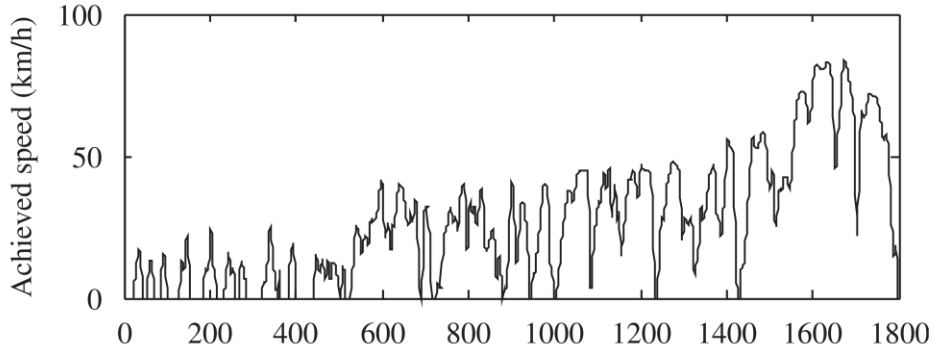

a. Driving cycle

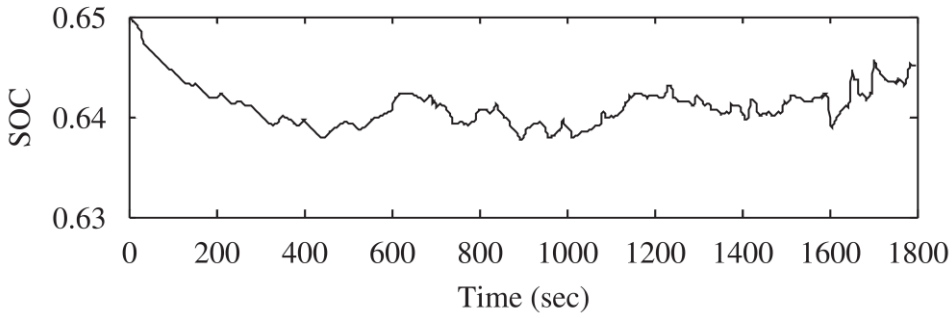

b. SOC history over TEH-CAR driving cycle

Figure 2-30: Simulation results for the genetic-fuzzy control strategy over the TEH-CAR driving cycle (source [85])

The fuzzy algorithm is also well suited for non-control applications. For example, in Brahama *et al.* [136], the fuzzy control theory is used to accurately design an HEV modelling tool, with multi-purpose applications.

2.4.2.2 Online optimisation based strategies

Online optimisation based strategies reduce global optimisation problems into a succession of local optimisation problems, thus reducing the associated computation effort. This eliminates the need for future driving information, thus making it implementable in real time. Despite yielding marginally sub-optimal results in comparison to global optimisation strategies, local optimisation strategies have received the greatest research attention in HEV control. ECMS (Equivalent Consumption Minimisation Strategy) [116, 137-140] and PMP (Pontryagin's minimum principle) [141, 142] are the most popular of these techniques among researchers. Other online optimisation based strategies being researched today include artificial neural network, particle swarm optimisation (PSO) and model predictive control (MPC).

2.4.2.2.1 Pontryagin's minimum principle

Pontryagin's minimum principle (PMP), formulated in 1956 by the Russian mathematician Lev Pontryagin and his students, is a special case of Euler-Lagrange equation of the calculus of variations. The principle stipulates that the optimal solution to the global optimisation problem must satisfy the condition of optimality. PMP is based on the instantaneous minimisation of a Hamiltonian function over a driving cycle [142, 143]. Under the assumption that the trajectory obtained from PMP is unique and satisfies the necessary constraints and boundary conditions, the optimal trajectory obtained by PMP can be considered a global optimal trajectory [142, 144-149]. In Geering [145] and Serrao *et al.* [146], the process of formulating a global optimisation problem into a local optimisation problem, and solving it using PMP is discussed.

Kim *et al.* [149, 150] applied PMP to find the optimal control law for a plug-in HEV. They showed that by setting a correct initial estimate of the co-state, the instantaneous minimisation of the Hamiltonian function over a driving cycle yields a control policy that closely matches results from dynamic programming, when the state boundary conditions are met (Table 2-17). They also showed that under the assumption that the battery resistance and voltage are independent of SOC, the co-state could be considered a constant, and the resulting controller would still compare very closely in performance to the PMP variation with a variable co-state (Table 2-17 and Figure 2-31).

Method	**DP**	**PMP**	
		Exact solution ($p(0) = -301.1$)	Constant co-state ($p(0) = -293.4$)
FE (km/l)	65.716	65.621	65.358

Table 2-17: Optimal fuel economies for PHEVs under different techniques (source [149])

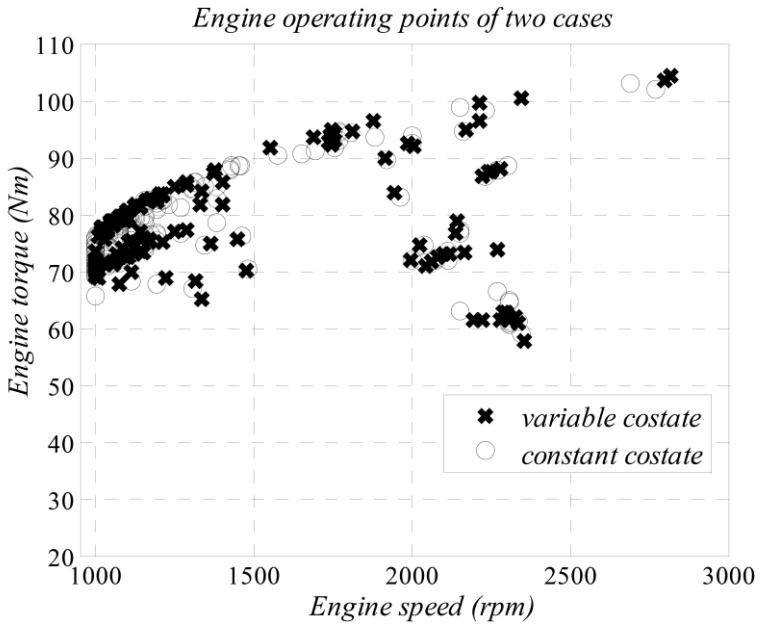

Figure 2-31: Engine operation points for a PMP controller with constant co-state and variable co-state (source [149])

Stockar *et al.* [151] proposed a PMP-inspired model-based control strategy to minimise CO_2 on a plug-in HEV (Figure 2-33). By examining the state of energy evolution for different co-state values, it was concluded that the performance of the PMP controller is very sensitive to the estimated co-state value. In the particular example considered (Figure 2-32), it was found that for a co-state value greater than 10, the model-based PMP control strategy forces the vehicle to deplete the battery, and when the lower SOE (state of energy) bound is reached, it switches to a charge-sustaining mode. Similarly, when the co-state value is equal to 6, the model-based PMP strategy allows the battery to be gradually depleted during the cycle, reaching the lower SOE boundary only at the end of the driving pattern, avoiding any charge-sustaining operations. This operation, which is known as blended mode, allows for the achievement of the minimum vehicle fuel consumption along a prescribed driving cycle. The findings from Stockar *et al.*

[151] suggest that PMP is a shooting method that solves a boundary value optimisation problem. Consequently, the resulting optimal control strategy is non-causal and cannot be implemented in real time.

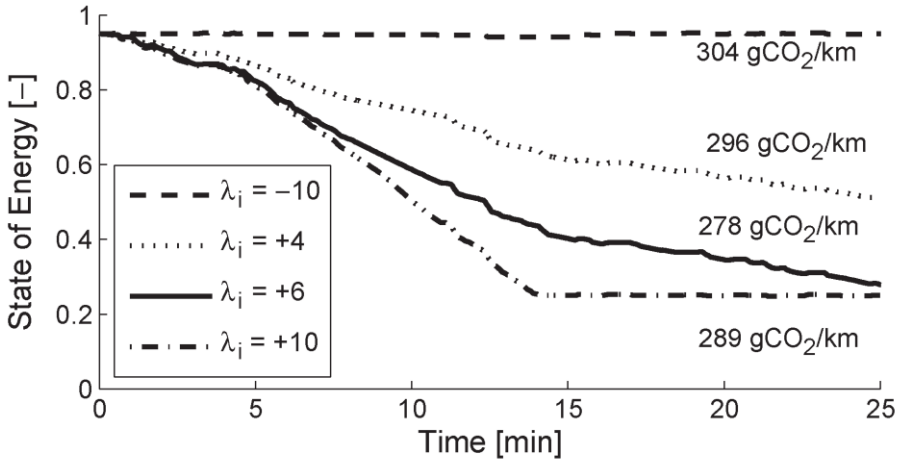

Figure 2-32: Battery SOE profile during the driving cycle for μ_i = 18 varying λ_i (cycle Path 3, U.S. scenario) (source [151])

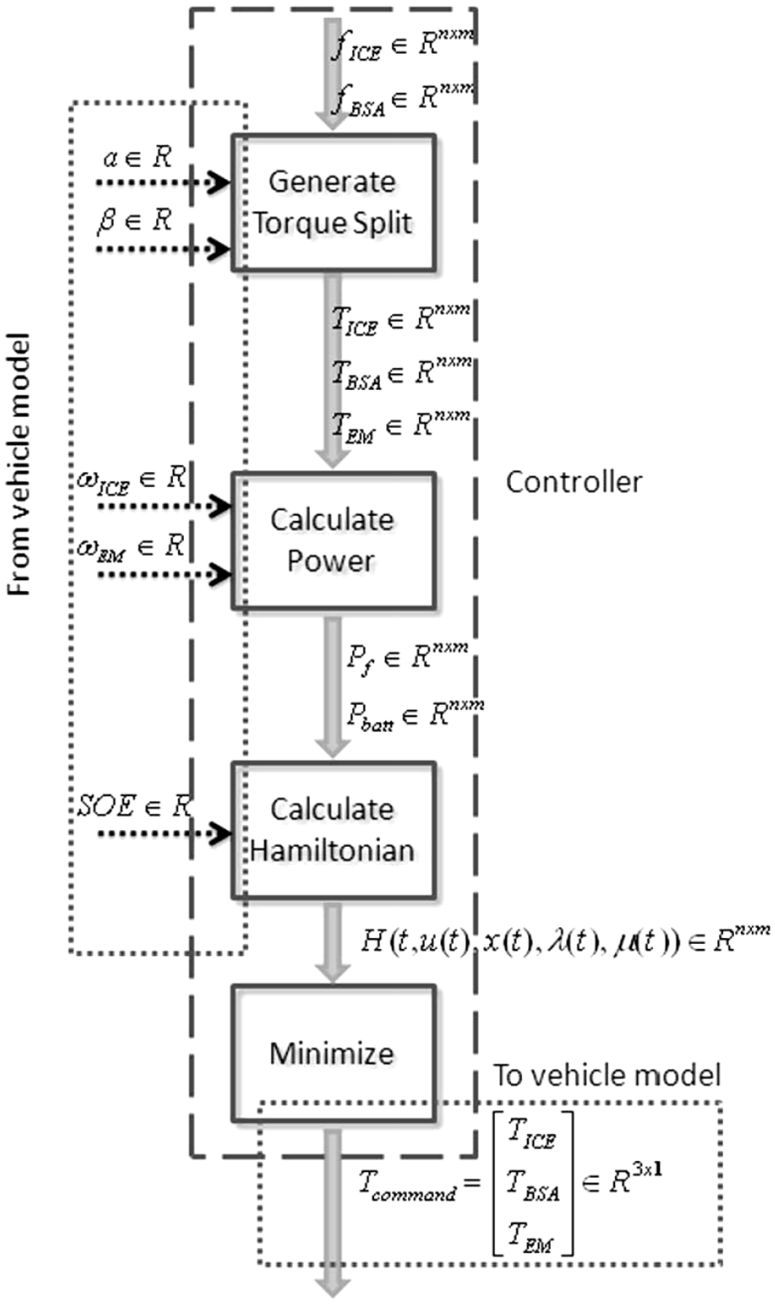

Figure 2-33: Flow chart describing the model-based PMP control strategy (source [151])

2.4.2.2.2 Equivalent consumption minimisation strategy

A more readily implementable local optimisation approach is the Equivalent Consumption Minimisation Strategy (ECMS) [137, 140, 143, 152-159]. ECMS was first developed based on the heuristic concept that the energy used to drive a vehicle over a driving cycle ultimately comes from the engine. As such, the hybrid system merely serves as an energy buffer [137]. This strategy is based on the instantaneous minimisation of a cost index, which is the sum of a number of operation metrics weighted by equivalence factors. The commonly used metrics in ECMS HEV control are engine fuel cost and battery fuel cost. It does not require prior knowledge of driving pattern and is thus implementable online. Variations to ECMS optimisation control strategy have been reported by a number of studies. Some of such variations include the Adaptive ECMS [152, 160] and Telemetry ECMS [161], which adjust the equivalence factor based on past driving data and future prediction. The downside to these adaptive techniques is the need for predictive equipment like GPS, which comes at an additional cost.

Paganelli *et al.* [153] implemented an ECMS strategy to minimise fuel consumption and pollutant emissions on a sport utility vehicle operating in charge-sustaining mode. To implement the global constraint of charge-sustaining operation, the optimum power split is biased using a non-linear penalty function of the battery state of charge deviation from its target value. Results from this study show that using the ECMS strategy, a charge-sustaining reduction in emissions can be achieved with no additional penalty to fuel economy.

Similar observations were made in Gao *et al.* [162] (Table 2-18) and Rousseau *et al.* [163] (Figure 2-34). Results from both studies show that even in the absence of

driving information, ECMS still yields near-optimal results for fuel consumption minimisation.

	Fuel consumption (l/100 km)		
	IM240	ECE_EUDC_LOW	MANHATTAN
Thermostat Control Strategy (TCS)	34.7	47.8	63.8
Power Follower Control Strategy (PFC)	36.5	45.7	56.5
Equivalent Fuel Consumption Optimal Control Strategy (EFCOCS)	32.9	42.3	54.7
Global optimisation (DP – Dynamic Programming controller)	30.2	38.5	49.3

Table 2-18: Comparison between the fuel economy performance of the TCS, PFC, EFC0CS and DP HEV control strategies (source [162])

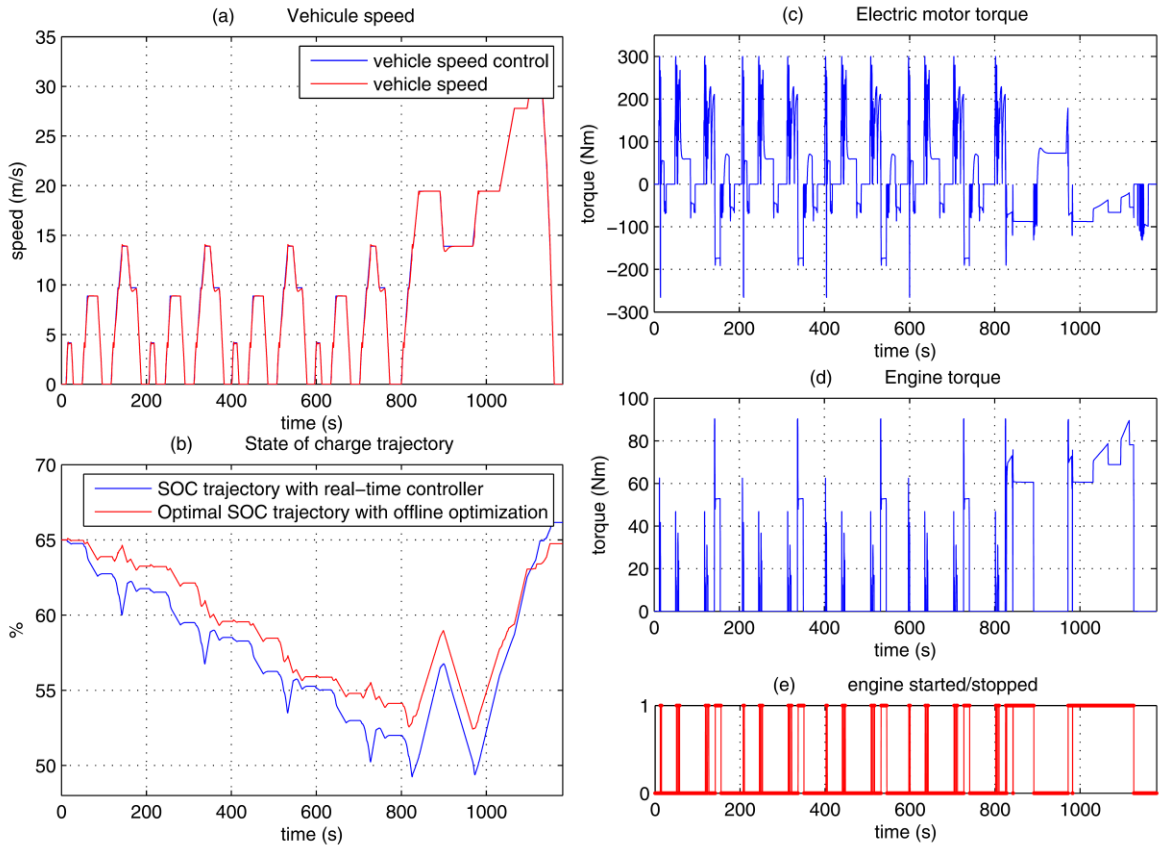

Figure 2-34: Results obtained with a sub-optimal ECMS strategy (source [163])

In Mursado *et al.* [152], an adaptive equivalent consumption minimisation strategy (A-ECMS), is proposed for the real-time energy management of an HEV (Figure 2-35). This strategy works by continuously updating the control parameter (equivalence factor) according to road load conditions, such that charge-sustaining, quasi-optimal control signals are obtained. By comparing the results obtained from the A-ECMS controller to those from an optimal controller (based on dynamic programming), the authors concluded that "a very slightly sub-optimal solution can be achieved with a technique much simpler than the one leading to the optimal policy" (Table 2-19). A similar inference was made in Sciarretta *et. al* [140] and Marano *et. al* [164]. Mursado *et al.* [152] also analysed the sensitivity of

equivalence factors on battery charge sustenance (Figure 2-36). Results from this analysis show that the control performance of a classical ECMS control strategy is very sensitive to the variation of equivalence factors. In fact, as shown in Figure 2-36, small perturbations of the equivalence factor leads to a non-charge-sustaining operation.

Driving Cycle	**Pure Thermal** mpg	**DP**		**ECMS opt**		**A-ECMS**	
		mpg	improve	mpg	improve	mpg	improve
FUDS	22.1	25.7	16.4%	25.7	16.3%	25.5	15.5%
FHDS	24.8	26.0	4.9%	25.8	4.1%	25.8	3.9%
ECE	20.8	24.5	18.2%	24.5	18.0%	24.5	17.9%
EUDC	23.3	24.8	6.3%	24.7	6.2%	24.7	6.1%
NEDC	22.2	24.5	10.7%	24.5	10.7%	24.4	10.1%
JP1015	21.0	25.1	20.1%	25.1	19.8%	24.8	18.2%

Table 2-19: Comparison of fuel economy for a baseline vehicle, dynamic programming controller, ECMS optimal controller and adaptive ECMS controller (source [152])

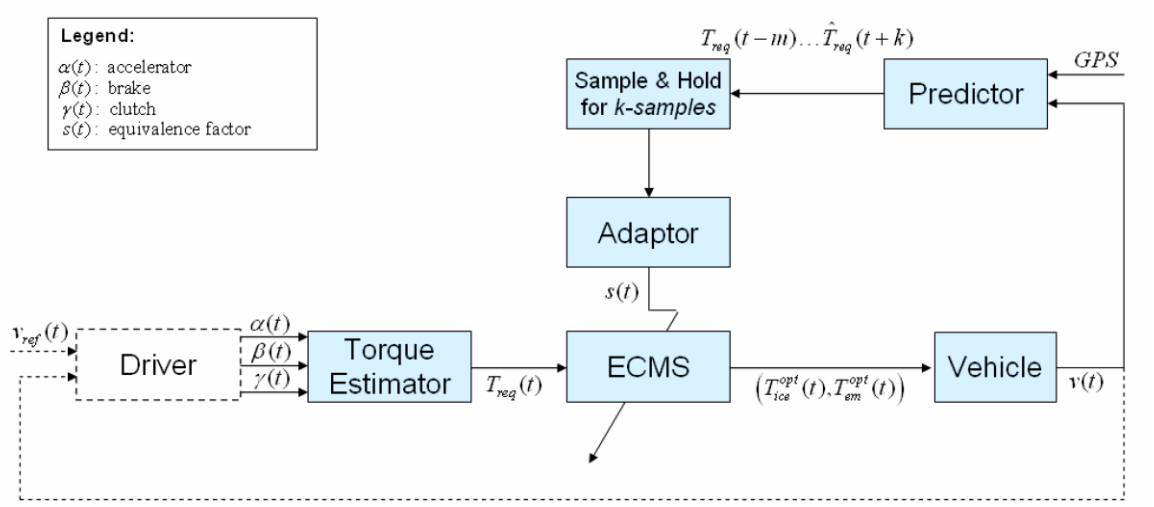

Figure 2-35: Control block diagram of A-ECMS (source [152])

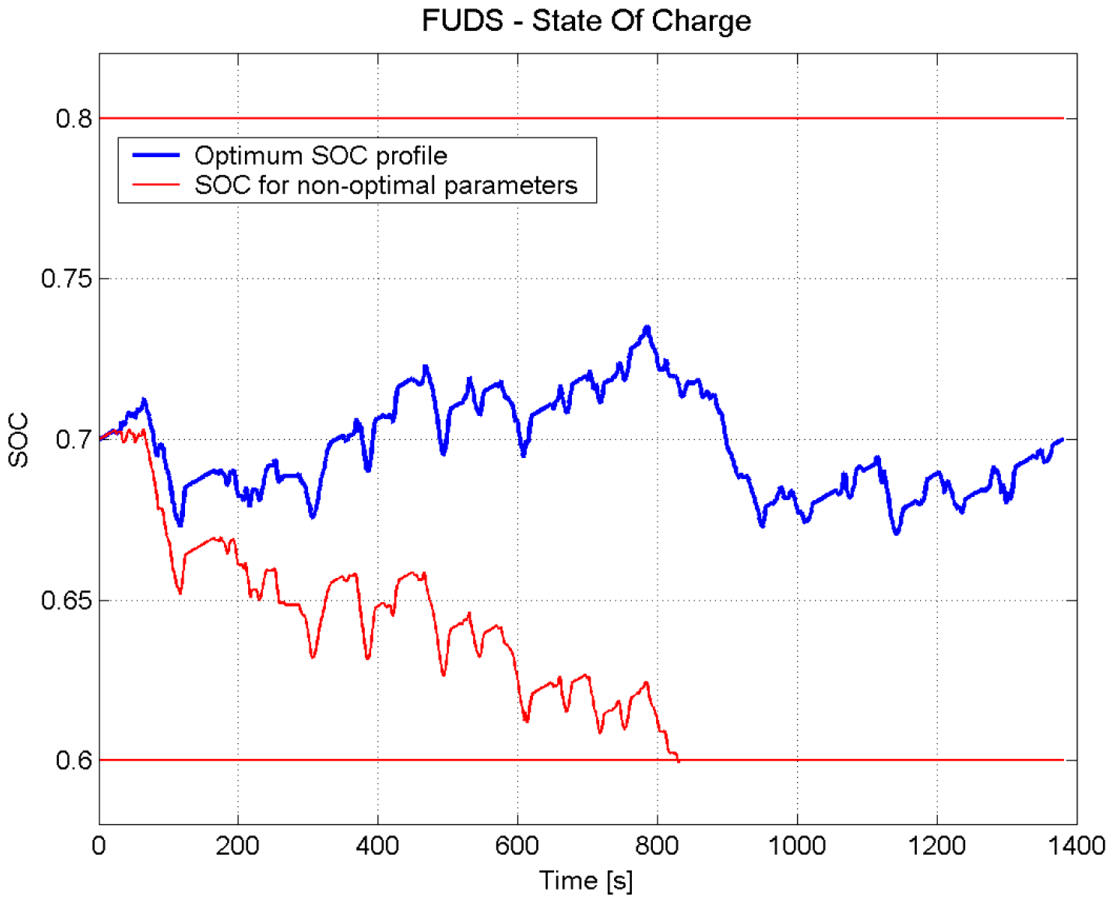

Figure 2-36: SOC for optimal and non-optimal equivalence factors (source [152])

In *Gu et al.* [159], a driving pattern recognition (DPR) approach to ECMS real-time adaptation is proposed to obtain a better estimation of the equivalence factor under different driving conditions (Figure 2-37). The proposed control strategy is articulated as follows: first, 18 standard driving cycles are analysed. Twenty-one different cycle-characterising quantities, such as average velocity, are extracted. Using the ideas of principal component analysis (PCA) and statistical clustering, driving cycles are classified into four classes. While the vehicle is running, a time window of past driving conditions is analysed periodically and recognised as one of the representative driving patterns. Under the assumption that the current driving

pattern does not change significantly compared to the past pattern, the equivalence factor is updated. Results obtained in this research show that with the proposed A-ECMS strategy, driving conditions can be successfully recognised, and good control performance can be achieved in various driving conditions while sustaining battery SOC within desired limits. In He *et al.* [165], telemetry ECMS (using predictive speed profiles) for energy management of plug-in HEVs is proposed. Using an optimal window size, the following improvements in cumulative fuel consumption were realized: 14–31% for the UDDS driving cycle, 1–15% for the HWFET driving cycle, and 1–8% for the US06 driving cycle (depending upon the total length of travel and operating modes).

In Won *et al.* [154], a multi-objective non-linear ECMS is proposed. First, a multi-objective non-linear optimal torque distribution strategy is formulated and converted into a single objective linear optimisation problem, by defining an equivalent energy consumption rate for fuel flow rate and battery state of charge. A vehicle-mode-based state of charge compensator is then applied to the optimal torque distribution strategy. Simulation results show that by linearising a non-linear optimisation problem, computation time could be reduced by up to 38% over standard driving cycles, with little or no penalty to the optimality of the solution obtained.

In Tulpule *et al.* [166], an ECMS approach is formulated to optimise fuel economy by estimating equivalence factors based on known total trip distance, instead of driving pattern information. The proposed approach estimates equivalence factors based on a battery SOC reference, which varies inversely with increasing trip distance.

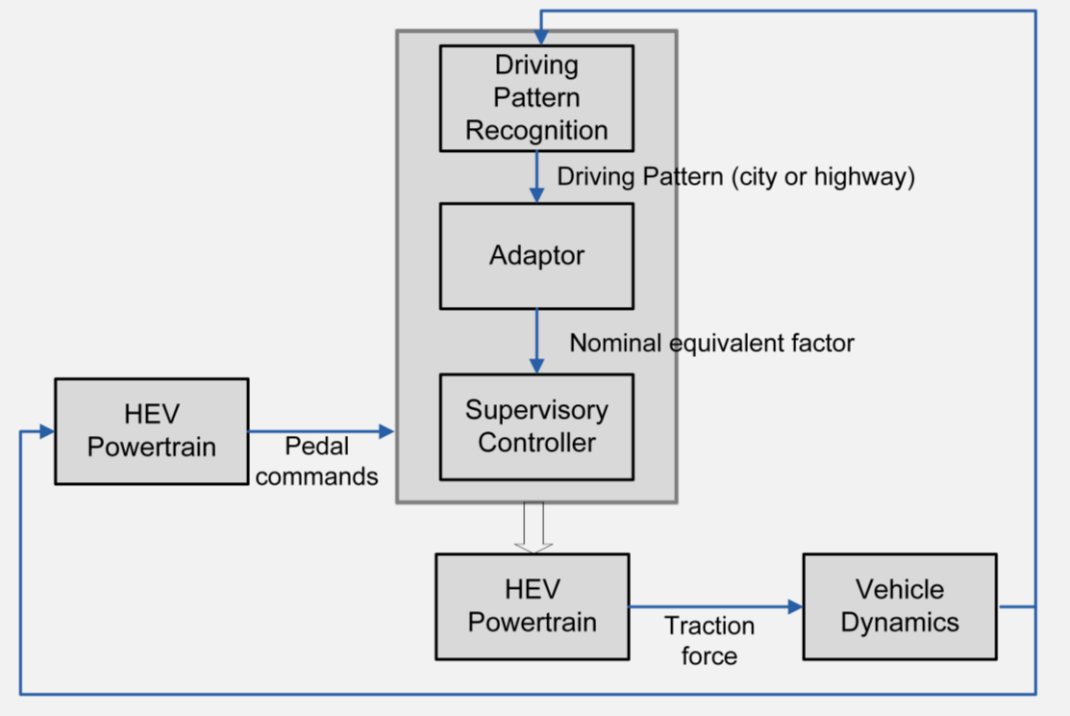

Figure 2-37: Driving pattern recognition based A-ECMS strategy (source [159])

2.4.2.2.3 Model predictive control strategy

Model predictive control (MPC) makes explicit use of a model of a plant process in order to obtain the control signal, which minimises the objective function. Model predictive control generally represents the solution of a standard optimal control problem over a finite horizon. It is performed online by using a model to predict the effect of a control on the system output.

It works by instantaneously calculating the optimal control for the prediction horizon, but only applying the first element; then at the next time step, the prediction horizon is displaced towards the future. The working principle of MPC relies heavily on high model accuracy, as well as prior knowledge of reference trajectories which are not directly possible in vehicular applications. However, MPC has been shown by Salman *et al.* [167] to be an effective real-time predictive

optimal control strategy, when used with a navigation system. In this study, a generalised predictive optimal control framework is used to find the conditions under which the predictive strategies will give superior fuel economy compared to instantaneous strategies. Mixed integer linear programming with no assumptions on the control structure is used subsequently to formulate the optimal predictive energy management strategy.

Typically, the information supplied by the navigation system, corresponding to future states is sampled in the look-ahead window along a planned route. Then, the optimal control theory is applied to solve the energy management problem in real time using a preview of driving pattern and driving route information. In the absence of a navigation system, a static and clustering based analysis method is used to predict future driving conditions from past and present recorded driving data. This method operates on the assumption that the driving conditions in future will remain relatively consistent.

MPC control strategy has been shown to yield as much as 31.6% fuel savings compared to a rule-based control strategy (Table 2-20) [168].

Driving cycle	**NEDC**	**UDDS**	**WVUSUB**
Strategies	L/100km	L/100km	L/100km
Rule-based control strategy	5.32	5.32	5.30
Predictive control strategy	3.64	3.82	3.76

Table 2-20: Fuel consumption results of a rule-based control strategy and a predictive control strategy (source [168])

Detailed implementation steps for MPC are outlined in “Implementation of Model Predictive Control Strategy”, extracted from Lerenzo *et al.* [169] - Figure 2-38.

Implementation of model predictive control strategy

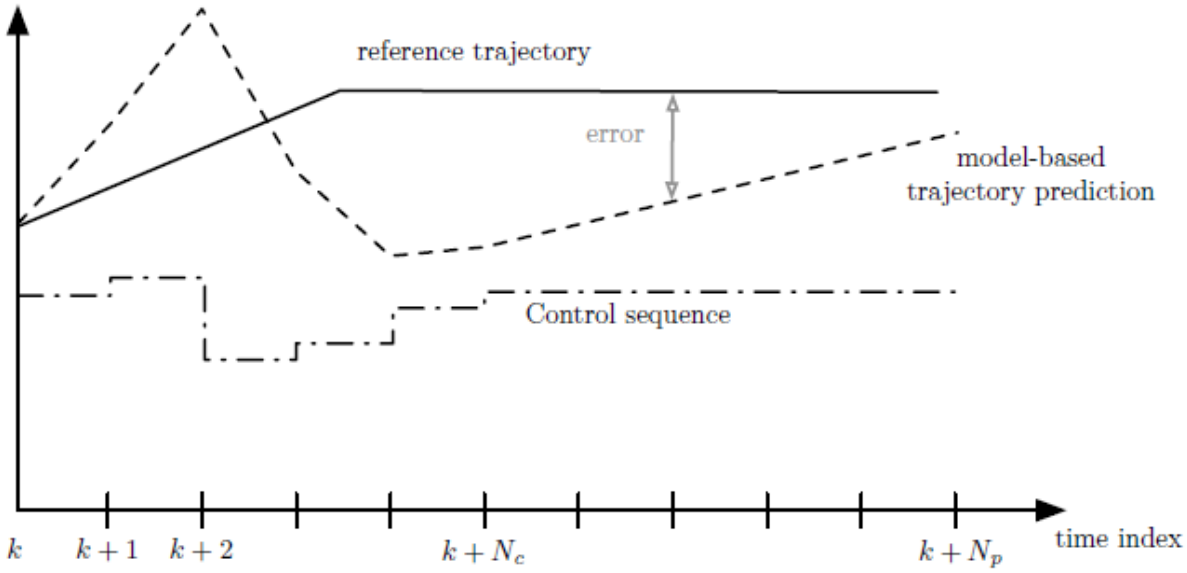

Figure 2-38: Sample reference trajectory, actual trajectory, and control sequence for MPC (source [169])

1. *The future outputs y for a determined horizon Np, called the prediction horizon, are predicted at each instant k using the process model. These predicted outputs y(k + i| k), i = 1, ..., Np depend on the known values up to instant k (past inputs and outputs) and on the future control signals u(k + i | k), i = 0, ..., Nc - 1, which are those to be sent to the system and to be calculated. Np indicates the length of the prediction horizon and Nc ≤ Np is the length of the control horizon (expressed in number of time steps).*

2. *The set of future control signals (from time k to time k + Nc - 1) is calculated by optimising a given criterion in order to keep the process as close as possible to the reference trajectory or set point. This criterion usually takes the form of a quadratic function of the errors between the predicted output and the reference trajectory. The control effort is included in the objective function in most cases. An explicit solution can be obtained if the criterion is quadratic, the model is linear and there are no constraints, otherwise an iterative optimisation method has to be used.*

3. *The control signal u(k | k) (i.e., the control at time k calculated based on the information available at time k) is sent to the process while the next control signals (u(k + 1 | k), u(k + 2 | k) etc.) are calculated but not used, because at the next sampling instant y(k + 1) will be known and thus the optimal control value will be recalculated. The procedure is repeated with this new value and the entire sequence is brought up to date. Then u(k + 1|k + 1) is calculated (which in principle will be different from u(k + 1 | k) because of the new information available) using the receding horizon concept.*

Few researchers [22, 167, 170-177] have successfully applied MPC to the energy management of HEVs. In Back *et al.* [45], an MPC energy management strategy is formulated for a parallel HEV. In their computation, they assumed a constant vehicle speed, and using GPS information, were able to estimate the road grade over the prediction horizon. Dynamic programming was then used to obtain the optimal control sequence which minimises fuel consumption. Simulation results

show that by extending the prediction horizon to the entire route, a fuel savings potential as high as 20% could be achieved by the model predictive controller.

Nuijten *et al.* [178] also successfully applied a similar approach (the receding horizon dynamic programming) on a conventional vehicle with a 42-volts electric power net and an alternator which is able to supplement torque to the driveline as required. Vito *et al.* [179] also presented a similar approach on a fuel cell hybrid vehicle. In this study, the MPC algorithm uses the linearised model of the fuel cell to predict its dynamic response, thus deciding what battery power is needed in order to satisfy the vehicle power demand, whilst minimising the objective function. The proposed approach consists of a two-level control architecture. The lower level scheme controls the fuel cell acting on the compressor command and on the back pressure valves of the anode and the cathode. The higher control level is devoted to manage the power absorbed by the motor and the one provided by the fuel cell.

In a study by West *et al.* [180], MPC is applied simultaneously to enhance battery life, vehicle driving range, as well as reduce emissions, fuel consumption and drive train oscillations for HEVs. In Rajagopalan *et al.* [122], traffic information in the form of road speed limits, and topological data from GPS over an entire trip was used alongside a fuzzy logic controller to determine the power split between the internal combustion engine and the electric motor, based on efficiency and emissions. In Sciaretta *et al.* [140] and Borhan *et al.* [181], an MPC framework with no need for future driving conditions is proposed for the control of parallel HEVs. In Sciaretta *et al.* [140], the fuel equivalent of electrical energy is estimated online as a function of current system status, and used to near-optimally adapt the MPC controller. Simulation results over an ECE driving cycle indicate a fuel consumption

reduction of around 50% over a typical urban driving scenario. In Borhan *et al.* [181], the global fuel minimisation problem is converted to a finite horizon optimal control problem with an approximated cost-to-go, using the relationship between the Hamilton-Jacobi-Bellman (HJB) equation and the Pontryagin's minimum principle. A non-linear MPC framework is employed subsequently, to solve the problem in real time. Simulation results indicate that compared to a rule-based control strategy, the non-linear MPC control strategy offers remarkable improvements in fuel economy over the US06, SC03, JC08 and NYCC driving cycles, with minimum penalty to the final battery state of charge (Table 2-21).

US06 cycle			
Controller	**Initial SOC**	**Final SOC**	**Fuel Economy (mpg)**
Rule-based	0.7	0.62	45.4
	0.6	0.6	42.8
Non-linear MPC	0.7	0.69	42.49
	0.69	0.69	46.01
SC03 cycle			
Controller	**Initial SOC**	**Final SOC**	**Fuel Economy (mpg)**
Rule-based	0.7	0.68	71.29
	0.68	0.68	69
Non-linear MPC	0.7	0.69	76.66
	0.69	0.69	74.77
JC08 cycle			
Controller	**Initial SOC**	**Final SOC**	**Fuel Economy (mpg)**
Rule-based	0.7	0.67	85.67
	0.67	0.67	81
Non-linear MPC	0.7	0.71	82
	0.71	0.71	83.6
NYCC			
Controller	**Initial SOC**	**Final SOC**	**Fuel Economy (mpg)**
Rule-based	0.7	0.66	68.68
	0.64	0.64	52.6
Non-linear MPC	0.7	0.67	66.47
	0.67	0.67	58.25

Table 2-21: Comparison between a non-linear MPC strategy and a rule-based strategy over the US06, SC03, JC08 and NYCC driving cycles (source [181])

Ripaccioli *et al.* [182] proposed a hybrid MPC strategy to coordinate powertrains and enforce state and control constraints. At first, the authors developed a hybrid dynamic model using a linear and piecewise affine identification method, and then designed an MPC strategy to reduce fuel consumption and emissions. In another study by Ripaccioli *et al.* [183], a stochastic model predictive control (SMPC) framework was developed for the power management of a series HEV. The power demand from the driver was modelled as a Markov chain, estimated on several driving cycles and used to generate scenarios in the SMPC control law. Simulation results show that the SMPC solution governs the engine, motor, and battery operations in a causal, time-invariant, state-feedback way, thus resulting in an improved fuel economy and vehicle performance, compared to deterministic receding horizon control techniques.

In Vogal *et al.* [184], a predictive MPC model based on driving route prediction is proposed and tuned using inverse reinforcement learning for fuel efficiency optimisation. In a more practical context, the proposed approach considers routes that the driver is likely to take, and then computes an optimal mix of engine and battery power. Using simulation analysis, this approach was shown to increase average vehicle fuel efficiency by 1.22%, without requiring any hardware modification or change in driver behaviour.

In Borhan *et al.* [185], a complex MPC control strategy articulated in two steps is proposed and applied to a power-split HEV (Figure 2-39). In the first step, a supervisory MPC is developed and used to calculate the future control sequences that minimise the chosen performance index. The supervisory MPC is made up of a quadratic cost function which characterises the HEV optimal control problem. The formulated problem is solved online using a linear time-varying MPC approach. In

the second step, an additional cost function is introduced by dividing the fuel consumption cost into a stage cost and an approximation of the cost-to-go as a function of the battery state of charge. Simulation results show that, compared to a linear time-varying MPC strategy, the proposed two-step non-linear MPC strategy yields a significant increase in fuel economy over standard driving cycles.

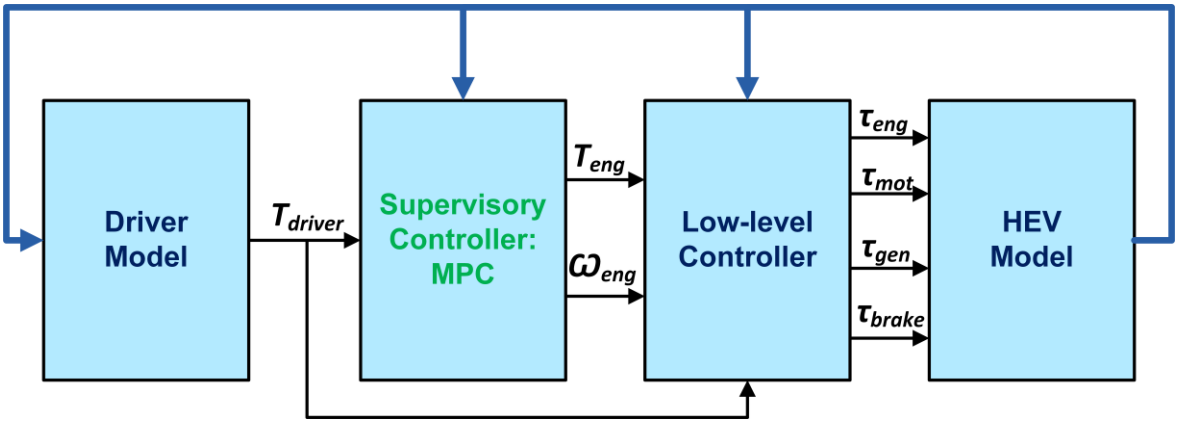

Figure 2-39: Control block diagram of a two-step MPC strategy (source [185])

Poramapojana *et al.* [176] proposed an MPC-based control strategy (Figure 2-40) for fuel consumption minimisation and charge sustenance, based on future torque demand predictions (estimated from desired battery SOC and desired vehicle speed). Simulation results show the feasibility of using an MPC controller to improve vehicle performance and minimise fuel consumption.

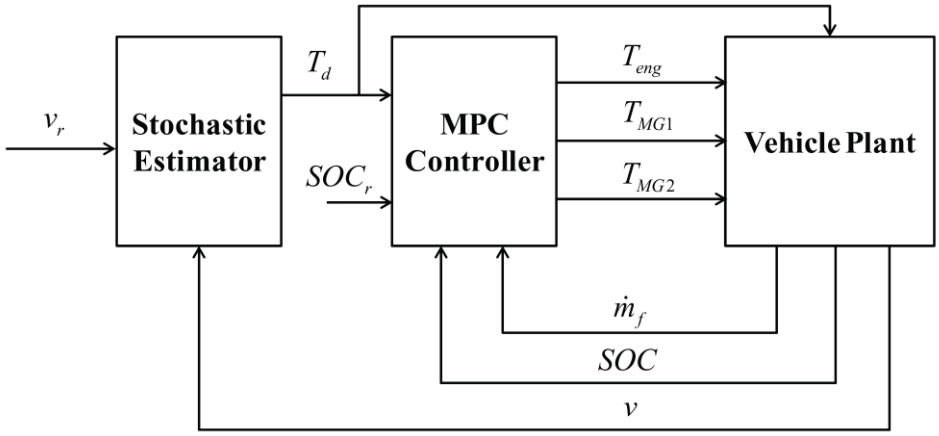

Figure 2-40: The control architecture of the MPC-based vehicle control system (source [176])

In Sampathnarayanan *et al.* [172] and Kermani *et al.* [22], MPC is combined with other global optimisation strategies to yield a near-optimal HEV control strategy in real time. In Sampathnarayanan *et al.* [172], MPC is combined with quadratic programming, to solve an optimal HEV control problem. Simulation results show that a long prediction horizon and high prediction accuracy do not yield better results than a shorter horizon. The results also show that prediction accuracy is only meaningful for long prediction horizons. In Kermani *et al.* [22], a Lagrange formula based MPC global optimisation approach is proposed. The resulting controller is made up of a two stage algorithm. The lower stage deals with solving a receding horizon optimisation problem, while the upper stage deals with prediction error compensation and disturbance rejection.

2.4.2.2.4 Artificial neural network (ANN)

Artificial neural network (ANN) is a computing system made up of a number of simple highly interconnected processing elements, which process information using their dynamic state response to external inputs. The concept of ANN was originally developed by McCulloh and Pitts in 1943 and further improved with the addition of the first learning rule by Hebb in 1949. Neural networks can be trained to learn a highly non-linear input/output relationship, by adjusting weights to minimise the error between the actual and predicted output patterns of a training set [186]. This form of supervised learning is facilitated by the back propagation method.

The adaptive structure of neural network makes it suitable for HEV energy management applications. Using neural network, it is possible to learn and replicate the non-linear relationships between inputs and outputs of a well-defined energy management network.

Baumann *et al.* [187] developed a control strategy that combines artificial neural network and fuzzy logic to implement a load-levelling strategy for improved fuel economy and reduced emissions for different drivers and different driving patterns. In Arsie *et al.* [47], a dynamic model is used to describe the driver-vehicle interaction for a generic transient and to simulate the vehicle driveline, the internal combustion engine and the electric motor/generator (EM). In the absence of traffic preview information, vehicle load is estimated in real time through the implementation of a time delay neural network (TDNN) and used to optimise the supervisory control strategy. Simulation results show a 45% improvement in fuel economy compared to a conventional vehicle with the same thermal engine.

In Mohebbi *et al.* [105], an adaptive neuro-fuzzy inference system controller is proposed and implemented to maximise fuel economy and minimise emissions in an HEV. The proposed approach is designed based on the torque required for driving and the battery state of charge. The output of the controller is the throttle angle of the internal combustion engine.

In Suzuki *et al.* [188], the neural network control framework is further improved to account for more multi-objectives including: torque distribution optimisation, fuel efficiency optimisation and electric current consumption minimisation. The entire optimisation process is articulated using the flowchart, shown in Figure 2-41. Controller sampling time, about several minutes, is defined as a parameter. During the sampling time, required vehicle torque demand, engine speed, regenerating current and battery SOC are estimated using neural network. The hybrid controller is then used to iteratively determine the optimal assist torque distribution. Simulation results show a 7% improvement in fuel economy compared with a heuristic HEV control algorithm.

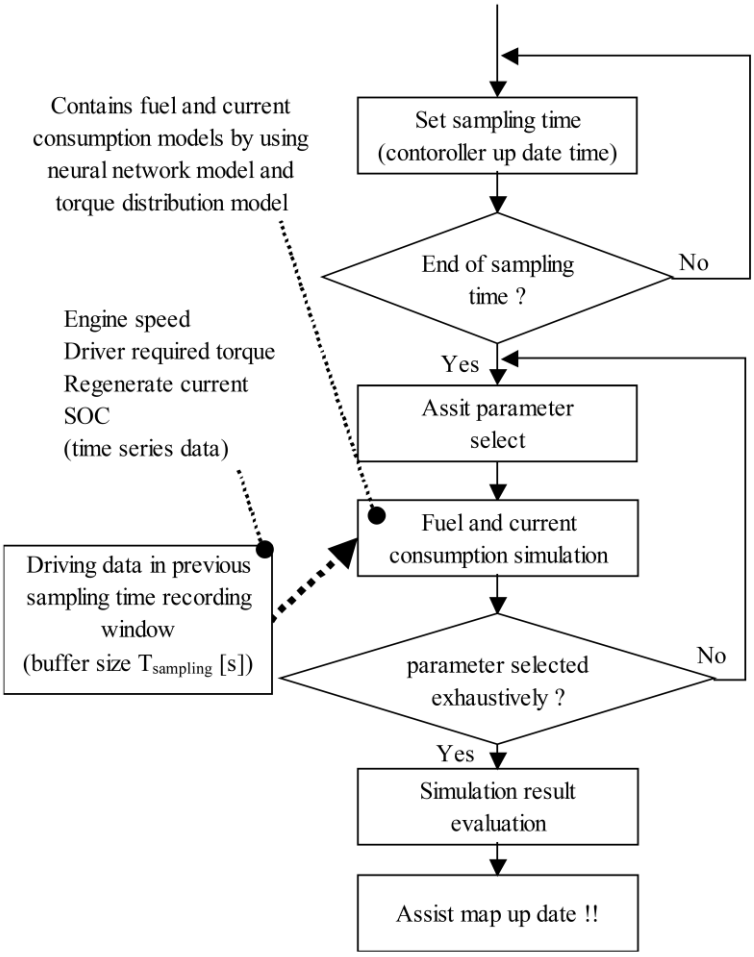

Figure 2-41: Flow chart for a neuro-fuzzy controller (source [188])

Prokhorov *et al.* [189] proposed a neural network controller for the Toyota Prius HEV. This approach is based on recurrent neural network using online and offline training including extended Kalman filtering and simultaneous perturbation stochastic approximation. A combination of the online and offline control methods was reported in this study to yield an improved average fuel efficiency of 17% over standard driving cycles. It was also shown to reduce the SOC variance over all the tested driving cycles by at least 25%. In Gong *et al.* [190] and Boyali *et al.* [191] neural network-based controllers are developed to consider variation in driving

patterns. In Gong *et al.* [190], a neural network-based trip model was developed for a highway trip. The simulation results show that the obtained trip model using neural network can greatly improve the trip modelling accuracy, and thus improve the fuel economy. In Boyali *et al.* [191], a neuro-dynamic programming (NDP) method for real-time HEV control is proposed. In this approach, the complex solution structure of dynamic programming optimal control is approximated using artificial learning algorithms for real-time application. Simulation results over two randomly generated urban driving cycles show that although the NDP controller is able to effectively sustain the battery energy in real time, it yields highly sub-optimal fuel economy, when compared to the dynamic programming optimal controller (Table 2-22). In Liu *et al.* [192], a high accuracy fuzzy neural network (FNN) controller is proposed and optimised using a modified genetic algorithm and an error-compensation approach.

	Fuel consumption	Improvement	ΔSOC
Conventional	10.99 L/100km	-	-
DP Solution	9.39 L/100km	14.5%	0%
NDP Solution	10.53 L/100km	4.12 %	1.7%

a. Randomly generated urban driving cycle 1

	Fuel consumption	Improvement	ΔSOC
Conventional	9.24 L/100km	-	-
DP Solution	8.07 L/100km	12.6%	0%
NDP Solution	8.84 L/100km	4.35 %	1.14%

b. Randomly generated urban driving cycle 2

Table 2-22: Comparison of simulation results from a dynamic programming controller (DP) and a neuro-dynamic programming controller (NDP) (source [191])

2.5 Existing research gaps in HEV energy management

As reviewed thus far, vehicle hybridisation poses new challenges in the form of: how to optimally split energy demand in real time between various competing power sources. In the case of braking, this answer is straightforward because while braking, the focus of the strategy is to maximise energy recovery in the battery by using the motor as much as possible. Simple solutions however, prove inefficient when the vehicle power demand is positive.

The first step in solving energy management problems when the vehicle power demand is positive lies in the formation of an objective function representing the

objectives to be minimised (e.g. fuel consumption, emissions). Another aspect of great importance in solving energy management problems lies in the control of the battery state of charge. This control is implemented to constantly keep the battery SOC within safe prescribed boundaries to ensure battery durability, and to ensure appropriate and convenient exploitation of the energy stored in the battery. The resulting energy management problem is a classical constrained optimisation problem which has been addressed by various studies, as reviewed in section 2.4.

Despite the improvements in fuel consumption and emissions reported by most studies, HEV control strategies are still lacking in some key areas, which are identified in this section and addressed in the succeeding chapters.

1. **Rule-based control strategies:** Rule-based control strategies are by nature sub-optimal, and unable to guarantee the fulfilment of integral constraints such as charge sustenance. They also require rigorous tuning to optimise rules for specific driving scenarios. This affects the robustness of the controller, consequently leading to highly sub-optimal online performances. The problem is further worsened in the absence of route preview information.

2. **Dynamic programming:** Although known to yield global optimal solutions to HEV energy management problems, dynamic programming present non-causal results which are non-implementable in real time, but can be used to create or benchmark sub-optimal controllers. The possibility of deriving useful real-time control policies from dynamic programming has been widely investigated in literature. Despite the research advances made, some of the resulting sub-optimal control

policies have been found to yield selective performances, which are charge-depleting in highway driving scenarios or charge-hoarding in urban driving scenarios.

3. **ECMS:** The equivalent consumption minimisation strategy is a local optimisation approach based on the heuristic concept that the energy used to drive a vehicle over a driving cycle ultimately comes from the engine, and as such the hybrid system merely serves as an energy buffer [137]. The resulting controller thus impacts the relative advantage of both heuristic controllers and optimal controllers. Consequently, the ECMS has received considerable amount of attention in literature, with several variations in the form of adaptive ECMS and telemetry ECMS being proposed. Despite these research advances, the ECMS technique in its present form is still unable to guarantee a charge-sustaining optimisation performance in real time. In a study by Silvertsonn *et al.* [193], the final battery SOC of sub-optimal ECMS strategies were shown to deviate by as much as 20% over standard driving cycles (Figure 2-42). This result shows that the equivalence factor of ECMS strategies are highly sensitive and cycle dependent i.e. the optimal equivalence factor for one driving cycle might lead to a poor performance on another driving cycle.

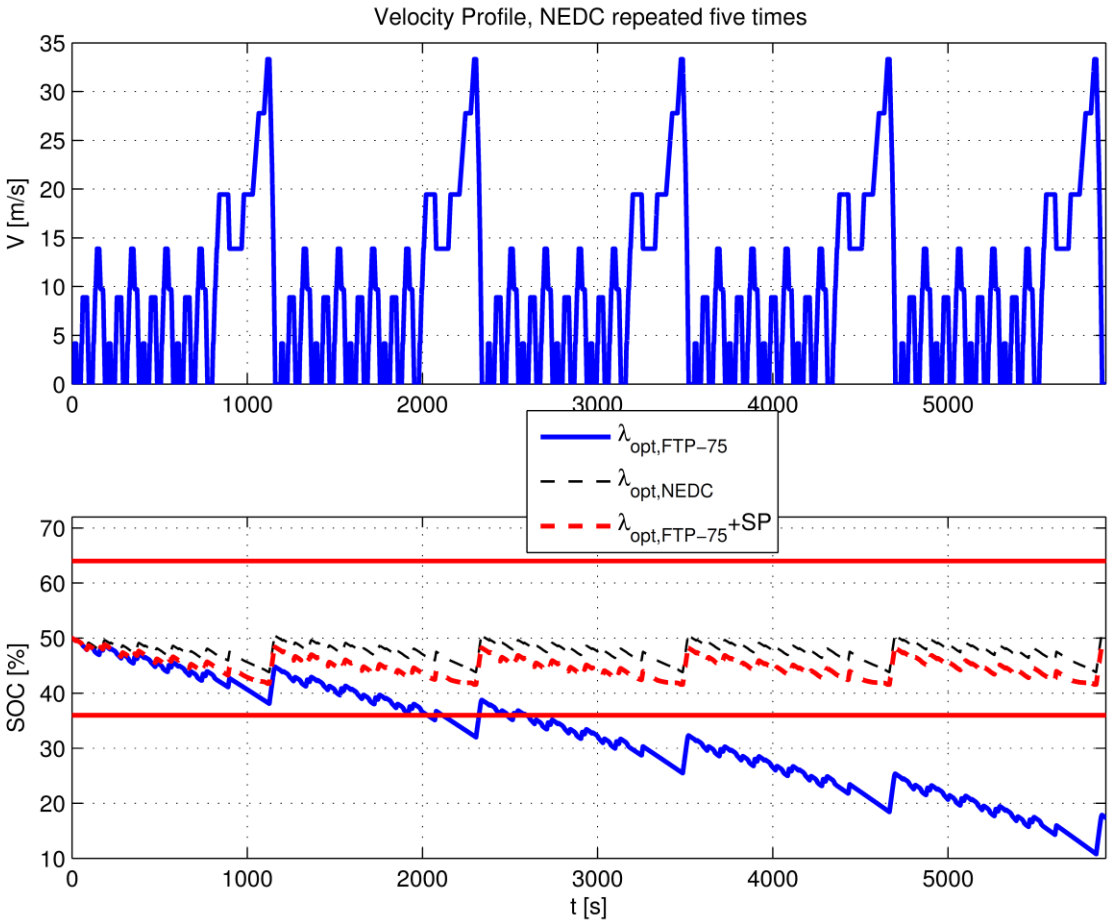

Figure 2-42: Impact of equivalence factor on battery state of charge (source [193])

4. **MPC strategy:** Owing to improved vehicular computational capabilities, and the wide availability of partial route preview information, model predictive control (MPC) strategies have gained significant attention, as a viable charge-sustaining energy management approach for HEVs. According to most literatures, future driving information can be predicted and incorporated into MPC strategies in two forms:
    i. Directly through real-time navigation systems

ii. Through the clustering based analysis of past recorded driving data.

Although both methods have been successfully implemented in literature, future driving information prediction based on navigation systems, have witnessed a wider appreciation. This is due to the computational burden associated with static and clustering based analysis. In most production vehicles today, the MPC framework is formulated using heuristics, which decide when the battery should be charged or discharged accordingly. Consequently, the resulting controller contains no form of optimisation and is not defined to account for charge sustenance.

In addition to the foregoing research gaps, the concept of vehicle speed control is relatively new and has only been investigated by a few researchers [194-197]. With the research area in its early days, most of the proposed vehicle speed control models are overly simplified and often yield non-realisable fuel-optimal speed trajectories. For example, the author was unable to find any study that considered engine braking effects in the formulation of fuel-optimal vehicle speed trajectories. By ignoring these real-world effects, the resulting speed trajectory is only of academic interest.

2.6 Chapter conclusions

Owing to the prospect of improved fuel economy and vehicle performance, HEVs continue to enjoy a wide research attention from academics and industrial researchers alike. With increased government funding and industrial cost optimisations, HEVs are becoming more affordable and accessible than ever.

To meet the energy demands of different HEV configurations, several energy management strategies have been proposed in literature. This chapter presents a comprehensive review of relevant literatures pertaining to modelling and control of parallel hybrid electric vehicles. HEV control strategies were reviewed at depth on two main tiers: HEV offline and online control strategies. This detailed appraisal is aimed at highlighting the control structure of the reviewed techniques, their novelty, as well as contributions towards the satisfaction of several optimisation objectives, which include but are not limited to: reduction of fuel consumption and emissions, charge sustenance, optimisation of braking energy regeneration, and improvement of vehicle driveability.

Exploitable research gaps pertaining to rule-based control strategies, dynamic programming, the equivalent consumption minimisation strategy (ECMS) and model predictive control (MPC) strategies were also identified. These identified research gaps suggest that current HEV control strategies are still lacking primarily in the aspects of: optimisation of braking energy regeneration and charge-sustaining sub-optimal control using partial route preview information and no route preview information. These research gaps will be addressed subsequently in this thesis.

3 HEV DYNAMIC MODELLING, VALIDATION AND SIMULATION

3.1 Introduction

In a control application where reduction in fuel consumption is the primary objective, it is important to develop vehicle models with a robust and accurate ability to predict fuel consumption even under rapid transients.

This chapter aims to develop a detailed modelling and heuristic simulation of the research vehicle, identifying all assumptions made. Vehicle subsystems for the presented vehicle will model, to a high level of accuracy, vehicle components which significantly affect fuel consumption. Using the validated model, the following case studies will be examined:

1. Impact of gear shift strategy on fuel consumption.
2. HEV performance under simple heuristic control.
3. Impact of braking patterns on kinetic energy regeneration.

3.2 Driving cycle definition and classification

A driving cycle is a standardised driving pattern, described by means of a velocity-time table and road grade, used to assess fuel consumption and pollutant emissions of a vehicle in a normalised way, so that different vehicles can be objectively compared. The primary intention of driving cycles is to provide a realistic and practical basis for a vehicle emissions test. Interactions among driving cycles or driving patterns, the driver and the vehicle are represented in Figure 3-1 [198]. There are two main categories of driving cycles: legislative cycles employed

in type-approval test for vehicle emissions certification and non-legislative cycles used mainly in research.

For light-duty vehicles, various vehicle dynamometer driving cycles are employed in type-approval tests for emissions certification. Such driving cycles include but are not limited to: the NEDC in Europe, JC08 in Japan and FTP-72 in the United States. The NEDC driving cycle includes four urban driving cycle segments characterised by low vehicle speed, low engine load and low exhaust gas temperature, followed by one extra-urban segment to account for more aggressive and high speed driving. JC08 represents congested city driving, including idling periods and frequently alternating acceleration and deceleration. The FTP-72 is a transient cycle produced from real measurements in Los Angeles [199].

When compared to conventional vehicles, HEVs are more sensitive to driving patterns. For example, if an HEV controller is not controlled properly for the chosen driving pattern, the battery end state of charge may violate its recommended limits, leading to deteriorated fuel economy. As a mitigating action, careful selection of driving cycles representing various real world driving scenarios is needed to ensure that the resultant HEV energy management controller will yield a charge-sustaining optimal performance in real time.

In this study, 11 standard driving cycles (detailed in Table 3-1) represent different driving scenarios. To emphasise the peculiarity of each selected driving cycle to this study, a novel two-class grouping system is proposed as shown in Table 3-2.

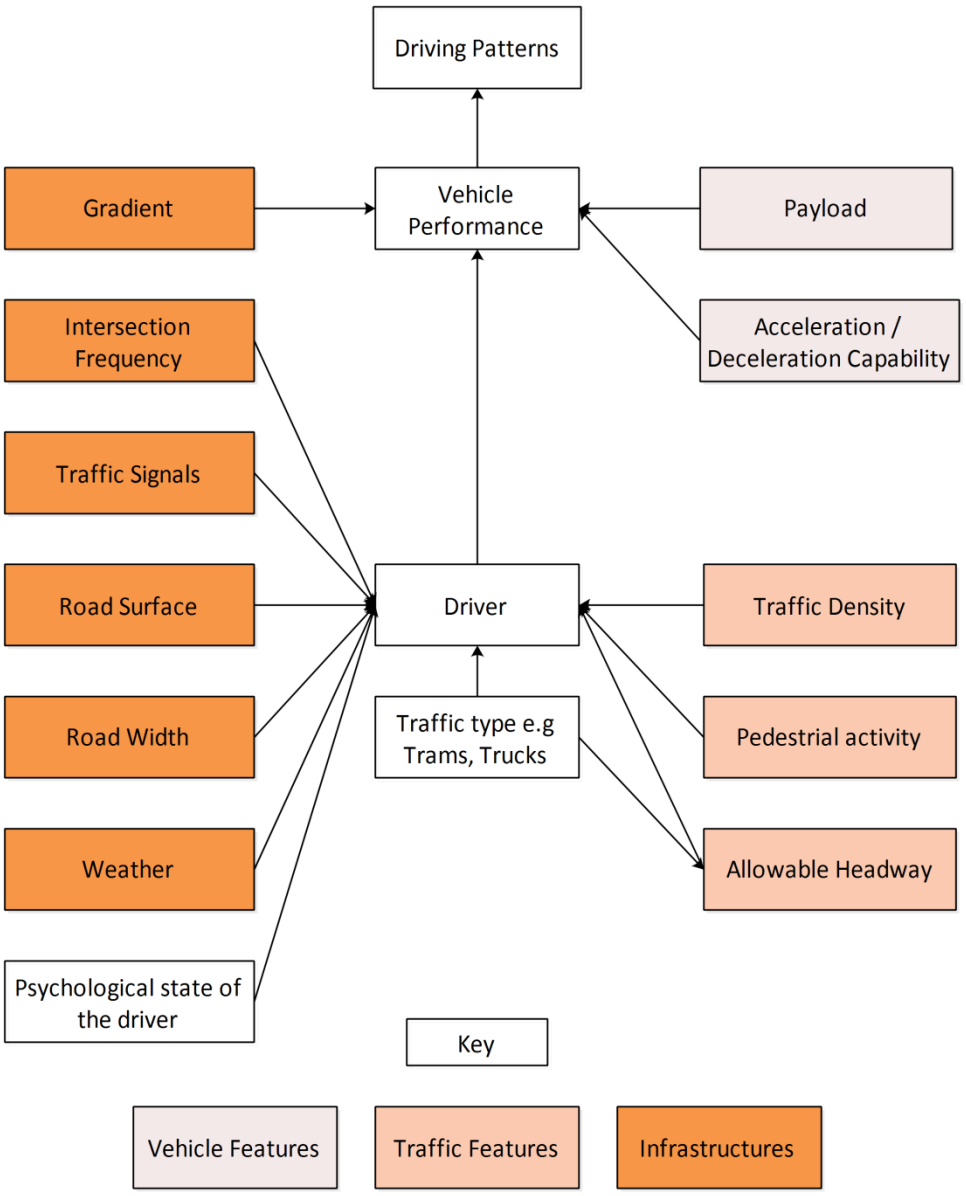

Figure 3-1: Representation of information influencing the driving cycle (source [198])

Standard driving cycle characteristics					
Driving cycle type	**Total distance (m)**	**Total time (s)**	**Average positive acceleration (m/s^2)**	**Average driving speed (Km/h)**	**Aggressivity factor (m^2/s^3)**
NEDC	11017	1180	0.53	42.24	3.10
FTP-72	11997	1369	0.43	36.60	4.36
JAPAN1015	4165	660	0.37	30.73	1.58
SC03	5766	596	0.42	40.38	4.76
NYCC	1903	598	0.47	16.63	2.15
HWFET	16503	765	0.16	77.76	3.39
IM240	3154	240	0.36	47.51	4.75
US06	12894	596	0.54	79.62	11.97
LA92	15802	1435	0.50	45.22	6.31
ARTEMIS U130	28737	1068	0.27	97.60	7.40
WLTC 3	23262	1800	0.41	46.50	5.30

Table 3-1: Standard driving cycle characteristics and aggressivity factors (source for cycle characteristics [200])

		Aggressivity Classification		
		Calm (AGF < $4m^2/s^3$)	**Moderate ($4m^2/s^3 \leq$ AGF $\leq 6m^2/s^3$)**	**Aggressive (AGF > $6m^2/s^3$)**
Driving type based on road type	**Neighbourhood driving (Average driving speed < 32km/h)**	JAPAN1015, NYCC		
	Urban driving (32Km/h < Average driving speed < 72km/h)	NEDC	FTP-72, SC03, IM240, WLTC 3	LA92
	Highway driving (Average driving speed > 72km/h)	HWFET		US06 ARTERMIS U130

Table 3-2: Standard driving cycle classification based on road type and aggressivity

In this grouping system, driving cycles are classed based on aggressivity; quantified as aggressivity factor (AGF) and road type. The road type classification is based on the speed class grouping system originally proposed by Berry [199], while the AGF is calculated using Equation 3-1. The resulting AGF for different standard driving cycles are detailed in the last column of Table 3-1.

$$Aggressivity\ (AGF) = \tau_{acf} \left(\frac{dV_v}{dt}\right)_{avg\ pos\ accel} V_{v_{avg\ driving\ spd}} \quad 3\text{-}1$$

Where:

τ_{acf} is the aggressivity compensation factor

$\left(\frac{dV_v}{dt}\right)_{avg\ pos\ accel}$ is the average positive vehicle acceleration

$V_{v_{avg\ driving\ speed}}$ is the average vehicle driving speed

$\tau_{acf} = 1$ for non-modal driving cycles (NYCC, FTP-72, SC03, IM240, WLTC 3, LA92, ARTEMIS U130, US06 and HWFET driving cycles) and real-world driving profiles

$\tau_{acf} = 0.5$ for modal driving cycles (NEDC and JAPAN 1015 driving cycles)

τ_{acf} is assumed low for modal driving cycles, to account for their stylistic nature when calculating the cycle aggressivity.

Based on this classification system, the NEDC driving cycle, for example, represents a calm urban driving scenario, while the LA92 cycle represents an aggressive urban driving scenario. The same interpretation applies to the rest of the driving cycles in this study.

3.3 Drivetrain configuration for the study vehicle

The vehicle considered for this study is a Citroen Berlingo van with a parallel HEV powertrain architecture as shown below in Figure 3-2 (See Appendix 1 for vehicle details). In this configuration, there are two drivelines to the wheels. The first driveline is the conventional thermal driveline, constituted by the engine, clutch, gearbox and differential. The second is the electrical driveline constituted by the battery, power electronics, electric motor, fixed coupling gearing and differential.

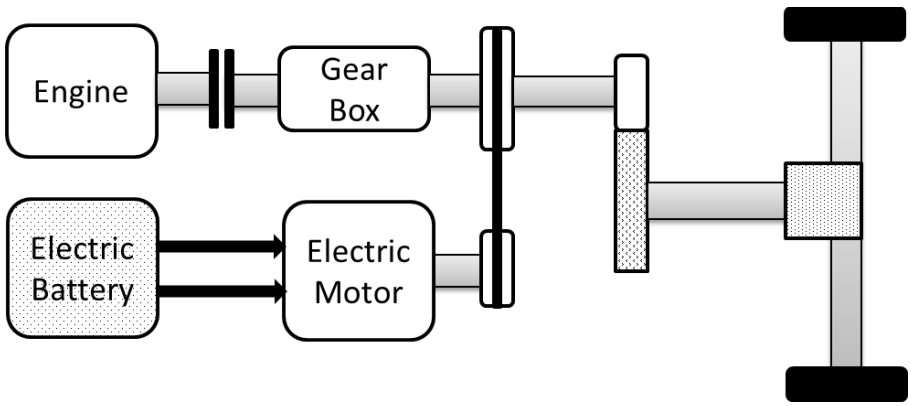

Figure 3-2: Parallel HEV architecture

As coupling between both drivelines occurs after the gear box, the architecture is specifically identified as a post-transmission parallel HEV [153]. The coupling device in use here is a fixed gearing, which transfers torque from the motor shaft

to the shaft exiting from the gearbox. As such, the torque delivered to the wheels equals the torque produced by the engine and torque produced by the electric motor, multiplied by the transmission ratio and transmission efficiency of their respective paths to the wheel. On the thermal driveline, there are 5 manual transmission gears and the differential, while the electrical driveline has a fixed gearing and a differential. In this configuration, although the engine can be disconnected from the wheels by means of the clutch between the engine and the gear box, the electric motor is connected to the wheels at all times. This configuration advantageously offers a range of functioning modes, thus making it possible for power requests to be fulfilled by either the thermal driveline alone, electric driveline alone or jointly by both drivelines.

The vehicle is a charge-sustaining hybrid (not rechargeable through electric grid) equipped with a 4 cylinder, 1.6 litre diesel common rail engine delivering a peak power of 90hp (68kW) at 4,000 RPM. The electric driveline is composed of an 8.23kW electric motor connected to a 16Ah lithium ion electric battery with a nominal voltage of 79.2V and a max continuous discharge current of 80A. Though rated at 16Ah, the capacity of the battery in reality is slightly lower. This is due to the limited battery state of charge range (40% to 80%) imposed to ensure durability.

3.4 Definition of performance metrics and modelling constraints

3.4.1 Degree of hybridisation

The degree of hybridisation is defined as the driving capacity of the electric motor relative to that of the ICE. Accordingly, the research vehicle is a charge-sustaining "full parallel HEV", which implies that depending on the vehicular power request, the vehicle can be driven independently or cooperatively by the ICE and the electric motor. In this case, the electric battery works as an energy buffer by storing regenerative braking energy and releasing it on demand.

3.4.2 Hybridisation ratio

Electric hybridisation ratio (EHR) indicates to what extent the propulsion system tends toward being a pure electric vehicle. In general, EHR is the ratio between the maximum electric power and the maximum total traction power [201] as illustrated in Equation 3-2 for a parallel HEV [202, 203].

$$HR = \frac{P_{motor_{max}}}{P_{motor_{max}} + P_{ICE_{max}}} \qquad 3\text{-}2$$

A summary of the electric hybridisation ratios for different parallel HEVs are detailed in Table 3-3.

HEV TYPE	DESCRIPTION	TYPICAL HYBRIDISATION RATIO
Micro HEV	Contains a small electric motor essentially used as an integrated starter generator (ISG)	HR ≈ 5%
Mild HEV	Similar to a micro HEV, but with an increased size of electric motor and battery which permits power assist during vehicle propulsion	HR ≈ 10 – 15 %
Full HEV	Electric motor and batteries are significantly bigger than that of the micro HEVs and mild HEVs. As such, depending on the vehicle power demand and battery state of charge, the electric motor can be used as the sole power source	HR ≈ 30 – 45 %
Plug-in HEV	Same configuration as full HEVs but with the addition of an external electric grid charging plug, much bigger electrical components (electric motor and battery) and a downsized engine.	HR > 50 %

Table 3-3: Summary of hybridisation ratios for different HEVs (source [204])

With a peak engine power of 68kW and a peak electric motor power of 8.23kW, the research vehicle powertrain has a hybridisation ratio of 38% which, according to Table 3-3, is typical for full HEVs and implies the following:

1. The electric motor is able to fulfil most of the vehicle's regenerative braking requirement.
2. Depending on the battery state of charge and vehicle power demand, the electric motor is able to solely power the vehicle during cruises or assist the ICE during acceleration.

3.4.3 Definition of vehicle modes

The research vehicle (Figure 3-2), being a full HEV, can be operated in different modes, which are illustrated in Figure 3-3 and subsequently described.

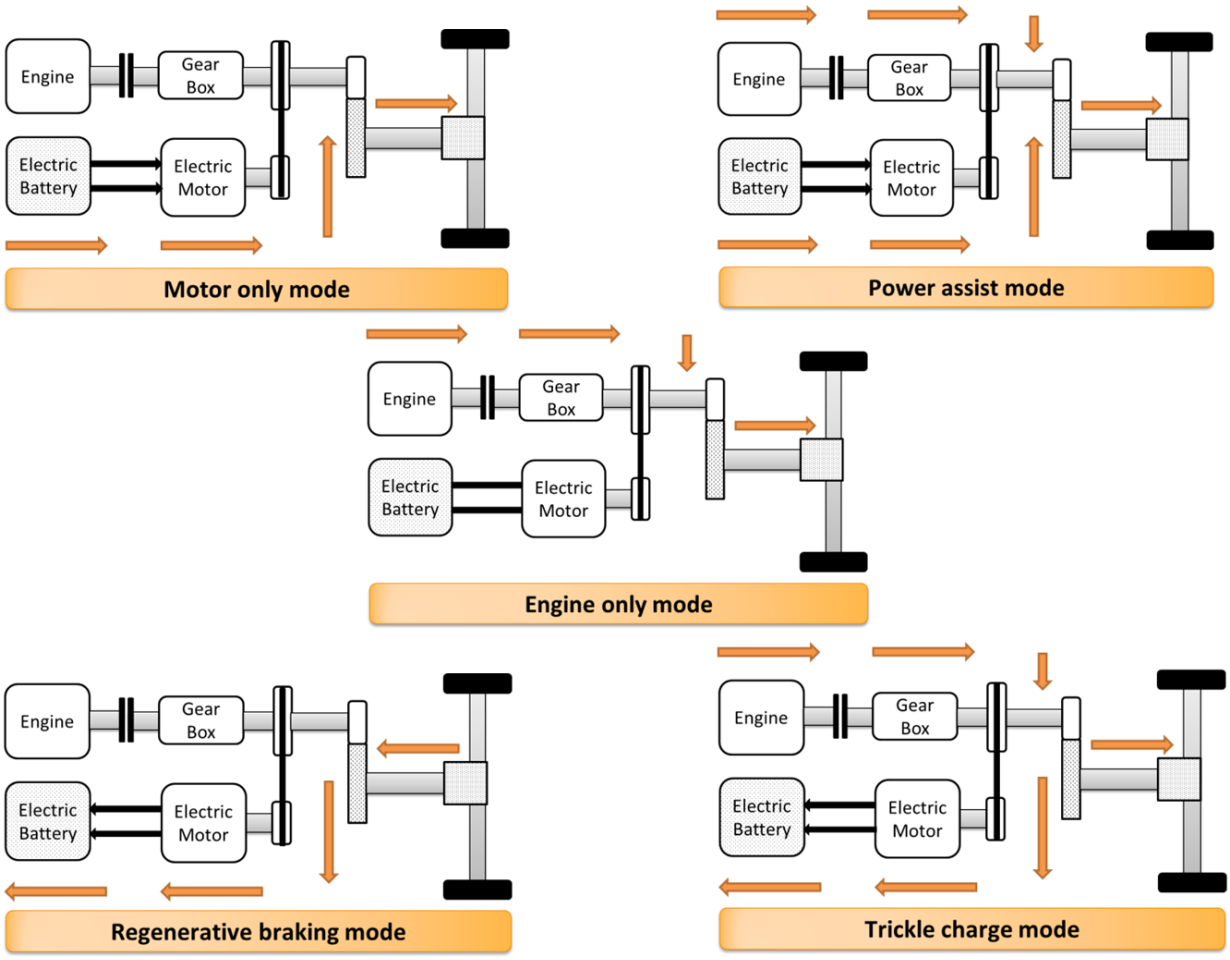

Figure 3-3: HEV operating modes with power flow

Motor only mode

In this mode, the HEV operates mainly as an electric vehicle, in which case the engine is disengaged from the drivetrain by means of a clutch and allowed to idle. Operating the HEV in this mode means that the entire energy which drives the drivetrain comes from the batteries.

Power-assist mode

In this mode, the electric motor operates to assist the engine in regions of low engine efficiency or high vehicle power demand.

Engine only mode

In this mode, HEV load and speed request are met solely by the ICE. This mode is preferred when the ICE operates in its peak-efficiency region.

Regenerative braking mode

In this mode, the HEV uses the electric motor to recover kinetic braking energy which would otherwise have been lost as heat to the mechanical brakes. The captured braking kinetic energy is converted to electrical energy and stored in the battery for use during the motor only mode or power-assist mode.

Trickle charge mode

In this mode, the engine is used to drive the road load, maintain the driving cycle speed request and recharge the batteries via the electric motor. Operating an HEV in this mode imposes an extra cost (fuel consumption), which is one of the reasons why such a practice is strongly discouraged, except on occasions where the battery SOC (state of charge) has dropped below the recommended lower boundary and needs to be brought back up to avoid damaging the battery cells.

3.4.4 Modelling assumptions

The following assumptions are made throughout this thesis:

1. Steady state maps of the ICE and electric motor are used throughout the modelling and applied to transient events.
2. Hot operation of ICE is assumed at all times (engine warm-up effects are neglected).
3. Frequency of driving data is 1s.
4. In calculating of vehicular energy demand, auxiliary loads such as HVAC (heating ventilation and air conditioning) and lighting loads are neglected.
5. The HEV model is purely longitudinal and does not account for lateral or vertical motion.
6. The vehicle is considered as a point mass and only its static mass is taken into account.
7. Fuel is cut off during vehicle braking.
8. When not used to meet vehicle power demand, the engine idles at 750 RPM.
9. Driver model is only suitable for fuel consumption and emissions studies and cannot be used for specific driver behaviour analysis.
10. Minimum permissible battery SOC is 40%.
11. Maximum permissible battery SOC is 80%.
12. Initial battery SOC is 60%.

3.4.5 Performance metrics

Performance metrics are the criterion used to evaluate the different HEV control strategies. The following are the main performance metrics considered in this study:

1. Optimality of fuel consumption.
2. Ability to control the SOC during and at the end of driving, thus leading to a near charge-sustaining performance ($\pm$5% deviation between the initial and final battery SOC).
3. Controller robustness, which ensures that the control strategies are insensitive, to different driving cycles.

3.5 HEV dynamic model set up

Based on the comparative analysis presented in section 2.3, a Simulink-based quasi-static (forward simulation) model is considered in this study [28]. From a control development stand-point, this model is preferred as it maintains the physical causality of the real system, allowing the same controller inputs/outputs from the simulator to be used in the real system. In the quasi-static HEV model, the driving cycle is subdivided into small time intervals (typically 1s) during which the driver model (typically a PID model) determines throttle and brake commands to meet the target speed at the next time instance of the driving cycle, from the present speed. The throttle command is then translated into vehicle power demand. The control strategy is then applied to split the demanded power between the ICE and the electric motor. Each powertrain component is modelled using a steady state efficiency or fuel consumption map, which brings to bear the

relationship between the losses in the component and the present operating conditions.

The rest of this section intends to synthetically present the model employed in this study, and is structured as follows: First, vehicle energy balance is analysed. Next, the powertrain components are modelled. Finally, the model is validated against experimental data.

3.5.1 Driver modelling

The driver in this HEV model is designed as a simple PID controller with the addition of an anti-windup on the integrator. At each simulation time, the extra wheel torque needed for the vehicle to achieve the required vehicle speed is calculated using Equation 3-3.

$$T_{extra} = K_p(V_c - V_v) + K_i \int (V_c - V_v)\, dt + K_d \frac{d(V_c - V_v)}{dt} \quad 3\text{-}3$$

From Equation 3-3, the extra tractive force needed for the vehicle to achieve the required vehicle speed can be calculated thus:

$$F_{extra} = \frac{T_{extra}}{R_w} \quad 3\text{-}4$$

The cycle speed is given as a look up table of speed and time. The gain values of the PID driver model were tuned using parameter estimation in MATLAB to find the values which best enable the vehicle to follow the required speed-time trace. The values obtained from tuning are: $K_p = 0.272,\ K_i = 0.35,\ K_d = 2.$

3.5.2 Vehicle dynamics modelling

A vehicle typically consists of thousands of components, most of which come from various manufacturers, making it difficult, extremely time consuming and sometimes impossible to model a vehicle completely at a component level. However, for the purpose of a control strategy development, a sophisticated mechanical and mathematical model representing the longitudinal performance of the vehicle (Figure 3-2) will be outlined in details in this section.

The total traction force necessary to accelerate the vehicle can be split into four contributions, which include:

1. Aerodynamic drag
2. Grade resistance
3. Rolling resistance
4. Inertia resistance

Aerodynamic drag

A vehicle travelling at a particular speed in air encounters a force resisting its motion. This force, known as aerodynamic drag, results mainly from two components: shape drag and skin drag [38], [104], [205].

Shape drag:

The forward motion of the vehicle pushes the air in front of it. Since the air is unable to move out of the way, the air pressure tends to increase with the vehicle speed, thus resulting in high air pressure in front of the vehicle. At the rear of the vehicle, the air behind cannot instantaneously fill the space left by the forward motion of the vehicle, thus creating areas of low pressure behind the vehicle. The

resultant motion therefore creates two zones of pressure that oppose the motion of the vehicle by pushing it forward in the front and backward at the back, thus causing a shape drag.

Skin drag:

In the case of skin drag, air close to the skin of the vehicle moves almost at the same speed with the vehicle, while air far from the vehicle remains still. On the in-between, air molecules move at a range of speeds. The difference in speed between both air molecules produces a skin drag effect.

Aerodynamic force (F_{aero}), is a function of the vehicle speed, vehicle frontal area, vehicle density and the coefficient of air drag, which can be expressed mathematically as detailed in Equation 3-5.

$$F_{aero} = 0.5\rho A_f C_d (V_v - V_a)^2 \quad \text{3-5}$$

Grade resistance

As a vehicle goes up or down a slope, its weight produces a component, which is always directed in the downward direction. This component either opposes the forward motion (grade climbing) or supports the forward motion (grade descending). The grade resistance is given by:

$$F_{grade} = mg\sin(\beta) \quad \text{3-6}$$

Rolling resistance

When a vehicle is in forward motion, the movement produced by the forward shift of the ground reaction force is called the rolling resistance moment, expressed in Equation 3-7. This moment occurs as a result of the deformation of the tyre material and the road surface. On road surfaces, the hysteresis due to the deformation of the tyre material produces an uneven pressure distribution at the contact surface with the roadway, such that the ground reaction force is shifted towards the direction of the vehicle movement from the wheel axle [205].

$$T_{rolling} = \mu N_c \cos(\beta)\, R_w \qquad 3\text{-}7$$

To keep the wheel rolling, a force: $F_{rolling}$ acting through the centre of the wheel is required to balance the rolling resistance moment [205], [38]. This force can be expressed thus:

$$F_{rolling} = \mu N_c \cos(\beta) \qquad 3\text{-}8$$

The coefficient of rolling resistance μ is a function of the tyre material, structure, temperature, inflation pressure and geometry.

Inertia resistance

Vehicle acceleration creates rotational inertial resistance, which can be expressed using Newton's second law of motion thus:

$$F_{inert} = m\frac{dV_v}{dt} \quad \text{3-9}$$

The inertia force F_{inert} is always positive when the vehicle is accelerating and negative during deceleration. The grade force F_{grade} is positive when the vehicle is driven uphill and negative when it is going downhill. The rolling resistance and aerodynamic forces are dissipative, and thus always positive.

Combining the vehicle loads derived thus far in accordance with Newton's second law, the engine torque and speed can be expressed thus for a parallel HEV.

$$T_{ICE} = \frac{(m\frac{dV_v}{dt} + \sum(F_{aero} + F_{rolling} + F_{grade} + F_{extra}))R_w}{FDR\ G_E\ \eta_{drivetrain}} - \frac{T_{motor}\ G_M}{G_E} \quad \text{3-10}$$

Where:

$$T_{motor} = \frac{P_{motor}}{G_M\ FDR\ \omega_{wheel}\ \frac{2\pi}{60}}$$

The engine torque demand expressed in Equation 3-10 can be further expressed thus:

$$T_{ICE} = \frac{(m\frac{dV_v}{dt} + \sum(F_{aero} + F_{rolling} + F_{grade} + F_{extra}))R_w}{FDR\ G_E\ \eta_{drivetrain}} - \frac{P_{motor}}{G_E\ FDR\ \omega_{wheel}\ \frac{2\pi}{60}} \quad \text{3-11}$$

The general engine speed equation can be expressed thus:

$$\omega_{ICE} = \omega_{wheel}\, FDR\, G_E \qquad 3\text{-}12$$

Where:

$$\omega_{wheel} = \frac{V_v}{R_w}\ \frac{60}{2\pi} \qquad 3\text{-}13$$

3.5.3 Engine modelling

Engine modelling in the development of an HEV control strategy centres mainly on the use of mathematical and statistical methods to accurately predict the objective function to be minimised (fuel consumption).

During the operation of this parallel HEV, the engine is only a functional part of the powertrain during the following operating modes: the power-assist mode, trickle charge mode and the engine only mode. This means that the engine idles when not in use. During braking, however, no fuel is injected into the engine.

A conceptual sketch of the engine model is shown in Figure 3-4. This model is static and neglects crank-angle dynamics and torque oscillations due to alternating inertia and combustion cycles. The maximum torque curve represents the highest ICE torque achievable for any speed, which is used to saturate the engine torque request, thus ensuring the feasibility of the engine operating point.

Fuel consumption can be expressed as a function of engine torque and speed, as shown in Figure 3-4. Using the engine torque and speed values derived from

Equations 3-11 and 3-12 respectively, the instantaneous fuel consumption rate for each engine torque-speed point can be read off the "engine fuel consumption map" shown in Figure 3-4.

Data used in creating this map was obtained experimentally using the Chassis Dynamometer facility at the University of Bath, UK. Obtaining the engine fuel consumption map in this manner implies that transmission losses have already been accounted for. Consequently, $\eta_{drivetrain}$ in Equations 3-11 and 3-12 is taken as 100%.

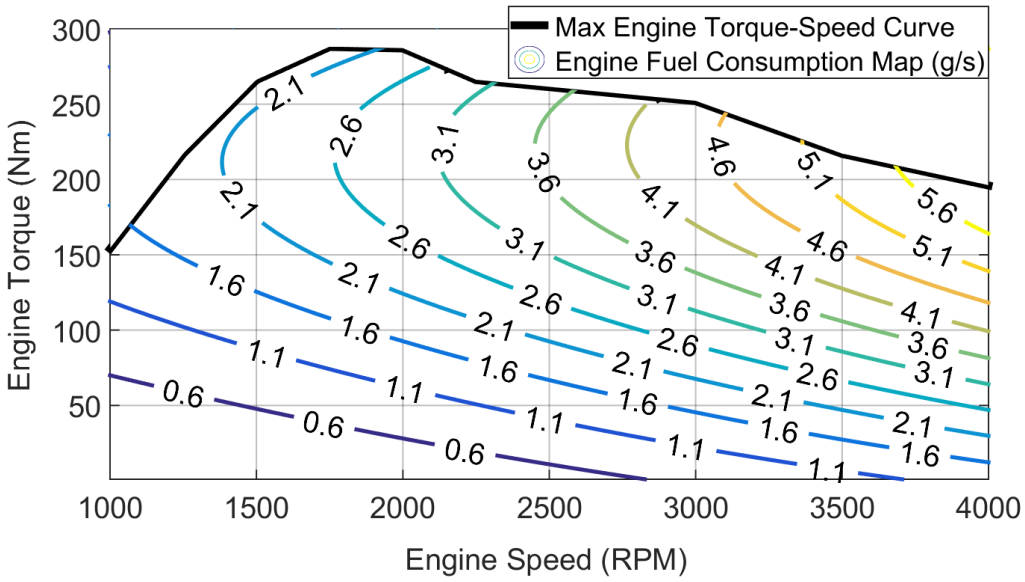

Figure 3-4: Engine fuel consumption map

3.5.4 Gear shift strategy

Several ways exist for defining the gear shift over a driving cycle. André *et al.* [206] pioneered the strategy now known as the "Artemis strategy". This strategy simultaneously considers the driving condition (engine speed and power demand)

and driving styles (database used includes measurement values for various drivers) [207].

The NEDC gear shift strategy performs gear shift on set vehicle speed values. This makes it easy to implement as it depends mainly on vehicle kinematics. However, this strategy is only well adapted to steady-speed cycles with few speed transients (such as the NEDC driving cycle) but is less suitable for real world driving cycles. This is because in most real-world driving cycles the vehicle speed is not steady and often varies around the shift threshold speed, which means that the time spent in a given gear can be very short. Over the NEDC, the gear shift strategy for a 5 speed gear vehicle is defined thus [207]:

0 < V_v(t) < 15 Km/h: ratio = 1

15 < V_v(t) < 35 Km/h: ratio = 2

35 < V_v(t) < 50 Km/h: ratio = 3

50 < V_v(t) < 70 Km/h: ratio = 4

V_v(t) > 70 Km/h: ratio = 5

Where V_v(t) is the vehicle speed (km/h)

In this thesis, a simple “Engine RPM” gear shift strategy is proposed for the vehicle thus:

If RPM(t) > 2000 : ratio(t+1) = ratio(t) + 1 (Upshift)

If RPM(t) < 1000 : ratio(t+1) = ratio(t) – 1 (Downshift)

If V_v(t) = 0 : ratio(t+1) = Neutral

If V_v(t) > 0 : 1 ≤ ratio (t) ≤ 5

This strategy takes into consideration the vehicle kinematic parameters and the vehicle characteristics in the gearshift pattern. In order to avoid frequent and unrealistic gear changes, a minimum 5 seconds delay is imposed on each gear, subject to the engine still being able to provide the vehicle torque requirement at that gear.

3.5.5 Electric motor modelling

A wide range of electrical machines are available, depending on the area of application. Generally electric machines can be categorised mainly into DC and AC machines, synchronous, asynchronous, etc. For the purpose of powertrain control strategy development, electrical machines can be modelled using a system-level approach (similar to the one used for the engine) which makes use of a 0D black box model to find the electrical efficiency of the electrical machine at each torque and speed point. The efficiency of the electrical machine η_{motor} is dynamically adjusted with respect to its speed (ω_{motor}) and torque (T_{motor}).

Depending on the instantaneous motor torque and speed, a look up table is used to estimate the electrical efficiency of the machine. The electric machine model presented here simulates electromechanical energy conversion in two directions: the motor mode and generator mode. During energy conversion in the electric machine, energy is lost due to copper losses caused by electrical resistance of the wires (and brushes), iron losses caused by hysteresis and eddy currents in the rotor, friction and windage losses [208].

The electrical power exchange between the battery and the electrical machine can be modelled thus:

$$P_{electric}(discharge) = \frac{1}{\eta_{motor}} P_{motor} \quad 3\text{-}14$$

$$P_{electric}(charge) = -\eta_{motor} P_{motor} \quad 3\text{-}15$$

Figure 3-5 shows the electric motor efficiency map. There exists a maximum torque for both the traction and regeneration performance of the electric motor. This maximum torque varies with motor speed, as shown in Figure 3-5. Data used in creating this map were obtained experimentally and supplied by Perm Motor, Germany.

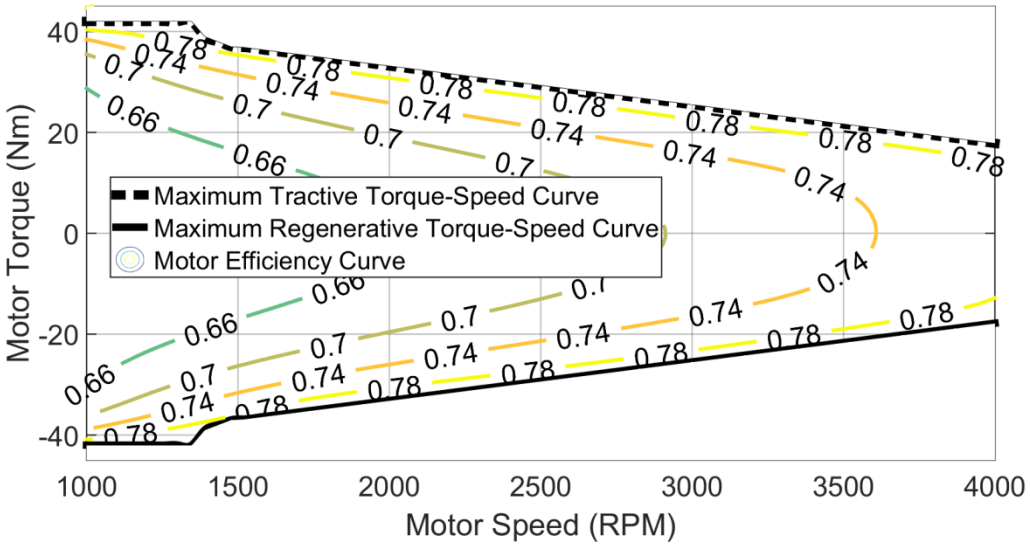

Figure 3-5: Electric motor efficiency map

3.5.6 Electric battery modelling

Many models have been developed to represent the actual behaviour of batteries. The simplest form of these models is based on the battery's electrochemistry. Electrochemical battery models ignore thermodynamic and quanta effects, and consequently are unable to model phenomena such as the time rate of change of

voltage under load. They are also unable to represent the battery's temperature and aging effects [209].

Another well-known battery model type commonly used in HEV control strategy development is the equivalent circuit battery model. In this sort of battery model, the capacity of the battery is modelled by a capacitor, the effect of the voltage deviation in the battery terminal is caused by temperature, and the battery state of charge is modelled by means of variable resistors and controlled voltage sources.

In this study, a simplified form of the circuit battery model, as shown in Figure 3-6, is applied. The series resistance R_{batt} represents Ohmic losses due to the actual resistance of wires and electrodes.

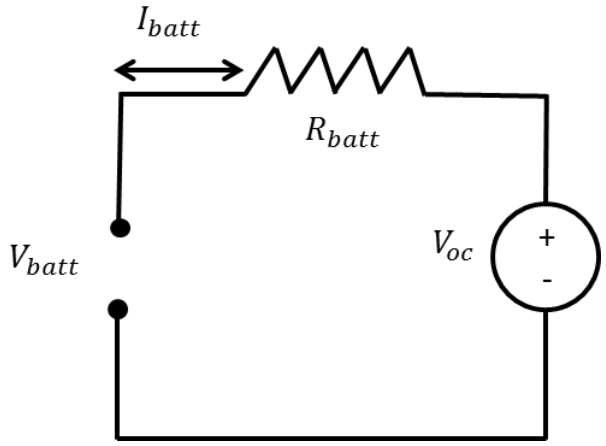

Figure 3-6: Battery circuit model

The objective of a battery model in a vehicle simulator is to predict the change in state of charge given the electrical load [210].

The battery state of charge (SOC) is a measure of charge left in a battery as a proportion of the maximum possible charge of the battery. In simulation, the

battery state of charge is calculated as an integral of battery current (I_{batt}) over the maximum possible battery charge.

The evolution of the battery state of charge as a function of the battery current can be expressed thus:

$$SOC_{t+1} = SOC_t \pm \int_t^{t+1} \frac{I_{batt_t}}{Q_{batt}}\ dt \qquad 3\text{-}16$$

Charge: (+), Discharge: (-)

Where I_{batt} is the battery current and Q_{batt} is the battery capacity.

In reality, the battery capacity changes according to the magnitude of current and battery age. However, these effects have been ignored for simplicity reasons. As such, the battery state of charge is calculated in terms of nominal capacity and not actual capacity. Battery aging does not affect battery performance in the short term, and so can be ignored. Using Equation 3-16, the SOC profile is computed stepwise over the driving cycle, starting from the initial SOC value.

In a typical discharge and charge operation in an HEV, the power flow to and from the battery can be modelled thus:

$$P_{batt}(discharge) = \frac{1}{\eta_{dis}}\ P_{electric} \qquad 3\text{-}17$$

$$P_{batt}(charge) = -\eta_{chg}\ \eta_{faradaic}\ P_{electric} \qquad 3\text{-}18$$

Equations 3-17 and 3-18 can be further expressed thus:

$$P_{batt}(discharge) = + \frac{1}{\eta_{dis}} \frac{1}{\eta_{motor}} P_{motor} \quad 3\text{-}19$$

$$P_{batt}(charge) = -\eta_{chg}\, \eta_{faradaic}\, \eta_{motor}\, P_{motor} \quad 3\text{-}20$$

η_{chg} and η_{dis} are assumed to be 80%, which is typical for lithium ion batteries (the battery in the study vehicle: see Appendix 1). The faradaic efficiency of the battery $(\eta_{faradaic} = 0.4)$ is assumed low to account for charge losses due to unproductive reactions.

The voltage across the battery terminals can be represented mathematically as:

$$V_{batt} = V_{oc} - I_{batt} R_{batt} \quad 3\text{-}21$$

Where V_{oc} is the open circuit voltage of the battery.

From Equation 3-21, the battery current (I_{batt}) and voltage (V_{batt}) can be related to its power using Equation 3-22 below:

$$P_{batt} = I_{batt}\, V_{oc} - {I_{batt}}^2 R_{batt} \quad 3\text{-}22$$

To derive the battery current, Equation 3-22 can be solved using the quadratic formula for battery discharge and recharge, as shown in Equation 3-23 and Equation 3-24, respectively:

$$I_{batt} = \frac{V_{oc}}{2R_{batt}} - \frac{\sqrt{{V_{oc}}^2 - 4R_{batt}\frac{1}{\eta_{dis}}\frac{1}{\eta_{motor}}P_{motor}}}{2R_{batt}} \quad 3\text{-}23$$

$$I_{batt} = \frac{V_{oc}}{2R_{batt}} - \frac{\sqrt{{V_{oc}}^2 - 4R_{batt}\,\eta_{chg}\,\eta_{faradaic}\,\eta_{motor}\,P_{motor}}}{2R_{batt}} \quad 3\text{-}24$$

By combining Equation 3-16 with Equation 3-23 and Equation 3-24, the evolution of the battery state of charge as a function of motor power can be expressed for battery discharge and recharge, as shown in Equation 3-25 and Equation 3-26, respectively:

$$SOC_{t+1} = SOC_t - \frac{V_{oc} - \sqrt{{V_{oc}}^2 - 4R_{batt}\frac{1}{\eta_{dis}}\frac{1}{\eta_{motor}}P_{motor_t}}}{2R_{batt}\,Q_{batt}} \quad 3\text{-}25$$

$$SOC_{t+1} = SOC_t + \frac{V_{oc} - \sqrt{{V_{oc}}^2 - 4R_{batt}\,\eta_{chg}\,\eta_{faradaic}\,\eta_{motor}\,P_{motor_t}}}{2R_{batt}\,Q_{batt}} \quad 3\text{-}26$$

3.5.7 SOC correction

Fuel consumption in an HEV is regarded as absolute only if it is charge-sustaining, i.e. the final SOC is equal to the initial SOC. For non-charge-sustaining journeys, an SOC correction procedure is required to estimate the fuel lost or gained due to non-charge sustenance, thus creating a paradigm for fair comparison of different HEV controllers. To make these estimations, Equation 3-27 is proposed and

applied to this study. Similarly, Equations 3-28 and 3-29 are defined to calculate the anticipated fuel savings in mass and percentage assuming charge sustenance.

$$FC_{savings\ deviation}(g) = \left(\left(\frac{SOC_{ref}}{2SOC_{ref} - SOC_f}\right)^{n_c} - 1\right) FC_{savings}(g) \quad \text{3-27}$$

$$FC_{savings\ _{charge\ sustaining}}(g) = \left(FC_{savings\ deviation}(g) + FC_{savings}(g)\right) \quad \text{3-28}$$

$$FC_{savings\ _{charge\ sustaining}}(\%) = \left(\frac{FC_{charge\ sustaining}\ (g)}{FC_{baseline}(g)}\right) 100 \quad \text{3-29}$$

Where:

$n_c = 1$ for charge-hoarding controllers

$n_c = 3$ for charge-depleting controllers

$n_c = 3$ is used in charge-depleting controllers to account for the charge losses and thus the fuel consumption penalties associated with battery recharge due to unproductive reactions.

There is an alternative approach to SOC correction, which involves using the lower heating value of fuel (J/g) to estimate the fuel mass differential for non-charge-sustaining controllers. However, the proposed approach is preferred as it takes in to account the performance of each controller in the estimation, and appropriately penalises charge-depleting controllers.

3.6 HEV model validation

The longitudinal simulation model of the study vehicle is validated in this subsection over the NEDC driving cycle. Rather than validating every subsystem in the vehicle, emphasis is laid on validating the vehicle's ability to:

1. Accurately track the driving cycle speed reference.
2. Accurately predict fuel consumption, which in this case is the optimisation cost function.

The experimental data used for the model validation was obtained via an NEDC transient test on a chassis dynamometer with the hybrid system turned off. For the sake of consistency, while obtaining the model validation data, the NEDC standard gear shift points were used both for experimental testing and model simulation.

3.6.1 Driver subsystem validation

The PID driver model's ability to follow the required vehicle speed trace is shown in Figure 3-7. The PID driver model is shown to command good track-ability over the NEDC, US06 and FTP-72 driving cycles, as shown in Figure 3-7a to Figure 3-7c respectively, despite the high level of aggressive driving characteristics which make up the US06 and FTP-72 driving cycles. Phasing of the driver tracking is believed to be the cause of the errors observed. These errors, though slightly significant, were found to have little or no effect on cumulative fuel consumption. As such, a further optimisation effort for the driver model was not necessary.

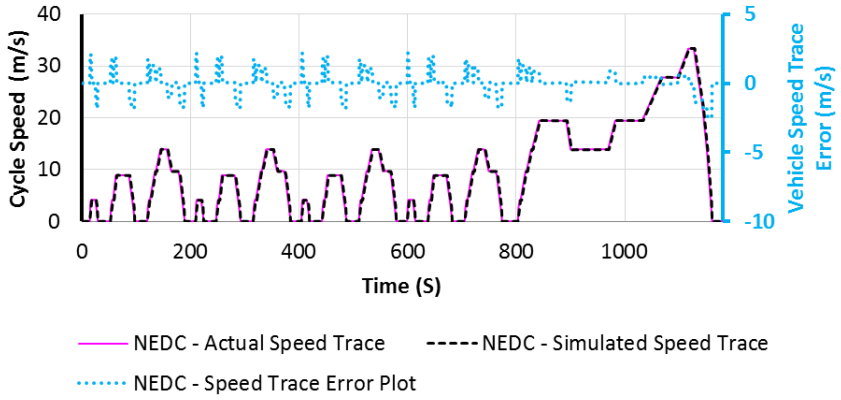

(a) NEDC driving cycle

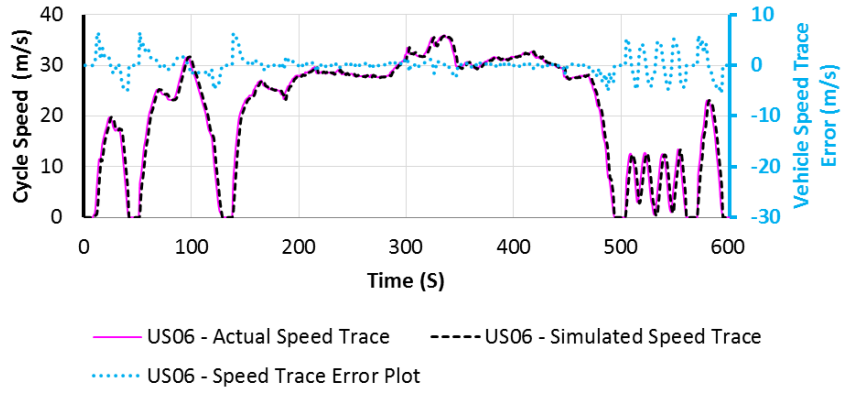

(b) US06 driving cycle

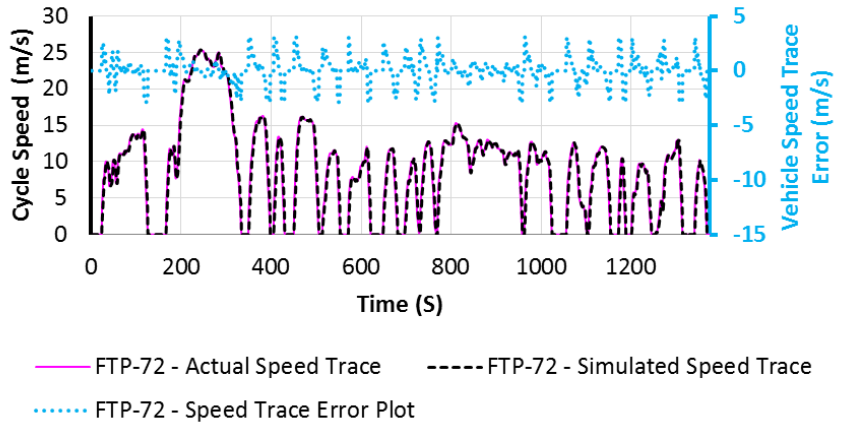

(c) FTP-72 driving cycle

Figure 3-7: PID driver tracking ability over the NEDC, US06 and FTP-72 driving cycle

3.6.2 Vehicle model baseline validation

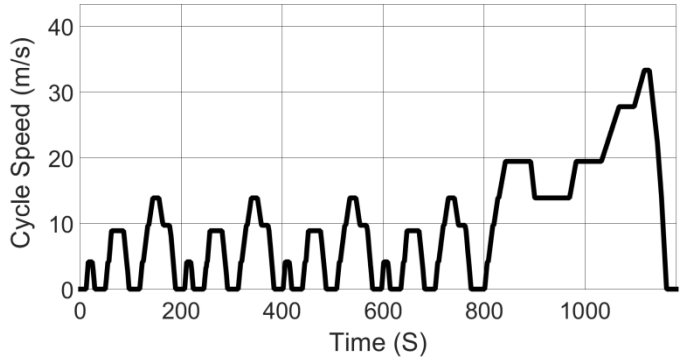

(a) NEDC driving cycle profile

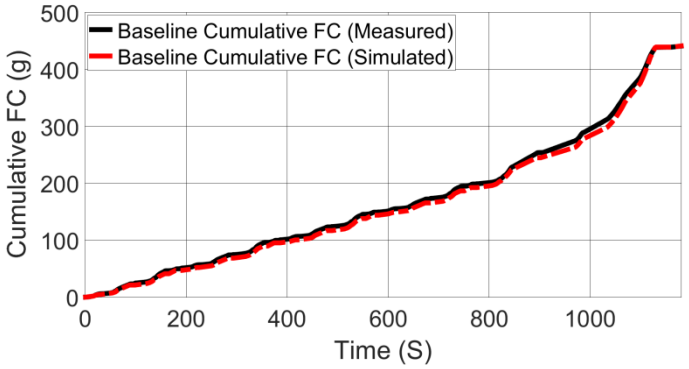

(b) Cumulative fuel consumption validation plot

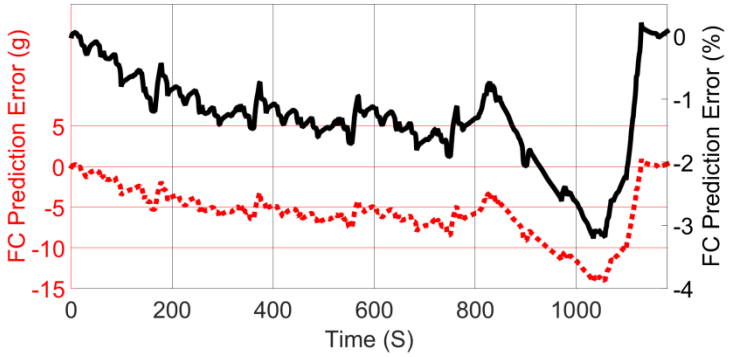

(c) Mass and percentage error in predicted fuel consumption

Figure 3-8: Model validation over the NEDC driving cycle

As shown in Figure 3-8b, the simulated baseline cumulative fuel consumption profile of the vehicle compares very closely to the experimentally obtained profile. A $\pm$3% error range in the model's predictability is observed over the NEDC driving cycle, as shown in Figure 3-8c.

3.7 Case studies

In the foregoing sections, a longitudinal model of the study vehicle is presented and validated. Validation results prove the fidelity of this model regarding the aspects of fuel consumption predictions and driving performance. The modularity of the proposed model is expected to allow substantial improvements, both at a component level and at a system level.

Building on the validated model, three case studies are undertaken in this section. At first, investigations are made into the impact of gear shift strategy on fuel consumption. Next, a novel and simple heuristic control strategy with no preview to prior driving information is developed and implemented with a view to better understand HEV dynamics, as well as identifying the most promising ICE operating points for fuel consumption minimisation. The resulting heuristic controller is analysed over different driving scenarios and appraised accordingly, with much emphasis on its performance gaps and opportunities for further improvements. The identified improvements are implemented in a modified heuristic controller, and its performance is then compared to that of the originally proposed heuristic controller over different driving scenarios. Finally, the impact of braking patterns on kinetic energy regeneration is investigated.

3.7.1 Impact of gear shift strategy on fuel consumption

In this section, the gear shift strategy proposed in section 3.5.4 is used to investigate the impact of up-shift RPM on baseline fuel consumption, as shown in Figure 3-9.

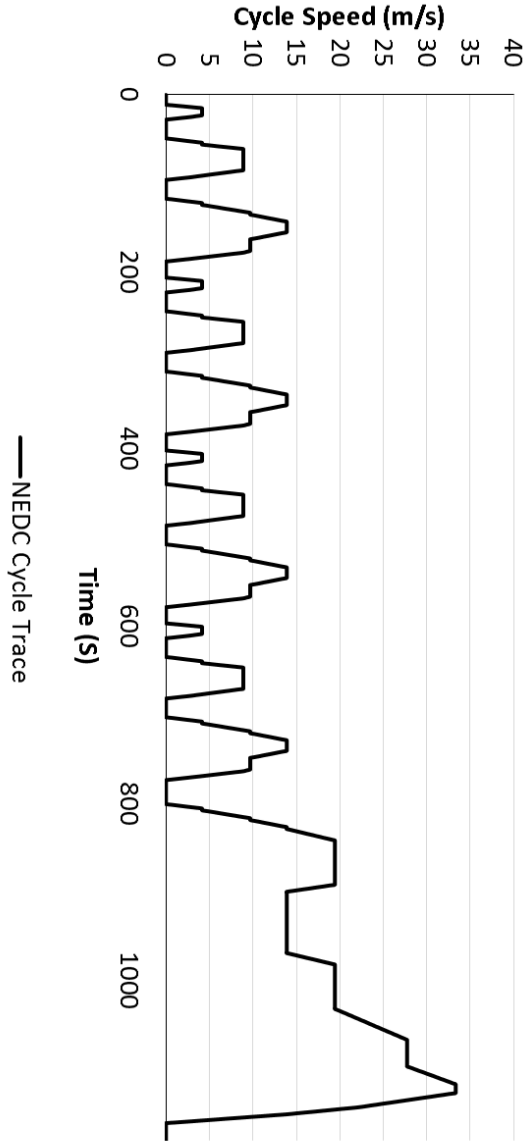

(a) NEDC driving cycle profile

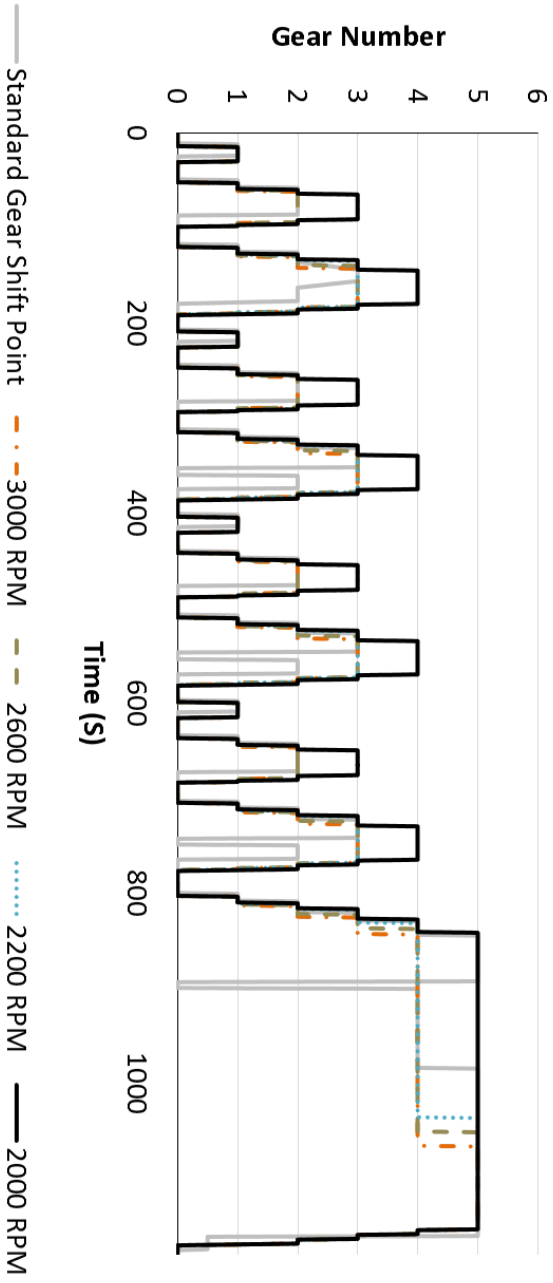

(b) Proposed NEDC gear shift schedule

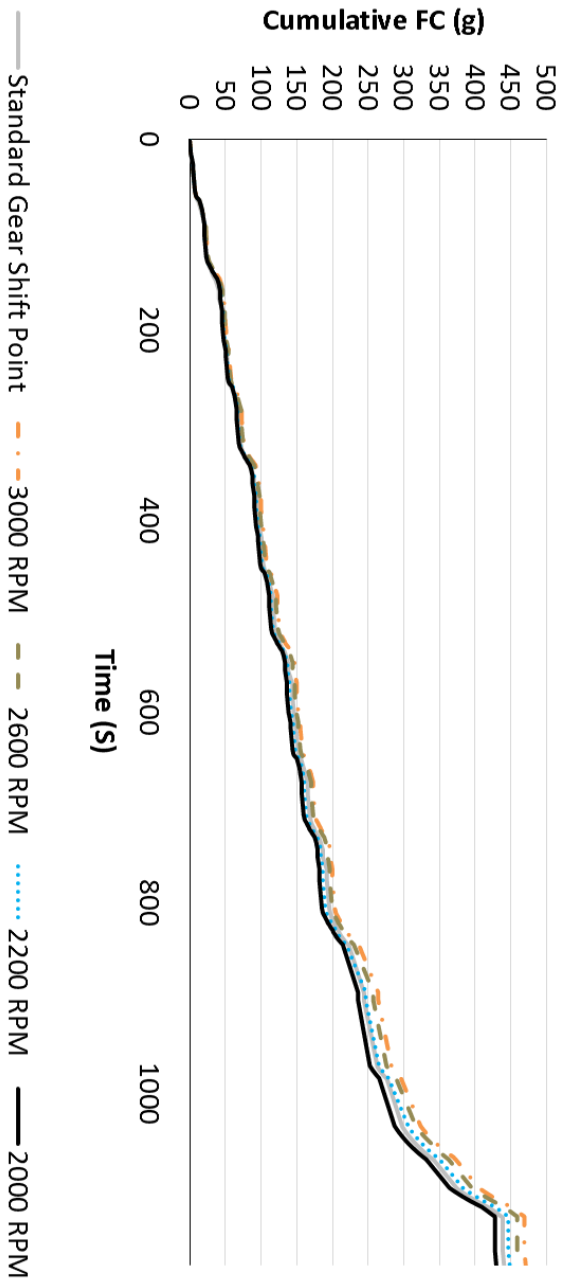

(c) Cumulative fuel consumption profile

Figure 3-9: Impact of upshift engine RPM on fuel consumption (NEDC)

This analysis shows a decrease in cumulative fuel consumption (Figure 3-9c) as the up-shift engine RPM decreases (Figure 3-9b). Whilst it is evident that a low upshift engine RPM will lead to lower fuel consumption, this advantage must be weighed against driveability constraints, such as meeting torque requirements and driver comfort. Compared to the defined NEDC standard shift strategy, this sensitivity analysis shows that a 2.5% fuel savings can be achieved using an early engine speed upshift.

3.7.2 Heuristic controller set up and simulation

This section aims to outline the design and implementation of a novel and simple heuristic power-assist control strategy on the research vehicle (a parallel HEV). In this control strategy, the internal combustion engine works as the main source of power, and the electric motor is used to supply power-assist to the engine during periods of high power demand, or supply additional power when the power demanded by the vehicle is greater than that which can be supplied by the engine. The electric motor is also used, depending on the battery state of charge, for regenerative braking. The online implementation of the power-assist heuristic control strategy is done using STATEFLOW, as will be explained and shown in the upcoming subsections.

Modelling a control strategy with STATEFLOW involves the use of states and transitions to form the basic building blocks of the system. The states of the controller decide the vehicle's operating mode. The transitions are requirements which must be met in order to permit the transition from one vehicle operating mode to the other.

The heuristic control strategy proposed makes use of a "charge non-sustaining" control logic in real time, as it does not guarantee the sustainability of battery state of charge at the end of the driving cycle. However, a lower and upper bound to the battery state of charge has been imposed on the controller to ensure better battery durability (lower bound: 40%, upper bound: 80%). For all simulations, a 60% battery state of charge is used as the initial battery energy level.

3.7.2.1 Control logic set up

As shown in Figure 3-10, the "vehicle power demand" input is used here as the global transition rule which dictates whether the HEV operates in traction mode, braking mode, or simply idles.

The global transition, as shown in Figure 3-10, can be expressed thus:

If $P_{demand} > 0$ *: Vehicle operates in traction mode*

If $P_{demand} == 0$ *: Vehicle idles*

If $P_{demand} < 0$ *: Vehicle operates in braking mode*

Figure 3-10 also outlines the inter-mode control logic, which governs how the electric motor is being utilised both for traction and for regenerative braking.

3.7.2.2 Braking mode controller

The heuristic control logic shown in Figure 3-10 has been modelled in such a way that during braking, the electric motor speed is used via a lookup table to estimate the maximum braking power capability of the electric motor at that instant (*"*P_{max_regen}*")*. The estimated value is then passed into the controller, where it is

used alongside the battery state of charge as proposed in Table 3-4 to decide the appropriate mode of braking:

Rule	**Activated mode**	**Resulting control action**
$P_{demand} < P_{max\_regen}$ & $SOC_t < SOC_{max}$	Regenerative braking	$P_{motor} = P_{demand}$
$P_{demand} \geq P_{max\_regen}$ & $SOC_t < SOC_{max}$	Regenerative braking and mechanical braking	$P_{motor} = P_{\max\_regen}$ $P_{mech\_brake} = P_{demand} - P_{max\_regen}$
$SOC_t \geq SOC_{max}$	Mechanical braking	$P_{mech\_brake} = P_{demand}$

Table 3-4: Heuristic braking control logic

3.7.2.3 Traction model controller

During the traction mode, a "switch parameter" (α_{sp}) is used alongside the battery state of charge to decide if the vehicle is to operate in any of the following modes:

(i) Engine only mode

(ii) Motor only mode

(iii) Assist mode

α_{sp} is determined outside the controller, and can be computed thus:

$$\alpha_{sp} = X_{pf}\ P_{motor_{max}} \qquad 3\text{-}30$$

Where X_{pf} is the "motor power allocation factor" (0.1 – 1).

Maximum motor tractive power varies with motor speed and as such can be estimated via a lookup table of (motor speed vs. maximum motor tractive power).

Computing α_{sp} using the method proposed in Equation 3-30 implies that the α_{sp} is a function of a known variable (maximum motor tractive power) and an unknown variable "X_{pf}" (motor power allocation factor), which can be optimally tuned over different driving cycles. The method used in determining a suitable value of "motor power allocation factor" for the heuristic controller will be discussed in the next subsection. Before then, it is important to understand the role "α_{sp}" plays in the traction mode controller. These details will be discussed in the rest of this subsection.

α_{sp} in this controller is an indication of the maximum level of power contribution the electric motor is allowed to make at any instant when the traction mode is active.

During traction mode, α_{sp} is used alongside the battery energy indicator (state of charge) to decide the appropriate power split between the electric motor and the internal combustion engine, as shown in Table 3-5.

Rule	**Activated mode**	**Resulting control action**
$P_{demand} < \alpha_{sp}$ & $SOC_t > SOC_{min}$	Motor only mode	$P_{motor} = P_{demand}$
$P_{demand} \geq \alpha_{sp}$ & $SOC_t > SOC_{min}$	Assist mode	$P_{motor} = \alpha_{sp}$ $P_{ICE} = P_{demand} - \alpha_{sp}$
$SOC_t \leq SOC_{min}$	Engine only mode	$P_{ICE} = P_{demand}$

Table 3-5: Heuristic traction control logic

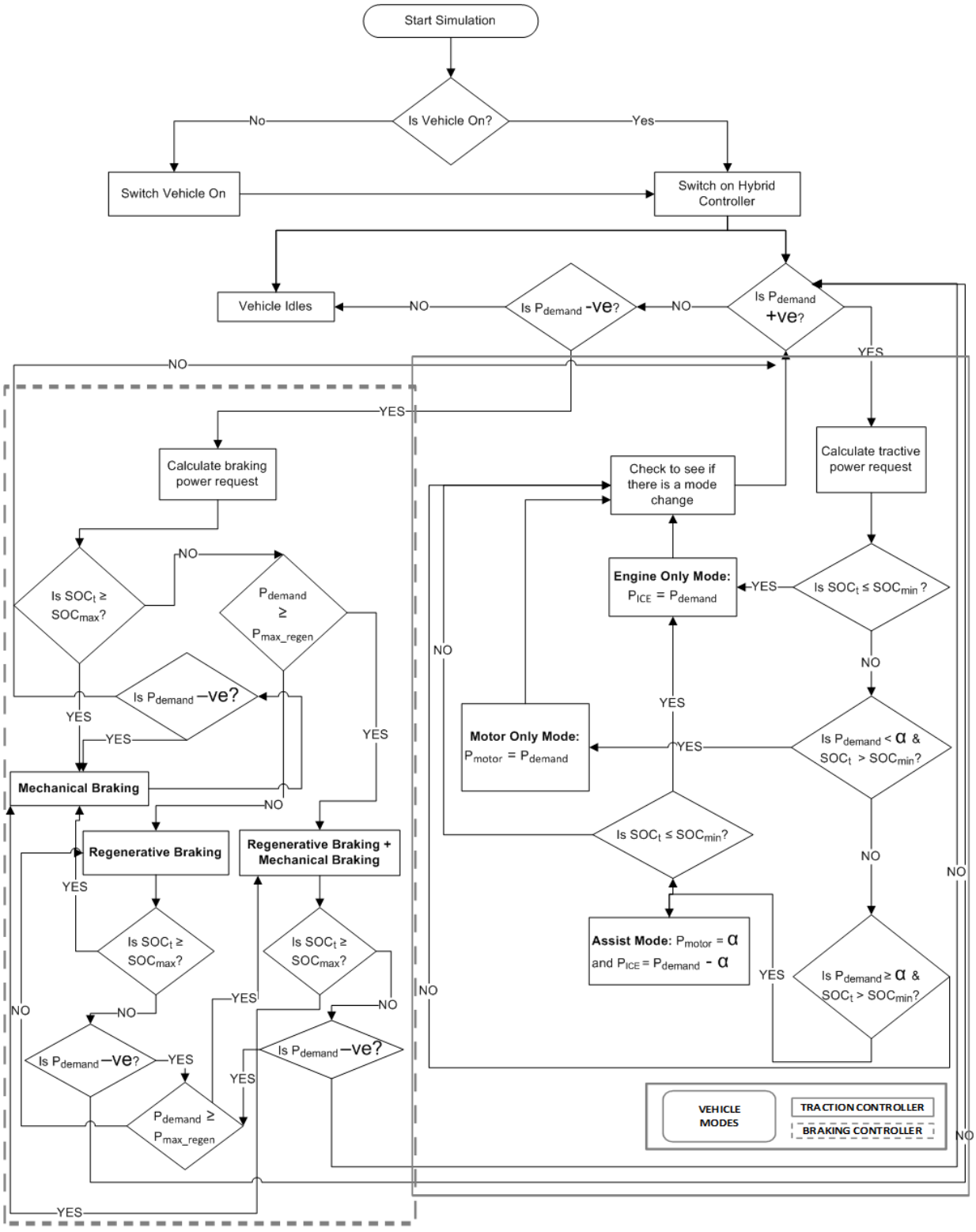

Figure 3-10: Heuristic control logic

3.7.2.4 Estimation of motor power allocation factor "$\boldsymbol{X_{pf}}$"

In section 3.7.2.3, the relevance of the "switch parameter" (α_{sp}) to the functionality of the proposed heuristic control strategy is outlined. This parameter, as shown in Equation 3-30, contains one known variable (maximum motor tractive power) and one unknown variable, "X_{pf}" (motor power allocation factor).

In order to estimate an appropriate value of "motor power allocation factor" for the proposed controller, a sensitivity analysis of its impact on cumulative fuel savings and battery state of charge was carried out over the NEDC, FTP-72 and JAPAN1015 driving cycles, as shown in Figure 3-11 - Figure 3-13. This analysis was made by simply running controller simulations for all values of "motor power allocation factor" and noting the corresponding percentage of cumulative fuel savings (%), final battery state of charge (%) and cumulative motor tractive energy (MJ) value in each case. The noted values are then used to plot the graphs shown in Figure 3-11 - Figure 3-13.

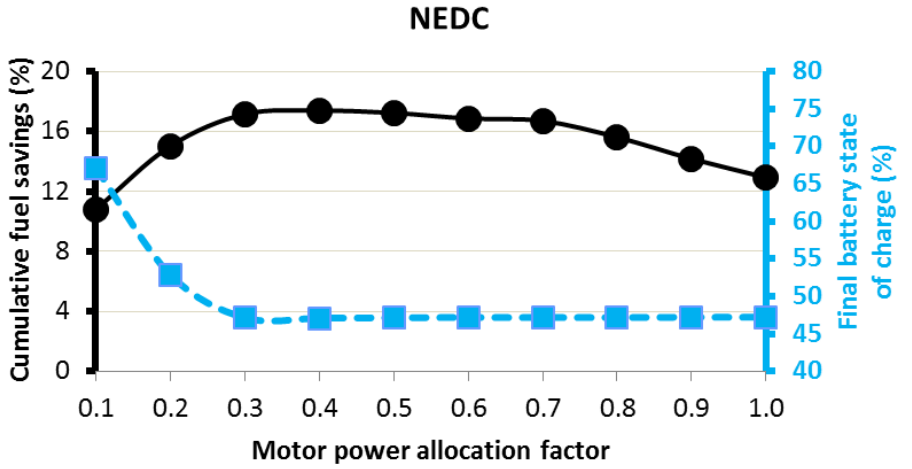

(a) Impact of motor power allocation factor on cumulative fuel savings and battery state of charge

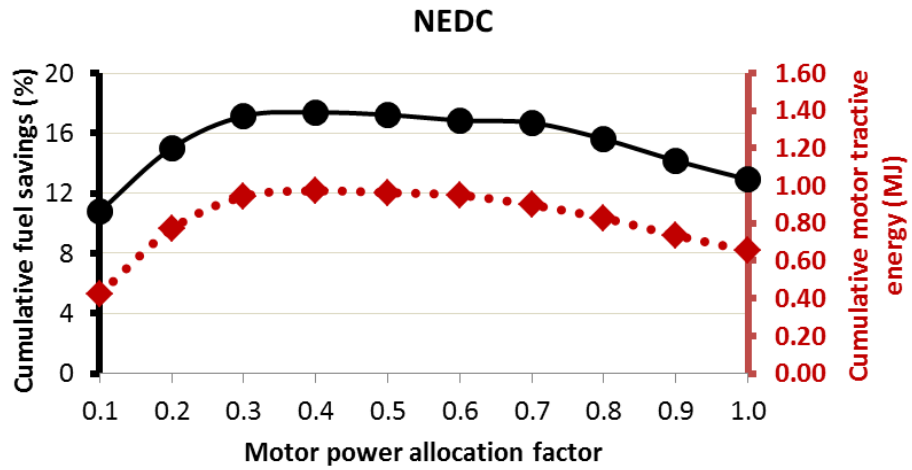

(b) Impact of motor power allocation factor on cumulative fuel savings and cumulative motor tractive energy

Figure 3-11: Motor power allocation factor analysis for the NEDC driving cycle

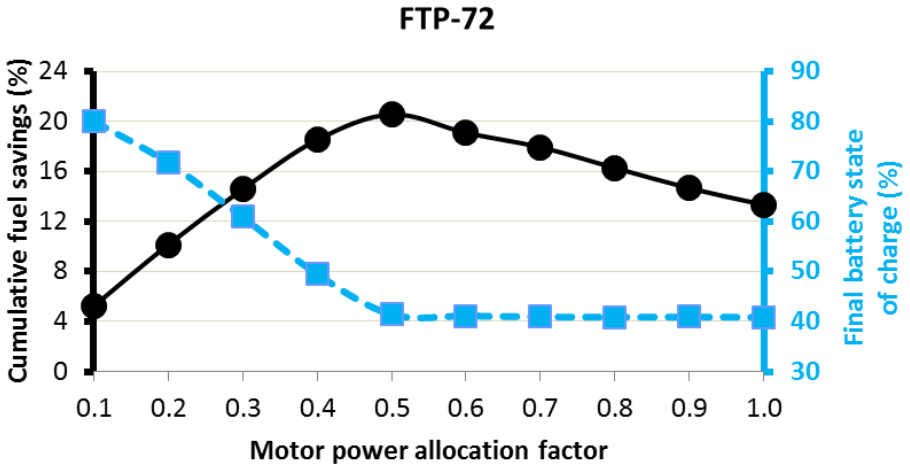

(a) Impact of motor power allocation factor on cumulative fuel savings and battery state of charge

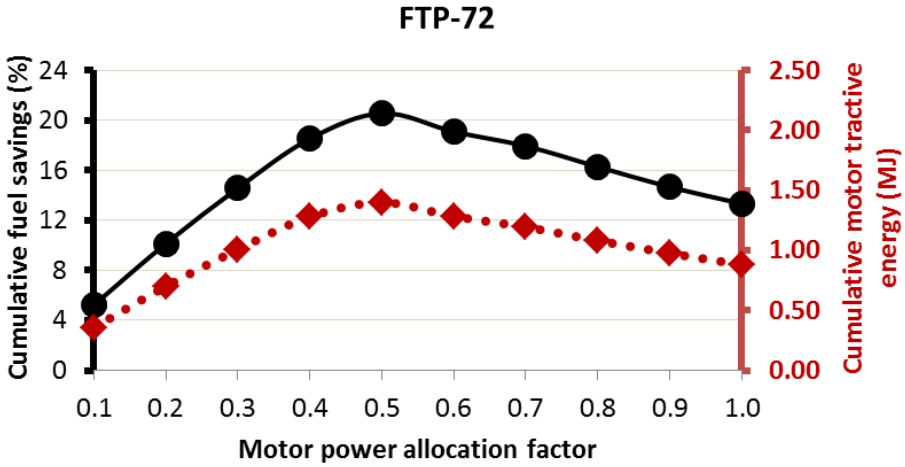

(b) Impact of motor power allocation factor on cumulative fuel savings and cumulative motor tractive energy

Figure 3-12: Motor power allocation factor analysis for the FTP-72 driving cycle

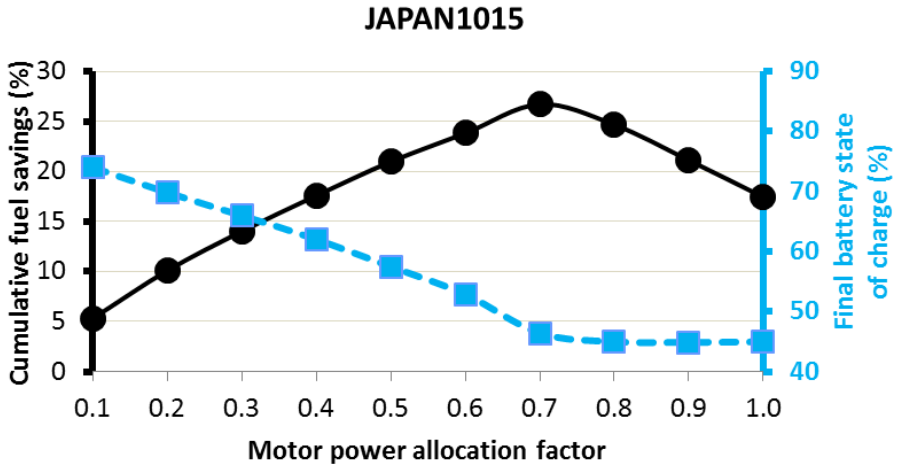

(a) Impact of motor power allocation factor on cumulative fuel savings and battery state of charge

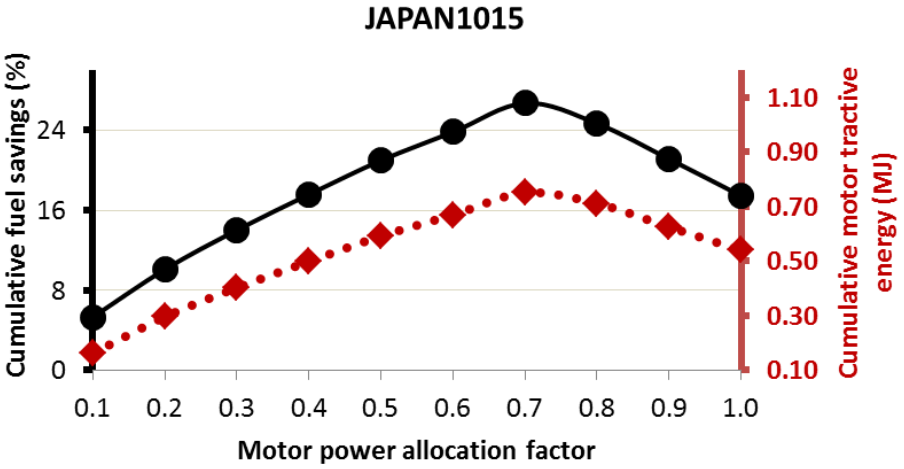

(b) Impact of motor power allocation factor on cumulative fuel savings and cumulative motor tractive energy

Figure 3-13: Motor power allocation factor analysis for the JAPAN1015 driving cycle

On all 3 driving cycles analysed, a decline in battery state of charge is observed for increased “motor power allocation factor”. This trend stems directly from the fact that as the motor power allocation factor is increased, the magnitude of motor power contributed at each instant of power assist also increases, thus leading to rapid instantaneous depletion in battery state of charge and a corresponding decrease in the final battery state of charge.

As shown in Figure 3-11b, Figure 3-12b and Figure 3-13b for the NEDC, FTP-72 and JAPAN1015 driving cycles respectively, an initial increase in “motor power allocation factor” corresponds to an increase in cumulative motor tractive energy and cumulative fuel savings. This trend is however reversed in each driving cycle once the peak cumulative motor tractive energy and peak cumulative fuel savings are reached, such that further increase in motor power allocation factor corresponds to a decrease in cumulative motor tractive energy and cumulative fuel savings. Saturation in instantaneous battery state of charge is believed to be responsible for the reversed trend observed in both cases. In this region, the rapid instantaneous depletion in battery state of charge associated with increased motor power allocation factor appears to be inhibitive to the overall motor tractive energy contribution. This happens due to fact that as the “motor power allocation factor” increases, the battery energy gets used up in a non-efficient way (cumulative fuel savings reduces further with increasing “motor power allocation factor”, while the battery state of charge remains the same after being depleted to the minimum level), quicker and earlier in the driving cycle. Consequently, there is no battery energy left to facilitate further use of the electric motor for the rest of the driving cycle.

From Figure 3-11 - Figure 3-13, it could also be inferred that for each driving cycle there exists a unique "motor power allocation factor" which simultaneously guarantees fuel savings and sustainability of battery state of charge over the entire driving cycle. A summary of the heuristic controller results under charge sustenance are detailed in Table 3-6.

Driving cycle type	Motor power allocation factor	Baseline cumulative fuel consumption (g)	Heuristic controller cumulative fuel consumption (g)	Cumulative fuel consumption savings (%)	Final battery state of charge (%)
NEDC	0.148	441.40	384.40	12.91	60.00
FTP-72	0.300	455.50	388.60	14.69	
JAPAN1015	0.447	184.09	148.80	19.17	

Table 3-6: Heuristic controller results under charge sustainability

Estimating this unique "motor power allocation factor" for different driving scenarios in real time is not possible, however, due to the iterative nature of the solution process. Despite this challenge, it is possible to obtain a single tuned "motor power allocation factor" which will, in real time, guarantee some fuel savings, whilst still minimising the difference between the initial and final battery state of charge.

In order to obtain this single value, the following steps were undertaken:

1. For each "motor power allocation factor", combine the cumulative fuel savings (%) values from all 3 analysed driving cycles (NEDC, FTP-72, JAPAN1015) and average them out.

2. For each “motor power allocation factor”, combine the final battery state of charge values from all 3 analysed driving cycles and average them out.
3. Using the derived results, create the graph shown in Figure 3-14.

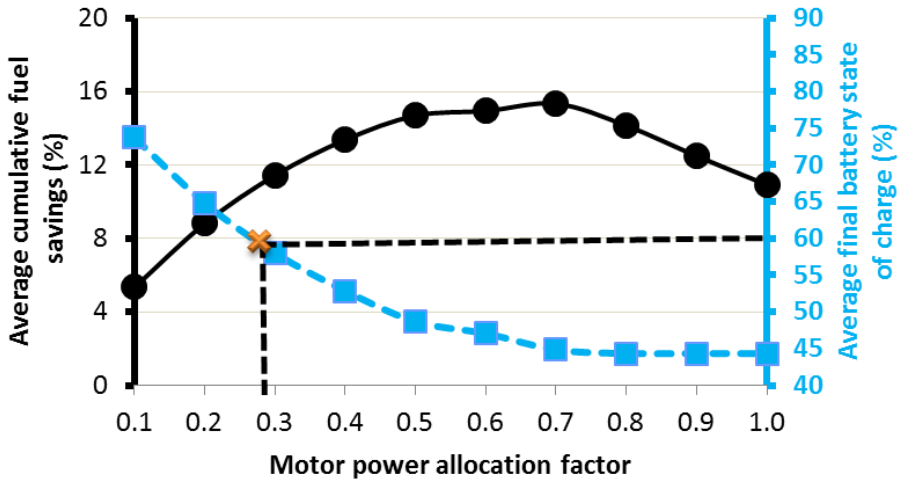

Figure 3-14: Impact of “motor power allocation factor” on average cumulative fuel savings and average final battery state of charge

From Figure 3-14, the appropriate “motor power allocation factor” which is applicable in real time to the proposed heuristic controller is decided on the basis of average final battery state charge sustenance to be 0.29.

3.7.2.5 Heuristic controller implementation and evaluation

In this section, the hybridisation potentials of the proposed heuristic control strategy is assessed over the NEDC, FTP-72 and JAPAN1015 driving cycles in real time, as shown in Figure 3-15 to Figure 3-17 and summarised in Table 3-7. In order to achieve this potential, the “motor power allocation” factor of 0.29, estimated in section 3.7.2.4, is applied to the controller in real time.

Observations from this simulation study can be summarised as follows, for different driving cycles:

NEDC driving cycle (Figure 3-15)

1. Over this driving cycle, the heuristic control strategy employed results in a hugely charge-depleting performance (SOC deviation of −13.02%).

JAPAN1015 driving cycle (Figure 3-16)

1. Gentle braking patterns are found to promote kinetic energy regeneration, thus resulting in significant increase of the battery SOC profile at each braking instant.
2. Over this driving cycle, the heuristic control strategy employed results in a charge-hoarding performance (SOC deviation of 66.35%).

FTP-72 driving cycle (Figure 3-17)

1 The aggressive braking patterns that characterised the FTP-72 driving cycle are found to be inhibitive to braking energy regeneration, thus leading to a narrow SOC range.

2 Over this driving cycle, the heuristic control strategy employed results in a near charge-sustaining performance (SOC deviation of 2.01%).

Driving cycle type	Motor power allocation factor	Baseline cumulative fuel consumption (g)	Heuristic controller fuel savings (g)	Cumulative fuel consumption savings (%)	Final battery state of charge (%)
NEDC	0.29	441.40	75.33	17.07	47.12
FTP-72		455.38	64.42	14.15	62.01
JAPAN1015		184.09	25.12	13.65	66.35

Table 3-7: Heuristic controller results with a "motor power allocation factor" of 0.29

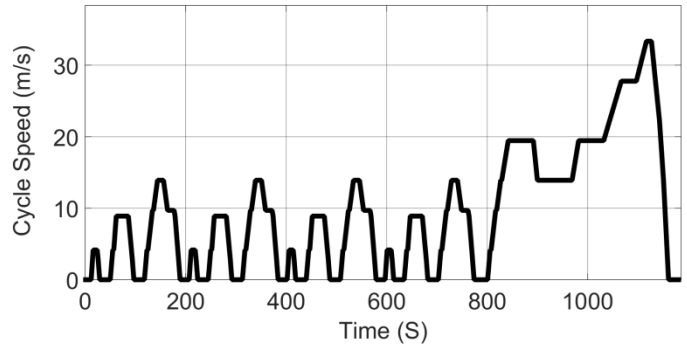

(a) NEDC driving cycle

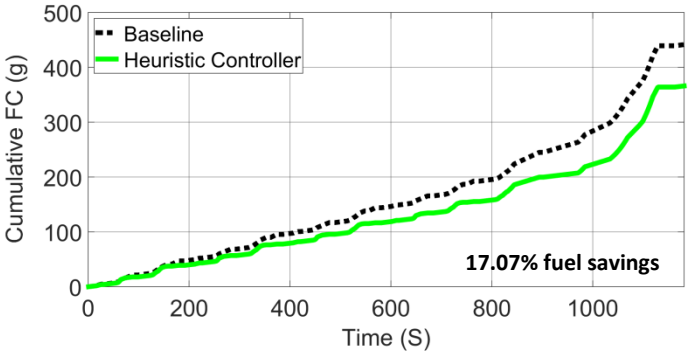

(a) Cumulative fuel consumption profile

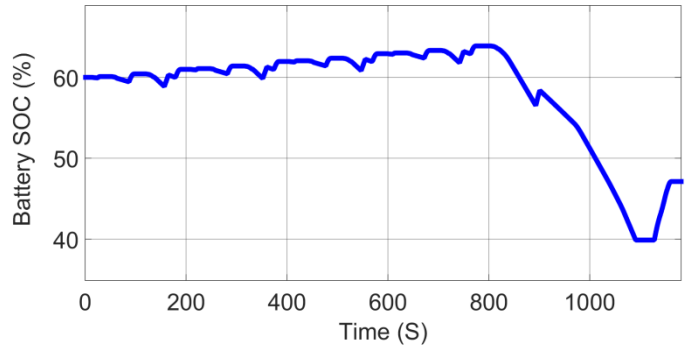

(b) Battery state of charge

Figure 3-15: Heuristic controller simulation results for NEDC driving cycle

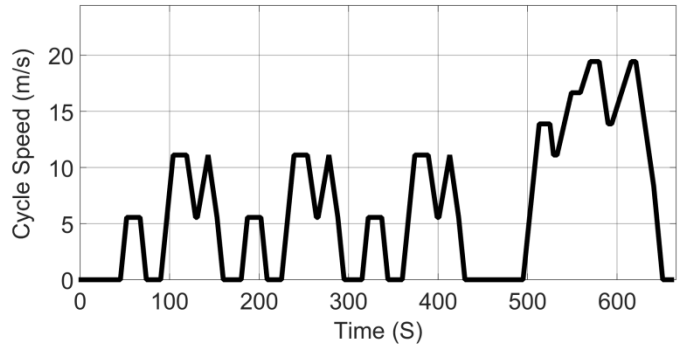

(a) JAPAN1015 driving cycle

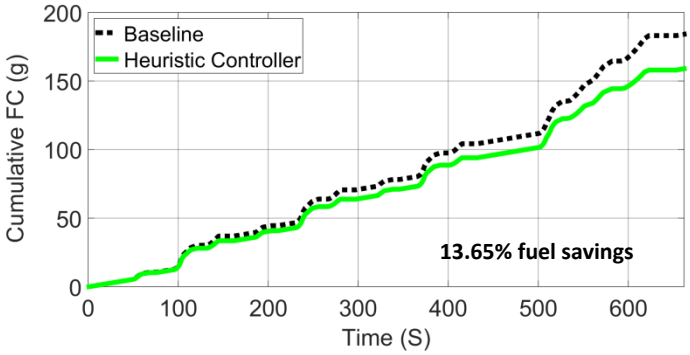

(b) Cumulative fuel consumption profile

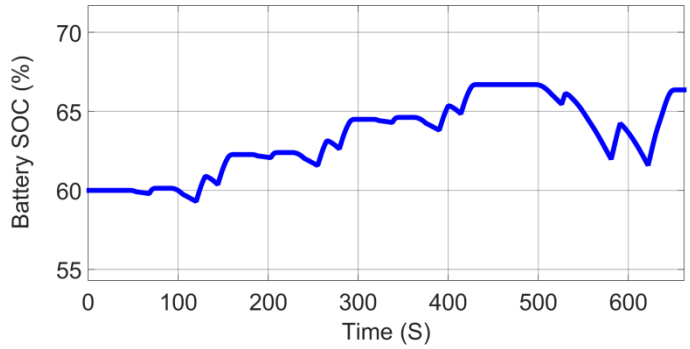

(c) Battery state of charge profile

Figure 3-16: Heuristic controller simulation results for JAPAN1015 driving cycle

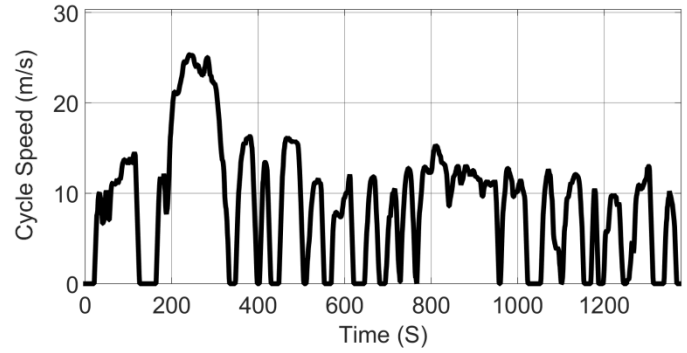

(a) FTP-72 driving cycle

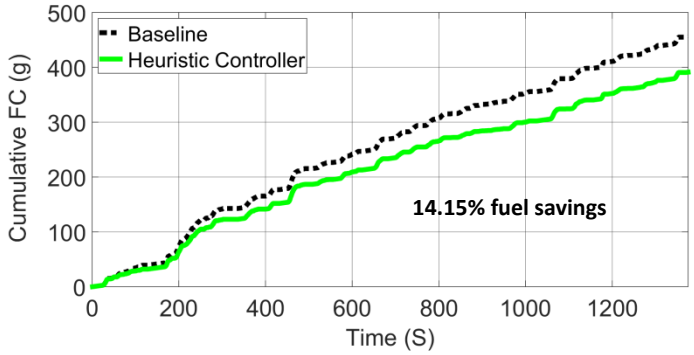

(b) Cumulative fuel consumption profile

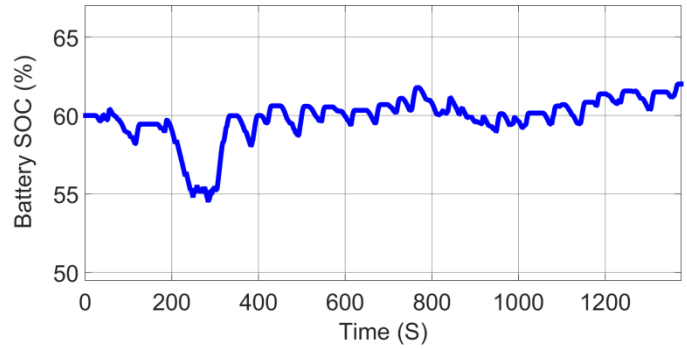

(c) Battery state of charge profile

Figure 3-17: Heuristic controller simulation results for FTP-72 driving cycle

Although the foregoing observations clearly infer that the proposed heuristic control strategy in its present form is unable to achieve the charge sustenance performance criterion defined in section 3.4.5, it however identifies two useful and interesting areas described below, for further investigation and possible improvement.

3.7.2.5.1 Heuristic controller performance gaps and areas for possible improvement

1. Over the NEDC and JAPAN1015 driving cycles, which are characterised by modal braking patterns, kinetic energy regeneration is found to be more significant. Sequel to this observation, the impact of braking patterns on kinetic energy regeneration will be quantitatively investigated in the succeeding section.
2. The non-charge-sustaining performance of the heuristic controller is as a result of inefficient use of braking energy over the driving cycle. In order to mitigate this problem, a two-step solution is proposed and subsequently implemented. The first step is a simulation study of different ICE operating points, with a view to identifying areas where significant fuel savings can be achieved at reduced battery SOC cost. The next step is the use of an SOC adaptation technique to regulate the "motor power allocation factor" online, such that the relative convenience of thermal and electric operation is impacted in a charge-sustaining manner. The resulting heuristic controller dubbed (HST-modified) is simulated and appraised accordingly over different driving scenarios.

3.7.2.6 Impact of braking patterns on kinetic energy recovery

When braking a vehicle from a speed of V_v(m/s) to a complete stop, the kinetic energy available for recovery can be characterised using Equation 3-31 below.

$$E_k = \frac{1}{2} m V_v^2 \qquad 3\text{-}31$$

This implies that irrespective of the braking deceleration, kinetic energy available for capture remains constant for each "initial braking speed" as shown in Figure 3-18.

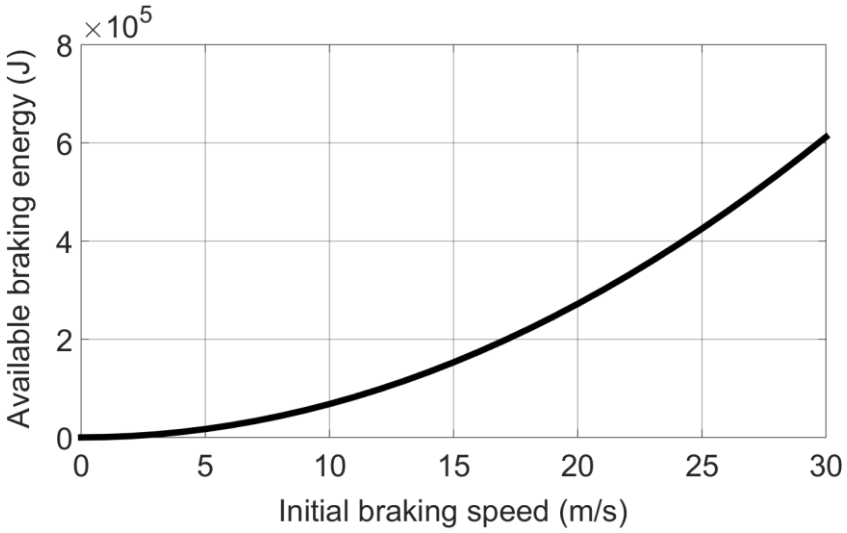

Figure 3-18: Available braking energy

With an objective of energy regeneration in mind, the imperative question then becomes: how best can braking be carried out so energy regeneration is optimised?

In order to address this problem, five braking patterns with different constant decelerations have been investigated, as shown in Figure 3-19.

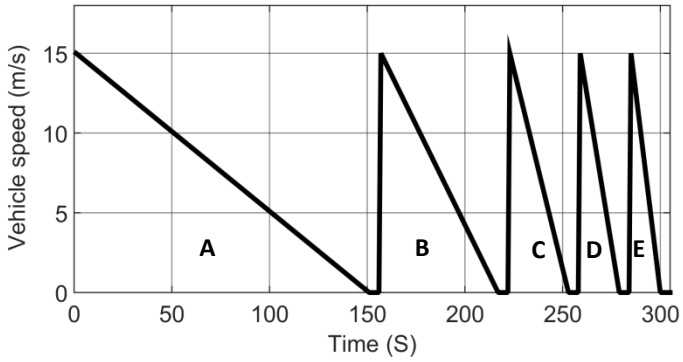

(a) Braking patterns

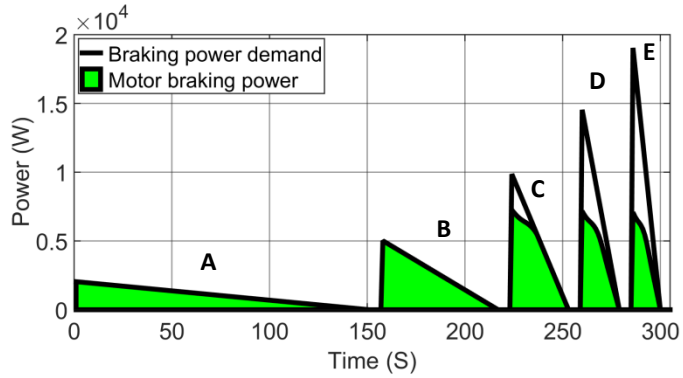

(b) Braking power distribution

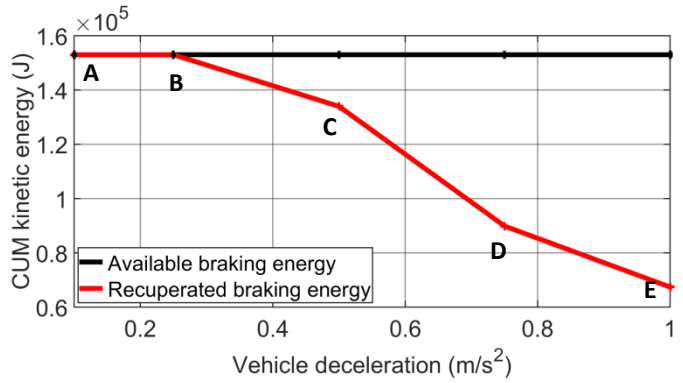

(c) Impact of vehicle deceleration on braking energy regeneration

Figure 3-19: Braking pattern analysis

The braking patterns considered, as shown in Figure 3-19a, represent vehicle braking from 15 m/s to 0 m/s under different constant rates of deceleration: A (0.10 m/s^2), B (0.25 m/s^2), C (0.50 m/s^2), D (0.75 m/s^2) and E (1.00 m/s^2). This implies that the kinetic energy available in each case is the same as shown in Figure 3-19c. Although in reality cars do not brake under constant deceleration, representing vehicle braking patterns in this manner is mainly for simplification reasons. This study also assumes an ideal regenerative braking system; as such, the only impedance to energy regeneration is the instantaneous power limit of the electric motor which varies with motor speed.

As shown in Figure 3-19c, an increase in vehicle deceleration beyond 0.25 m/s^2 corresponds to a decrease in kinetic energy regeneration by the electric motor. This trend can be understood by looking at Figure 3-19b. According to this figure, as vehicle deceleration increases, the braking time significantly reduces, however the instantaneous braking power demand increases significantly. Owing to limitations in the instantaneous braking power of the electric motor, increased energy loss is observed as vehicle deceleration increases.

The study presented in Figure 3-19 is further expanded in Figure 3-20 to feature a range of constant vehicle decelerations occurring at different initial vehicle braking speeds. Observations from this graph further confirm the inferences made in Figure 3-19, where for each initial vehicle braking speed, the percentage of kinetic energy regenerated decreases with increased vehicle deceleration. As shown in Figure 3-20, for most initial vehicle braking speeds, optimisation of braking energy regeneration is possible if braking occurs at deceleration rates below 0.5 m/s^2.

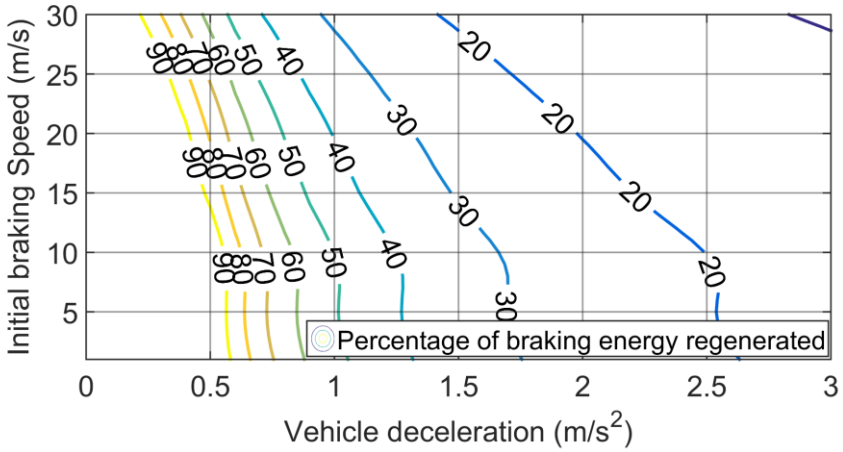

Figure 3-20: Impact of vehicle deceleration on braking energy regeneration

3.7.2.7 Heuristic controller improvements

3.7.2.7.1 Impact of vehicle operating points on fuel savings

This simulation study features a constant power-assist scenario occurring at different engine speeds, as shown in Figure 3-21. Observations from this plot show that increased engine speed at constant power demand and constant motor power supply is found to correspond to increasing fuel consumption. This is mainly because of the shift in engine operating point from an efficient high torque-low speed area to an inefficient low torque-high speed area, as shown in Figure 3-22. The latter operating region, though detrimental in terms of fuel consumption, does present the opportunity for significant fuel savings to be achieved at reduced battery SOC cost. This observation is notable in Figure 3-23 where for a constant motor power supply (approximate constant battery SOC), fuel savings is found to increase with increasing engine speed. The term “approximate” is used here to account for the slight deviations in the battery SOC caused by the difference in motor speeds across the different operating points. The foregoing observations

and inferences are assumed valid for other constant power demand and constant motor power supply operating points.

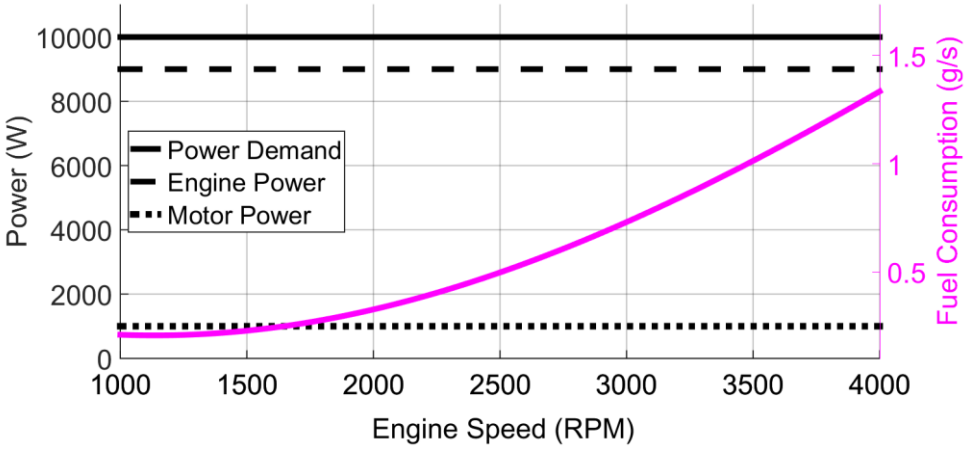

Figure 3-21: Impact of increasing engine speed, constant power demand and constant motor power supply on fuel consumption

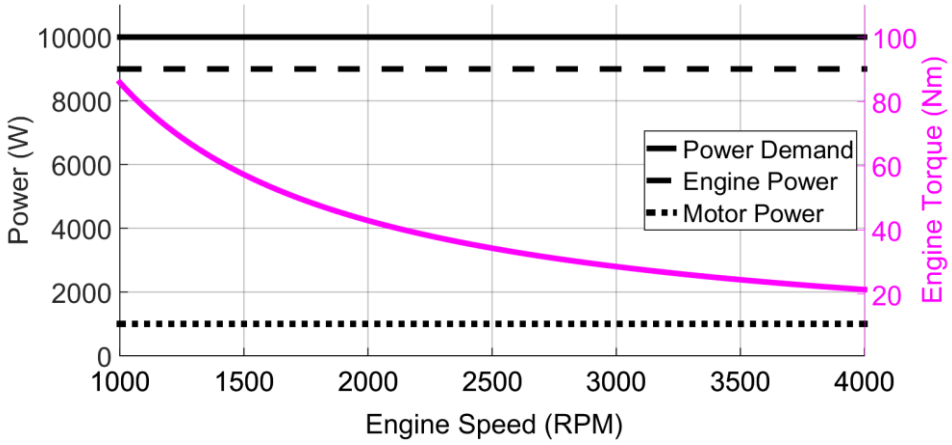

Figure 3-22: Impact of increasing engine speed, constant power demand and constant motor power supply on engine torque

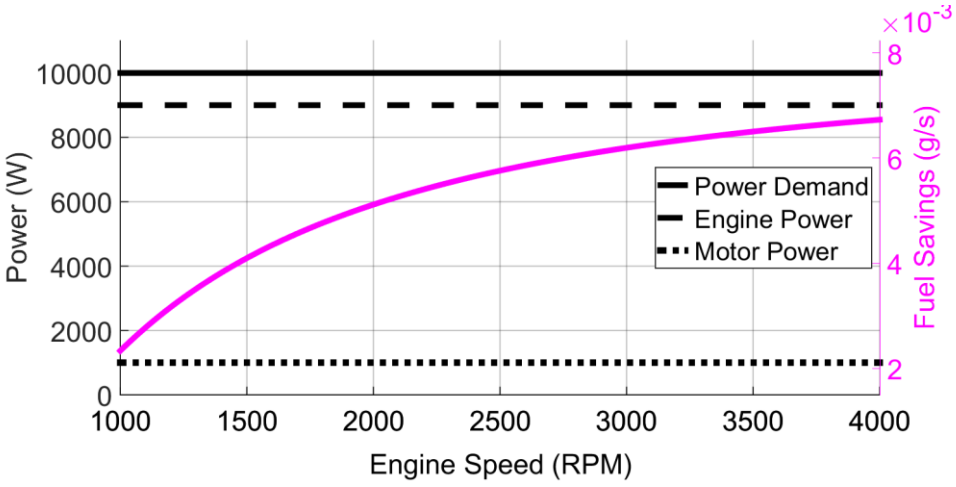

Figure 3-23: Impact of increasing engine speed, constant power demand and constant motor power supply on fuel savings

3.7.2.7.2 Implementation of improvements to the proposed heuristic control strategy

Building on observations from the simulation study detailed in section 3.7.2.7.1, 1,200 RPM is selected as the engine speed threshold for electric motor use. This selection is based particularly on the observation made in Figure 3-21. In this plot it could be observed that below 1,200 RPM, the fuel consumption curve asymptotes towards the idling fuel consumption value (0.12 g/s) where significant fuel savings is infeasible. The resulting modification implies that below 1,200 RPM an engine only operation is used, thus reserving the battery energy for use at more beneficial ICE operating points, where the ratio of fuel savings to battery SOC cost can be maximised.

Consequently, in the modified heuristic control logic (HST-modified), an engine only operation is activated when the battery SOC reduces beyond its minimum

permissible SOC threshold, as shown in Figure 3-10, or when the engine speed reduces below 1,200 RPM.

In order to properly regulate the battery SOC during and at the end of the driving cycle, an SOC based adaptation strategy is proposed in Equation 3-32 and applied to the modified heuristic controller. The proposed adaptation strategy ensures charge sustenance by adapting online the motor power allocation factor, thus impacting the relative convenience of thermal and electric operation.

$$X_{pf_{adapted}} = X_{pf} + X_{pf}\left(SOC_t - SOC_{ref}\right) \quad \text{3-32}$$

Where: $0.01 < X_{pf_{adapted}} < 1$ and $X_{pf} = 0.29$

3.7.2.8 Modified heuristic controller (HST-modified) evaluation

In this section, the performance of the modified heuristic control strategy is simulated and appraised accordingly over the NEDC, FTP-72, JAPAN1015, US06, LA92, ARTEMIS U130 and HWFET driving cycles (already introduced in Section 3.2) as summarised in Table 3-8. Simulation results from the originally proposed heuristic controller are included for comparative reasons, to highlight the importance of the implemented improvements.

In order to accurately compare the performance of different HEV control strategies, they must yield a perfectly charge-sustaining performance ($SOC_f = 60$). In a case where the controller is not perfectly charge-sustaining, an SOC correction is required to account for the fuel lost or gained due to non-charge sustenance. In this study, Equations 3-28 and 3-29 (section 3.5.7) are proposed for the SOC correction. Using these equations, the mass and percentage of anticipated fuel savings assuming charge sustenance is estimated for both strategies over different driving scenarios, as detailed in Table 3-8.

HST controller						
Driving cycle	**Baseline fuel consumption (g)**	**Cumulative fuel savings (actual) (g)**	**Final battery SOC (%)**	**Cumulative fuel savings (actual) (%)**	**Cumulative fuel savings (Assuming charge sustenance) (g)**	**Cumulative fuel savings (Assuming charge sustenance) (%)**
NEDC	441.40	75.33	47.12	17.07	38.13	8.64
FTP-72	455.38	64.42	62.01	14.15	66.65	14.64
JAPAN1015	184.09	25.12	66.35	13.65	28.10	15.26
US06	606.50	44.99	62.18	7.42	46.69	7.70
LA92	767.31	83.01	56.33	10.82	67.45	8.79
ARTEMIS U130	2221.40	212.67	46.81	9.57	106.06	4.77
HWFET	421.44	63.77	45.59	15.13	30.02	7.12

HST-modified controller						
Driving cycle	**Baseline fuel consumption (g)**	**Cumulative fuel savings (actual) (g)**	**Final battery SOC (%)**	**Cumulative fuel savings (actual) (%)**	**Cumulative fuel savings (Assuming charge sustenance) (g)**	**Cumulative fuel savings (Assuming charge sustenance) (%)**
NEDC	441.40	58.79	62.21	13.32	61.04	13.83
FTP-72	455.38	66.17	61.04	14.53	67.33	14.79
JAPAN1015	184.09	27.04	63.98	14.69	28.96	15.73
US06	606.50	45.51	62.31	7.50	47.33	7.80
LA92	767.31	81.75	61.79	10.65	84.27	10.98
ARTEMIS U130	2221.40	206.24	61.66	9.28	212.12	9.55
HWFET	421.44	38.25	63.97	9.08	40.96	9.72

Table 3-8: Simulation results for the HST controller and HST-modified controller over the NEDC, FTP-72, JAPAN1015, US06, LA92, ARTEMIS U130 and HWFET driving cycles

Table 3-10 presents a nomenclature-based comparison for both heuristic control strategies. By comparing the cumulative fuel savings assuming charge sustenance, both controllers are rated on the basis of efficiency, as detailed in Table 3-10. A controller is rated as "more efficient" if its cumulative fuel savings assuming charge sustenance is of higher value. Another comparative metric used in Table 3-10 is the "charge sustenance status" for each controller, which is defined in Table 3-9 below.

Final SOC value	**Charge sustenance status**
$SOC_f < 55$	"charge-depleting"
$55 < SOC_f < 59.95$	"near charge-sustaining"
$SOC_f = 60$	"charge-sustaining"
$59.95 < SOC_f < 60.05$	"near-perfectly charge-sustaining"
$60.05 < SOC_f < 65$	"near charge-sustaining"
$SOC_{final} > 65$	"charge-hoarding"

Table 3-9: Logic defining charge sustenance status

From the nomenclature-based controller comparison detailed in Table 3-10, it could be inferred that the modified heuristic controller (HST-modified) clearly outperforms the HST controller on the basis of charge sustenance and efficiency, over most of the driving cycles analysed.

	HST controller		HST-modified controller	
Driving cycle	**Charge sustenance status**	**Efficiency rating (Assuming charge sustenance)**	**Charge sustenance status**	**Efficiency rating (Assuming charge sustenance)**
NEDC	Charge-depleting	Less efficient	Near charge-sustaining	More efficient
FTP-72	Near charge-sustaining	Less efficient	Near charge-sustaining	More efficient
JAPAN1015	Charge-hoarding	Less efficient	Near charge-sustaining	More efficient
US06	Near charge-sustaining	Less efficient	Near charge-sustaining	More efficient
LA92	Near charge-sustaining	Less efficient	Near charge-sustaining	More efficient
ARTEMIS U130	Charge-depleting	Less efficient	Near charge-sustaining	More efficient
HWFET	Charge-depleting	Less efficient	Near charge-sustaining	More efficient

Key	Desired	Undesired

Table 3-10: Subjective performance comparison between the HST controller and the HST-modified controller over the NEDC, FTP-72, JAPAN1015, US06, LA92, ARTEMIS U130 and HWFET driving cycles

3.8 Chapter conclusions

This chapter presents detailed longitudinal quasi-static modelling and validation of a parallel HEV. Using the validated model, further analysis was carried out over the NEDC driving cycle to investigate the effect of gear shift strategy on cumulative fuel consumption. Results from this analysis showed that gear upshift at a lower engine speed saves more fuel than carrying out the same manoeuvre at a higher engine speed. However, legislative tests define gear change time in many cases. Gentle braking patterns were found to promote kinetic energy regeneration by the electric motor. Vehicle deceleration less than 0.5 m/s^2 was also found to optimise braking energy regeneration.

A simple heuristic control strategy which uses a tuneable parameter "motor power allocation factor" to decide the tractive power split between the electric motor and the internal combustion engine was modelled and applied to the parallel HEV. Based on simulation studies over the NEDC, JAPAN1015 and FTP-72 driving cycles, some performance gaps and thus improvement opportunities were identified and incorporated into a "modified heuristic controller".

A comparative study between the "heuristic controller" and the "modified heuristic controller", over the NEDC, FTP-72, JAPAN1015, US06, LA92, ARTEMIS U130 and HWFET driving cycles was undertaken. Simulation results prove the "modified heuristic controller" to be a better controller with a "more efficient" and "near charge-sustaining" performance over most driving cycles analysed.

Though easy to design, simple to implement in real time, and capable of impressive real-time charge-sustaining fuel savings, the "modified heuristic controller" and thus any heuristic controller is unable to guarantee optimality of

the cost function (fuel consumption). Without an optimal controller benchmark, it is impossible to fairly assess the performance of the "modified heuristic controller". As a result, the next chapter will aim to develop an HEV optimal controller with the assumption of full route preview information.

4 HEV OPTIMAL CONTROL WITH FULL ROUTE PREVIEW INFORMATION (A DYNAMIC PROGRAMMING-INSPIRED APPROACH)

4.1 Introduction

In the preceding Chapter, detailed longitudinal quasi-static modelling and validation of the research vehicle was presented. A simple heuristic energy management controller was also designed, implemented and simulated. By simulating the heuristic controller over different driving scenarios, possible improvement opportunities were identified and incorporated into the modified heuristic controller. In a simulation study, both controllers were compared over 7 different driving scenarios, and this proved the modified heuristic controller to be the superior controller in terms of “charge sustenance” and “efficiency”.

By definition, all heuristic controllers are “near-optimal” at best. Consequently, an optimal controller is required to serve as the ultimate performance benchmark. In this chapter, a theoretical framework for a dynamic programming-based optimal controller (with full route preview information) will be designed and evaluated over different driving scenarios. Though non-causal (requires the entire driving cycle to be known in advance) in nature, the optimal controller will be used subsequently in two ways. First, the simulation results will be used to benchmark the performance of other controllers. These results will then be formulated into a Markov chains model and used to develop a novel real-time near-optimal controller (causal) with an inherent optimal property. Comparative performance evaluations between the developed near-optimal controller and another

literature-based dynamic programming-inspired real-time controller will be undertaken over different driving scenarios.

4.2 Problem statement

Energy management in HEVs consists of determining the instantaneous operating mode and power split of the vehicle using a single control parameter. The scope of an optimal control strategy in an HEV is to determine the optimal power split between the energy sources on board (ICE and electric motor) over the driving horizon. The decision for what is optimal depends on the specific application; typically, the objective is to minimise fuel consumption, but could also be extended to include minimisation of pollutant emissions, maximisation of power delivery, driveability improvement, battery life durability, or a compromise among all these competing, but often conflicting goals.

Once a suitable optimisation cost function has been determined, the optimal control problem consists of minimising the total cost (an integral function) using a sequence of instantaneous actions. By definition, the optimal control problem assumes the availability of prior driving information and is therefore non-causal in nature.

4.3 Definition of optimal control problems for HEVs

The optimal control strategy is tasked with finding a control law for the HEV such that the total fuel consumption cost is minimised within the defined driving horizon. In this study, the sequence of control variables is represented by the instantaneous power distribution between the energy sources.

In more formal terms, the research vehicle can be considered as a generic dynamic system with the state as defined in Equations 4-1 and 4-2 respectively for the battery discharge and recharge operations. The state equation is an indication of the battery state of charge evolution as a function of the control policy (P_{motor_t}).

$$S\dot{O}C_t = -\frac{\frac{V_{oc}}{2R_{batt}} - \frac{\sqrt{{V_{oc}}^2 - 4R_{batt}\frac{1}{\eta_{dis}}\frac{1}{\eta_{motor}}P_{motor_t}}}{2R_{batt}}}{Q_{batt}} \quad 4\text{-}1$$

$$S\dot{O}C_t = -\frac{\frac{V_{oc}}{2R_{batt}} - \frac{\sqrt{{V_{oc}}^2 - 4R_{batt}\,\eta_{chg}\,\eta_{faradaic}\,\eta_{motor}\,P_{motor_t}}}{2R_{batt}}}{Q_{batt}} \quad 4\text{-}2$$

Similarly, the cost function can be expressed mathematically as follows:

$$C_{t+1} = \sum_{t=0}^{t_f-1} L\left(\omega_{ICE_t}, P_{motor_t}\right) \quad 4\text{-}3$$

Where t_f is the duration of the driving cycle, L is the instantaneous fuel consumption rate and C_{t+1} is the cost function (fuel consumption) to be minimised. ω_{ICE} is the engine speed. P_{motor} is the vector of control variables.

The cost function formulated in Equation 4-3 does not impose a charge-sustaining policy and, as such, the optimisation algorithm will tend to deplete the battery in order to attain minimal fuel consumption. Charge sustenance is imposed by adding a soft quadratic penalty to the overall cost function outlined in Equation 4-3, such that the new cost function for the charge-sustaining optimisation problem becomes:

$$C_{t+1} = \sum_{t=0}^{t_f-1} L\left(\omega_{ICE_t}, P_{motor_t}\right) + \emptyset(SOC(t) - SOC_f)^2 \qquad 4\text{-}4$$

Where SOC_f is the desired final battery state of charge at the end of the driving cycle and $\emptyset$ is the terminal cost (cost due to the final value of the state), which physically translates to the fuel lost or gained in order to attain charge sustenance. The soft quadratic penalty is a product of the terminal cost, and the square of the difference between the final battery state of charge and the desired battery state of charge.

In the absence of plug-in charging facilities on parallel HEVs, enforcing a charge-sustaining constraint at the end of the driving cycle ensures that the hybrid system is readily available for use at any time and that the durability of the battery (battery life) is increased via reduced depth of discharge (DOD). Battery life directly depends on the total energy throughput that its active chemicals can tolerate. Ignoring other ageing effects, the total energy throughput is fixed, such that 1

cycle of 100% DOD is roughly equivalent to 2 cycles at 50% DOD, 10 cycles at 10% DOD and 100 cycles at 1% DOD.

The aim of the optimisation is to find the optimal control variables P_{motor} (motor mechanical power) which minimises the total cost function "C_{t+1}" (Equation 4-1) over the entire driving cycle, as expressed in Equation 4-5.

$$P_{motor_t}{}^{*} = \arg\min \left[\sum_{t=0}^{t_f} L(\omega_{ICE_t}, P_{motor_t}) \right] \quad 4\text{-}5$$

Subject to the state and control constraints specified in Table 4-1.

Constraint	**Implication**
$P_{demand_t} \leq P_{motor_{max_t}} + P_{ICE_{max_t}}$	Power demand should not exceed the powertrain limits to avoid damage to the powertrain components.
$SOC_{min} \leq SOC_t \leq SOC_{max}$	The battery must operate within its safe limits.
$P_{motor_t} \leq P_{motor_{max_t}}(\omega_{motor})$	Instantaneous motor power must be lower or equal to the maximum permissible motor power at the current speed.
$P_{ICE_t} \leq P_{ICE_{max_t}}$	Instantaneous engine power must be lower or equal to the maximum permissible engine power at the current speed.
$SOC_{t_0} = SOC_{t_f} = SOC_f = 60$	The HEV operation must be charge-sustaining.

Table 4-1: Optimal control constraints

The foregoing constraints are imposed as hard constraints [140], which imply that infringing control variables are simply discarded. Conversely, the terminal cost "Ø" is imposed as a soft constraint which modifies the cost function, as shown in Equation 4-4, such that the final value of the constrained variable (battery state of charge) is close but not necessarily identical to the desired target. The electric motor used is relatively small in size. As such, the battery charge and discharge rate is not constrained.

The optimal control variables to be determined equal the number of time points of the driving cycle. With each time point having a continuous feasible range of candidate control variables, finding the optimal global solution within a reasonable simulation time is a difficult task. Dynamic programming is a well suited optimal technique that can yield global optimal solutions to energy management problems within a reasonable time frame, using a systematic approach [26, 44, 45, 47-49, 211].

4.4 Dynamic programming

4.4.1 Dynamic programming basis

The dynamic programming technique, originally proposed and defined by Richard Bellman, is a multi-stage numerical method applicable to discrete optimisation problems. It is based on a recursive procedure that starts with a small subset of the optimisation problem, and subsequently develops the solution to the whole problem.

As defined by Bellman, the principle of optimality can be expressed verbally thus:

> *An optimal control policy has the property that no matter what the previous decision (i.e., controls) have been, the remaining decisions must constitute an optimal policy with regard to the state resulting from those previous decisions [42].*

Consequently, the dynamic programming algorithm is a discrete multi-stage optimisation problem by which a decision based on the optimisation criterion (cost function) is chosen from a finite number of candidate decision variables at each time step.

Mathematically, the Bellman principle of optimality can be expressed as follows:

Considering the dynamic system introduced in Equations 4-1 and 4-2, of which the control policies are:

$$\pi = \left\{P_{motor_0}, P_{motor_1} \dots \dots \dots, P_{motor_{t_f-1}}\right\} \quad 4\text{-}6$$

The cost of the control policy π starting at SOC_0 can be represented as:

$$C_\pi(SOC_0) = L_{t_f}\left(\omega_{ICE_{t_f}}, P_{motor_{t_f}}\right) + \sum_{t=0}^{t_f-1} L_t\left(\omega_{ICE_t}, P_{motor_t}\right) \quad 4\text{-}7$$

Where $L_t\left(\omega_{ICE_t}, P_{motor_t}\right)$ is the transition cost at the state SOC_t with the control variable: P_{motor_t} and $L_{t_f}\left(\omega_{ICE_{t_f}}, P_{motor_{t_f}}\right)$ is the terminal cost that represents the penalty cost for deviating from the final desired battery state of charge.

The optimal control policy defined in Equation 4-9 is the policy that minimises the cost function in Equation 4-7, as per the optimisation criterion in Equation 4-8.

$$C^*(SOC_0) = \min_{\pi} C_\pi(SOC_0) \quad 4\text{-}8$$

$$\pi^* = \left\{P_{motor_0}{}^*, P_{motor_1}{}^* \dots\dots\dots, P_{motor_{t_f-1}}{}^*\right\} \quad 4\text{-}9$$

Proceeding backwards in time, the cost $C_0(SOC_0)$ generated at the last time step, is equal to the optimum cost (minimum cost) $C^*(SOC_0)$. In other words, it is possible to determine the optimal sequence of control policies proceeding backwards from the final state, choosing at each step the path that minimises the cost-to-go (integral cost from that time step until the final state).

Bellman's dynamic programming algorithm can be applied using two methods: the backward recursive method and the forward method. In the backward recursive method, the optimal sequence of control variables is obtained proceeding backwards from the final state and choosing at each time step the path that minimises the cost-to-go (Integral cost from that time step until the final state). By

symmetry, most dynamic programming problems solved using the backward recursive method could also be solved using the forward dynamic programming technique. Although both techniques do lead to the same set of optimal control policies for the entire problem, there is a difference in the "by-products" produced by both methods. When solving a problem using the backward dynamic programming technique, the by-products obtained are the optimal values from every state in every stage to the end; whereas in solving a problem using forward dynamic programming, the corresponding by-products would be the optimal values from the initial state(s) in the first stage to every state in the remaining stages.

4.4.2 Dynamic programming offline numerical implementation in HEVs

Numerical implementation of dynamic programming to solve energy management problems in HEVs involves three important steps: (1) calculation of the cost matrix, (2) calculation of the control-time grid, and (3) calculation of the state-time grid, all of which are discussed elaborately in the following subsections.

4.4.2.1 Calculation of cost matrix

As defined in Section 4.3, electric motor mechanical power is used as the control variable in this study. Consequently, the control vector consists of a set of discrete feasible control variables (resolution of 0.01kW) applicable at each time step. The control variable resolution is selected minute enough, to guarantee a computationally efficient optimisation routine, whilst ensuring that the control policies do not get trapped in a local optimum.

Mathematically, the control vector can be expressed as follows:

$$P_{motor_{\{admissible\ set\}}} = P_{motor_{min}} : P_{motor_{resolution}}(0.01kW) : P_{motor_{max}} \quad 4\text{-}10$$

Once the grid of possible power splits or solution candidates are created for each time step, the procedure outlined in Section 4.4.2 can be applied, by associating a cost to each solution candidate, thus producing a cost matrix of size $N_{P_{motor\{admissible\ set\}}} \times N_t$. Proceeding backwards from the end of the driving cycle, the optimal cost-to-go is calculated for each grid point. At the end of the driving cycle, the path with the lowest total cost (integral cost-to-go) represents the optimal solution. During the dynamic programming routine, constraints to engine operating points are implemented in the form of adjustments to the cost function as detailed in Table 4-2.

Event	**Fuel consumption cost**	**Reason**
$P_{demand} > 0$ & $P_{motor} = P_{demand}$	0.12 g/s	Engine idling
$P_{demand} = 0$	0.12 g/s	Engine idling
$P_{demand} < 0$	0 g/s	Vehicle braking therefore fuel has been cut off
$T_{ICE} > T_{ICE_{max}}$ $\omega_{ICE} > \omega_{ICE_{max}}$ $\omega_{ICE} < \omega_{ICE_{min}}$ $P_{demand} > P_{motor} + P_{ICE}$ $P_{ICE} < 0$	Infinite cost	Infeasible operating area

Table 4-2: Cost adjustments during dynamic programming

4.4.2.2 Grid set up

For dynamic programming, two main grid set ups (detailed below) are necessary.

1. Control-time grid
2. State-time grid

The time grid "t" has the same length as the duration of the driving cycle. The control-time grid is defined in Equation 4-10. The state-time grid is made of a vector of feasible discretised battery state of charge, which can be expressed mathematically as follows:

$$SOC_{admissible\ set} = SOC_{min} : SOC_{resolution}(0.001) : SOC_{max} \quad \text{4-11}$$

The state resolution is selected minute enough, to avoid state approximation errors.

4.4.2.3 Dynamic programming routine

An illustrative model of the dynamic programming routine using the backward recursive approach is shown in Figure 4-1. The nodes (a, b, c etc.) refer to the "state-time grid nodes".

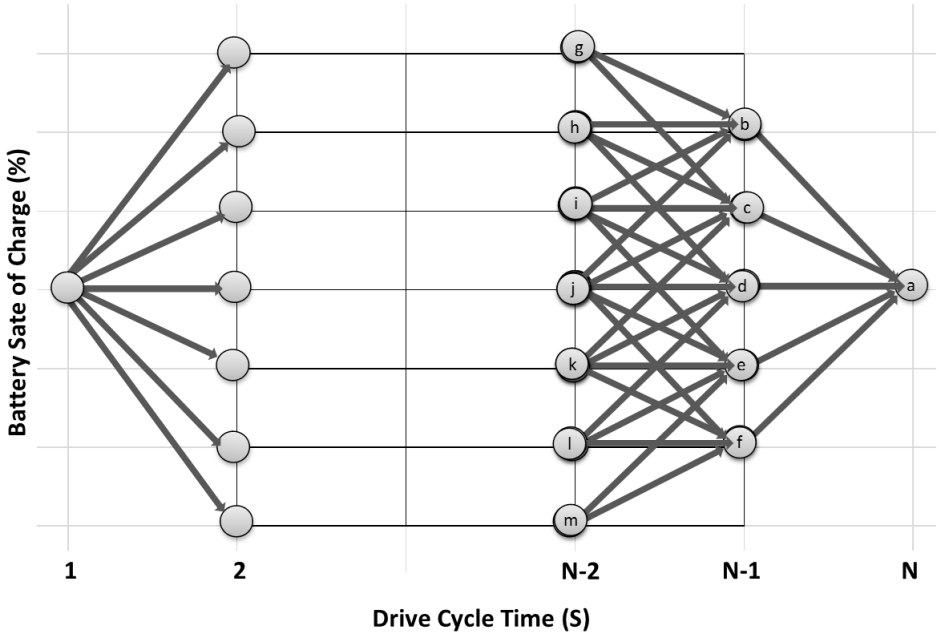

Figure 4-1: Dynamic programming implementation to an HEV

At each node (a, b, c etc.), the minimum cost-to-go to the final state is stored alongside the corresponding control variable(s).

At the start of the simulation, an infinite cost-to-go is applied at each node of the state-time grid. Starting from the last time step "N" and working backwards in time, a cost-to-go value of "0" is applied at node "a". It is important to note that this new cost-to-go will replace the pre-populated infinite cost-to-go, which was applied by default to all nodes. At time step "N-1", the admissible set of the control variables defined in Equation 4-10 is applied to all the states starting from the state at node "b". The control cost in each case is read off the pre-computed

cost matrix. The control variable which offers the least cost from the state at node "b" time step "N-1" to the state at node "a" in the final time step "N" is stored at node "b" alongside its corresponding cost. Still at time step "N-1", the same procedure is applied sequentially to nodes c, d, e, f and the corresponding control variable which offers the least cost from the state at each of those nodes to the state at nodes "a" is stored alongside the corresponding cost at the respective nodes. The cost value stored at node b, c , d, e, f at this point is known as the cost-to-go to the final state which is the same as the cost-to-go to node "a". At time step "N-2" starting from the state at node "g", the control variable which leads to a state transition from the state at node "g", time step "N-2" to the state at node "b", time step "N-1" is stored alongside its corresponding cost at node "g".

The optimal cost-to-go from node "g" to node "a" via node "b" is calculated as follows:

$$C_{optimal\ cost-to-go_{node\ (g,b,a)}} = C_{node\ (g\ to\ b)} + C_{optimal\ cost-to-go_{node\ (b,a)}} \quad 4\text{-}12$$

This procedure is also applied for transitions from node "g" to node "a" via nodes c, d, e, and f, and each time there is a lower cost-to-go leading from node "g" to node "a" via any of the other intermediate nodes c, d, e and f, the cost and control variables for such a path are updated at node "g". The updated cost is known as the new optimal cost-to-go from node "g" to node "a". The same process is applied to the rest of the nodes at time step "N-2" e.g. h, i, j, k, l, m and the optimal cost-to-go from these nodes at time step "N-2" to node "a" at time step "N" is saved at each of the respective nodes alongside the corresponding control variables. This procedure is applied to all other time steps until the final time step

of “t=1” is reached, thus ensuring that all possibilities have been checked for each time step. By definition, the optimal control policy is therefore the set of control variables resulting in the optimal cost-to-go from the “initial state” at time step “t=1” to the “final state” at time step “t=N”.

In this study, the foregoing recursive approach is implemented below, using the “generic dynamic programming tool” developed by Sundstrom *et al.* [212].

At step $t_f - 1$

$$C_{t_f-1}{}^{*}\left(SOC\left(t_f - 1\right)\right)$$

$$= \underset{P_{motor}}{min}{}_{t_f-1}\left[L(SOC\left(t_f - 1\right), P_{motor}\left(t_f - 1\right)) + \emptyset(SOC(t_f) - SOC_f)^2\right]$$

At step t for $0 \leq t \leq t_f - 1$

$$C_t^*(SOC(t)) = \underset{P_{motor}(t)}{min}\ [L(S0C(t), P_{motor}(t)) + C_{t+1}^*(SOC(t+1))]$$

Where t_f is the duration of the driving cycle.

4.4.3 Dynamic programming real-time implementation issues

Dynamic programming offers a mathematically global optimal solution to HEV energy management problems. Despite yielding globally optimal results, the dynamic programming procedure is non-causal and thus inherently offline for two main reasons:

1. The solution has to be calculated backwards, and therefore necessitates prior knowledge of the entire driving cycle.
2. It is a computationally heavy procedure, requiring huge computational time and space. In dynamic programming, the state-time grid size can be regarded as a tuning parameter in the sense that a high number generates a finer quantisation, and therefore a solution closer to that of the continuous optimum, but also increases the total computational and memory requirement of the algorithm. The high memory requirement is in fact more limiting, considering the need to store the optimal cost-to-go matrix at the "state-time grid nodes".

Despite these shortcomings, dynamic programming results can be used for benchmarking the performance of other causal or real-time implementable control strategies. These results can also be used as a guide for the development of real-time sub-optimal controllers with some inherent optimal properties. Both of these derivatives of dynamic programming are of interest, and will be explored further.

4.5 Dynamic programming optimal controller evaluation

In this section, simulation results obtained from the offline implementation of dynamic programming over the NEDC, FTP-72, JAPAN1015, US06, LA92, ARTEMIS U130 and HWFET driving cycles (already introduced in Section 3.2) are reported. Although all 7 driving cycles are analysed, only 4 of them (FTP-72, US06, ARTEMIS U130 and HWFET driving cycles) with distinct trends are discussed in detail. These 4 driving cycles are selected on purpose to represent 1 urban (FTP-72 driving cycle) and 3 highway (US06, ARTEMIS U130 and HWFET driving cycles) driving scenarios. This ensures that observed trends could be crosschecked for repeatability. For convenience, the term “power split ratio” (PSR) is introduced subsequently, and represents the ratio of motor power to vehicle power demand.

Over the FTP-72 driving cycle (Figure 4-3a), which represents a “moderate” urban driving scenario (Table 3-2), a narrow battery SOC range is observed (Figure 4-3c). This trend is believed to be as a result of the aggressive braking patterns that characterises the FTP-72 driving cycle. As previously discussed in Section 3.7.2.6, as vehicle deceleration increases, the braking time significantly reduces. However, the instantaneous braking power demand increases significantly. Due to limitations in the instantaneous braking power of the electric motor, increased energy loss is observed as vehicle deceleration increases. Consequently, this limits the battery SOC increase, and therefore the availability of battery energy for future motor use.

Over the FTP-72 driving cycle an even distribution of power split ratios is observed, as shown in Figure 4-2. The “power split ratio” however decreases with increasing power demand. The former trend is believed to be as a result of the “moderate”

nature of the FTP-72 driving cycle, which implies that a significant amount of its tractive power demand can be met by the electric motor. This results in an ultimate fuel savings potential of 16.63% (75.72g of fuel), as shown in Figure 4-3b. The latter trend is believed to be as a result of the electric motor tractive power limitation which increases with increased power demand.

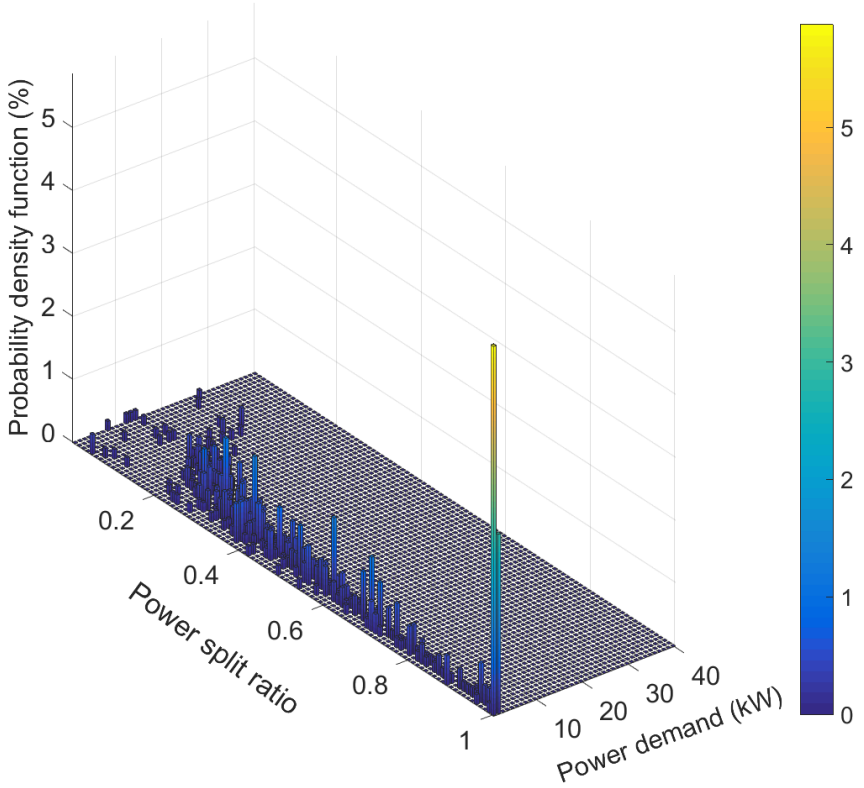

Figure 4-2: Percentage distribution of power split ratios over the FTP-72 driving cycle

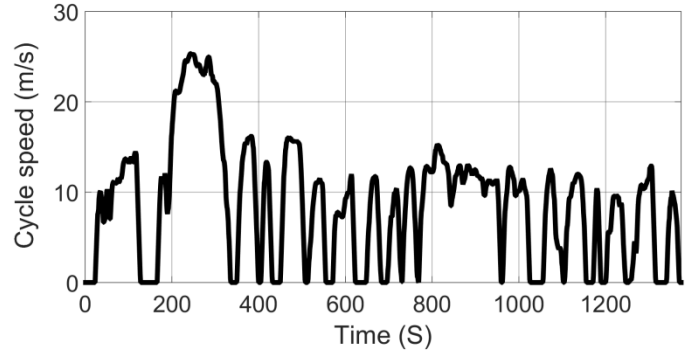

(a) FTP-72 driving cycle

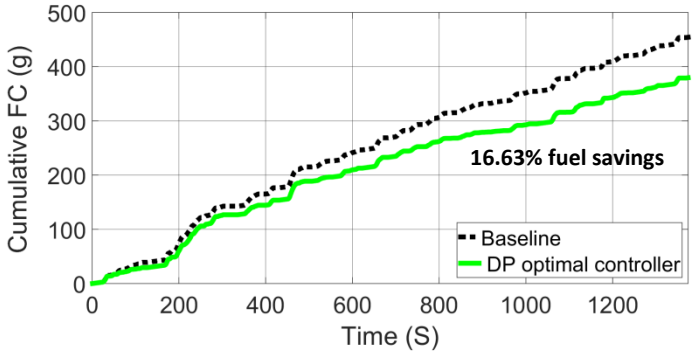

(b) Cumulative fuel consumption

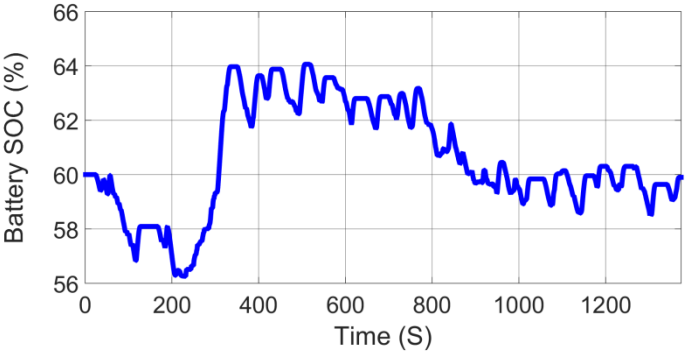

(c) Battery state of charge

Figure 4-3: Dynamic programming optimal controller simulation results over the FTP-72 driving cycle

Over the ARTEMIS U130 driving cycle (Figure 4-5a), which represents an aggressive highway driving scenario (Table 3-2), a more extensive use of the battery is observed (Figure 4-5c) compared to the FTP-72 driving cycle. Unlike the FTP-72 driving cycle, the ARTEMIS U130 driving cycle contains a significant phase with gentle braking patterns, which promotes the regeneration of braking energy, thus increasing the availability of battery energy for future use. Similar to the observations made over the FTP-72 driving cycle, an even distribution of power split ratios which decreases with increasing power demand is observed over the ARTEMIS U130 driving cycle, as shown in Figure 4-4. The ultimate fuel savings potential over this driving cycle is 13.18% (292.86g of fuel), as shown in Figure 4-5b.

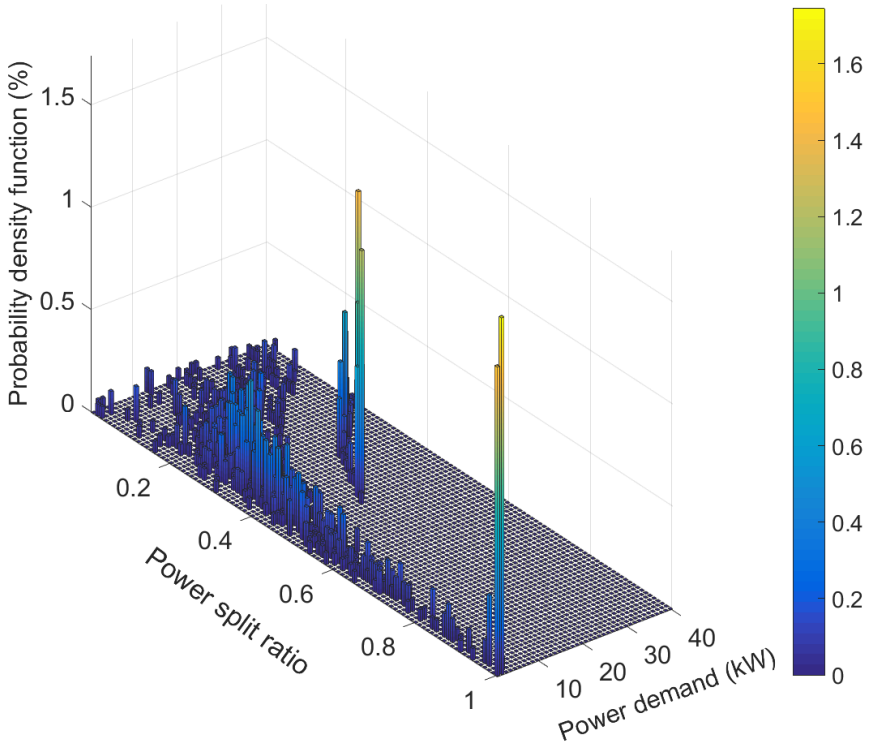

Figure 4-4: Percentage distribution of power split ratios over the ARTEMIS U130 driving cycle

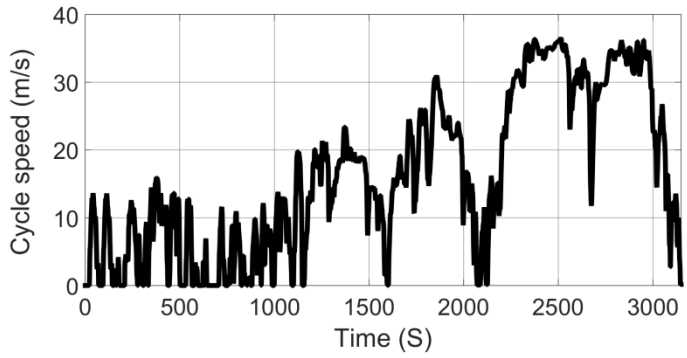

(a) ARTEMIS U130 driving cycle

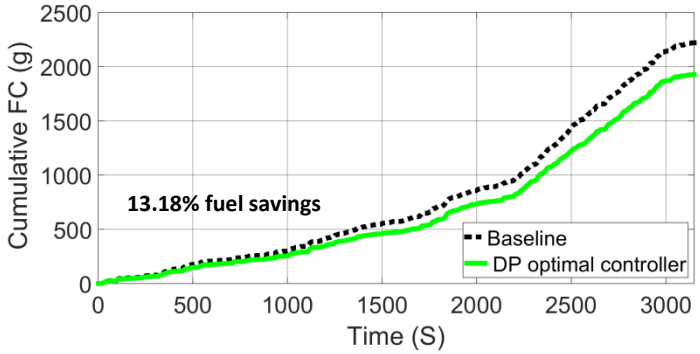

(b) Cumulative fuel consumption

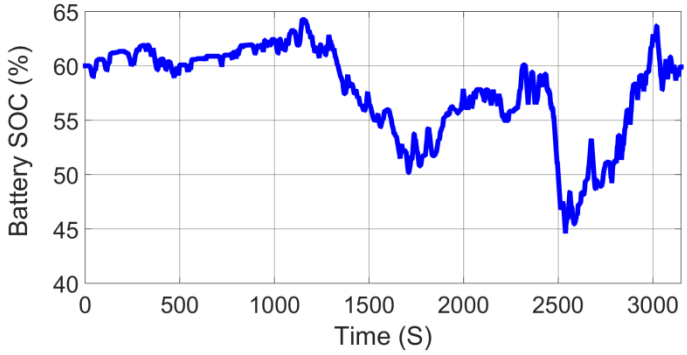

(c) Battery state of charge

Figure 4-5: Dynamic programming optimal controller simulation results over the ARTEMIS U130 driving cycle

The HWFET driving cycle (Figure 4-7a) represents a “calm” highway driving scenario (Table 3-2), which is typically characterised by a low number of braking events. Though few in number, these braking events have gentle patterns that promote braking energy regeneration. The resulting effect is a wide battery SOC range, as shown in Figure 4-7c. Over this driving cycle, a predominant distribution of electric motor utility (indicated by the distribution of power split ratios) at low vehicle power demand is observed (Figure 4-6). This implies that the HWFET driving cycle by definition is a low-power highway driving cycle. The ultimate hybridisation potential over this driving cycle is 11.74% (49.46g of fuel), as shown in Figure 4-7b.

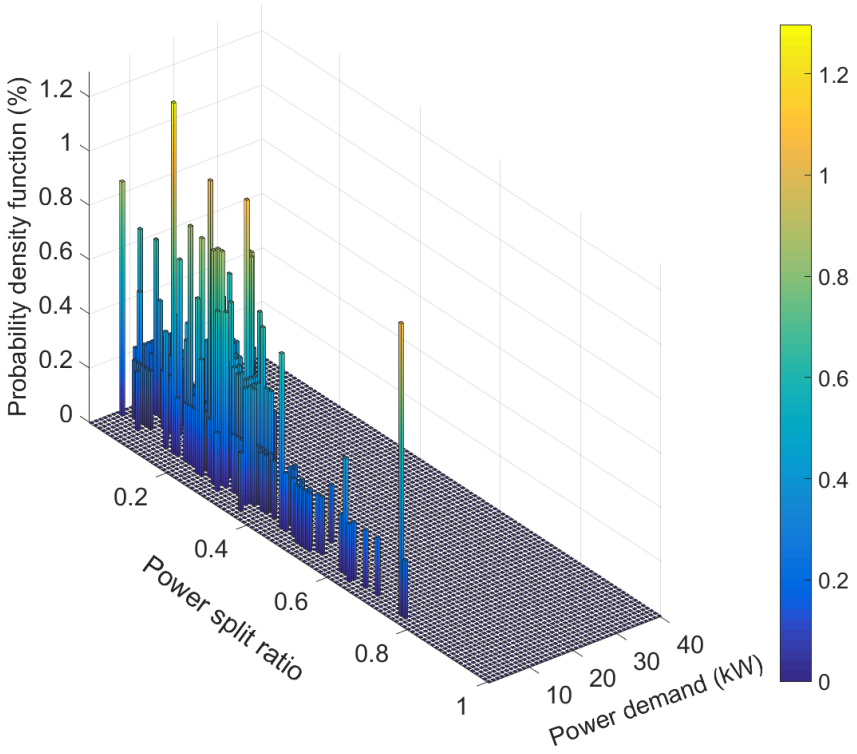

Figure 4-6: Percentage distribution of power split ratios over the HWFET driving cycle

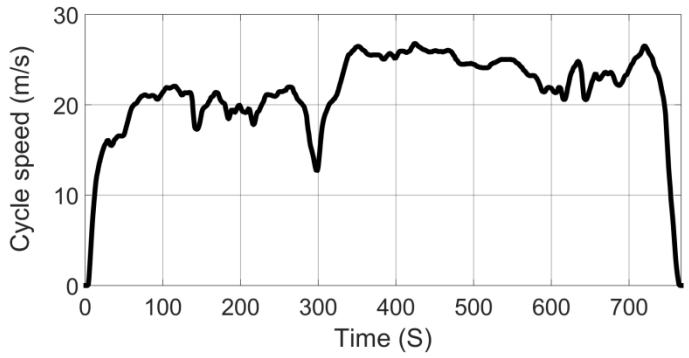

(a) HWFET driving cycle

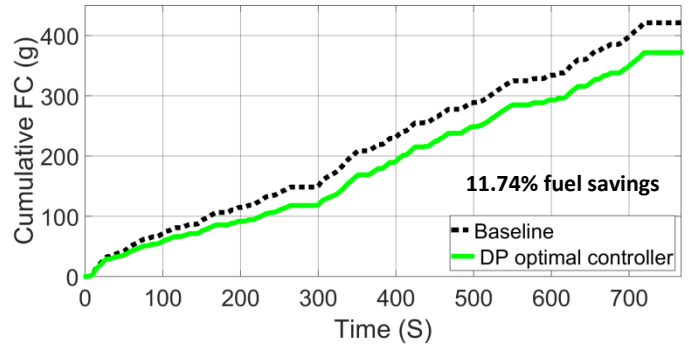

(b) Cumulative fuel consumption

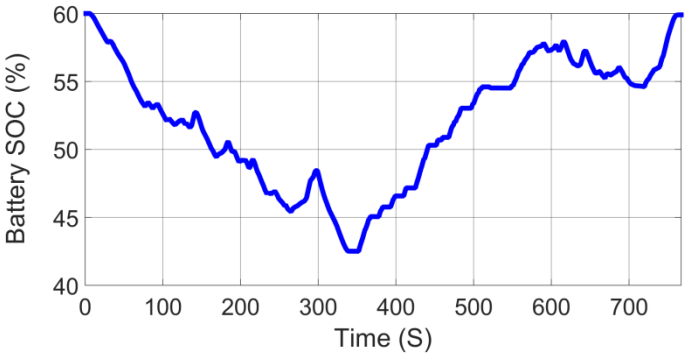

(c) Battery state of charge

Figure 4-7: Dynamic programming optimal controller simulation results over the HWFET driving cycle

The US06 driving cycle (Figure 4-9a) represents an “aggressive” highway (Table 3-2) driving scenario. This cycle by definition is characterised by a low number of aggressive braking events which does not effectively promote braking energy regeneration. The resulting effect is a relatively narrow battery SOC range (Figure 4-9c), and a low utility of the electric motor capacity, as shown in Figure 4-8. The ultimate fuel savings potential over this driving cycle is 9.68% (58.71g of fuel), as shown in Figure 4-9b.

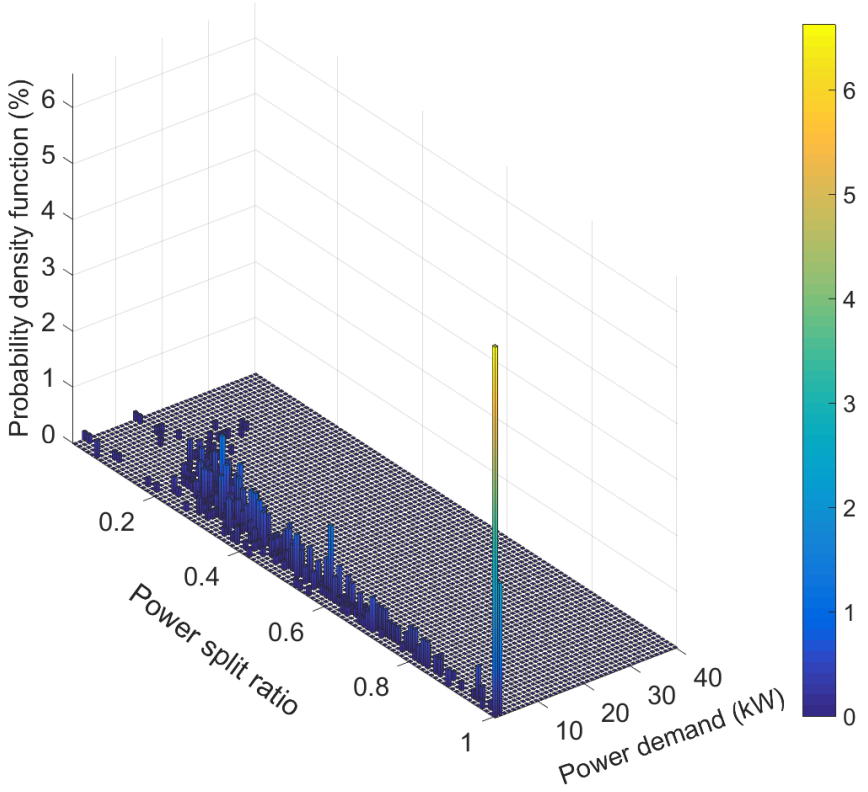

Figure 4-8: Percentage distribution of power split ratios over the US06 driving cycle

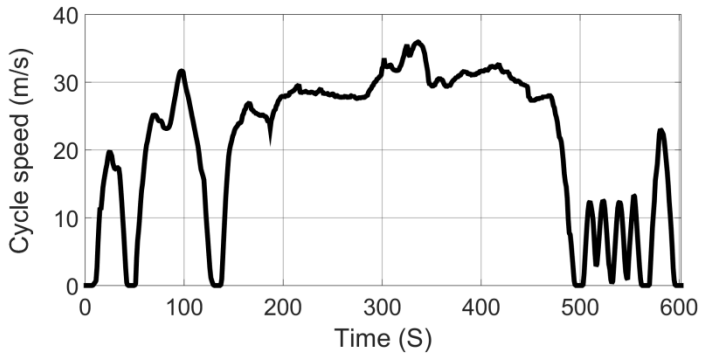

(a) US06 driving cycle

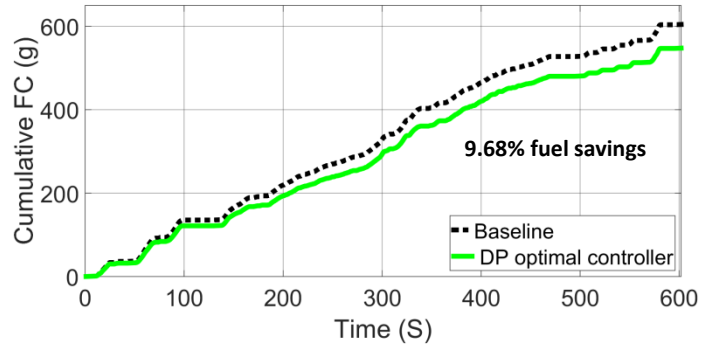

(b) Cumulative fuel consumption

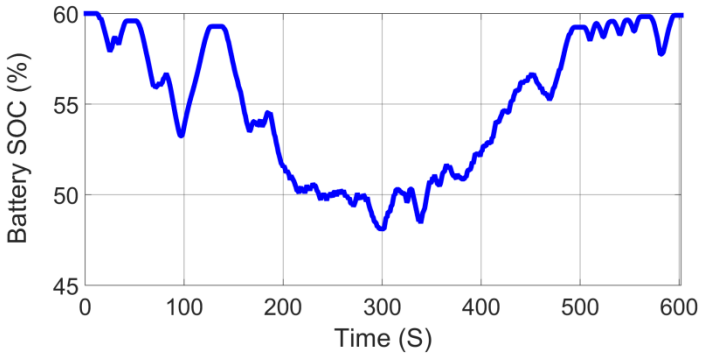

(c) Battery state of charge

Figure 4-9: Dynamic programming optimal controller simulation results over the US06 driving cycle

Table 4-3 summarizes the ultimate fuel savings potential of the research vehicle over the 7 driving cycles analysed (NEDC, FTP-72, JAPAN1015, US06, LA92, ARTEMIS U130 and HWFET).

The ultimate fuel savings potential of dynamic programming is further evidenced by the engine torque distribution plot over the FTP-72 driving cycle (Figure 4-10) and ARTEMIS U130 driving cycle (Figure 4-11). Both graphs show a notable reduction in engine torque with the dynamic programming optimal controller. With a fixed engine speed, the reduced engine torque translates to increased fuel savings.

	Baseline vehicle	**DP optimal controller**		
Driving cycle	Baseline fuel consumption (g)	DP cumulative fuel consumption (g)	Cumulative fuel savings (g)	Cumulative fuel savings (%)
NEDC	441.40	372.64	68.76	15.58
FTP-72	455.38	379.66	75.72	16.63
JAPAN1015	184.09	137.97	46.12	25.05
US06	606.50	547.79	58.71	9.68
LA92	767.31	673.07	94.25	12.28
ARTEMIS U130	2221.40	1928.54	292.86	13.18
HWFET	421.44	371.98	49.46	11.74

Table 4-3: Dynamic programming optimal controller simulation results over the NEDC, FTP-72, JAPAN1015, US06, LA92, ARTEMIS U130 and HWFET driving cycles

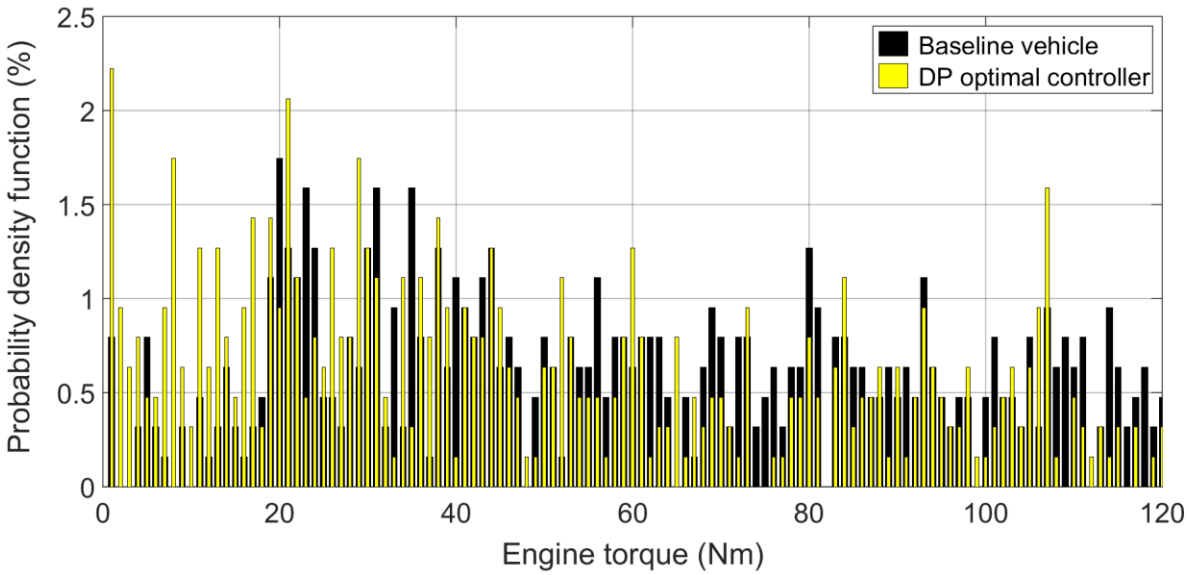

Figure 4-10: Dynamic programming engine torque distribution plot over the FTP-72 driving cycle

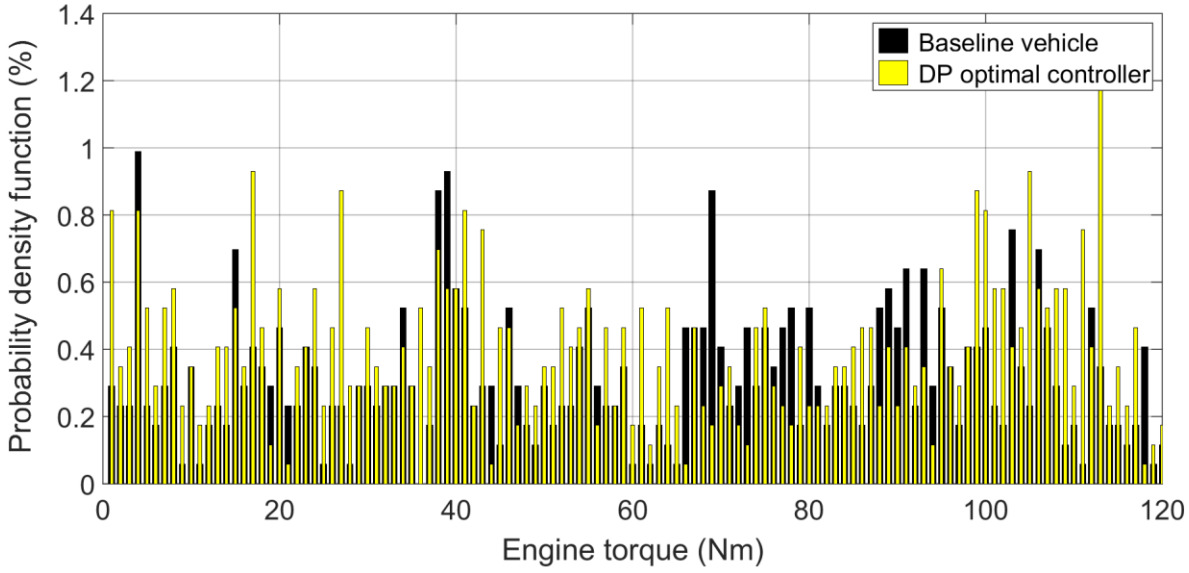

Figure 4-11: Dynamic programming engine torque distribution plot over the ARTEMIS U130 driving cycle

4.6 Dynamic programming-inspired near-optimal real-time controller development (DP-HST controller)

In the preceding sections, a mathematically based approach to solving the HEV energy management problem is explained. Based on this theoretical framework, the dynamic programming optimal control analogy was developed to assess the ultimate fuel savings potential of the research vehicle over different driving scenarios.

Although the dynamic programming approach yields an optimal solution, the resulting control policy is not implementable in real time due to the need for prior driving cycle information. Nonetheless, analysing optimal control policies determined through dynamic programming can provide insight into how fuel economy improvement is achieved. Consequently, in this section, a Markov chains-based approach is applied to extract real-time implementable near-optimal control policies from the dynamic programming algorithm. The resulting near-optimal controller (DP-HST) is a novel dynamic programming-inspired real-time sub-optimal controller with an inherent optimal property.

Comparative performance evaluations between DP-HST and other literature-based dynamic programming-inspired real-time controllers are undertaken over the NEDC, FTP-72, JAPAN1015, US06, LA92, ARTEMIS U130 and HWFET driving cycles, which represent different driving scenarios.

4.6.1 Development of a Markov-based controller framework

Derivation of real-time sub-optimal controllers from dynamic programming is a concept that has received significant attention for academic and industrial researchers alike [46, 48, 211, 213-215]. Most of these studies proposed the use of a time-series identification algorithm to first map online driving characteristics against similar pre-optimised driving cycles and then implement the optimal control policies (in the form of a multidimensional lookup model) associated with these pre-optimised driving cycles over a predefined look-ahead horizon [211, 215-219]. Although this approach can yield promising fuel savings [219], its control performance is limited in that it depends both on the size of the offline driving database, and the cycle identification algorithm in use.

Other attempts have been made to extract real-time implementable optimal control policies for developing and tuning heuristic controllers [46, 214]. Using this approach, Bianchi *et al.* [214] reported a charge-hoarding controller performance with final battery state of charge deviation above 5%. The foregoing shortcomings clearly indicate the need for an optimal control policy extraction approach which is capable of yielding a near-optimal charge-sustaining performance over different driving cycles in real time.

The proffered solution to this challenge is a “future energy variation compensation” approach couched in a “Markov chains” predictive model, which estimates future energy variations within a defined prediction horizon and then adjusts real-time control policies near-optimally, such that charge sustenance and optimisation of energy utilisation are achieved simultaneously.

With no access to route preview information, estimation of future energy variation is based on battery state of charge transitions, determined from the dynamic programming optimal state trajectory.

The optimal state trajectory (optimal battery state of charge) from dynamic programming (Figure 4-3, Figure 4-5, Figure 4-7 and Figure 4-9) can be interpreted as state transitions in the battery resulting from implementation of optimal control policies. Using Markov chains [217-219], these transitions can be expressed in the form of a state transition matrix containing transition probabilities.

4.6.1.1 Transition probabilities

A one-step state transition in a Markov chains model can be described using a state transition diagram, shown in its simplest form in Figure 4-12.

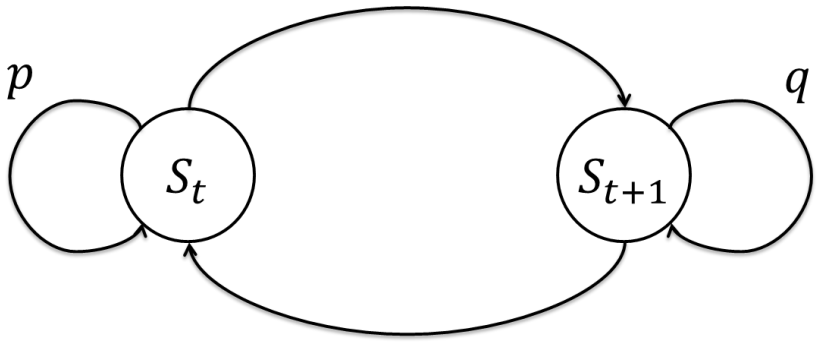

Figure 4-12: Markov chains state transition diagram

Mathematically, this one-step state transition diagram could be adapted to account for transition probabilities between different states, for each prediction horizon as follows:

$$\begin{matrix} & [S_t & S_{t+1}] \\ \begin{bmatrix} S_t \\ S_{t+1} \end{bmatrix} & \begin{bmatrix} p & 1-p \\ 1-q & q \end{bmatrix}^h \end{matrix} \quad \text{4-13}$$

Where h is the prediction horizon and $\begin{bmatrix} p & 1-p \\ 1-q & q \end{bmatrix}^h$ is the transition probability matrix (TPM).

The transition probability matrix maps the probability of occupying a new state based on the current state. Mathematically, the transition probability matrix consists of a K by K matrix that records the probability of moving from one state to another.

In this study, the transition probability matrix is estimated from the combined optimal state of charge trajectories of the NEDC, FTP-72, JAPAN1015 and LA92 driving cycles obtained through the offline implementation of dynamic programming, as shown in Figure 4-13.

The combined optimal battery state of charge trajectory for all 4 driving cycles are mapped into a sequence of quantised states using the nearest-neighbour method with a resolution of 0.01. Despite the stochastic nature of combined state trajectory, it can be assumed to have the Markov property, i.e. the property that given the present, the future is conditionally independent of the past.

The transition probabilities making up the transition probability matrix are estimated using the maximum likelihood estimation method, expressed mathematically in Equation 4-14.

$$P(S_t|S_{t+1}) = \frac{number\ of\ transitions\ from\ S_t\ to\ S_{t+1}}{number\ of\ times\ S_t\ occured} \quad 4\text{-}14$$

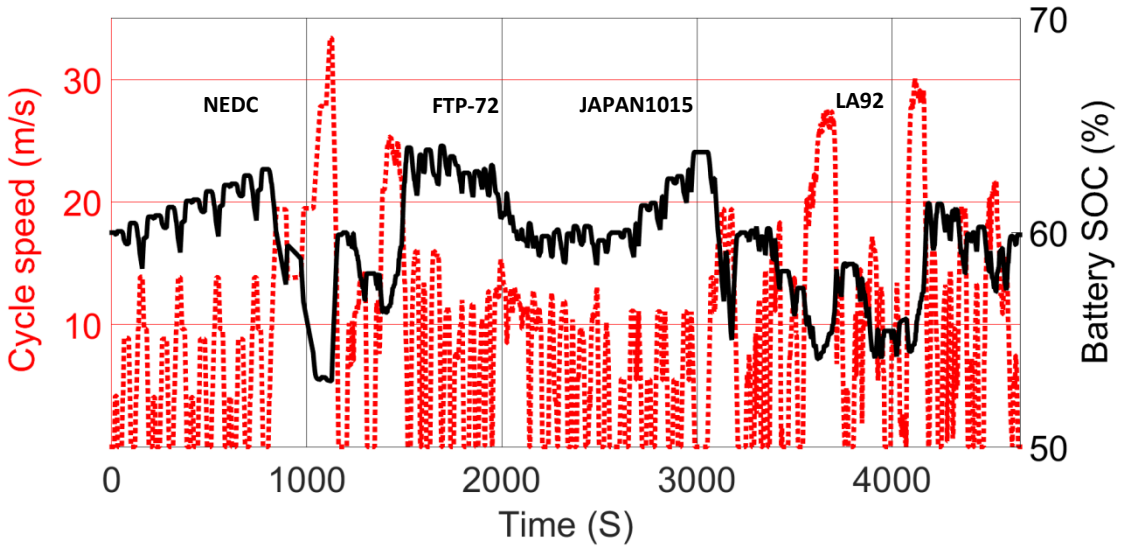

Figure 4-13: Combined optimal battery state of charge trajectory over the NEDC, FTP-72, JAPAN1015 and LA92 driving cycles

The resulting transition probability matrix for this study is shown graphically in Figure 4-14.

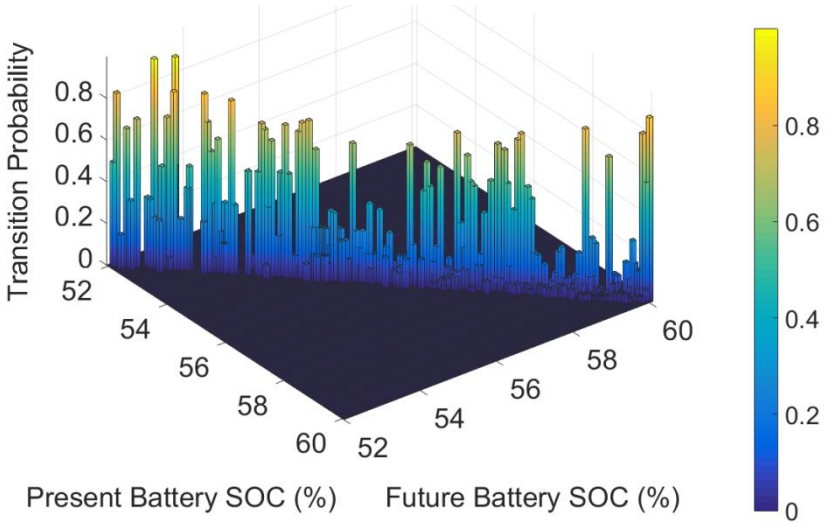

Figure 4-14: Battery state of charge transition probability matrix for the NEDC, FTP-72 and JAPAN1015 driving cycles

For each prediction horizon, state transition is based on the future state with the highest transition probability (calculated mathematically using Equation 4-15).

$$S_{t+1} = argmax\ (P(S_t|S_{t+1})) \qquad 4\text{-}15$$

Where:

$S_{t+1} \in [SOC_{min}, SOC_{max}]$

$P_{ij} \geq 0$

$\sum_j P_{ij} = 1 \ for\ all\ i.$

The Markov chains model used in this study is time-homogeneous, which implies that the transition matrix is the same after each step. As such, the k-step transition probability can be computed in accordance to Equation 4-13, as the k-th power of

the transition matrix, (TPM^k). The resulting variation in battery state of charge transition with prediction horizon is shown in Figure 4-15.

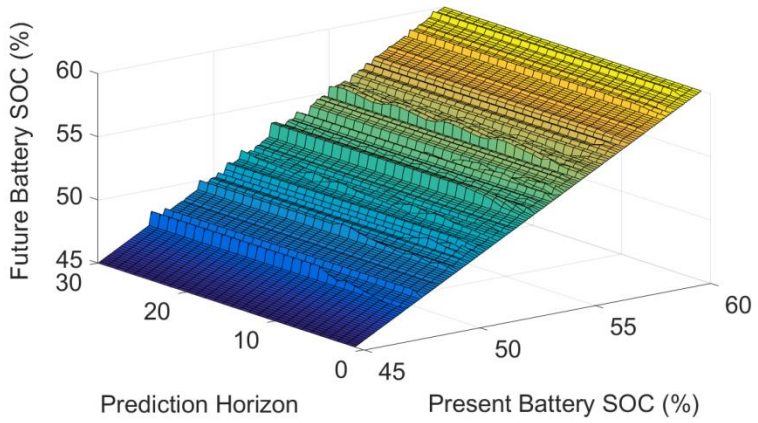

Figure 4-15: Variation in battery state of charge transition with prediction horizon

4.6.2 Estimation of net future energy variation

From Figure 4-15, it is possible to estimate the expected future battery state of charge, given the present state and the look-ahead horizon. Using this information, the expected net change in battery state of charge within the look-ahead horizon can be estimated as follows:

$$\Delta_{SOC_{\overrightarrow{t\ h}_t}} = SOC_h - SOC_t \qquad 4\text{-}16$$

Where h is the look-ahead horizon length.

By relating Equation 4-16 with the equation for the battery state of charge evolution (expressed in Equation 3-25 for battery discharge and Equation 3-26 for battery recharge), the expected net change in battery energy within the look-ahead horizon can be estimated as follows for an expected battery discharge operation (expressed in Equation 4-17):

Solution steps

$$\Delta_{SOC_{\overrightarrow{t\ h}_t}} = -\frac{V_{oc} - \sqrt{{V_{oc}}^2 - 4R_{batt}\frac{1}{\eta_{dis}}\frac{1}{\eta_{motor}}E_{\Delta_{SOC_{\overrightarrow{t\ h}}dischg_t}}}}{2R_{batt}\,Q_{batt}}$$

$$2\,\Delta_{SOC_{\overrightarrow{t\ h}_t}}\,R_{batt}\,Q_{batt} = -V_{oc} - \sqrt{{V_{oc}}^2 - 4R_{batt}\frac{1}{\eta_{dis}}\frac{1}{\eta_{motor}}E_{\Delta_{SOC_{\overrightarrow{t\ h}}dischg_t}}}$$

$$-\left(2\,\Delta_{SOC_{\overrightarrow{t\ h}_t}}\,R_{batt}\,Q_{batt}+\,V_{oc}\right)=\,\sqrt{{V_{oc}}^2-4R_{batt}\frac{1}{\eta_{dis}}\,\frac{1}{\eta_{motor}}E_{\Delta_{SOC_{\overrightarrow{t\ h}}dischg_t}}}$$

$$\left(2\,\Delta_{SOC_{\overrightarrow{t\ h}_t}}\,R_{batt}\,Q_{batt}+\,V_{oc}\right)^2=\,\left(\sqrt{{V_{oc}}^2-4R_{batt}\frac{1}{\eta_{dis}}\,\frac{1}{\eta_{motor}}E_{\Delta_{SOC_{\overrightarrow{t\ h}}dischg_t}}}\right)^2$$

$$\left(2\,\Delta_{SOC_{\overrightarrow{t\ h}_t}}\,R_{batt}\,Q_{batt}+\,V_{oc}\right)^2=\,{V_{oc}}^2-4R_{batt}\frac{1}{\eta_{dis}}\,\frac{1}{\eta_{motor}}E_{\Delta_{SOC_{\overrightarrow{t\ h}}dischg_t}}$$

$${V_{oc}}^2-\left(2\,\Delta_{SOC_{\overrightarrow{t\ h}_t}}\,R_{batt}\,Q_{batt}+\,V_{oc}\right)^2=\,4R_{batt}\frac{1}{\eta_{dis}}\,\frac{1}{\eta_{motor}}E_{\Delta_{SOC_{\overrightarrow{t\ h}}dischg_t}}$$

$$E_{\Delta_{SOC_{\overrightarrow{t\ h}}dischg_t}}=\left|\frac{\eta_{dis}\,\eta_{motor}\left({V_{oc}}^2-\left(2\,\Delta_{SOC_{\overrightarrow{t\ h}_t}}\,R_{batt}\,Q_{batt}+\,V_{oc}\right)^2\right)}{4R_{batt}}\right| \qquad 4\text{-}17$$

Similarly, for an expected battery *recharge* operation the expected net change in battery energy within the look ahead horizon can be estimated as follows (expressed in Equation 4-18):

Solution steps

$$\Delta_{SOC_{\overrightarrow{t\ h}_t}}=+\,\frac{V_{oc}-\sqrt{{V_{oc}}^2-4R_{batt}\,\eta_{chg}\,\eta_{faradaic}\,\eta_{motor}\,E_{\Delta_{SOC_{\overrightarrow{t\ h}}rechg_t}}}}{2R_{batt}\,Q_{batt}}$$

$$2\,\Delta_{SOC_{\overrightarrow{t\ h}_t}}\,R_{batt}\,Q_{batt}$$

$$= V_{oc} - \sqrt{{V_{oc}}^2 - 4R_{batt}\,\eta_{chg}\,\eta_{faradaic}\,\eta_{motor}\,E_{\Delta_{SOC_{\overrightarrow{t\ h}}rechg}{}_t}}$$

$$2\,\Delta_{SOC_{\overrightarrow{t\ h}_t}}R_{batt}\,Q_{batt} - V_{oc}$$

$$= \sqrt{{V_{oc}}^2 - 4R_{batt}\,\eta_{chg}\,\eta_{faradaic}\,\eta_{motor}\,E_{\Delta_{SOC_{\overrightarrow{t\ h}}rechg}{}_t}}$$

$$\left(2\,\Delta_{SOC_{\overrightarrow{t\ h}_t}}\,R_{batt}\,Q_{batt} - V_{oc}\right)^2$$

$$= \left(\sqrt{{V_{oc}}^2 - 4R_{batt}\,\eta_{chg}\,\eta_{faradaic}\,\eta_{motor}\,E_{\Delta_{SOC_{\overrightarrow{t\ h}}rechg}{}_t}}\right)^2$$

$$\left(2\,\Delta_{SOC_{\overrightarrow{t\ h}_t}}\,R_{batt}\,Q_{batt} - V_{oc}\right)^2$$

$$= {V_{oc}}^2 - 4R_{batt}\,\eta_{chg}\,\eta_{faradaic}\,\eta_{motor}\,E_{\Delta_{SOC_{\overrightarrow{t\ h}}rechg}{}_t}$$

$${V_{oc}}^2 - \left(2\,\Delta_{SOC_{\overrightarrow{t\ h}_t}}\,R_{batt}\,Q_{batt} - V_{oc}\right)^2$$

$$= 4R_{batt}\,\eta_{chg}\,\eta_{faradaic}\,\eta_{motor}\,E_{\Delta_{SOC_{\overrightarrow{t\ h}}rechg}{}_t}$$

$$E_{\Delta_{SOC_{\overrightarrow{t\ h}}rechg}{}_t} = \left|\frac{{V_{oc}}^2 - \left(2\,\Delta_{SOC_{\overrightarrow{t\ h}_t}}\,R_{batt}\,Q_{batt} - V_{oc}\right)^2}{4R_{batt}\,\eta_{chg}\,\eta_{faradaic}\,\eta_{motor}}\right| \qquad 4\text{-}18$$

Therefore:

If $\Delta_{SOC_{\overrightarrow{t\ h}_t}} < 0$: *(net battery discharge is expected within the look-ahead horizon)*

$$E_{\Delta_{SOC_{\overrightarrow{t\ h}}dischg}}{}_t = \left| \frac{\eta_{dis}\,\eta_{motor}\left({V_{oc}}^2 - \left(2\,\Delta_{SOC_{\overrightarrow{t\ h}_t}} R_{batt}\,Q_{batt} + V_{oc}\right)^2\right)}{4R_{batt}} \right|$$

If $\Delta_{SOC_{\overrightarrow{t\ h}_t}} > 0$: *(net battery recharge is expected within the look-ahead horizon)*

$$E_{\Delta_{SOC_{\overrightarrow{t\ h}}rechg}}{}_t = \left| \frac{{V_{oc}}^2 - \left(2\,\Delta_{SOC_{\overrightarrow{t\ h}_t}}\,R_{batt}\,Q_{batt} - V_{oc}\right)^2}{4R_{batt}\,\eta_{chg}\,\eta_{faradaic}\,\eta_{motor}} \right|$$

η_{chg} and η_{dis} are assumed to be 80%, which is typical for lithium ion batteries (the battery in the study vehicle, see Appendix 1). The faradaic efficiency of the battery $(\eta_{faradaic} = 0.4)$ is assumed low to account for charge losses due to unproductive reactions.

4.6.3 Compensation for future energy variation

Using the estimated future energy variation for expected battery discharge (Equation 4-17) and recharge (Equation 4-18) it is possible to adjust implemented control policies in real time, such that a charge-sustaining compensation effect is achieved.

In this study, future energy variation is compensated for using Equation 4-19 (for battery discharge operation) and Equation 4-20 (for battery recharge operation).

If $\Delta_{SOC_{\overrightarrow{t\ h}_t}} < 0$: *(net battery discharge is expected within the look-ahead horizon)*

$$P_{SOC_{regulator}}{}_t = \frac{E_{\Delta_{SOC_{\overrightarrow{t\ h}dischg}}}{}_t}{h}\ (SOC_t - SOC_{ref}) \quad \text{4-19}$$

If $\Delta_{SOC_{\overrightarrow{t\ h}_t}} > 0$: *(net battery recharge is expected within the look-ahead horizon)*

$$P_{SOC_{regulator}}{}_t = \frac{E_{\Delta_{SOC_{\overrightarrow{t\ h}rechg}}}{}_t}{h}\ (SOC_t - SOC_{ref}) \quad \text{4-20}$$

Where h is the look-ahead horizon.

4.6.4 Estimation of the optimal control policy lookup table

The control policy for this controller is estimated from a combination of optimal power split ratios for the NEDC, FTP-72, JAPAN1015 and LA92 driving cycles as shown in Figure 4-16.

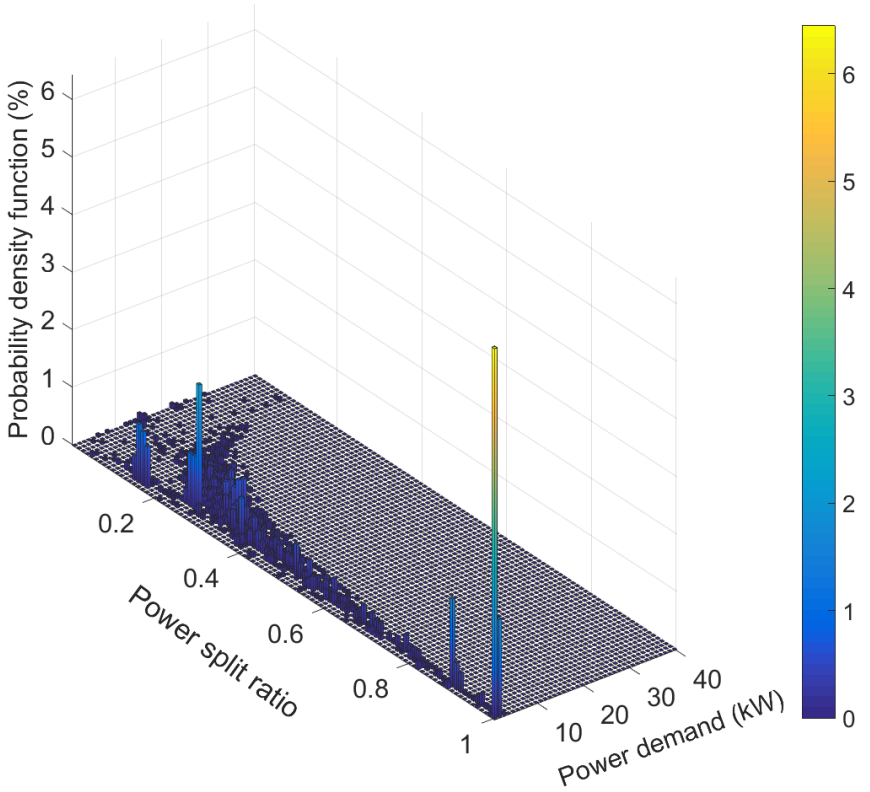

Figure 4-16: Combined optimal power split ratios for the NEDC, FTP-72, JAPAN1015 and LA92 driving cycles

Using the maximum likelihood estimation method, the optimal distribution of power splt ratios for this controller (P_{RSP}) could be estimated from Figure 4-16 as shown in Figure 4-17. As observed from Figure 4-17, optimal power split ratios are found to decrease with increasing power demand. This trend is similar to the trend

observed in Figure 4-2 and Figure 4-4 and is as a result of the electric motor tractive power limitation, which increases with increased power demand.

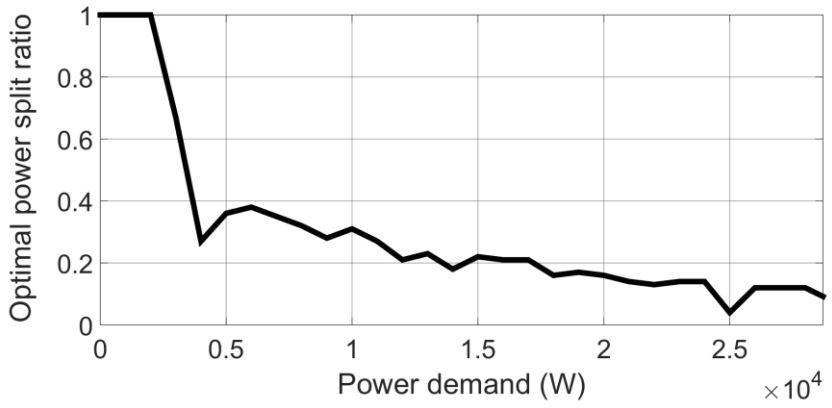

Figure 4-17: Variation of real-time optimal power split ratios with power demand

4.6.5 Real-time optimal control policy for the (DP-HST) controller

By combining the derivation in sections 4.6.3 and 4.6.4, the real-time optimal control policy for the DP-HST controller can be estimated as follows:

$$P_{motor_t} = P_{RSP}\, P_{demand} + P_{SOC_{regulator_t}} \qquad 4\text{-}21$$

Similarly, Equation 4-21 can be further expressed in Equation 4-22 for battery *discharge* operation and Equation 4-23 for battery *recharge* operation.

If $\Delta_{SOC_{\overrightarrow{t\ h_t}}} < 0$: *(net battery discharge is expected within the look-ahead horizon)*

$$P_{motor_t} = P_{PSR_t} P_{demand} + \frac{1}{h} \left| \frac{\eta_{dis}\, \eta_{motor} \left({V_{oc}}^2 - \left(2\, \Delta_{SOC_{\overrightarrow{t\ h_t}}} R_{batt}\, Q_{batt} + V_{oc} \right)^2 \right)}{4 R_{batt}} \right| (SOC_t - SOC_{ref}) \quad \text{4-22}$$

If $\Delta_{SOC_{\overrightarrow{t\ h_t}}} > 0$: *(net battery recharge is expected within the look-ahead horizon)*

$$P_{motor_t} = P_{PSR_t} P_{demand} + \frac{1}{h} \left| \frac{{V_{oc}}^2 - \left(2\, \Delta_{SOC_{\overrightarrow{t\ h_t}}} R_{batt}\, Q_{batt} - V_{oc} \right)^2}{4 R_{batt}\, \eta_{chg}\, \eta_{faradaic}\, \eta_{motor}} \right| (SOC_t - SOC_{ref}) \quad \text{4-23}$$

Where:

$\Delta_{SOC_{\overrightarrow{t\ h_t}}}$ *Expected net change in battery energy within the look-ahead horizon*

P_{PSR_t} *Optimal power split ratio*

P_{demand} *Vehicle power demand*

SOC_t *Present battery state of charge*

SOC_{ref} *Battery state of charge reference (assumed 60% in this study)*

The uniqueness of the proposed approach lies in its amalgamation of the two most important features of the dynamic programming optimal controller: the optimal control policy and the charge-sustaining energy compensation algorithm. As with any statistically based model, the DP-HST controller's exposure to estimation

errors is expected to increase with increasing preview length. As such, the “look-ahead horizon length” for this controller is 1s.

4.7 DP-HST controller evaluation

In this section, the performance of the proposed DP-HST controller is evaluated over the NEDC, FTP-72, JAPAN1015, US06, LA92, ARTEMIS U130 and HWFET driving cycles. Results from the DP-HST controller are compared to those from a dynamic programming-inspired multidimensional lookup model dubbed DP-LT, which is similar to the model proposed in [211, 215-219].

4.7.1 Set up of literature-based dynamic programming-inspired multidimensional look-up model (DP-LT controller)

The DP-LT control strategy is a multidimensional lookup model that maps vehicle inputs to the optimal control policies from dynamic programming using the relationship model shown in Figure 4-18.

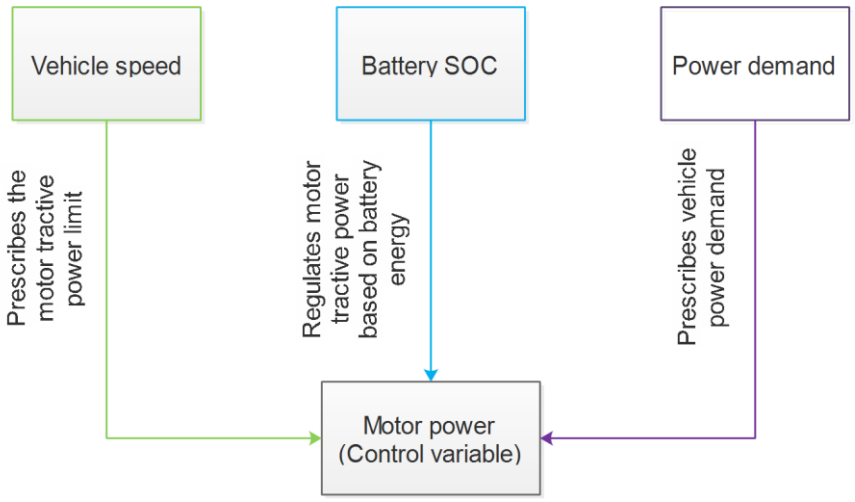

Figure 4-18: Flow chart showing relationships between vehicle inputs and the control variable

Neural network [216-222], is used to establish the statistical relationship between the inputs specified in Figure 4-18 and the control variable. Through appropriate training and adjustment of weights, an artificial neural network can approximate any continuous measurable function to a desired accuracy.

4.7.1.1 Neural network theoretical framework

Neural networks can be trained to learn a highly non-linear input/output relationship by adjusting weights to minimise the error between the actual and predicted output patterns of a training set [186]. This form of supervised learning is facilitated by the back propagation method (shown in Figure 4-19), which could be articulated in the following steps:

Feed Forward Approach

1. Using inputs (X_1 and X_2) to the prediction network, calculate the input to hidden layer neurons

$$N_{in_{1,1}} = X_1 W_{x_{1,1}} + X_2 W_{x_{2,1}} \quad \text{4-24}$$

$$N_{in_{1,2}} = X_1 W_{x_{1,2}} + X_2 W_{x_{2,2}}$$

2. Calculate the output from hidden layer neurons

$$N_{out_{1,1}} = \left(\frac{1}{(1 + e^{-N_{in_{1,1}}})}\right) \quad \text{4-25}$$

$$N_{out_{1,2}} = \left(\frac{1}{(1 + e^{-N_{in_{1,2}}})}\right)$$

3. Calculate the input to the output neuron

$$Y_{in} = N_{out_{1,1}} W_{N_{1,1}} + N_{out_{1,2}} W_{N_{1,2}} \quad \text{4-26}$$

4. Calculate the output from the neural network

$$Y_p = \left(\frac{1}{(1 + e^{-Y_{in}})}\right) \quad \text{4-27}$$

5. Calculate the prediction error

$$Y_{actual} - Y_p = error \quad \text{4-28}$$

Back propagation approach

6. Calculate local gradients of output and hidden layers

$$\delta_{N_{1,1}} = \frac{1}{1 + e^{-N_{in_{1,1}}}} \left[1 - \frac{1}{1 + e^{-N_{in_{1,1}}}}\right] \delta_y W_{N_{1,1}} \quad \text{4-29}$$

$$\delta_{N_{1,2}} = \frac{1}{1 + e^{-N_{in_{1,2}}}} \left[1 - \frac{1}{1 + e^{-N_{in_{1,2}}}}\right] \delta_y W_{N_{1,2}}$$

7. Adjust the weight of the network using the gradient descent learning rule

$$W_{x_{1,1}\,new} = W_{x_{1,1}\,old}(1 + \sigma) + \delta_{N_{1,1}} X_1 \quad \text{4-30}$$

$$W_{x_{1,2}\,new} = W_{x_{1,2}\,old}(1 + \sigma) + \delta_{N_{1,2}} X_1$$

$$W_{x_{2,1}\,new} = W_{x_{2,1}\,old}(1 + \sigma) + \delta_{N_{1,1}} X_2$$

$$W_{x_{2,2}\,new} = W_{x_{2,2}\,old}(1 + \sigma) + \delta_{N_{1,2}} X_2$$

$$W_{N_{1,1}\,new} = W_{N_{1,1}\,old}(1 + \sigma) + \delta_y N_{out_{1,1}}$$

$$W_{N_{1,2}\,new} = W_{N_{1,2}\,old}(1 + \sigma) + \delta_y N_{out_{1,2}}$$

8. Using the recomputed weights, perform steps 1-7 again while:

$(Y_{actual} - Y_p) > set\ threshold$

Note: Steps 1 to 8 could be applied to networks with more inputs, hidden layers and outputs.

Summarily, the back propagation algorithm adjusts the weights of each unit in such a way that the error between the desired output and actual output is reduced. This process requires the computation of an error derivative for each weight, which is a measure of how the error changes as each weight is increased or decreased.

The DP-LT controller neural network is made up of 20 hidden layers, 3 inputs and 1 output, as specified in Figure 4-18. Although neural network predictability is expected to increase with increasing hidden layer size, a hidden layer size of 20 is

selected for the DP-LT controller in order to avoid the estimation errors associated with "over estimation" which tends to increase with increasing hidden layer size.

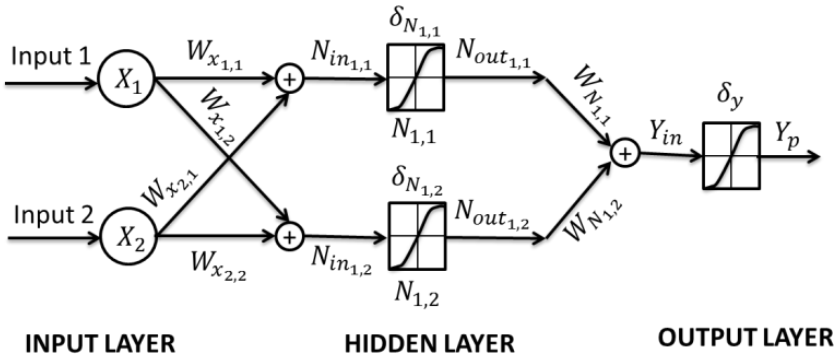

Figure 4-19: Network schematics for an artificial neural network predictor with two inputs and one output

Where:

$W_{x_{1,1}}$ $W_{x_{1,2}}$ $W_{x_{2,1}}$ $W_{x_{2,2}}$	Randomly generated input weights	X_1 X_2	Inputs to neural network
$N_{1,1}$ $N_{1,2}$	Neurons in hidden layer nodes	$N_{in_{1,1}}$ $N_{in_{1,2}}$	Inputs to hidden layer neurons.
σ	Learning rate	$N_{out_{1,1}}$ $N_{out_{1,2}}$	Outputs from hidden layer neurons
$\delta_{N_{1,1}}$ $\delta_{N_{1,2}}$ δ_y	Local gradients	$W_{N_{1,1}}$ $W_{N_{1,2}}$	Randomly generated hidden layer weights
Y_{in}	Input to output neuron	Y_p	Predicted output

Table 4-4: Notation definition for an artificial neural network predictor

4.7.2 Simulation results of DP-HST and DP-LT controllers over standard driving cycles

In this section, the performance of the proposed Markov chains-based, dynamic programming-inspired controller (DP-HST) is simulated and appraised accordingly over the NEDC, FTP-72, JAPAN1015, US06, LA92, ARTEMIS U130 and HWFET driving cycles, as summarised in Table 4-5. Simulation results from a literature-based dynamic programming-inspired lookup model [211, 215-219] are also included for comparative reasons, and to highlight the importance of the proposed controller.

In order to achieve a "like for like" comparison, the SOC correction proposed in section 3.5.7 is applied to both sets of simulation results (Table 4-5), to calculate the mass and percentage of anticipated fuel savings assuming charge sustenance. The nomenclature based comparative analogies developed in Table 3-9 is also applied to the simulation results from both controllers, as detailed in Table 4-6. Using these comparative analogies, simulation results from each controller are classified either as "near charge-sustaining", "charge-sustaining", "charge-depleting" or "charge-hoarding". Both controllers are also rated on the basis of efficiency (Table 4-6), where a controller is rated as "more efficient" if its fuel savings assuming charge sustenance is of higher value.

From the comparative analysis detailed in Table 4-5 and Table 4-6, it could be inferred that over most driving cycles analysed, the DP-HST controller, clearly outperforms the DP-LT controller on the basis of charge sustenance and efficiency. In Table 4-7, the fuel savings potential of the DP-HST controller is compared with that of the global optimal controller, over standard driving cycles. Simulation results show that the DP-HST controller maintains a near-optimal performance

which differs only slightly from the performance of the global optimal controller (maximum difference of 3.71% fuel savings, which occurs over the ARTEMIS U130 driving cycle).

The importance of the proposed “future energy variation compensation strategy” is also highlighted, with the inclusion of Table 4-8 which details controller simulation results for the DP-HST controller with no compensation for future energy variation. Results from this analysis show that without the proposed “future energy variation compensation strategy”, the DP-HST controller yields a predominantly charge-depleting performance similar to the one detailed in Table 4-5 for the DP-LT controller.

DP-LT controller						
Driving cycle	**Baseline fuel consumption (g)**	**Fuel savings (actual) (g)**	**Final battery SOC (%)**	**Fuel savings (actual) (%)**	**Fuel savings (Assuming charge sustenance) (g)**	**Fuel savings (Assuming charge sustenance) (%)**
NEDC	441.40	76.00	46.94	17.22	38.15	8.64
FTP-72	455.38	77.63	56.80	17.05	64.74	14.22
JAPAN1015	184.09	29.68	64.26	16.12	31.95	17.36
US06	606.50	14.22	70.05	2.35	17.09	2.82
LA92	767.31	103.47	47.31	13.48	52.86	6.89
ARTEMIS U130	2221.40	235.63	43.85	10.61	102.29	4.60
HWFET	421.44	37.57	67.67	8.92	43.08	10.22

DP-HST controller						
Driving cycle	**Baseline fuel consumption (g)**	**Fuel savings (actual) (g)**	**Final battery SOC (%)**	**Fuel savings (actual) (%)**	**Fuel savings (Assuming charge sustenance) (g)**	**Fuel savings (Assuming charge sustenance) (%)**
NEDC	441.40	64.59	63.54	14.63	68.64	15.55
FTP-72	455.38	66.86	60.21	14.68	67.10	14.74
JAPAN1015	184.09	43.43	63.33	23.59	45.98	24.98
US06	606.50	48.06	60.28	7.92	48.29	7.96
LA92	767.31	81.07	61.02	10.57	82.47	10.75
ARTEMIS U130	2221.40	205.78	61.32	9.26	210.41	9.47
HWFET	421.44	40.58	62.02	9.63	41.99	9.96

Table 4-5: Simulation results for the DP-LT controller and DP-HST controller over the NEDC, FTP-72, JAPAN1015, US06, LA92, ARTEMIS U130 and HWFET driving cycles

	DP-LT controller		DP-HST controller	
Driving cycle	**Charge sustenance status**	**Efficiency rating (Assuming charge sustenance)**	**Charge sustenance status**	**Efficiency rating (Assuming charge sustenance)**
NEDC	Charge-depleting	Less efficient	Near charge-sustaining	More efficient
FTP-72	Near charge-sustaining	Less efficient	Near charge-sustaining	More efficient
JAPAN1015	Near charge-sustaining	Less efficient	Near charge-sustaining	More efficient
US06	Charge-hoarding	Less efficient	Near charge-sustaining	More efficient
LA92	Charge-depleting	Less efficient	Near charge-sustaining	More efficient
ARTEMIS U130	Charge-depleting	Less efficient	Near charge-sustaining	More efficient
HWFET	Charge-hoarding	More efficient	Near charge-sustaining	Less efficient

Key	Desired	Undesired

Table 4-6: Subjective performance comparison between the DP-LT controller and the DP-HST controller over the NEDC, FTP-72, JAPAN1015, US06, LA92, ARTEMIS U130 and HWFET driving cycles

	DP optimal controller		DP-HST controller			Fuel saving benefits of the DP controller over the DP-HST (%)
Driving cycle	**Fuel savings (Actual) (g)**	**Fuel Savings (Assuming charge sustenance) (%)**	**Final battery SOC (%)**	**Fuel savings (Actual) (g)**	**Fuel Savings (Assuming charge sustenance) (%)**	
NEDC	68.76	15.58	63.54	68.64	15.55	0.03
FTP-72	75.72	16.63	60.21	67.10	14.74	1.89
JAPAN1015	137.97	25.05	63.33	45.98	24.98	0.07
US06	58.71	9.68	60.28	48.29	7.96	1.72
LA92	94.25	12.28	61.02	82.47	10.75	1.53
ARTEMIS U130	292.86	13.18	61.32	210.41	9.47	3.71
HWFET	49.46	11.74	62.02	41.99	9.96	1.77

Table 4-7: Performance comparison between the dynamic programming optimal controller and the DP-HST controller over the NEDC, FTP-72, JAPAN1015, US06, LA92, ARTEMIS U130 and HWFET driving cycles

Driving cycle	Baseline fuel consumption (g)	Fuel savings (Actual) (g)	Final battery SOC (%)	Fuel savings (Actual) (%)	Fuel savings (Assuming charge sustenance) (g)	Fuel savings (Assuming charge sustenance) (%)
NEDC	441.40	70.86	47.17	16.05	35.97	8.15
FTP-72	455.38	69.75	40.84	15.32	26.44	5.81
JAPAN1015	184.09	44.72	44.71	24.30	20.21	10.98
US06	606.50	56.88	41.87	9.38	22.57	3.72
LA92	767.31	86.42	41.53	11.26	33.78	4.40
ARTEMIS U130	2221.40	173.91	40.74	7.83	65.65	2.96
HWFET	421.44	49.32	45.20	11.70	22.80	5.41

Table 4-8: Simulation results for the DP-HST controller with no compensation for future energy variation over the NEDC, FTP-72, JAPAN1015, US06, LA92, ARTEMIS U130 and HWFET driving cycles

4.8 Chapter conclusions

In this chapter, a theoretical framework for a dynamic programming optimal controller was designed and evaluated over different driving scenarios. Though non-causal (requires the entire driving cycle to be known in advance) in nature, simulation results from the dynamic programming optimal controller proved useful in the following ways: first as an optimal benchmark for evaluating the performance of other sub-optimal controllers and then as a basis for the formulation of a Markov chains-based controller (DP-HST). The theoretical framework of the DP-HST controller which is based on "future energy variation compensation", was given a detailed appraisal. A literature-based dynamic programming-inspired lookup model (DP-LT) was also developed for the purpose of comparing its performance with that of the proposed DP-HST controller.

A comparative study of both controllers (DP-HST and DP-LT) was undertaken in real time over the NEDC, FTP-72, JAPAN1015, US06, LA92, ARTEMIS U130 and HWFET driving cycles. Simulation results from this analysis prove the DP-HST controller to be a better controller with a "more efficient" and "near charge-sustaining" performance over most of the driving cycles analysed. Similarly, the fuel savings potential of the DP-HST controller was compared with that of the global optimal controller. Simulation results show a maximum performance difference of 3.71% (over the ARTEMIS U130 driving cycle) between both controllers. The significance of this performance becomes even greater when considered in the context that, unlike the global optimal controller, the DP-HST controller has no access to route preview information.

The importance of the proposed “future energy variation compensation” strategy was further highlighted by comparing simulation results from a DP-HST controller with no future energy variation compensation to simulation results from the proposed controller. From this analysis, the DP-HST controller with no future energy variation compensation yields a “charge-depleting” performance over all the driving cycles analysed.

Summarily, the benefits of the proposed novel DP-HST controller can be elucidated as follows:

1. It proves useful as a “near-optimal” and “charge-sustaining” derivative of the global optimal dynamic programming controller.
2. It replaces the need for expensive telematics to estimate future vehicular energy variations.
3. Previously, the application of Markov chains to solve HEV energy management problems was limited only to the development of a stochastic dynamic programming controller, which is non-causal and commands a very high computational burden [66, 223]. In this study, a more practical and causal application of Markov chains to solving HEV energy management problems is proposed.

The foregoing trends generally do suggest that the optimality of a causal controller derived from dynamic programming varies depending on the sophistication of the rules extraction process employed. Without a formalised approach for extracting sub-optimal control rules from offline optimisation techniques in general, the problem of finding a suitable extraction technique becomes even more subjective and non-trivial. In contrast, online optimisation techniques have a more formalised rules extraction process involving the estimation and calibration of few control

parameters, which represent fuel equivalence weighting factors [116, 137-140]. Consequently, an online optimisation technique based on the equivalent consumption minimisation strategy (ECMS) is proposed in the next chapter.

5 HEV REAL-TIME OPTIMAL CONTROL WITH NO ROUTE PREVIEW INFORMATION (AN ECMS-INSPIRED APPROACH)

5.1 Introduction

In Chapter 4, the optimal HEV energy management problem for a parallel HEV was defined and solved using the dynamic programming algorithm. Being non-causal in nature, the simulation results obtained over different driving scenarios served two main purposes: first as an ultimate performance benchmark for other controllers and then as a basis for the derivation of a quasi-optimal real-time control strategy, which estimates and compensates for future energy variations using Markov chains (DP-HST).

The DP-HST controller was compared with a dynamic programming-inspired multidimensional lookup model (DP-LT), over the NEDC, FTP-72, JAPAN1015, US06, LA92, ARTEMIS U130 and HWFET driving cycles. Obtained simulation results proved the DP-HST controller to be a better controller with a “more efficient” and “near charge-sustaining” performance over most of the driving cycles analysed. From the simulation results, it was also inferred that the optimality of a causal controller derived from dynamic programming, varied depending on the sophistication of the rules extraction process employed.

Without a formalised approach for extracting sub-optimal control rules from offline optimisation techniques in general, the problem of finding a suitable extraction technique becomes even more subjective and non-trivial. In contrast, online optimisation techniques have a more formalised rules extraction process involving the estimation and calibration of few control parameters, which

represent fuel equivalence weighting factors [116, 137-140]. Consequently, an online optimisation technique based on the equivalent consumption minimisation Strategy is proposed in this chapter.

The global optimisation problem will be solved using an instantaneous optimisation approach based on the ECMS. The ECMS, originally derived as a real-time realisation of Pontryagin's Minimum Principle, mathematically reformulates a global optimisation problem into a local optimisation problem, where the equivalent fuel consumed is minimised at each instant. This eliminates the need for future driving information, making it possible for the strategy to be implemented in real time.

The disposition of this chapter is outlined as follows: first, the local optimisation energy management problem for a parallel HEV will be quantified and defined, after which a quick derivation of the ECMS strategy is carried out using Pontryagin's minimum principle. Next, a quick overview about the challenges currently facing the commercialisation of ECMS strategies will be discussed alongside the different solutions that have been proposed by different studies in literature. Afterwards, a novel and robust proportional ECMS control strategy dubbed (RPEC) will be developed, tuned and simulated over some standard driving cycles in real time. Finally, simulation results from the RPEC strategy will then be compared to results obtained from other ECMS controllers published in literature.

5.2 ECMS formulation for HEV energy management

The ECMS is based on the engineering intuition that, in a charge-sustaining HEV, the energy used to propel the vehicle ultimately comes from the fuel, and the battery is only used as an energy buffer. The analogy goes as follows: in a charge-sustaining HEV, any chemical energy disturbance in the battery needs to be rectified in the future. Consequently, a present battery discharge needs to be rectified by future recharge, which consumes fuel energy. Similarly, a present recharge needs to be rectified by future discharge, thus saving more fuel. The fuel consumed or saved in the rectifying process is the battery fuel cost. The ECMS, originally derived as a real-time realisation of Pontryagin's minimum principle, mathematically reformulates a global optimisation problem into a local optimisation problem, where the equivalent fuel consumed is minimised at each instant.

Pontryagin's minimum principle, originally proposed by the Russian mathematician Lev Pontryagin in 1958 [224], provides a set of conditions necessary to ensure the optimisation of the control policy. PMP is a special case of the Euler-Lagrange equation of variational calculus, in which the principle lies in the definition of the Hamiltonian function of the system.

PMP [142, 225] is a mathematical theorem that provides a set of necessary conditions for the solution of a constrained optimal control problem to be globally optimal. This implies that the optimal solution to the global optimisation problem must satisfy these conditions (which are not, by themselves, a guarantee of optimality). The set of control laws that satisfies these conditions is known as the

extremal solutions to the control problem. If the optimal solution exists, then it is also *extremal*.

In a charge-sustaining HEV application, the principle is applied using the following steps:

Step 1: The Hamiltonian function or cost function to be minimised is defined as shown in Equation 5-1.

$$H\left(SOC_t, P_{motor_t}, \gamma_t, t\right) = \dot{m}_{f\ engine}\left(P_{motor_t}\right) + \gamma_t \dot{SOC}_t\left(P_{motor_t}\right) \quad 5\text{-}1$$

The Hamiltonian function defined in Equation 5-1 represents the instantaneous form of the integral optimisation cost function introduced in Equation 4-4 (Section 4.3).

Step 2: For optimality to be ensured, the control inputs P_{motor} are chosen such that the Hamiltonian condition below in Equation 5-2 is satisfied and the Hamiltonian is minimised, subject to the optimal control constraints specified in Table 4-1 (Section 4.3) and reintroduced below for emphasis.

$$H\left(SOC_t^*, P_{motor_t}^*, \gamma_t^*, t\right) \leq H\left(SOC_t, P_{motor_t}, \gamma_t, t\right) \quad 5\text{-}2$$

Constraint	Implication
$P_{demand_t} \leq P_{motor_{max_t}} + P_{ICE_{max_t}}$	Power demand should not exceed the powertrain limits to avoid damage to the components of the powertrain.
$SOC_{min} \leq SOC_t \leq SOC_{max}$	The battery must operate within its safe limits.
$P_{motor_t} \leq P_{motor_{max_t}}(\omega_{motor})$	Motor power must be lower or equal to the maximum permissible motor power at the current speed.
$P_{ICE_t} \leq P_{ICE_{max_t}}$	Engine power must be lower or equal to the maximum permissible engine power at the current speed.
$SOC_{t_0} = SOC_{t_f} = SOC_f = 60$	The HEV operation must be charge-sustaining

Table 5-1: Optimal control constraints

Step 3:

The state and co-state nonlinear boundary value differential equations are solved as follows:

State equation:

$$\dot{SOC}_t = -\left(\frac{I_{batt_t}}{Q_{batt}}\right) = \frac{dH}{d\gamma_t}\left(SOC_t, P_{motor_t}, \gamma_t, t\right) \quad 5\text{-}3$$

Where I_t (A) is the current flowing through the battery and $Q(Ah)$ is the maximum possible battery charge.

Co-state equation:

$$\dot{\gamma}_t = -\frac{dH}{dSOC}\left(SOC_t, P_{motor_t}, \gamma_t, t\right) \quad 5\text{-}4$$

If the Hamiltonian function in Equation 5-1 is combined with the system state in Equation 5-4, Equation 5-5 is obtained.

$$H\left(SOC_t, P_{motor_t}, \gamma_t, t\right) = \dot{m}_{f\ engine}\left(P_{motor_t}\right) - \gamma_t \frac{I_{batt_t}}{Q_{batt}} \quad 5\text{-}5$$

<u>When:</u>

$$I_{batt_t} = \frac{\eta_{motor}\ P_{motor_t}}{V_{batt}} \quad 5\text{-}6$$

is substituted in Equation 5-5, the Hamiltonian function can be re-expressed, as shown in Equation 5-7 below:

$$H\left(SOC_t, P_{motor_t}, \gamma_t, t\right) = \dot{m}_{f\ engine}\left(P_{motor_t}\right) - \gamma_t \frac{\eta_{motor}\ LHV\ P_{motor_t}}{Q_{batt}\ LHV\ V_{batt}} \quad 5\text{-}7$$

Where η_{motor} is the motor efficiency, LHV is the lower heating value of the fuel, V_{batt} is the battery voltage and γ_t is the co-state of the controller.

Under the definition of equivalence factor, as follows:

$$\varepsilon_t = \frac{LHV\ \gamma_t}{Q_{batt}\ V_{batt}} \quad \text{5-8}$$

Where - $\infty < \gamma_t < 0$, the Hamiltonian function can be expressed in Equation 5-9, as follows:

$$H\left(SOC_t, P_{motor_t}, \gamma_t, t\right) = \dot{m}_{f\ engine}\left(P_{motor_t}\right) + \varepsilon_t \frac{\eta_{motor}\ P_{motor_t}}{LHV} \quad \text{5-9}$$

Similarly:

Equation 5-9 can be expressed as:

$$\dot{m}_{f\ eq}\left(SOC_t, P_{motor_t}, \gamma_t, t\right) = \dot{m}_{f\ engine}\left(P_{motor_t}\right) + \varepsilon_t \frac{\eta_{motor}\ P_{motor_t}}{LHV} \quad \text{5-10}$$

Where $\dot{m}_{f\,eq}\left(SOC_t, P_{motor_t}, \gamma_t, t\right)$ is the equivalent fuel consumed by the vehicle. Under the assumption that the effect of the battery SOC on the equivalence factor is negligible [142], Equation 5-10 can be expressed as follows:

$$\dot{m}_{f\ eq}\left(SOC_t, P_{motor_t}, \gamma_t, t\right) = \dot{m}_{f\ engine}\left(P_{motor_t}\right) + \varepsilon \frac{\eta_{motor}\ P_{motor_t}}{LHV} \quad \text{5-11}$$

Where:

$0 < \varepsilon < \infty$

$\dot{m}_{f\ eq}\ (SOC_t, P_{motor}, \gamma_t, t)\ is$: Equivalent fuel cost (g/s)

$\dot{m}_{f\ engine}\ (P_{motor})\ is$: Engine fuel cost (g/s)

$\varepsilon \frac{\eta_{motor}\ P_{motor}}{LHV}\ is$: Battery fuel cost (g/s)

Physically, the equivalence factor ε can be explained as the equivalent conversion ratio between the thermal energy of fuel and electrical energy.

As could be inferred from Figure 5-1, a low equivalence factor implies that electrical energy is cheaper than using fuel; therefore the controller encourages battery use. Conversely, a high equivalence factor implies that using electrical energy is expensive. Therefore the controller reduces battery use.

Pictorially, the equivalent fuel cost function expressed in Equation 5-11 is shown in Figure 5-2. The lenticular nature of the equivalent fuel cost function means that the optimal solution is unique at each time instant.

Equation 5-11 is the mathematical representation of the ECMS that will be applied to the rest of this study for the development of the robust real-time HEV control strategy.

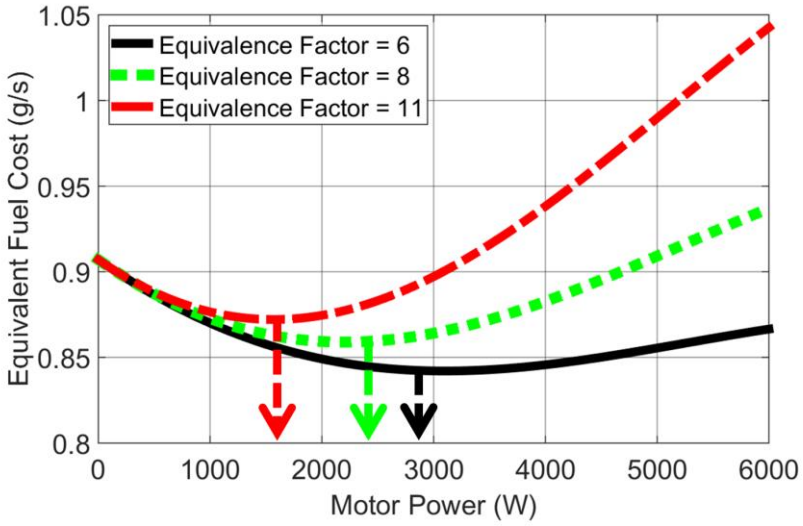

Figure 5-1: Impact of equivalence factor on optimal control input

(Power Demand = 40000 W, Motor Speed = 2000 RPM)

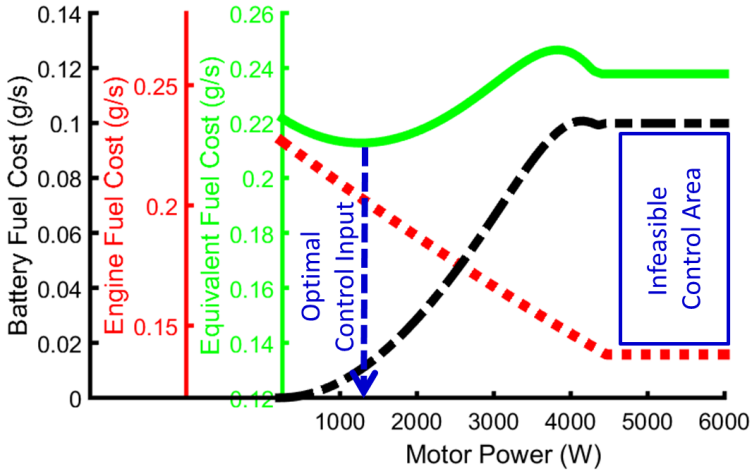

Figure 5-2: Impact of motor power on battery, engine and equivalent fuel cost (Power demand = 20000 W, Equivalence factor = 6, Motor speed = 1000 RPM)

5.3 Offline ECMS implementation

The underlying concept of the ECMS is to minimise the sum of the instantaneous fuel consumed by the internal combustion engine and the battery fuel cost, both of which make up the equivalent fuel cost.

An offline implementation of the ECMS strategy can be realised using the flow chart logic specified in Figure 5-3. At each time *t*, the admissible range of discretised control variables (discretisation resolution is 0.01kW) is calculated as specified in Figure 5-3, taking into consideration the control constraints imposed by the motor speed and vehicle power demand. The control variable resolution is selected minute enough to guarantee a computationally efficient optimisation routine, whilst ensuring that the control policies do not get trapped in a local optima.

The equivalent fuel cost for each control variable is calculated using Equation 5-11. The minimising control variable is applied as the optimal control variable. At the end of the optimisation horizon, the final battery state of charge is compared to the initial battery state of charge. The procedure is repeated each time with a new equivalence factor, until the final battery state of charge equals the initial battery state of charge. The charge-sustaining equivalence factor is the optimal equivalence factor for the specified driving schedule.

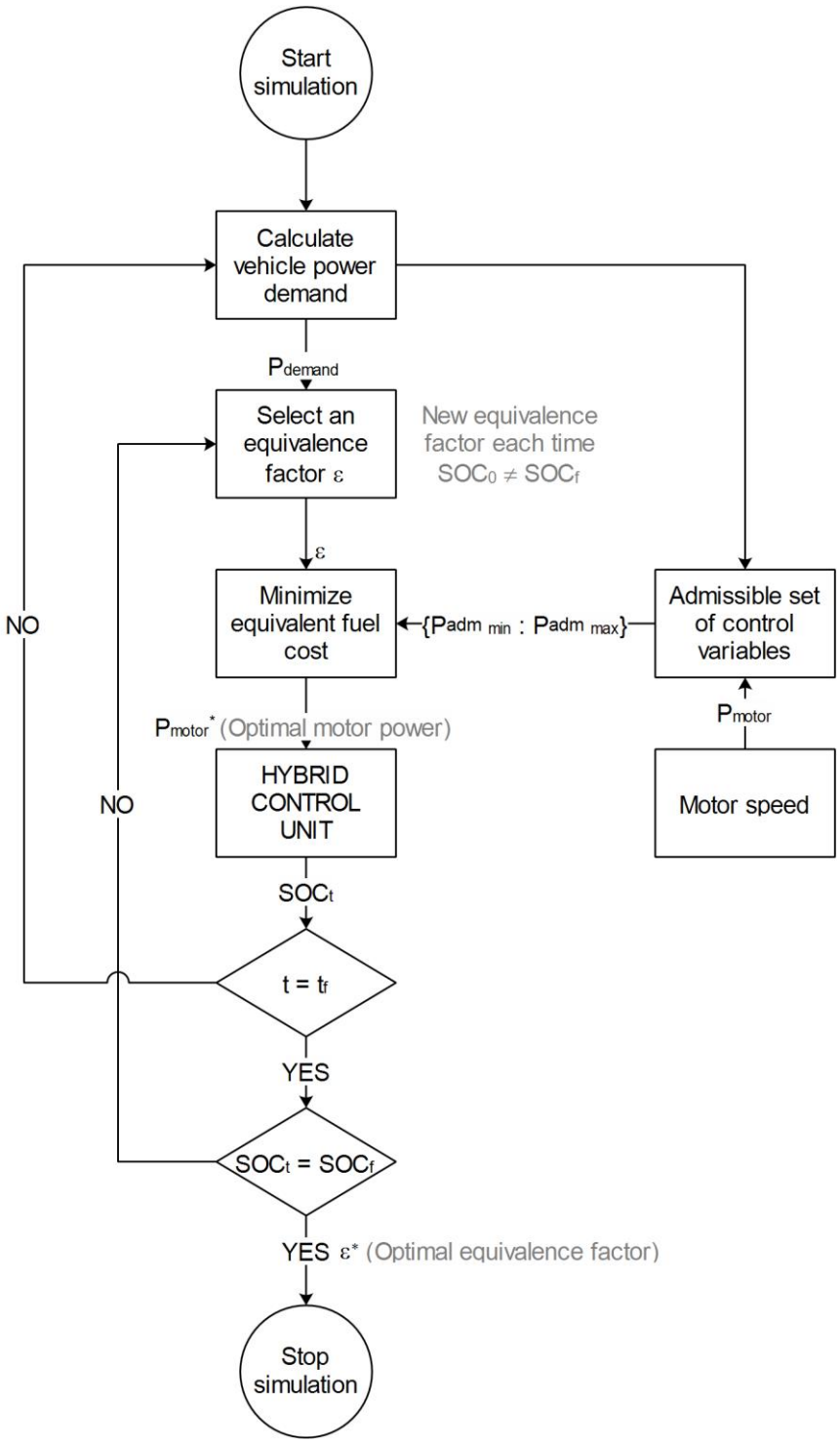

Figure 5-3: Flow chart for an offline ECMS solution

5.4 Impact of equivalence factor on HEV system dynamics

According to a number of studies [137, 143, 160, 226], there is a direct link between the equivalence factor and the battery state of charge usage over any driving cycle. The effect of this calibration is further shown in Figure 5-4, Figure 5-5 and Figure 5-6 over the NEDC, FTP-72 and HWFET driving cycles respectively. From these plots, three main observations are apparent. Firstly, a single but cycle-specific optimal equivalence factor is found to be responsible for charge sustenance (final battery SOC = 60%) over each driving cycle. Secondly, the ECMS control strategy in its present form is highly inflexible. Consequently, a slight deviation in the estimation of the optimal equivalence factor would yield an undesired controller performance that is non-charge-sustaining in real time. Finally, the equivalence factor is found to correlate inversely with cumulative fuel savings and proportionately with the final battery state of charge. In Figure 5-5, beyond an equivalence factor of 12, a decrease in cumulative fuel savings could be observed for a saturated and non-varying final battery state of charge. This trend is very similar to the observations made in Section 3.7.2.4. In this region, the rapid instantaneous depletion in battery state of charge associated with increased equivalence factor appears to be inhibitive to the overall motor tractive energy contribution. This happens due to the fact that as the equivalence factor increases, the battery energy gets used up in a non-efficient way (cumulative fuel savings reduces further with increasing equivalence factor, while the battery state of charge remains the same after being depleted to the minimum level), quicker and earlier in the driving cycle. Consequently, there is no battery energy left to facilitate further use of the electric motor for the rest of the driving cycle.

The peculiar nature of each equivalence factor as detailed in Table 5-2, which means that prior knowledge of the driving cycle is needed for the ECMS to produce charge-sustaining control policies, thus yielding an inherently offline control strategy.

Therefore, in order for ECMS to be employed online, the equivalence factor needs to be determined in an alternative way such that it does not rely on prior driving cycle information.

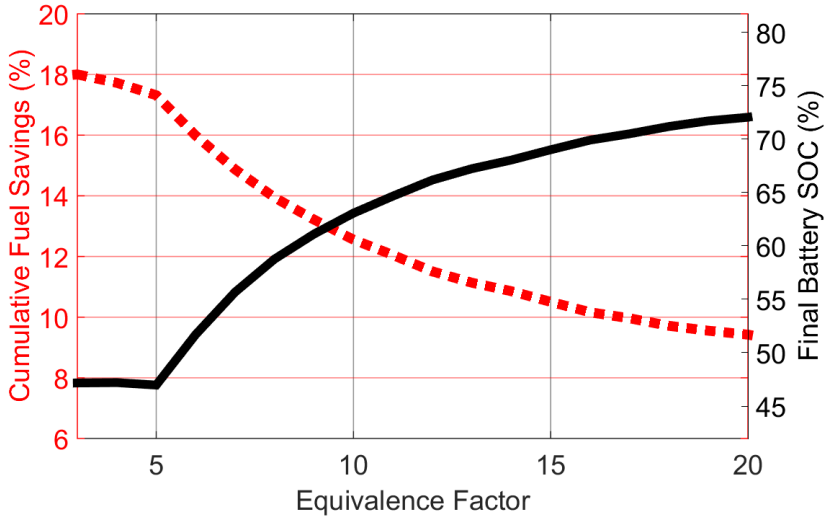

Figure 5-4: Impact of equivalence factor on cumulative fuel savings and final battery state of charge over the NEDC driving cycle

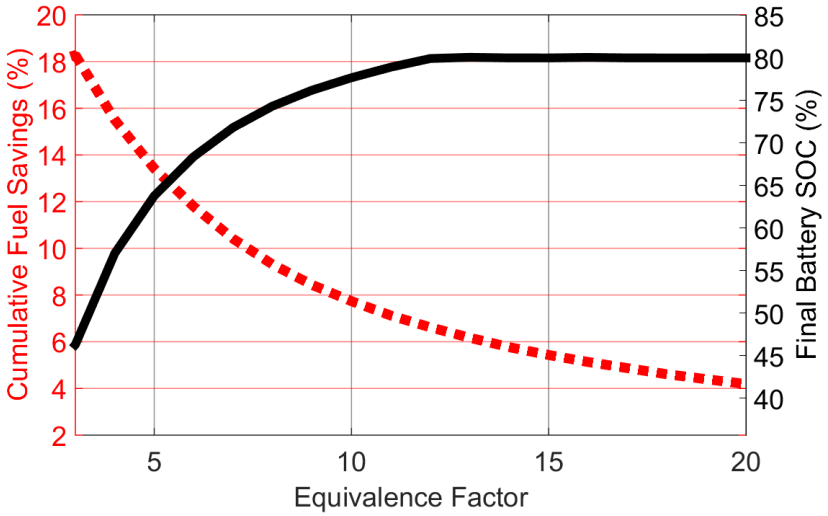

Figure 5-5: Impact of equivalence factor on cumulative fuel savings and final battery state of charge over the FTP-72 driving cycle

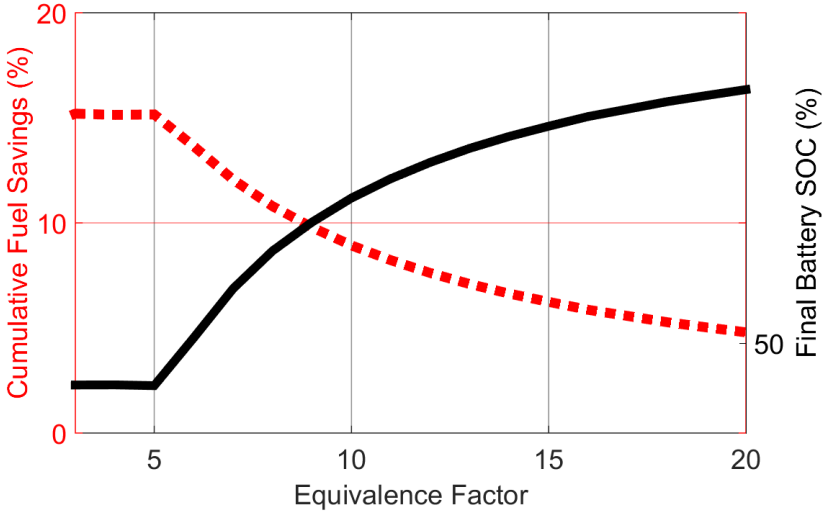

Figure 5-6: Impact of equivalence factor on cumulative fuel savings and final battery state of charge over the HWFET driving cycle

Driving cycle	Equivalence factor	Final battery SOC (%)	Cumulative fuel savings (%)
NEDC	8.512	60	13.57
FTP-72	4.515	60	14.47
HWFET	8.05	60	10.76

Table 5-2: Equivalence factor and controller results for NEDC, FTP-72 and HWFET driving cycles under charge sustenance

5.5 Existing equivalence factor adaptation strategies

Several techniques aimed at appropriately estimating or adapting the equivalence factor towards simultaneously achieving fuel savings and charge sustenance over different driving cycles in real time have been proposed since the introduction of the ECMS strategy. The first simplistic approach was setting the equivalence factor equal to one at all times and for any driving cycle [154]. This strategy was found to yield undesired controller results that were either charge-depleting or charge-hoarding, depending on the driving cycle in question. Consequently, strategies for adapting the equivalence factor online were created. Among relevant examples are equivalence factor adaptation based on driving cycle prediction using GPS [161], driving pattern recognition [227] and battery SOC feedback [62]. In the equivalence factor adaptation method using driving cycle prediction, future driving conditions over a discrete prediction horizon are estimated using a GPS or ITS device and are used to adapt the equivalence factor accordingly online.

In the equivalence factor adaptation method using driving pattern recognition, driving pattern recognition techniques are used online over discrete prediction windows to obtain an estimate of the optimal equivalence factors (pre-computed using offline optimisation) in different driving conditions. In the equivalence factor adaptation method using battery SOC feedback, the equivalence factor is dynamically adjusted to contrast the SOC variation, thus maintaining its value around the reference SOC value (60%), which is considered to be constant. In comparison to the other existing methods, equivalence factor adaptation based on SOC feedback appears to be the most promising, viable and cost-effective method of realising a charge-sustaining ECMS optimal control in real time, as detailed in

Table 5-3. However, this potential is currently offset by its lack of flexibility (non-adaptability to varying driving conditions – Section 2.5), which is the main inspiration for the studies detailed in this chapter.

Comparison factors	**Equivalence factor adaptation based on driving cycle prediction**	**Equivalence factor adaptation based on driving pattern recognition**	**Equivalence factor adaptation based on SOC feedback**
Computational load and cost	High	High	Low
Susceptibility to estimation errors	High	High	Low
Need for external prediction equipment	High	None	None
Real-time implementation cost	High	Average	Low
Adaptability to varying driving conditions	High	High	Low

Desired factors Undesired factors

Table 5-3: Comparison of different equivalence factor adaptation techniques

5.6 Proposed equivalence factor adaptation strategy

In view of the highlighted research gap with regard to equivalent factor adaptation, the use of a simple proportional controller was proposed, as shown in Figure 5-7. This adaptation strategy ensures charge sustainability by adapting online the equivalence factor, thus impacting the relative convenience of thermal and electric operation. When the battery SOC value is higher than the reference SOC value (60%), the proportional controller dynamically adapts the equivalence factor such that electrical energy is deemed cheap and therefore battery use is increased. The reverse happens when the battery SOC value falls below the reference SOC value.

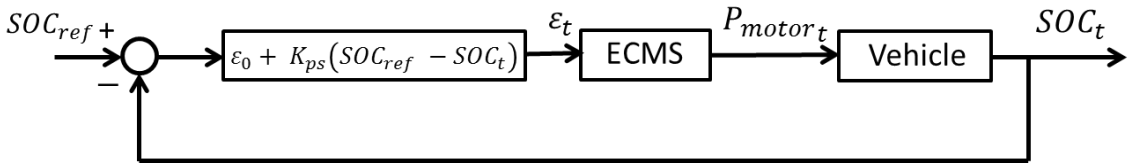

Figure 5-7: Equivalence factor adaptation based on a simple proportional controller

Where ε_0 *is the initial value of the equivalence factor,* K_{ps} *is the proportional controller gain and* SOC_{ref} *(charge-sustaining SOC) is 60%.*

The proposed adaptation strategy differs conceptually from other existing SOC feedback adaptation techniques in the sense that while existing methods propose the selection of the proportional controller gain K_{ps} alone, thus making the controller performance heavily dependent on the intuitive estimate of the initial equivalence factor ε_0, this method simultaneously optimises and selects the proportional controller gain and initial equivalence factor as single parameters that

can be applied in real time over any driving cycle. Unlike other existing SOC feedback methods, this approach solves a conflicting multi-objective optimisation control problem, thus ensuring that the obtained adaptation factors (K_{ps}, ε_0) are optimised for robustness, charge sustenance and fuel reduction.

In order to estimate an appropriate value for the initial equivalence factor ε_0 and the proportional controller gain K_{ps} for this controller, a sensitivity analysis of its impact on cumulative fuel savings and final battery state of charge was carried out over the NEDC, FTP-72 and HWFET driving cycles, as shown in Figure 5-8 to Figure 5-10.

From these figures, the following two key observations are made:

1. For all driving cycles analysed, an increase in proportional controller gain is found to correspond to an increase in controller robustness for SOC control, as well as a reduction in cumulative fuel savings (%) achieved.

2. As the proportional controller gain is increased, a significant change in gradient of the final battery SOC (%) curve is observed, thus resulting in a robust controller performance in which a change in initial equivalence factor has very little effect on the change in the final battery state of charge.

For each driving cycle, there exists a set of unique initial equivalence factors and proportional controller gains which yield a charge-sustaining performance. Considering the fuel savings potential posed by each set of cycle-specific controller adaptation factors, the control dilemma lies in simultaneously selecting an appropriate single initial equivalence factor and proportional controller gain which is optimised for fuel reduction, charge sustenance and robustness.

In order to select the appropriate value of initial equivalence factor and proportional controller gain for use in real time optimal control of the HEV, the following unique steps were taken:

1. A sensitivity analysis was carried out to outline the impact of initial equivalence factor and proportional controller gain on cumulative fuel savings and final battery state of charge over the NEDC, FTP-72, JAPAN1015, NYCC, SC03, HWFET and IM240 driving cycles.

2. For each controller gain and equivalence factor, the corresponding cumulative fuel savings (%) and final battery SOC (%) were averaged accordingly, as shown in Figure 5-11.

3. For each set of average charge-sustaining initial equivalence factor and proportional controller gain, the corresponding average cumulative fuel savings (%) were plotted out as shown in Figure 5-12.

4. The charge-sustaining adaptation parameter set (initial equivalence factor and proportional controller gain) with the highest average cumulative fuel savings (%) were then selected and applied to the ECMS controller in real time (Figure 5-12).

5. Based on the steps above, an initial equivalence factor value of 3.47 and a controller gain value of 1.725 were selected for the ECMS controller implementation in real time.

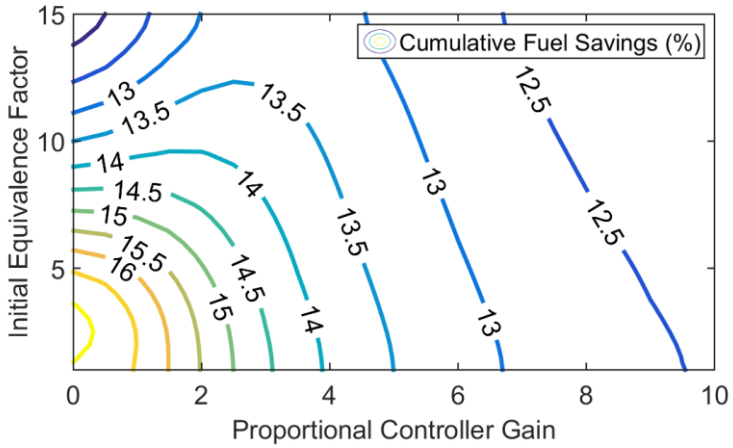

(a) Impact of initial equivalence factor and proportional controller gain on cumulative fuel savings

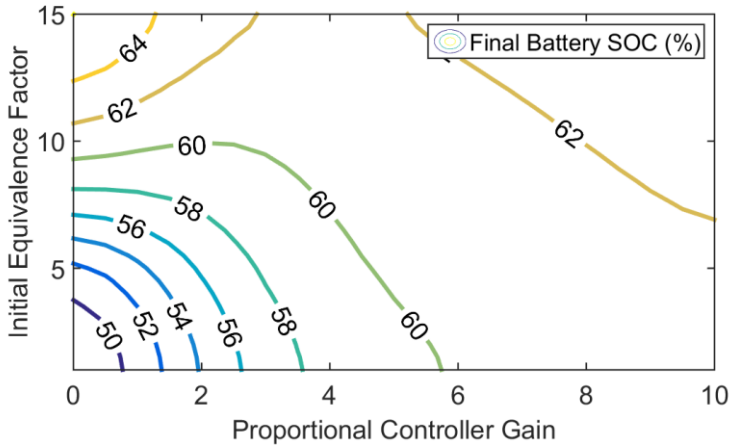

(b) Impact of initial equivalence factor and proportional controller gain on final battery SOC

Figure 5-8: Sensitivity analysis of initial equivalence factor and proportional controller gain over the NEDC driving cycle

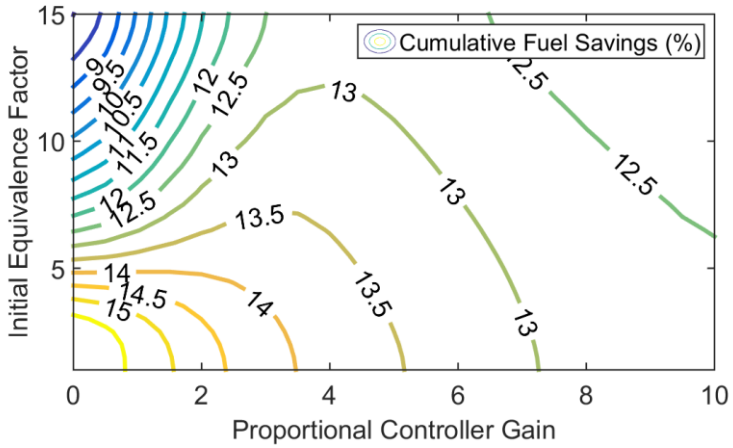

(a) Impact of initial equivalence factor and proportional controller gain on cumulative fuel savings

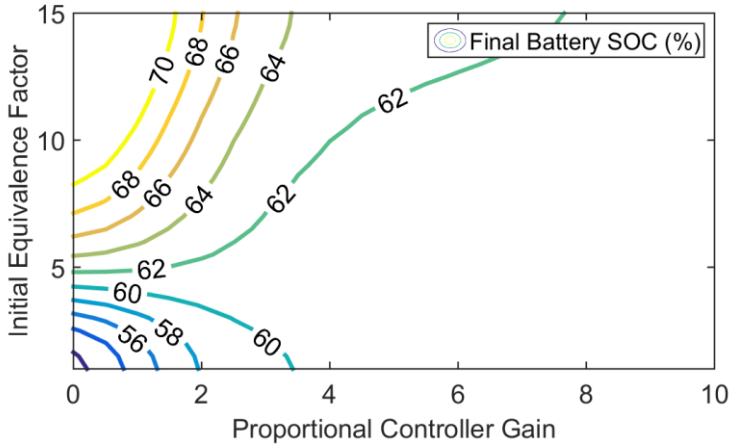

(b) Impact of initial equivalence factor and proportional controller gain on final battery SOC

Figure 5-9: Sensitivity analysis of initial equivalence factor and proportional controller gain over the FTP-72 driving cycle

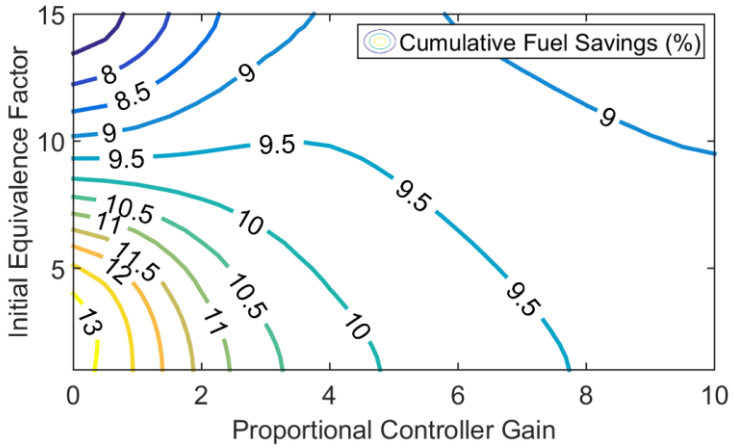

(a) Impact of initial equivalence factor and proportional controller gain on cumulative fuel savings

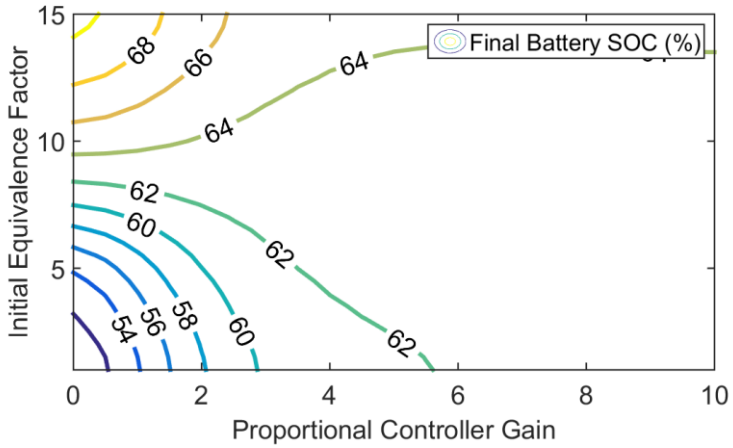

(b) Impact of initial equivalence factor and proportional controller gain on final battery SOC

Figure 5-10: Sensitivity analysis of initial equivalence factor and proportional controller gain over the HWFET driving cycle

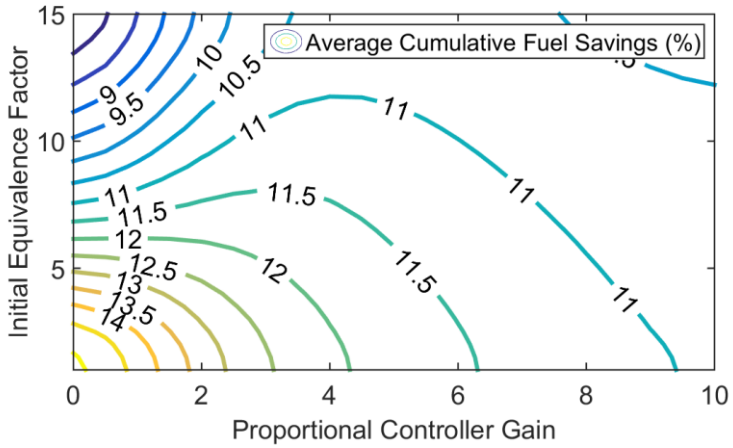

(a) Impact of initial equivalence factor and proportional controller gain on cumulative fuel savings

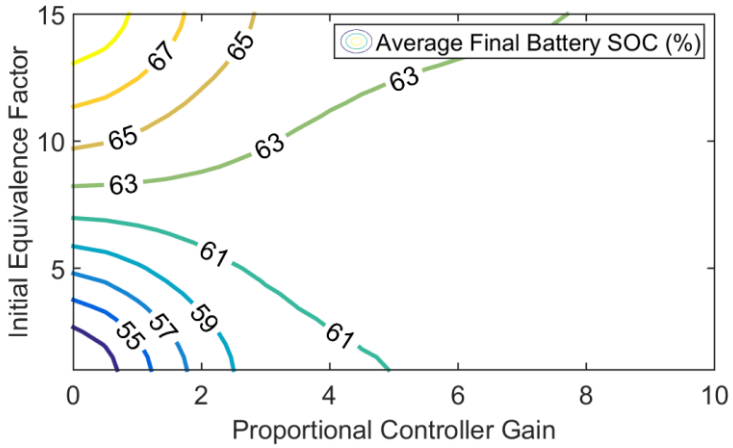

(b) Impact of initial equivalence factor and proportional controller gain on final battery SOC

Figure 5-11: Sensitivity analysis of initial equivalence factor and proportional controller gain: averaged over NEDC, FTP-72, JAPAN1015, NYCC, SC03, HWFET and IM240 driving cycles

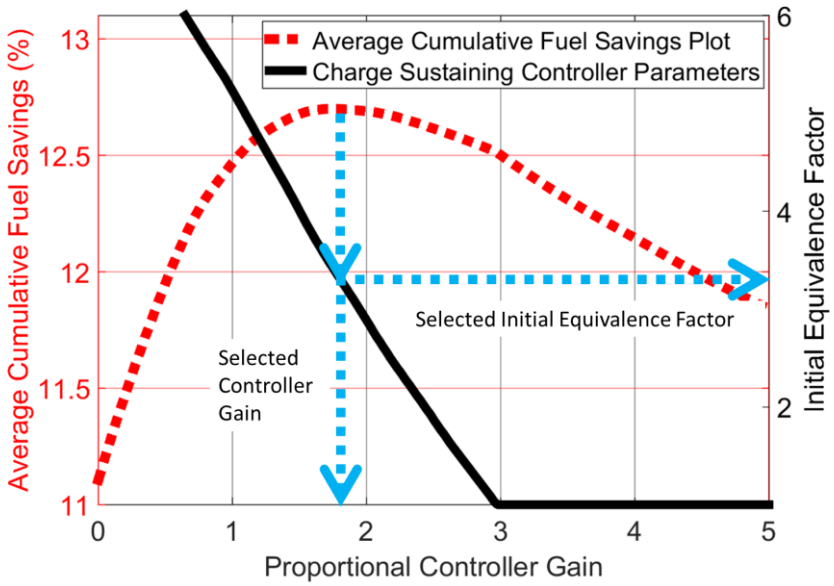

Figure 5-12: Selection of initial equivalence factor and proportional controller gain from a Pareto-set of charge sustaining control parameters, for real-time HEV control

5.7 Real-time evaluation of the proposed RPEC strategy

In this section, the hybridisation potentials of the proposed "Robust Proportional ECMS Control" strategy (RPEC) are assessed over the NEDC, FTP-72, JAPAN1015, US06, LA92, ARTEMIS U130, HWFET and WLTC 3 driving cycles in real time. In order to assess these potentials, the pre-estimated values of the initial equivalence factor (3.47) and the proportional controller gain (1.725), which were estimated in Section 5.6, are applied.

Over the US06 driving cycle (Figure 5-13a), which represents an aggressive highway driving scenario in the US (Table 3-2), the controller is found to be charge-depleting by 1.57% (Figure 5-13c), with a cumulative fuel savings of 8.40% (Figure 5-13b).

Unlike the US06 driving cycle, the LA92 driving cycle (Figure 5-14a) represents an aggressive urban driving scenario which typically offers more braking opportunities. Over this driving cycle, the motor was found to significantly participate in vehicle braking, which is believed to be the prime contributor to the near charge-sustaining performance of 60.61% (Figure 5-14c) achieved by the controller. In addition, a cumulative fuel savings of 10.40% was achieved over this driving cycle as shown in Figure 5-14b.

Unlike the US06 and LA92 driving cycles which represent aggressive American highway and urban driving scenarios respectively, the ARTEMIS U130 driving cycle (Figure 5-15a) has been introduced in this study to assess the hybridisation potentials of the controller over an aggressive highway driving scenario in Europe. Over the ARTEMIS U130 driving cycle, a near charge-sustaining balance in energy

of 59.28% (Figure 5-15c) is achieved with a cumulative fuel savings of 9.18% (Figure 5-15b).

The WLTC 3 driving cycle (Figure 5-16a) represents a moderate urban driving scenario in Europe. Unlike all other considered driving cycles in this section, the WLTC 3 driving cycle offers the opportunity to investigate the potency of the controller over a cycle which is representative of the most common urban driving scenario in Europe. The WLTC 3 driving cycle is characterised by numerous braking opportunities, which makes it possible for the controller to achieve a cumulative fuel savings of 13.73% (Figure 5-16b), with a final battery state of charge of 63.63% (Figure 5-16c).

A summary of the fuel savings potential derived from applying the RPEC strategy to different driving profiles is detailed in Table 5-4. In Table 5-4, estimations of average fuel savings assuming charge sustenance are also included to reflect the absolute fuel savings for the RPEC strategy over different standard driving cycles. These values are estimated from equations 3-28 and 3-29 (Section 3.5.7).

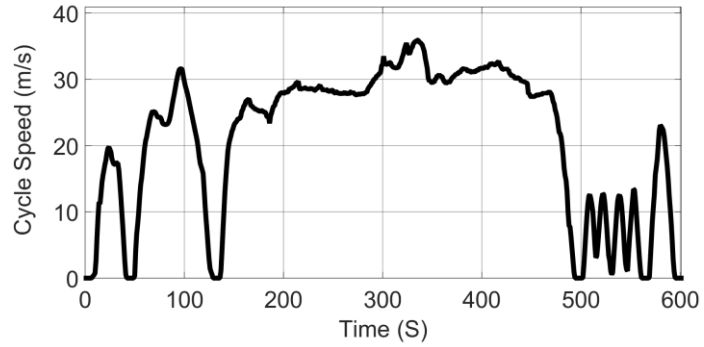

(a) US06 driving cycle

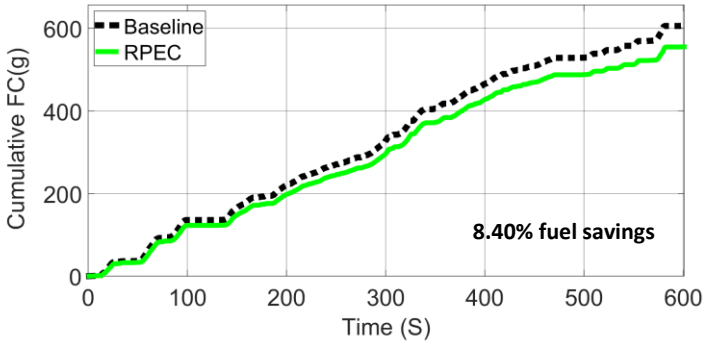

(b) Cumulative fuel consumption profile

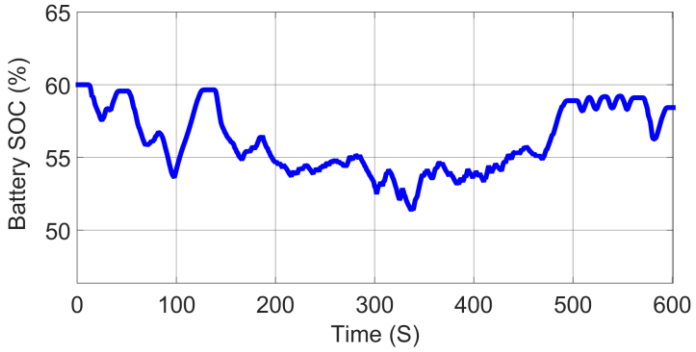

(c) Battery state of charge profile

Figure 5-13: RPEC strategy simulation results for US06 driving cycle

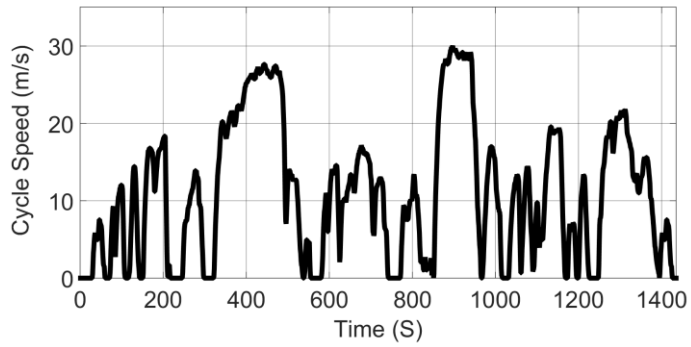

(a) LA92 driving cycle

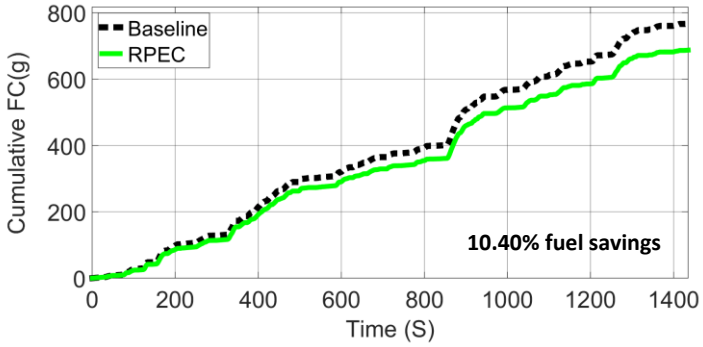

(b) Cumulative fuel consumption profile

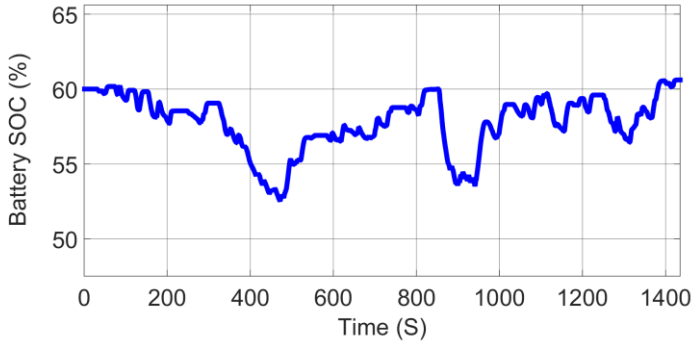

(c) Battery state of charge profile

Figure 5-14: RPEC strategy simulation results for LA92 driving cycle

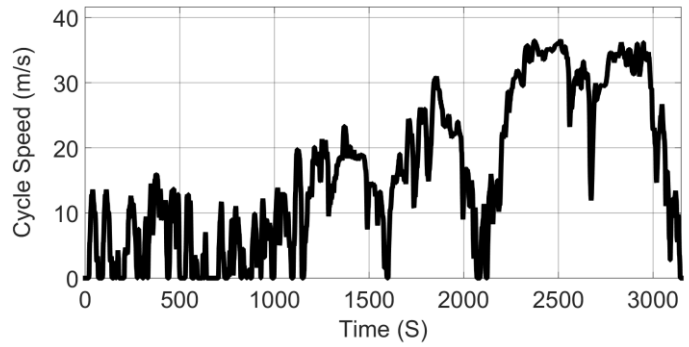

(a) ARTEMIS U130 driving cycle profile

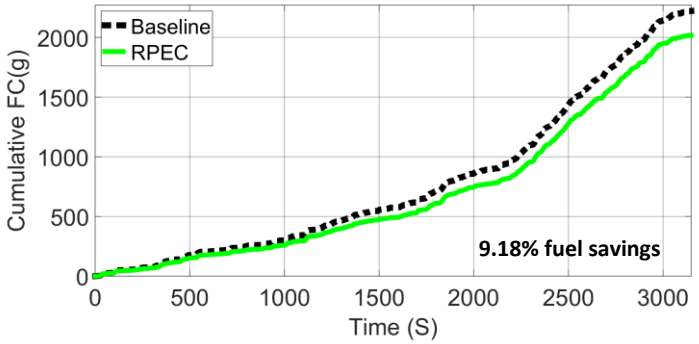

(b) Cumulative fuel consumption profile

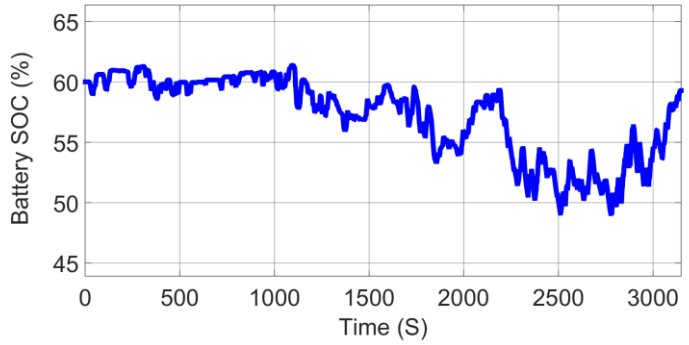

(c) Battery state of charge profile

Figure 5-15: RPEC strategy simulation results for ARTEMIS U130 driving cycle

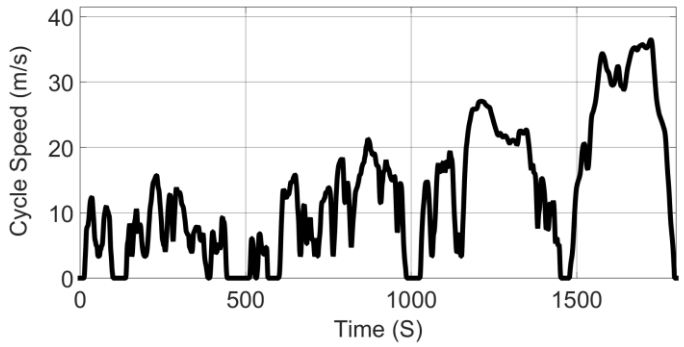

(a) WLTC 3 driving cycle profile

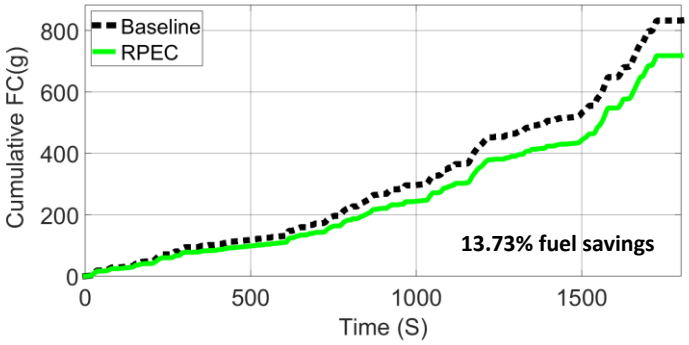

(b) Cumulative fuel consumption profile

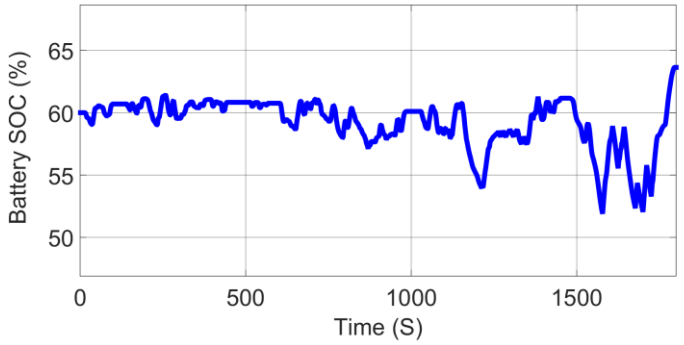

(c) Battery state of charge profile

Figure 5-16: RPEC strategy simulation results for WLTC 3 driving cycle

Driving cycle	Baseline fuel consumption (g)	Fuel savings (Actual) (g)	Final battery SOC (%)	Fuel savings (Actual) (%)	Fuel savings (Assuming charge sustenance) (g)	Fuel Savings (Assuming charge sustenance) (%)
NEDC	441.40	67.25	55.73	15.24	52.87	11.98
FTP-72	455.38	65.21	60.62	14.32	65.90	14.47
JAPAN1015	184.09	27.66	62.98	15.03	29.11	15.81
US06	606.50	50.92	58.43	8.40	46.51	7.67
LA92	767.31	79.81	60.61	10.40	80.63	10.51
ARTEMIS U130	2221.40	204.03	59.28	9.18	195.70	8.81
HWFET	421.44	45.58	59.98	10.81	45.51	10.80
WLTC 3	833.05	114.37	63.63	13.73	121.74	14.61

Table 5-4: Simulation results for the RPEC strategy with an initial equivalence factor of 3.470 and a proportional controller gain 1.725 over the NEDC, FTP-72, JAPAN1015, US06, LA92, ARTEMIS U130, HWFET and WLTC 3 driving cycles

5.8 Comparison of the RPEC strategy against existing SOC feedback ECMS controllers

In this section, the RPEC strategy is compared to existing SOC feedback controllers with different adaptation techniques over the US06, LA92 and ARTEMIS U130 driving cycles. Before carrying out this comparative analysis, it is imperative to introduce the existing SOC feedback controllers in question.

One of such controller is the "Static prediction based on SOC" (SP) controller [193], which is mathematically represented in Equation 5-12.

$$When\ SOC_t < SOC_{ref} \qquad 5\text{-}12$$

$$\varepsilon_t = \varepsilon_0 \left(1 + \left(\frac{tan\left(SOC_{ref} - SOC_t\right)\frac{\pi}{180}}{tan\left(SOC_{ref} - SOC_{min}\right)\frac{\pi}{180}} \right)^n \right)$$

$$When\ SOC_t > SOC_{ref}$$

$$\varepsilon_t = \varepsilon_0 \left(1 + \left(\frac{tan\left(SOC_{ref} - SOC_t\right)\frac{\pi}{180}}{tan\left(SOC_{ref} - SOC_{max}\right)\frac{\pi}{180}} \right)^n \right)$$

n = 2, $SOC_{ref} = 60\%$, $SOC_{min} = 40\%$, $SOC_{max} = 80\%$

The second controller being considered is the "Adaptive prediction based on SOC" (AP) controller [193], which is mathematically represented in Equation 5-13.

$When\ SOC_t < SOC_{ref}$ 5-13

$$\varepsilon_t = \varepsilon_{t-1}\left(1 + \left(\frac{tan\left(SOC_{ref} - SOC_t\right)\frac{\pi}{180}}{tan\left(SOC_{ref} - SOC_{min}\right)\frac{\pi}{180}}\right)^n\right)$$

$When\ SOC_t > SOC_{ref}$

$$\varepsilon_t = \varepsilon_{t-1}\left(1 + \left(\frac{tan\left(SOC_{ref} - SOC_t\right)\frac{\pi}{180}}{tan\left(SOC_{ref} - SOC_{max}\right)\frac{\pi}{180}}\right)^n\right)$$

$0 < \varepsilon_t < 40$ (Used to avoid integral build up), n = 2, $SOC_{ref} = 60\%$, $SOC_{min} = 40\%$, $SOC_{max} = 80\%$

Both AP and SP controllers employ the use of a tangent penalty function to regulate the battery SOC whenever it deviates from the reference SOC, which is 60%. In both controllers, whenever the battery SOC is close to the reference value, the penalty is negligible; however, the penalty function changes nonlinearly as the SOC deviates from the reference value. The exponential coefficient governing the shape of the penalty function is (n = 2).

In contrast to the SP controller, the AP controller introduces some adaptability into the system, such that the initial equivalence factor has a negligible effect on system performance. This adaptability is facilitated using the feedback of previous equivalence factors, such that the centre of the tangent function is made to change according to trending values of the equivalence factor. In order to avoid an integral build up in the system, the equivalence factor feedback for the “AP” controller is saturated at 40. From Figure 5-4, Figure 5-5 and Figure 5-6, for the NEDC, FTP-72 and HWFET driving cycles respectively, it could be observed that at

an equivalence factor of 20, most of the driving cycles edge closer towards the maximum battery state of charge (80%). With this in mind, the equivalence factor feedback for the “AP” controller is saturated at 40 to accommodate the possibility of using the RPEC strategy on an aggressively charge-depleting driving profile, which may not be close to reaching the maximum battery state of charge, at an equivalence factor of 20.

Over all the driving profiles analysed (Figure 5-17 to Figure 5-19), the SP controller performance is found to be greatly affected by the initial equivalence factor (Figure 5-17a, Figure 5-18a and Figure 5-19a), which weakens the robustness of the controller and makes it the least effective of all controllers compared. In comparison to the RPEC strategy, the AP controller is found to be inefficient over the US06, LA92 and ARTEMIS U130 driving cycles. Over these driving cycles, both controllers deplete similar levels of battery energy, but the RPEC strategy achieves higher fuel savings, as shown in Figure 5-17a, Figure 5-18a and Figure 5-19a, for the US06, LA92 and ARTEMIS U130 driving cycles respectively.

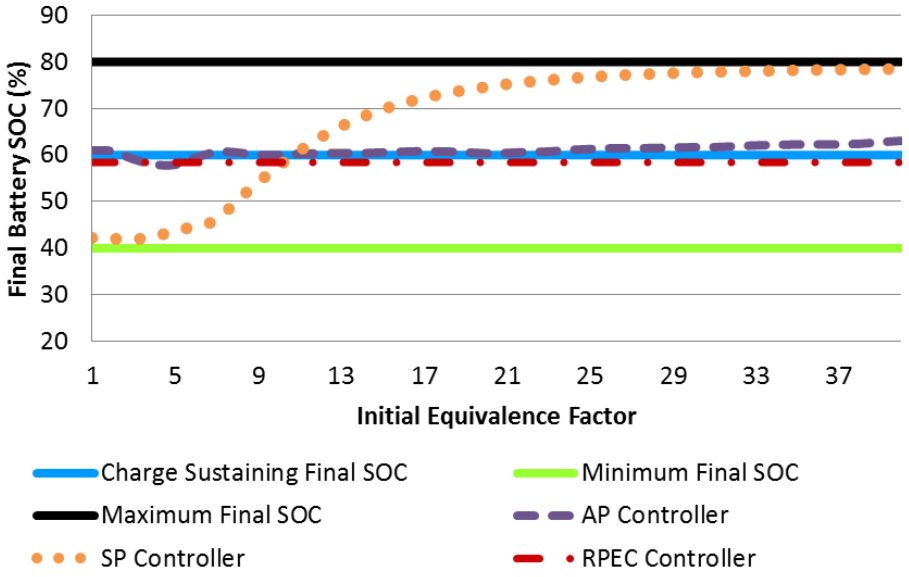

(a) Impact of initial equivalence factor on final battery state of charge

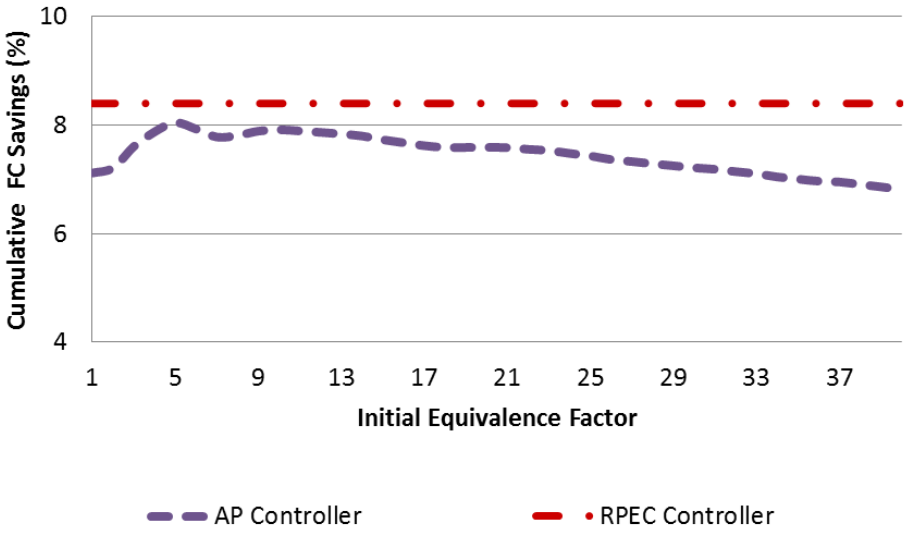

(b) Impact of initial equivalence factor on cumulative fuel savings

Figure 5-17: Comparison of SP, AP and RPEC strategies over the US06 driving cycle

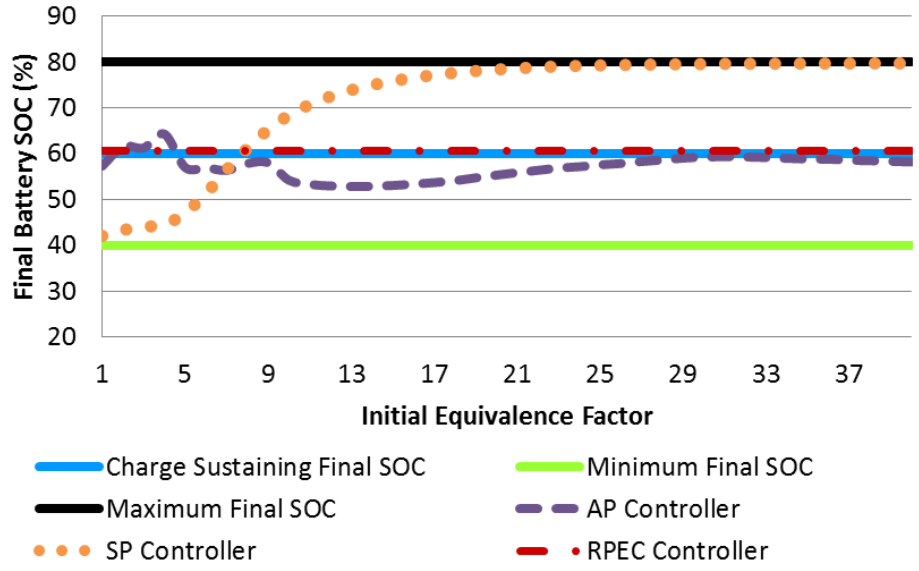

(a) Impact of initial equivalence factor on final battery state of charge

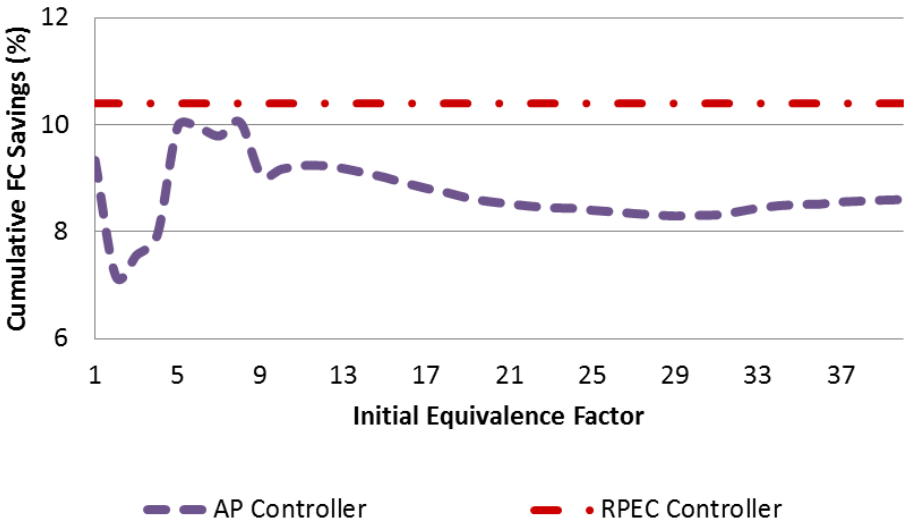

(b) Impact of initial equivalence factor on cumulative fuel savings

Figure 5-18: Comparison of SP, AP and RPEC strategies over the LA92 driving cycle

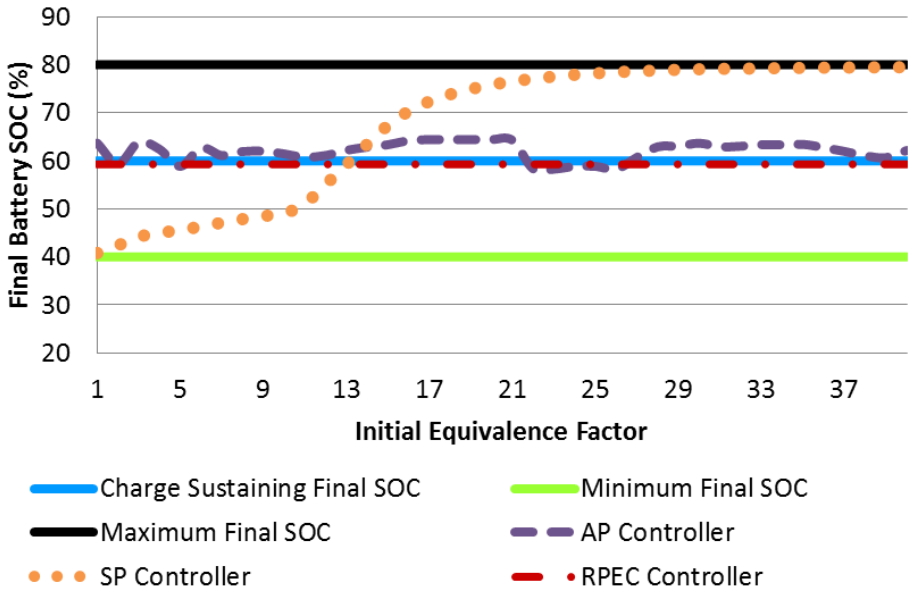

(a) Impact of initial equivalence factor on final battery state of charge

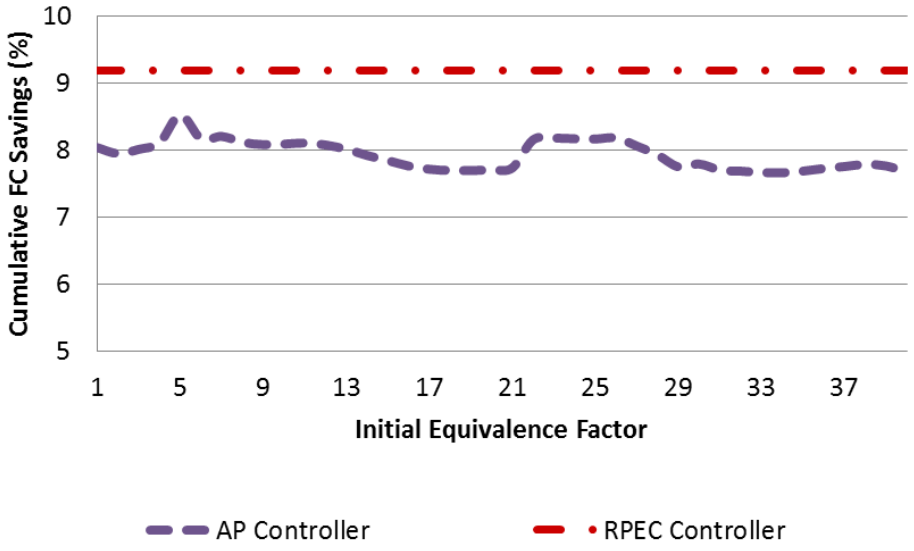

(b) Impact of initial equivalence factor on cumulative fuel savings

Figure 5-19: Comparison of SP, AP and RPEC strategies over the ARTEMIS U130 driving cycle

Based on the foregoing comparative analysis, the following general inferences could be drawn:

1. The SP controller performance is greatly affected by the intuitive estimate of the initial equivalence factor, which means that the controller can only provide promising and charge-sustaining results if an accurate estimate of the initial equivalence factor is made. This shortcoming limits the usefulness of the SP controller, and thus its viability for real-time implementation.

2. The AP controller introduces some adaptability into the control system by changing the centre of the tangent function in accordance with the trending values of the equivalence factor. By so doing, the AP controller is able to achieve a higher level of charge sustenance when compared to the SP controller. That notwithstanding, the AP controller suffers from efficiency issues in that over the US06, LA92 and ARTEMIS U130 driving cycles, it is found to deplete similar battery energy levels as the RPEC strategy but achieves less fuel savings.

3. The RPEC strategy performs consistently well across all cycles examined, minimising the final SOC error compared to the other controllers. Its robustness and simultaneous optimisation of adaptation factors for charge sustenance and fuel reduction make it a promising option for real-time implementation in commercial HEVs.

5.9 ECMS real-time implementation issues

5.9.1 Computational burden

Online implementation of the ECMS approach involves the calculation of an equivalent fuel cost at each time instant, for each candidate control variable. Although optimality can be improved by increasing the discretisation resolution of the candidate control variables, in a vehicle application, there needs to be a balance between this advantage and the associated computational burden which tends to increase with increasing discretisation resolution. To overcome this problem, pre-calculation of optimal control variables is recommended. This approach consists of calculating, offline, optimal control variables given all possible combinations of vehicle power demand, engine speed, motor speed, battery state of charge and equivalence factors. Typically, the equivalent fuel consumption is calculated for all combinations of vehicle operating conditions, and the optimal control variable corresponding to each set of operating conditions is calculated and stored in a multidimensional lookup model. During real-time vehicle operation, suitable optimal control variables are selected by matching online operating conditions to those stored in the lookup model. This approach is simple and guarantees reduction in processor requirements for ECMS online implementation.

5.9.2 Chattering issues

Another common problem with ECMS implementation on vehicles is the presence of chattering in the control outputs. This phenomenon occurs when the optimal control variables change very quickly and distinctively. The reason for this occurrence is that the control output is the minimising control variable, which can be very different at each time instant. The resultant effect is a high frequency of change in control outputs which can be uncomfortable for passengers. To solve this problem, filtering of control outputs and the introduction of hysteresis are recommended.

5.10 Chapter conclusions

This chapter offers a detailed insight into ECMS optimal control. First, a theoretical framework for the ECMS control is developed from Pontryagin's Minimum Principle. From this derivation it is shown that, based on the assumption that the effect of the battery SOC on the equivalence factor is negligible, the equivalence factor could be considered a constant parameter, thus reducing the complexity of the optimal control problem. Physically, the equivalence factor represents the equivalent conversion ratio between the thermal energy from fuel and electrical energy. Using a one-dimensional sensitivity analysis, a low equivalence factor was shown to imply that electrical energy is cheaper than fuel; therefore, the controller encourages battery use, while a high equivalence factor implies that using electrical energy is expensive. Therefore, the controller reduces battery use.

Analysis of the impact of the equivalence factor on the fuel savings potential of the modelled vehicle was undertaken over different driving cycles. The following useful inferences were drawn from this analysis: (1) A single but cycle-specific optimal equivalence factor is responsible for charge sustenance (final battery SOC = 60%) over each driving cycle. (2) A slight deviation in the estimation of the optimal equivalence factor would yield an undesired controller performance, which is non-charge-sustaining in real time. (3) The equivalence factor is found to correlate inversely with cumulative fuel savings and proportionately with final battery state of charge.

Based on observations from the aforementioned analysis, problems impeding the commercial implementation of ECMS optimal control were identified alongside some key solutions that have been proposed in literature. Despite the proposed

solutions, the problem of non-robustness (non-adaptability to varying driving conditions – Section 2.5) for ECMS controllers still remained unaddressed and, as such, was considered the main inspiration for this study.

In order to address the non-robustness issue currently associated with ECMS controllers, a proportional ECMS control strategy (RPEC) was proposed. This strategy works by adapting equivalence factors based on battery state of charge feedback. The proposed adaptation strategy differs conceptually from existing SOC feedback adaptation strategies in that the method simultaneously optimises and selects the adaptation factors (proportional controller gain and initial equivalence factor) as single parameters which can be applied in real time over any driving cycle. Unlike existing SOC feedback methods, this approach solves a conflicting multi-objective optimisation control problem, thus ensuring that the obtained adaptation factors are optimised for robustness, charge sustenance and fuel reduction.

Using a two-dimensional sensitivity analysis, the appropriate adaptation factors for application in real time were selected (initial equivalence factor = 3.47 and proportional controller gain = 1.725) and applied over a range of driving profiles. Hybridisation fuel savings potential of approximately 8.40%, 10.40%, 9.18% and 13.73% were observed over the US06, LA92, ARTEMIS U130 and WLTC 3 driving cycles respectively.

In comparison to existing SOC feedback ECMS controllers, the RPEC strategy was found to perform well, specifically in two key areas. The first being that the controller appears robust and unaffected by the intuitive estimate of the initial equivalence factor as in the case of the “SP controller” and the second being that the controller is highly efficient. Over the US06, LA92 and ARTEMIS U130 driving

cycles, it was shown that the “AP controller“ in comparison to the RPEC strategy, depleted similar levels of battery energy but achieved less fuel savings.

Despite the significant fuel savings realised by the RPEC strategy, the absence of route preview information from the proposed control framework means that route elevation changes are not being accounted for during the equivalence factor adaptation. As a result, the RPEC strategy may be unable to effectively manage energy fluctuations resulting from changing route elevations. This problem becomes even more significant in hilly environments where the RPEC strategy could result in a non-charge-sustaining performance. Route preview information is also important in ensuring that vehicular energy management problems are approached from a global perspective, with efficient utilisation of energy regeneration opportunities resulting from road grade. In the next chapter, the fuel savings potential of the research vehicle through the use of real-time predictive control strategies with access to partial route preview information are assessed.

6 HEV REAL-TIME OPTIMAL CONTROL WITH PARTIAL ROUTE PREVIEW INFORMATION

6.1 Introduction

In Chapter 5, the global optimisation problem defined in Section 4.3 is solved using an instantaneous optimisation approach based on the ECMS. Using an ECMS variation based on battery SOC feedback, a robust proportional ECMS controller (RPEC) with no access to route preview information was designed and simulated over 8 standard driving cycles representing various driving conditions.

Simulation results from this analysis proved the RPEC strategy to be a near-optimal controller, which is capable of yielding a near charge-sustaining energy management performance. With no access to route preview information, the RPEC strategy may be unable to effectively manage energy fluctuations resulting from changing route elevations. This problem becomes even more significant in uneven environments where the RPEC strategy could result in a non-charge-sustaining performance. Route preview information is also important in ensuring that vehicular energy management problems are approached from a global perspective, with efficient utilisation of energy regeneration opportunities resulting from road grade.

This chapter explores the fuel savings potential of the research vehicle through the use of real-time predictive control strategies with access to partial route preview information (future driving conditions). Route preview information can be estimated using the global positioning system (GPS), the geographic information system (GIS) and the intelligent transportation system (ITS). An interaction

between these systems and a real-time predictive control strategy is summarised in Figure 6-1. As shown in Figure 6-1, a predictive control strategy typically requires a receding horizon control approach whereby look-ahead driving information is predicted by the vehicle prediction systems (GPS, GIS and ITS) and then used to control the vehicle at the current time step.

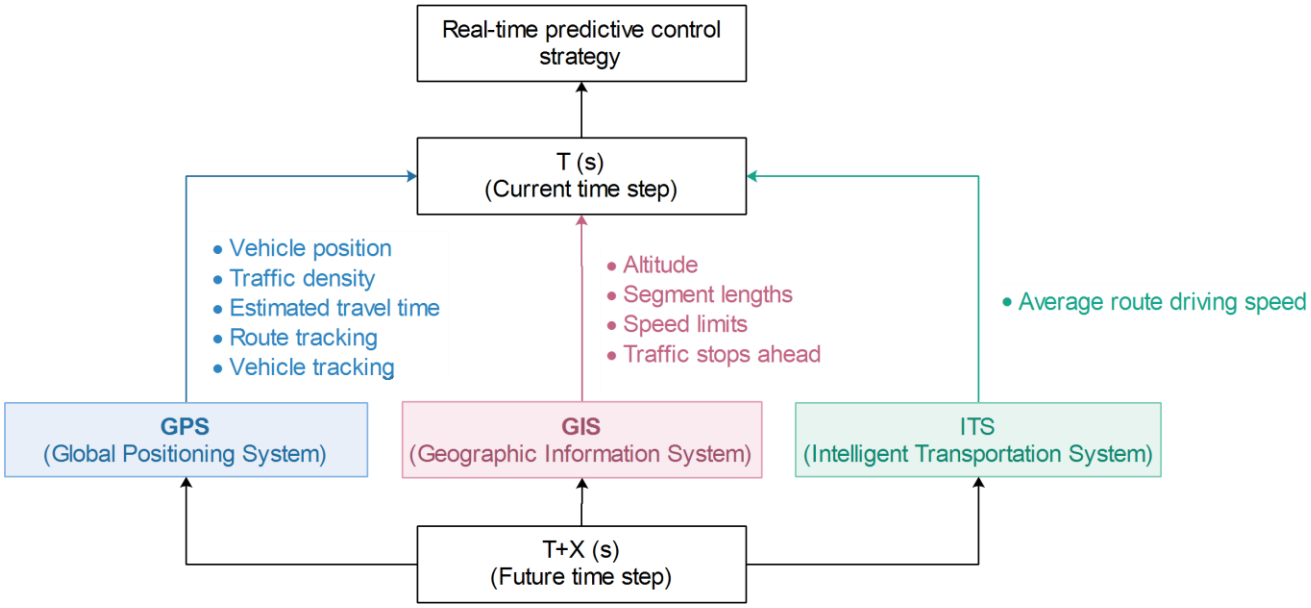

Figure 6-1: Diagram showing the interaction between vehicle prediction systems and a real-time predictive control strategy

Very few studies have attempted to develop a predictive HEV control strategy [45, 131, 167, 228, 229]. Typically, the easiest way to apply look-ahead driving information in an HEV control environment is in the form of heuristics. In this approach, speed and elevation information from vehicle predictive systems (GPS, GIS and ITS) are used in the form of control rules to optimise the predictive controller towards achieving optimal fuel savings. Heuristic-based predictive control strategies are subjective by definition and, as such, have performances which vary depending on the complexity of the control rules. With no standard

approach to the formation of control rules, and no way to determine a priori that the given set of rules is appropriate for the given application, heuristic-based predictive control strategies are generally unable to guarantee the optimality of the solution found. In a study by Adhikari [195], a receding horizon control approach to predictive HEV energy management was proposed. In this approach, future torque demand and speed demand are estimated from look-ahead speed and gradient information. The resulting energy demand estimations are then fed into a power management module, where the torque split ratios that minimises fuel consumption over the look-ahead horizon are selected and applied. The same procedure is repeated in the next time step with updated states.

In a study by Appelkvist *et al.* [230], an instantaneous optimisation approach to predictive HEV control was proposed. The research goal here was to lower the SOC reference signal before an important regeneration segment, in order to maximise battery energy regeneration without violating any constraints. This was achieved through the use of a linear programming algorithm to calculate the optimal start values of the battery state of charge for each recuperation segment, such that energy recuperation is maximised without violating any constraints. The performance of the resulting controller was found to be predominantly charge-hoarding (SOC deviations as high as 10%). There are at least two plausible reasons to explain the poor controller performance reported in this study. The first is the lack of a global outlook to the optimisation routine and the second is the non-inclusion of energy consuming segments during the optimisation procedure. Without both considerations, the resulting SOC reference trajectory is only optimal in a local sense.

To date, the author could find no research study performed to develop a global route-optimal predictive control strategy for real-time application. Developing such a predictive controller is a non-trivial task, and involves the formulation of route preview information (average route driving speed and altitude) into a global optimal reference trajectory which can be implemented in an HEV control framework. Building on this research gap, two main contributions to existing energy management literature are offered in this chapter.

The first contribution is a novel route-based ECMS control strategy, which uses a route optimised battery SOC trajectory to adapt the predictive controller towards achieving an optimal performance in real time. The route-optimised battery SOC trajectory in this case is formulated from route preview information in the form of average route driving speed and altitude. First, the "least expendable or regenerable energy across the driving route segments" will be calculated from the estimated route preview information (average route driving speed and altitude). Thereafter, the resulting energy profile will be used to formulate a route optimised battery state of charge reference trajectory. Finally, the route optimised battery SOC trajectory will then be incorporated into the RPEC framework. The resulting controller dubbed RBEC (route based ECMS control) will be simulated subsequently, in comparison with the RPEC strategy, over different real-world driving scenarios, with a view to investigating the additional benefits associated with incorporating route preview information into an HEV energy management control framework.

The second contribution is the development of two novel methods of achieving significant fuel savings through vehicle speed control. The first method is an optimal vehicle speed control approach based on deterministic dynamic

programming, while the second method is a real-time vehicle speed control approach which is based on smoothing the speed trajectory of the vehicle immediately ahead (lead vehicle). First, the theoretical frameworks for both methods will be developed. These models will then be used for comparative performance evaluations over different real-world driving scenarios.

6.2 Route optimised ECMS control of an HEV

6.2.1 Problem statement

In Chapter 5, a robust proportional ECMS controller (RPEC) was proposed with an equivalence factor with the characteristic equation shown in Equation 6-1.

$$\varepsilon_t = \varepsilon_0 + K_{ps}(SOC_{ref} - SOC_t) \quad \text{6-1}$$

Using the sensitivity analysis study in Section 5.6, the optimal initial equivalence factor (ε_0) and optimal proportional controller gain (K_{ps}) for this controller were estimated as 3.47 and 1.725 respectively. With no access to route preview information, SOC_{ref} was set to 60 (charge-sustaining SOC).

In this chapter, route preview information in the form of average route driving speed and altitude is used to formulate a route-optimised battery state of charge trajectory, which replaces the constant SOC_{ref} in Equation 6-1, thus resulting in a new controller dubbed RBEC (Route Based ECMS Control) with a characteristic equivalence factor equation as shown in Equation 6-2.

$$\varepsilon_t = \varepsilon_0 + K_{ps}(SOC_{route\ optimized} - SOC_t) \quad 6\text{-}2$$

The steps leading towards the route optimised SOC trajectory formulation will be detailed in the succeeding sections.

6.2.2 Modelling of route preview information

As shown in Figure 6-1, vehicle prediction systems (GPS, GIS and ITS) offer specific pieces of information. Among these information, average route driving speed and altitude have the most significant effect on HEV performance. As shown in Figure 6-2, a delicate balance between the ICE and the electric motor is required in order to maximise energy recovery over a route with varying altitude profile.

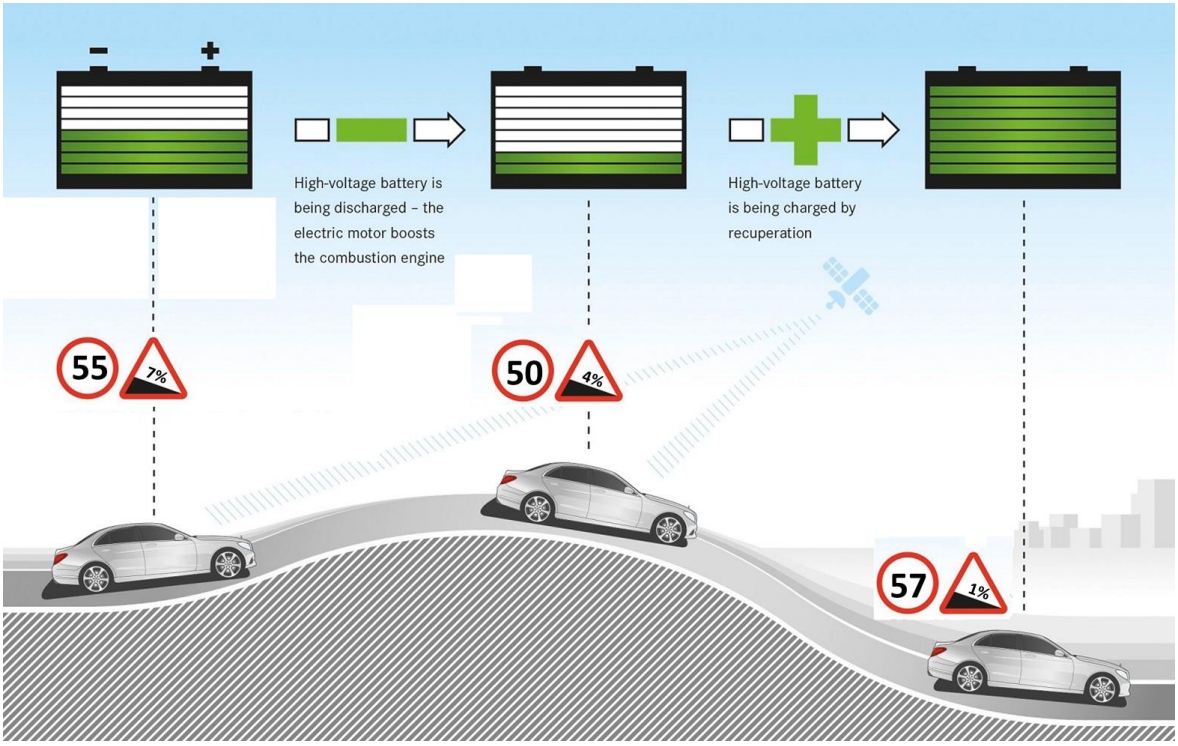

Figure 6-2: Impact of road grade on HEV battery state of charge (modified from [231])

In order to achieve this delicate balance, vehicular energy estimation over the route profile is required. An example of such estimation will be undertaken in the succeeding subsection, for a selected driving route in the UK (Bath Spa to Corsham) with properties as detailed in Table 6-1.

Travel routes	Distance (km)	Net altitude (m)	Estimated driving time (s)
Bath Spa	19.19	82	1,592.41
Corsham			

Table 6-1: Properties for a driving route from **Bath Spa to Corsham**

6.2.2.1 Route energy estimation

Route energy estimation in this section involves an estimation of the least possible energy consumption or recuperation along a route. As an example, route energy is estimated here for a driving route from Bath Spa to Corsham. The average route driving speed and altitude profile for this route are shown in Figure 6-3. Both sets of data were obtained via the Google API (Application Programming Interface). The free version which was used for this study only allows for a 10-waypoint average route driving speed data along a specified route. As shown in Figure 6-3, this approximates a constant average route driving speed across most route segments. Therefore, acceleration values cannot be estimated for the route. Consequently, acceleration effects are ignored, and the resulting energy demand profile represents the least possible instantaneous energy consumption or recuperation along the specified route.

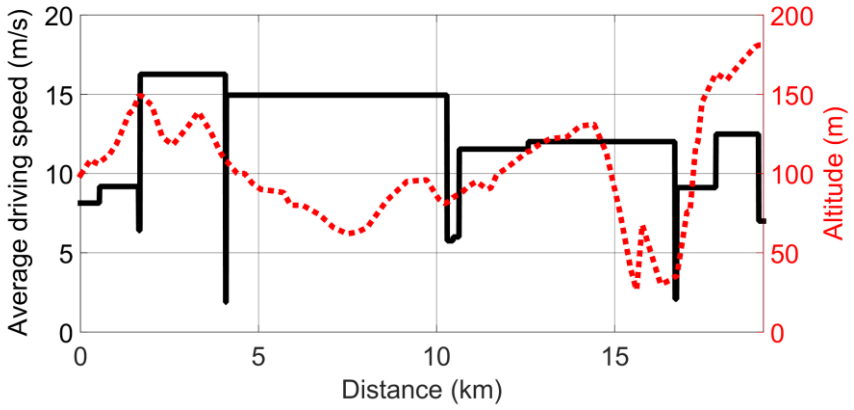

Figure 6-3: Average route driving speed and altitude for a driving route from **Bath Spa to Corsham**

The first step towards route energy estimation is route segmentation. Deciding the segmentation resolution for a route requires an optimal balance between accuracy and computational burden. In this section, a segmentation resolution of 1m (0.001km) is used. The number of route segments for each route can be calculated using Equation 6-3.

$$N_{seg} = \frac{Distance_{route}}{resolution} \quad 6\text{-}3$$

The road grade for each route segment can be calculated using Equation 6-4. The resulting road grade profile for this route is shown in Figure 6-4.

$$\propto_{seg} = \tan^{-1}\left(\frac{Altitude_{seg} - Altitude_{seg\,-\,resolution}}{resolution}\right) \quad 6\text{-}4$$

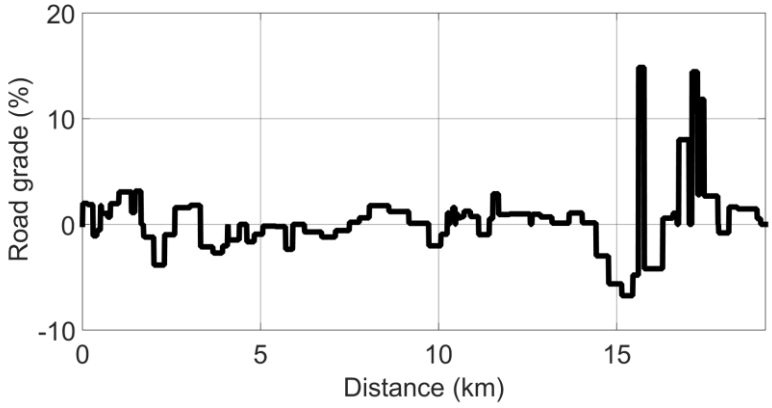

Figure 6-4: Road grade profile for a driving route from **Bath Spa to Corsham**

Similarly, by combining the road grade for each route segment ($\propto_{seg}$) with the average route driving speed for each route segment ($V_{avg_{seg}}$), the least possible instantaneous energy consumption or recuperation along a route segment could be estimated using Equation 6-5.

$$P_{seg_{min}} = 0.5\rho A_f C_d V_{avg_{seg}} (V_{avg_{seg}} - V_a)^2 + mg\, V_{avg_{seg}} \sin(\propto_{seg}) + \mu N_c V_{avg_{seg}} cos(\propto_{seg}) \quad 6\text{-}5$$

The resulting energy profile can be formulated into an optimal control problem, which can be solved using the dynamic programming algorithm. The solution process involves minimising the least total cost of operating the vehicle along the route, using a sequence of instantaneous control actions. These formulations will be undertaken in the next section.

6.2.3 Estimation of route-optimised battery state of charge trajectory

In the previous section, a mathematical relationship was formulated for the estimation of the least possible instantaneous energy consumption or recuperation along a route (Equation 6-5). In this section, Equation 6-5 is formulated into an optimal HEV control problem and solved using dynamic programming to obtain the route optimised battery state of charge trajectory.

6.2.3.1 Definition of a route-optimised SOC control problem

In more formal terms, the research vehicle can be considered a generic dynamic system with the state, as defined in Equations 6-6 and 6-7 respectively, for the battery discharge and recharge operation along a route.

$$S\dot{O}C_{seg} = -\frac{\frac{V_{oc}}{2R_{batt}} - \frac{\sqrt{{V_{oc}}^2 - 4R_{batt}\frac{1}{\eta_{dis}}\frac{1}{\eta_{motor}}P_{motor_{seg}}}}{2R_{batt}}}{Q_{batt}} \quad 6\text{-}6$$

$$S\dot{O}C_{seg} = -\frac{\frac{V_{oc}}{2R_{batt}} - \frac{\sqrt{{V_{oc}}^2 - 4R_{batt}\,\eta_{chg}\,\eta_{faradaic}\,\eta_{motor}\,P_{motor_{seg}}}}{2R_{batt}}}{Q_{batt}} \quad 6\text{-}7$$

Similarly, the charge-sustaining cost of operating the research vehicle along a route can be expressed mathematically as:

$$C_{seg+1} = \sum_{seg=0}^{N_{seg}-1} L_{seg}\left(\omega_{ICE\,seg}, P_{motor\,seg}\right) + \emptyset_{seg}\left(SOC(seg) - SOC_f\right)^2 \quad 6\text{-}8$$

Where:

$$\omega_{ICE\,seg} = \frac{V_{avg\,seg}}{R_w}\, FDR\, G_E\, \frac{60}{2\pi} \quad 6\text{-}9$$

N_{seg} is the number of route segments (Equation 6-3), L_{seg} is the instantaneous fuel consumption rate for each route segment, and C_{seg+1} is the cost function (fuel consumption) to be minimised. $\omega_{ICE\,seg}$ is the engine speed, $P_{motor\,seg}$ is the vector of control variables, SOC_{seg_f} is the desired final battery state of charge at the end of the route and $\emptyset_{seg}$ is the terminal cost (cost due to the final value of the state), which physically translates to the fuel lost or gained in order to attain charge sustenance at the end of the route.

The aim of the optimisation is to find the optimal control variables $P_{motor\,seg}$ (motor mechanical power for each route segment) which minimises the total cost function "C_{seg+1}" (Equation 6-8) over the entire route, as expressed in Equation 6-10.

$$P_{motor\,seg}{}^{*} = \arg\min\left[\sum_{seg=0}^{N_{seg}} L_{seg}\left(\omega_{ICE\,seg}, P_{motor\,seg}\right)\right] \quad 6\text{-}10$$

This is subject to the state and control constraints specified in Table 6-2. These constraints are imposed as hard constraints [140], which implies that infringing control variables are simply discarded. Conversely, the terminal cost "$\emptyset_{seg}$" is

imposed as a soft constraint that modifies the cost function, as shown in Equation 6-8, such that the final value of the constrained variable (battery state of charge) is close but not necessarily identical to the desired target.

Constraint	**Implication**
$P_{demand_{seg}} \leq P_{motor_{max_{seg}}} + P_{ICE_{max_{seg}}}$	Power demand for each route segment should not exceed the powertrain limits to avoid damage to the powertrain components.
$SOC_{min} \leq SOC_{seg} \leq SOC_{max}$	The battery must operate within its safe limits.
$P_{motor_{seg}} \leq P_{motor_{max_{seg}}}\left(\omega_{motor_{seg}}\right)$	Instantaneous motor power must be lower or equal to the maximum permissible motor power at the current speed.
$P_{ICE_{seg}} \leq P_{ICE_{max_{seg}}}(\omega_{ICE_{seg}})$	Instantaneous engine power must be lower or equal to the maximum permissible engine power at the current speed.
$SOC_{seg_f} = SOC_{seg_0} = SOC_f = 60$	The HEV operation must be charge-sustaining

Table 6-2: Route optimal control constraints

6.2.3.2 A dynamic programming solution approach to a route-optimised SOC control problem

Dynamic programming is a well suited approach for solving the route optimal control problem formulated in Equation 6-8. Considering the dynamic system introduced in Equations 6-6 and 6-7, of which the control policies are:

$$\pi_{seg} = \left\{P_{motor_0}, P_{motor_1} \dots \dots \dots, P_{motor_{N_{seg}-1}}\right\} \quad 6\text{-}11$$

The cost of the control policy π_{seg} starting at the beginning of the route seg_0 can be represented as:

$$C_{seg_{\pi_{seg}}}(SOC_0) \quad 6\text{-}12$$
$$= L_{N_{seg}}\left(\omega_{ICE_{N_{seg}}}, P_{motor_{N_{seg}}}\right) + \sum_{seg=0}^{N_{seg}-1} L_{seg}\left(\omega_{ICE_{seg}}, P_{motor_{seg}}\right)$$

Where $L_{seg}\left(\omega_{ICE_{seg}}, P_{motor_{seg}}\right)$ is the transition cost at the state SOC_{seg} with the control variable: $P_{motor_{seg}}$ and $L_{N_{seg}}\left(\omega_{ICE_{N_{seg}}}, P_{motor_{N_{seg}}}\right)$ is the terminal cost that represents the penalty cost for deviating from the final desired battery state of charge.

The optimal control policy defined in Equation 6-14 is the policy that minimises the cost function in Equation 6-12 as per the optimisation criterion in Equation 6-13.

$$C_{seg_{\pi_{seg}}}{}^{*}(SOC_0) = \min_{\pi_{seg}} C_{seg_{\pi_{seg}}}(SOC_0) \quad 6\text{-}13$$

$$\pi_{seg}{}^{*} = \left\{P_{motor_0}{}^{*}, P_{motor_1}{}^{*} \dots\dots\dots, P_{motor_{N_{seg}-1}}{}^{*}\right\} \quad 6\text{-}14$$

Proceeding backwards in time, the cost $C_{seg}(SOC_0)$, generated at the last time step, is equal to the optimum cost (minimum cost) $C_{seg}{}^{*}(SOC_0)$. In other words, it is possible to determine the optimal sequence of control policies proceeding backwards from the final state, choosing at each step the path that minimises the cost-to-go (integral cost from that time step until the final state).

The foregoing recursive approach, which can be expressed mathematically below, is implemented using the "generic dynamic programming tool" developed by Sundstrom *et al.* [212].

At step $N_{seg} - 1$

$$C_{seg_{N_{seg}-1}}{}^{*}\left(SOC\left(N_{seg}-1\right)\right) = \min_{P_{motor_{N_{seg}-1}}} \left[L\left(SOC\left(N_{seg}-1\right), P_{motor}\left(N_{seg}-1\right)\right) + \emptyset_{seg}\left(SOC(N_{seg}) - SOC_{seg_f}\right)^2\right]$$

At step seg for $0 \leq seg \leq N_{seg} - 1$

$$C_{seg}{}^{*}\left(SOC(seg)\right) = \min_{P_{motor}(seg)} \left[L(S0C(seg), P_{motor}(seg)) + C_{seg+1}{}^{*}(SOC(seg+1))\right]$$

Where N_{seg} is the number of route segments.

The resulting route-optimised SOC trajectory for the driving route under consideration is shown in Figure 6-5. This trajectory physically translates to the energy path which yields the least possible fuel consumption for an HEV, along a given route. Considering that distance is time-variant, the route-optimised SOC trajectory can also be expressed in real time simulation as a function of time as will be shown subsequently in the RBEC evaluation subsections.

Figure 6-5: A route-optimised SOC trajectory for a driving route from **Bath Spa to Corsham**

The steps leading towards the estimation of a route optimised battery state of charge trajectory could be summarised as follows:

1. Choose an intended travel route and obtain the average route driving speed and altitude profile for that route.
2. Using the altitude profile obtained, extract the grade variation for the route and apply the Newtonian equation of motion alongside relevant vehicle parameters to estimate the energy demand profile across the route.
3. Using the dynamic programming algorithm, solve for the route optimised battery state of charge reference.

6.2.4 RBEC logic set up

An overview of the route-based ECMS control strategy is shown in Figure 6-6. As shown in this figure, the RBEC approach involves three offline control steps and one online control step, which are detailed in the RBEC real-time control logic shown in Figure 6-7. Once a route-optimised SOC trajectory has been determined for a route, it can be applied in real time over the RBEC without requiring any further updates or access to route preview information. This implies that the RBEC strategy is non-causal by definition.

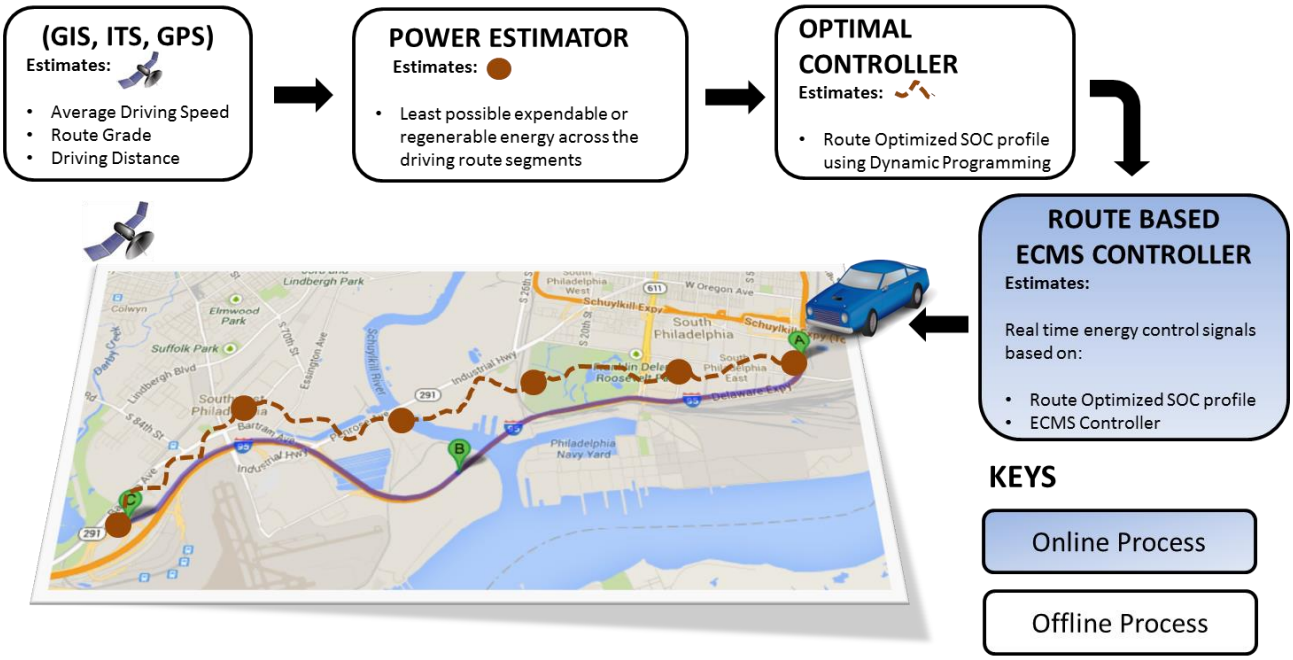

Figure 6-6: An overview of the route based ECMS control strategy (RBEC)

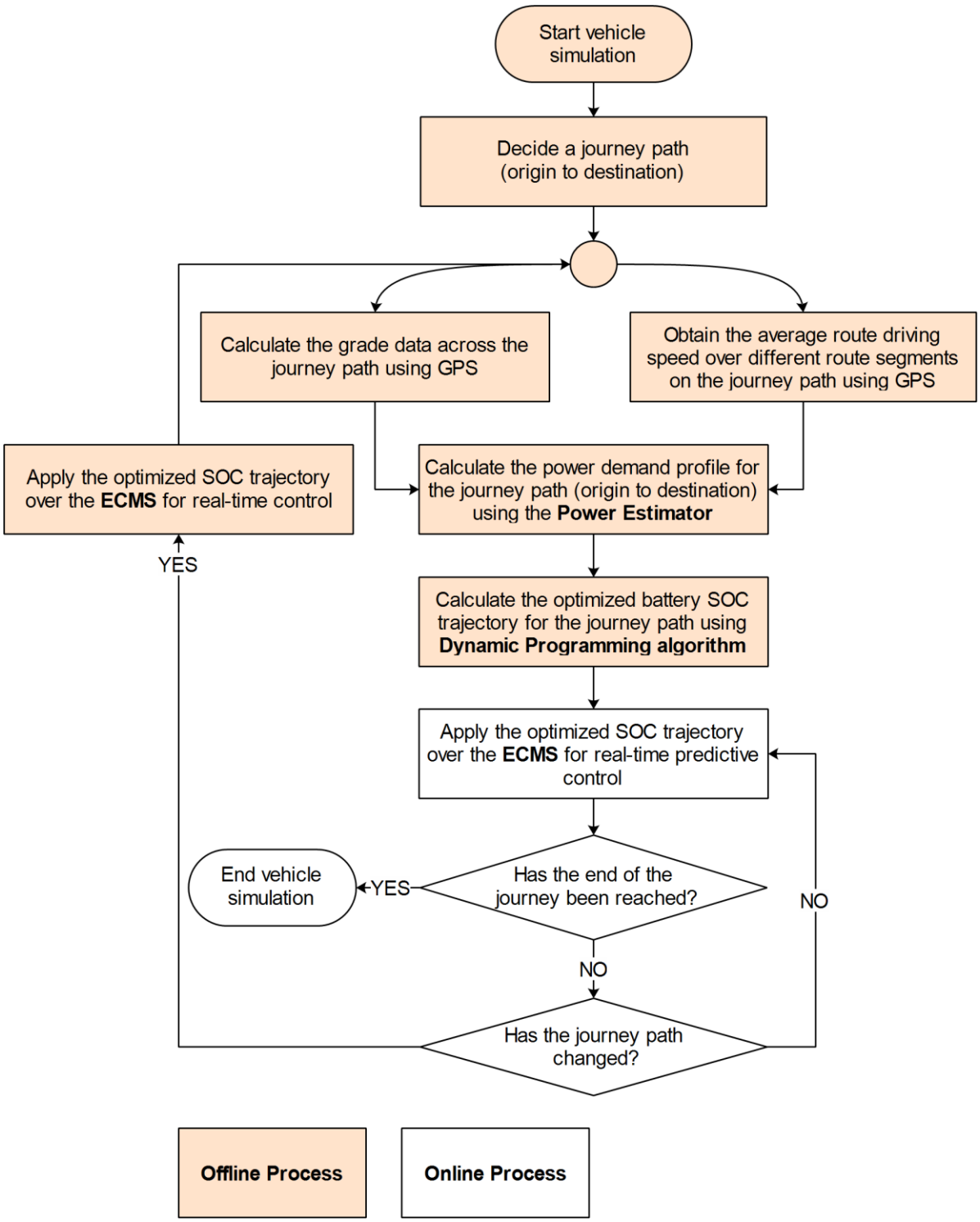

Figure 6-7: RBEC real-time logic

6.2.5 Real-time evaluation of the RBEC strategy

In this section, the performance of the route based ECMS control strategy is evaluated in real time, over 8 different journeys (8 real-world driving profiles) from Bath Spa to Corsham, as shown in Figure 6-12 to Figure 6-17. For this simulation study, the route-optimised SOC trajectory (Figure 6-5) is expressed as a function of time for clarity. Consequently, the resulting route-optimised SOC profile varies depending on the distance trajectory of the driving profile considered.

As could be observed, there are different journey times for all 8 driving profiles over the same route. This is as a result of the unique traffic conditions that characterise each journey. These many repeat journeys were included in order to ensure that the observed controller performance is repeatable.

Simulation results from the proposed RBEC strategy are compared to those of an optimal controller (dynamic programming controller) and those of the RPEC strategy. These comparative evaluations are aimed at highlighting the relative benefits of a real-time control strategy with access to route preview information.

In order to achieve a “like” for “like” comparison, the SOC correction proposed in Section 3.5.7 is applied to simulation results from the RBEC and RPEC strategies (Table 6-3) to calculate the mass and percentage of anticipated fuel savings assuming charge sustenance. The nomenclature-based comparative analogies developed in Table 3-9 are also applied to the simulation results from both controllers, as detailed in Table 6-4. Using these comparative analogies, simulation results from each controller are classified either as “near charge-sustaining”, “charge-sustaining”, “charge-depleting” or “charge-hoarding”. Both controllers are also rated on the basis of efficiency (Table 6-4), where a controller is rated as “more efficient” if its fuel savings assuming charge sustenance is of higher value.

Over all driving profiles analysed (Figure 6-12 to Figure 6-17), the RBEC strategy is found to perform near-optimally with a fuel consumption profile very similar to that of the global optimal controller. Comparatively, the RBEC strategy outperforms the RPEC strategy on the basis of charge sustenance and efficiency over all driving profiles analysed (Table 6-4). This performance is further confirmed by the comparative evaluation plot presented in Figure 6-8 and Figure 6-9. As shown in these figures, fuel saving benefits as high as 2.44% can be realised over a real-world driving route by using the RBEC strategy, as opposed to the RPEC strategy. The foregoing merits are as a result of the RBEC framework being able to impact the relative benefit of route preview information, to bring about improved controller robustness and near-optimal fuel savings, without the need for an expensive real-time route planning device.

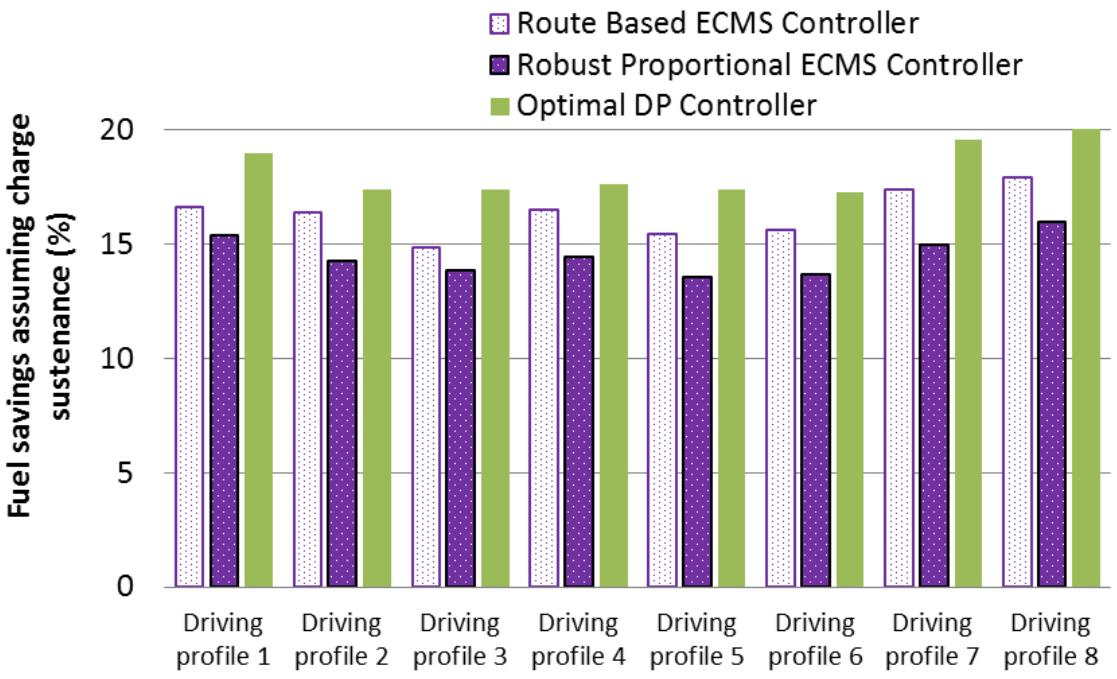

Figure 6-8: Comparative evaluation of the RBEC strategy, the RPEC strategy and the optimal controller over 8 real-world driving profiles from **Bath Spa to Corsham**

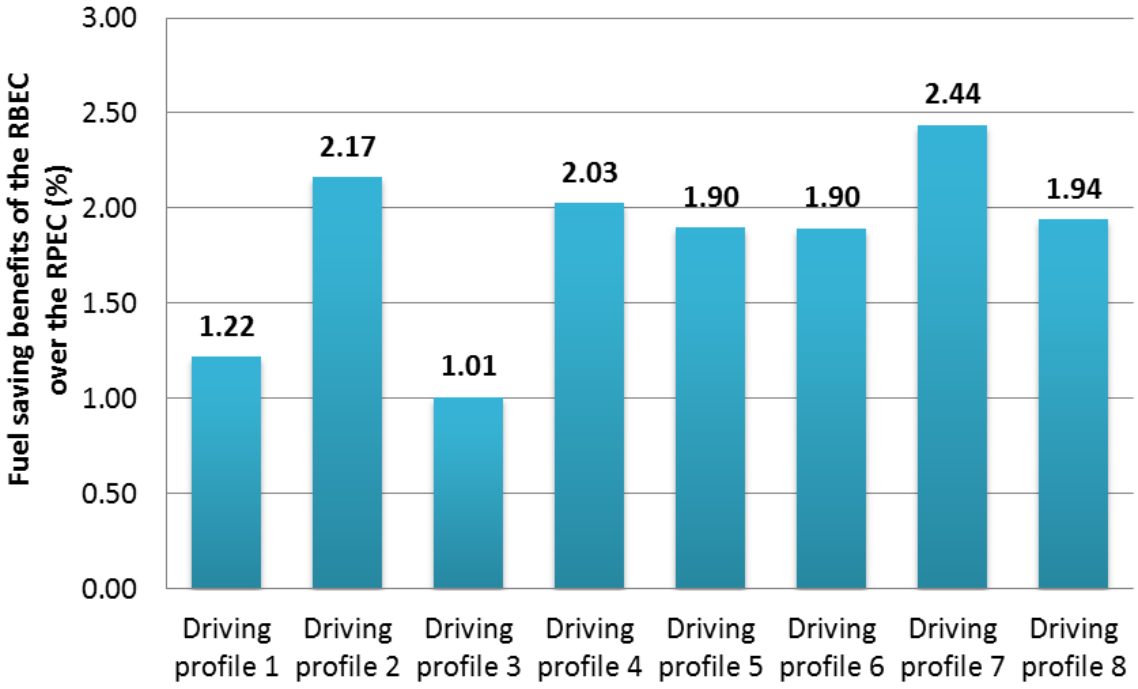

Figure 6-9: Fuel saving benefits of the RBEC strategy over RPEC for 8 real-world driving profiles from **Bath Spa to Corsham**

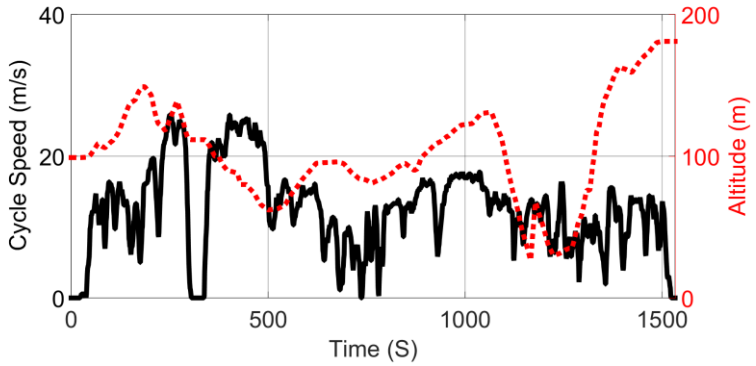

(a) Real-world driving profile

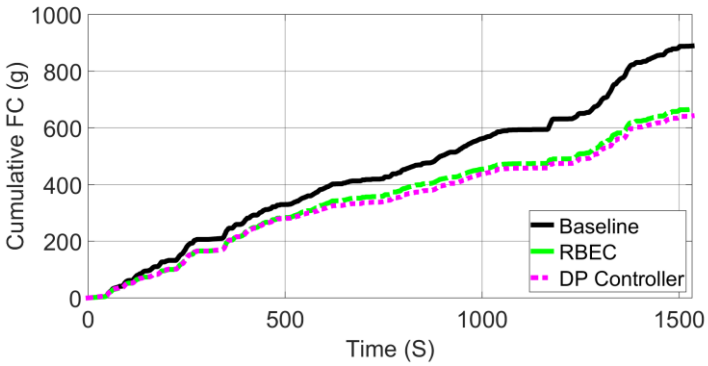

(b) Cumulative fuel consumption

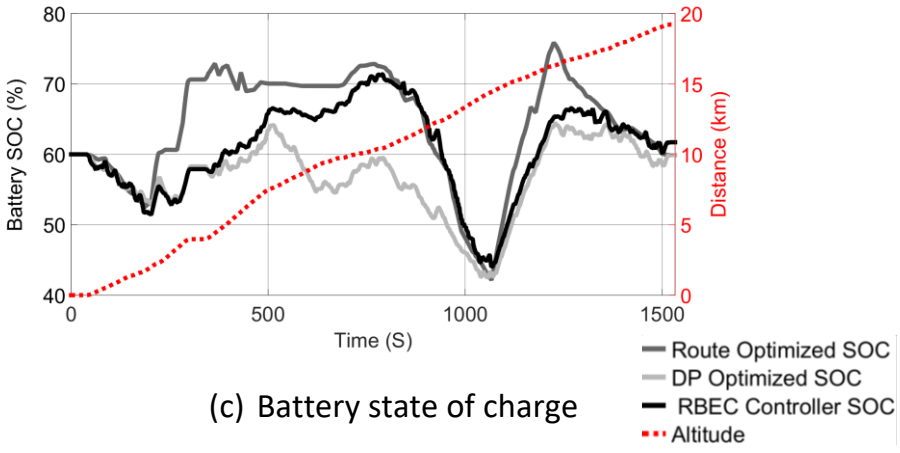

(c) Battery state of charge

Figure 6-10: RBEC strategy simulation results over a driving route from Bath Spa to Corsham **(Driving profile 1)**

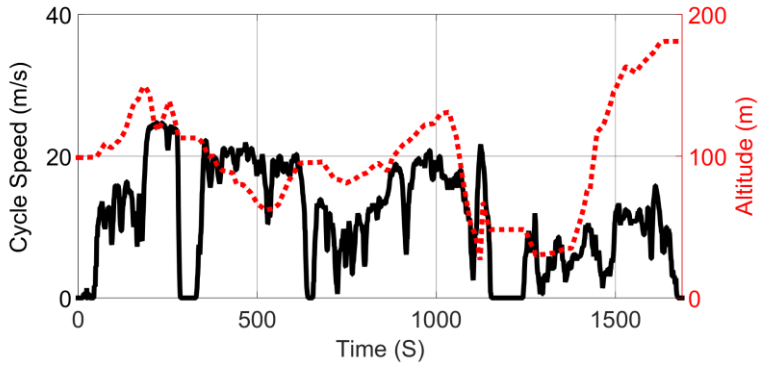

(a) Real-world driving profile

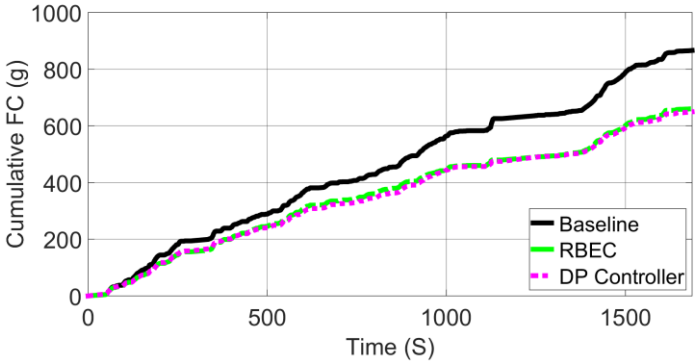

(b) Cumulative fuel consumption

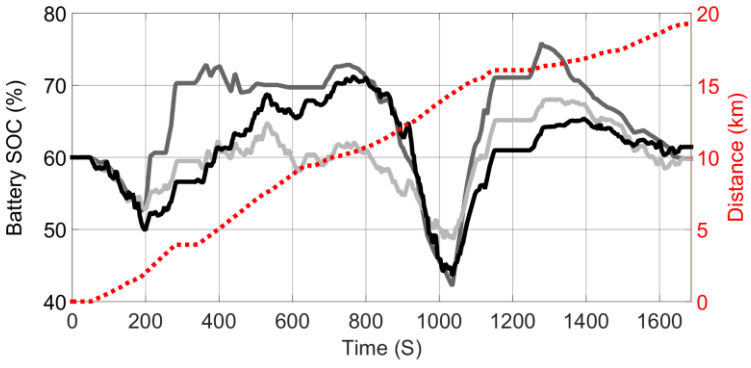

(c)

(d) Battery state of charge

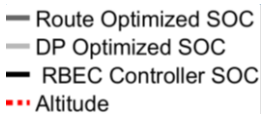

Figure 6-11: RBEC strategy simulation results over a driving route from Bath Spa to Corsham **(Driving profile 2)**

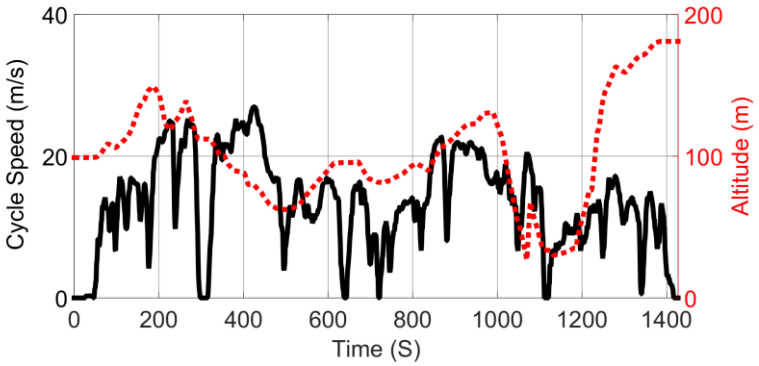

(a) Real-world driving profile

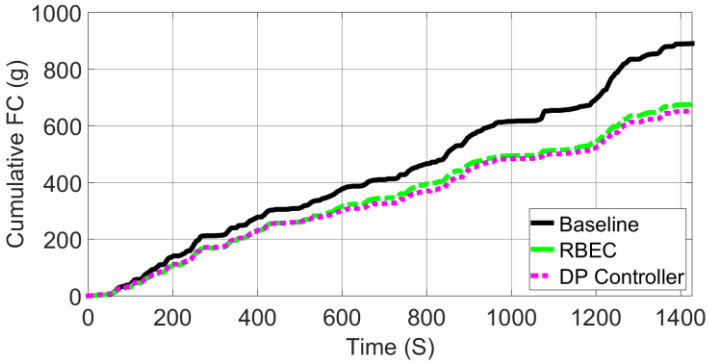

(b) Cumulative fuel consumption

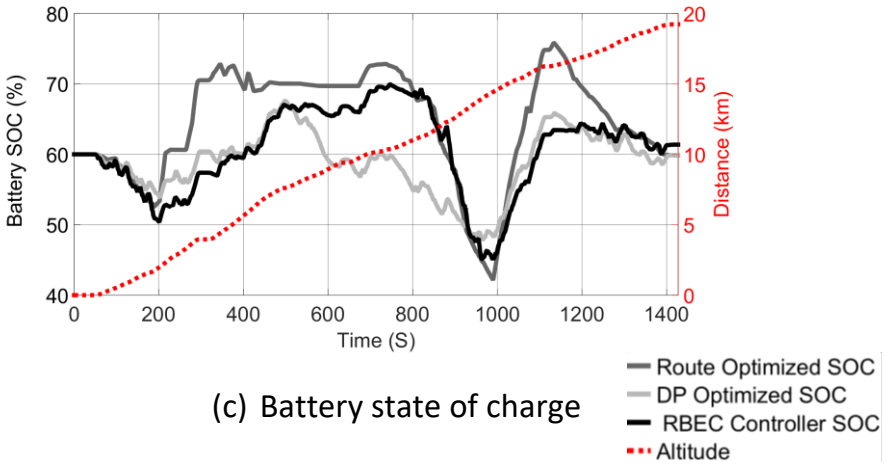

(c) Battery state of charge

Figure 6-12: RBEC strategy simulation results over a driving route from Bath Spa to Corsham **(Driving profile 3)**

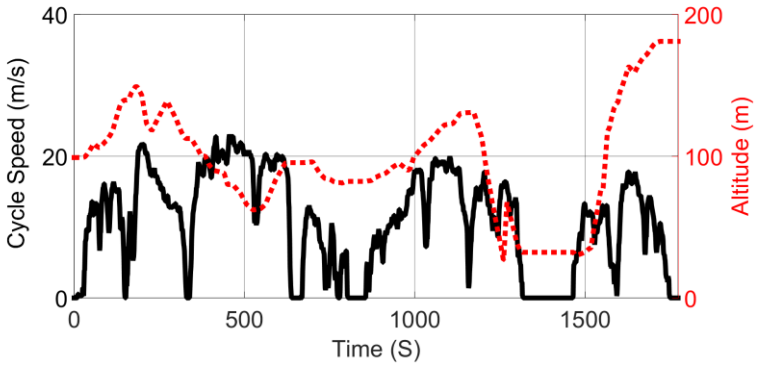

(a) Rea-world driving profile

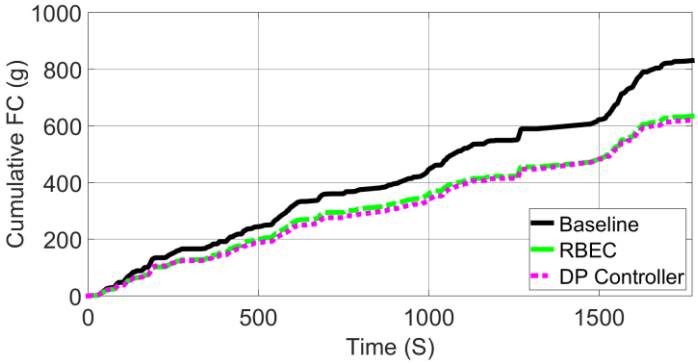

(b) Cumulative fuel consumption

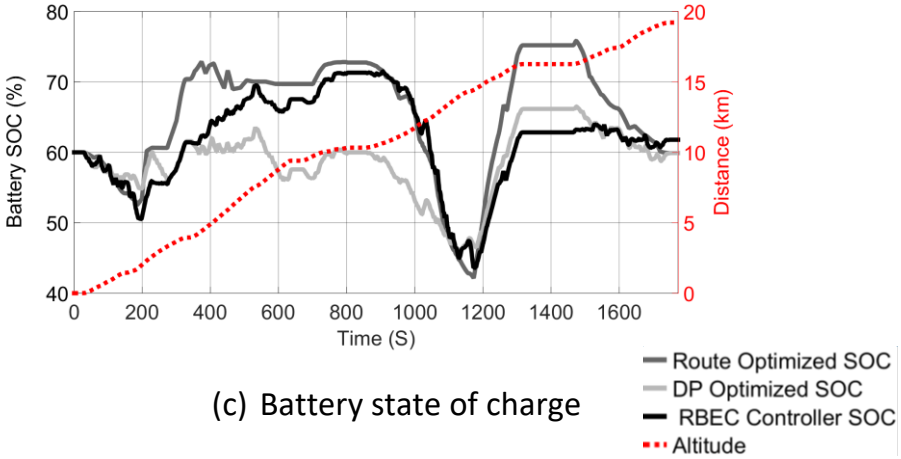

(c) Battery state of charge

Figure 6-13: RBEC strategy simulation results over a driving route from Bath Spa to Corsham **(Driving profile 4)**

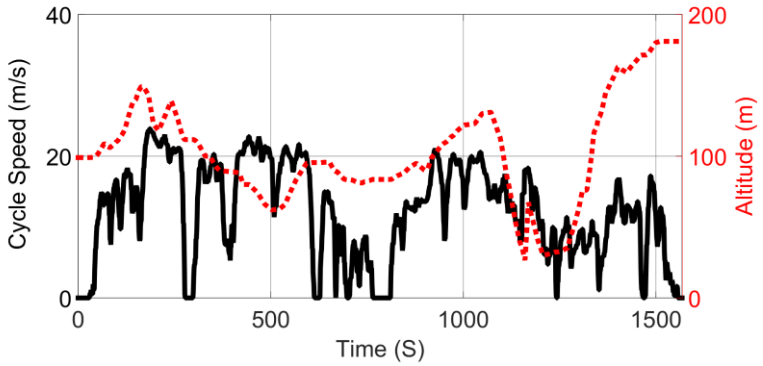

(a) Real-world driving profile

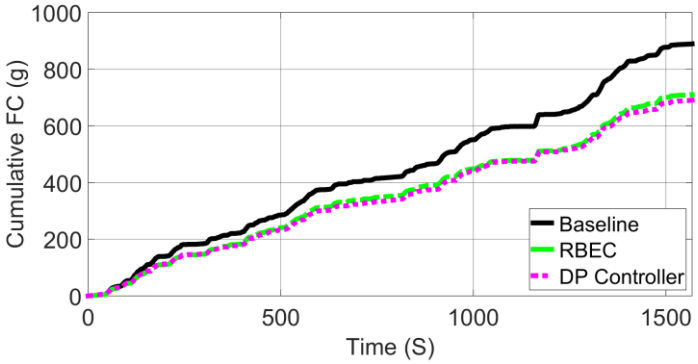

(b) Cumulative fuel consumption

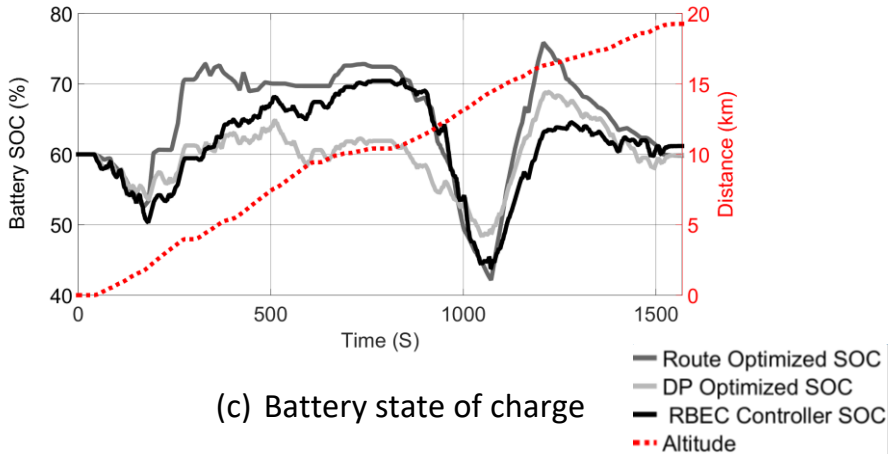

(c) Battery state of charge

Figure 6-14: RBEC strategy simulation results over a driving route from Bath Spa to Corsham **(Driving profile 5)**

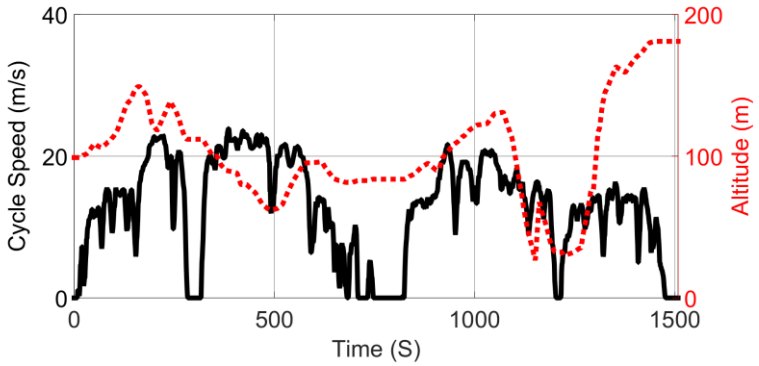

(a) Real-world driving profile

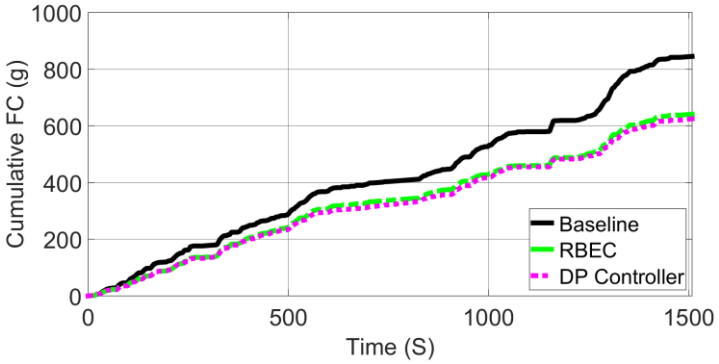

(b) Cumulative fuel consumption

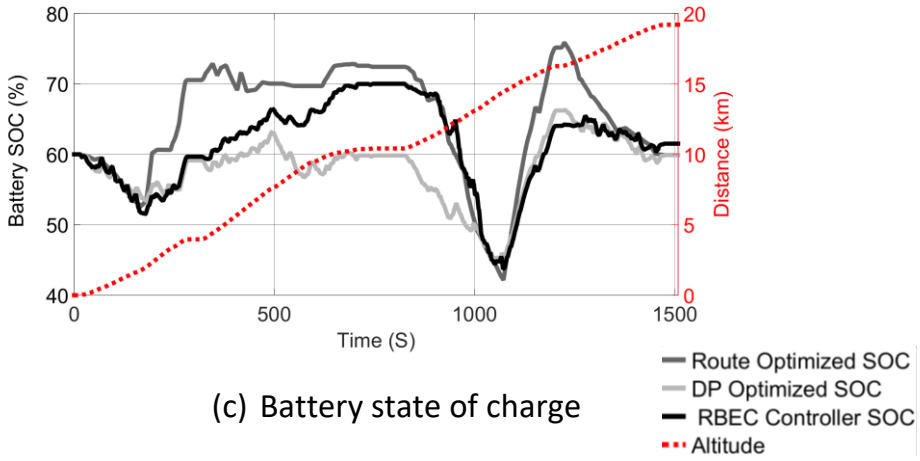

(c) Battery state of charge

Figure 6-15: RBEC strategy simulation results over a driving route from Bath Spa to Corsham **(Driving profile 6)**

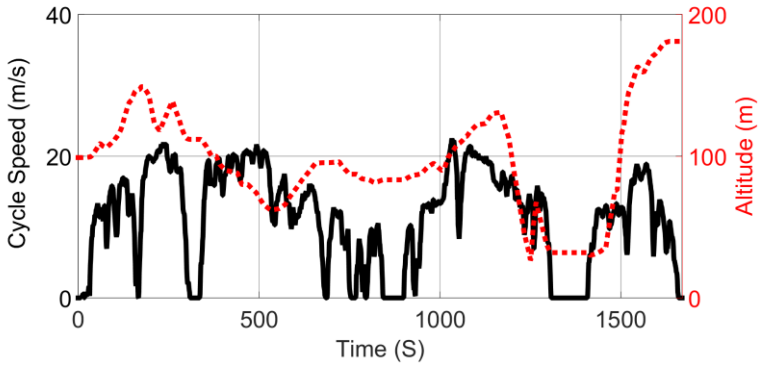

(a) Real-world driving profile

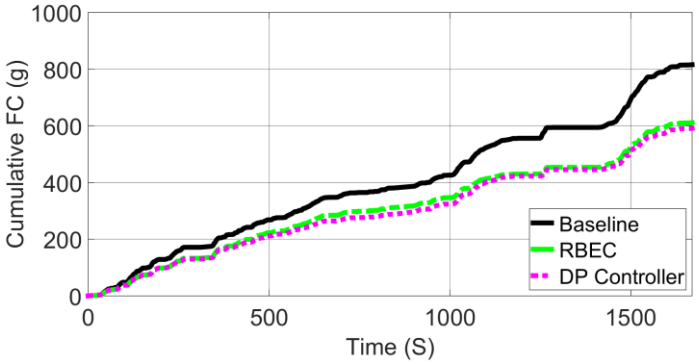

(b) Cumulative fuel consumption

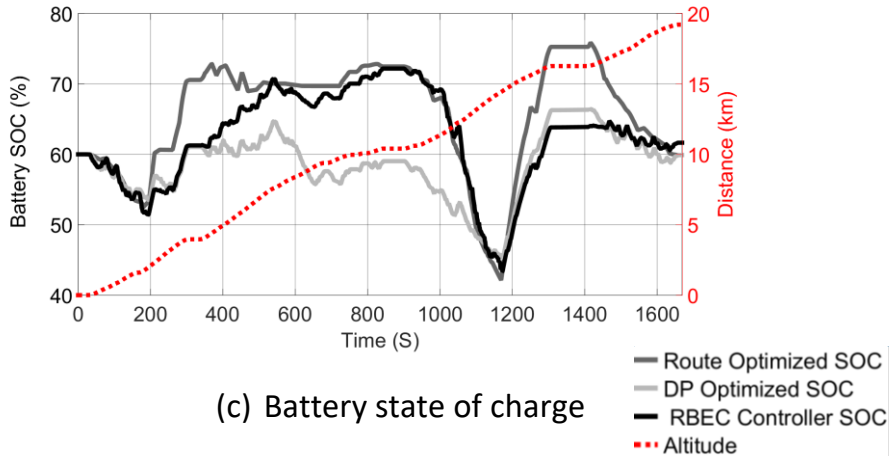

(c) Battery state of charge

Figure 6-16: RBEC strategy simulation results over a driving route from Bath Spa to Corsham **(Driving profile 7)**

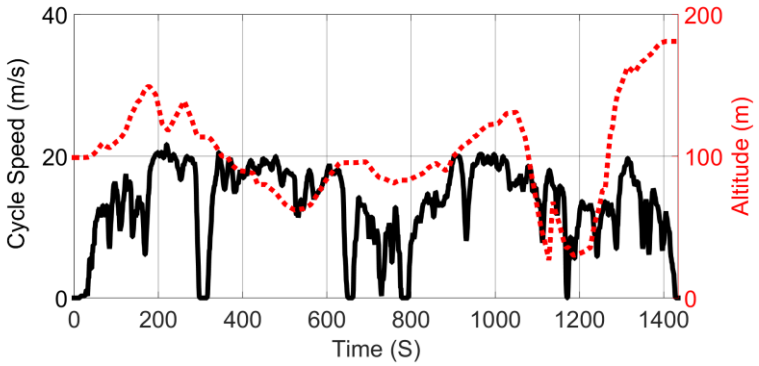

(a) Real-world driving profile

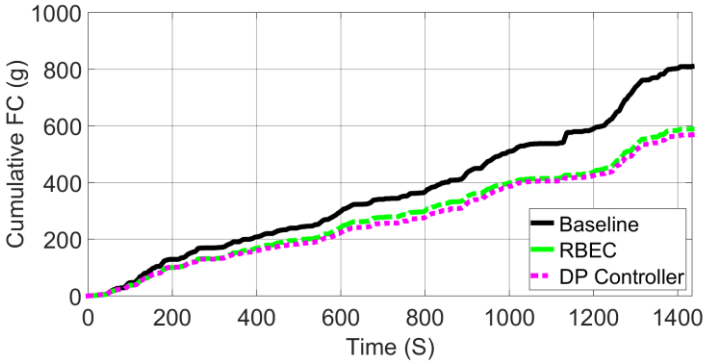

(b) Cumulative fuel consumption

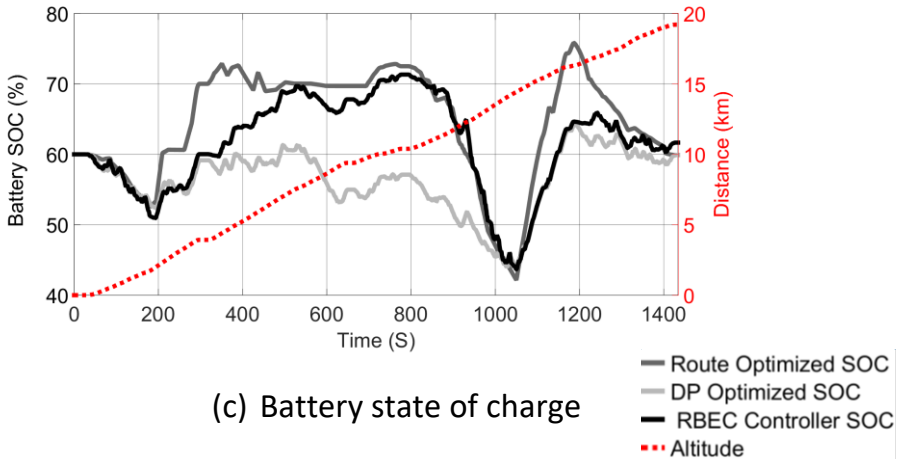

(c) Battery state of charge

Figure 6-17: RBEC strategy simulation results over a driving route from Bath Spa to Corsham **(Driving profile 8)**

RBEC strategy						
Driving cycle	**Baseline fuel consumption (g)**	**Fuel savings (Actual) (g)**	**Final battery SOC (%)**	**Fuel savings (Actual) (%)**	**Fuel savings (Assuming charge sustenance) (g)**	**Fuel savings (Assuming charge sustenance) (%)**
Driving profile 1	792.64	127.57	61.72	16.09	131.33	16.57
Driving profile 2	786.03	125.56	61.44	15.97	128.65	16.37
Driving profile 3	790.58	114.52	61.37	14.49	117.20	14.83
Driving profile 4	754.60	120.35	61.79	15.95	124.04	16.44
Driving profile 5	836.30	126.39	61.18	15.11	128.93	15.42
Driving profile 6	755.65	114.65	61.51	15.17	117.61	15.56
Driving profile 7	735.43	124.29	61.65	16.90	127.80	17.38
Driving profile 8	712.83	123.91	61.66	17.38	127.45	17.88

RPEC strategy						
Driving cycle	**Baseline fuel consumption (g)**	**Fuel savings (Actual) (g)**	**Final battery SOC (%)**	**Fuel savings (Actual) (%)**	**Fuel savings (Assuming charge sustenance) (g)**	**Fuel savings (Assuming charge sustenance) (%)**
Driving profile 1	792.64	124.98	59.54	15.77	121.65	15.35
Driving profile 2	786.03	127.21	57.72	16.18	111.62	14.20
Driving profile 3	790.58	119.49	58.44	15.11	109.22	13.81
Driving profile 4	754.60	123.16	57.83	16.32	108.73	14.41
Driving profile 5	836.30	127.82	57.86	15.28	113.03	13.52
Driving profile 6	755.65	114.86	58.15	15.20	103.27	13.67
Driving profile 7	735.43	123.88	57.90	16.84	109.85	14.94
Driving profile 8	712.83	125.37	58.29	17.59	113.60	15.94

Table 6-3: Simulation results for the RBEC strategy and the RPEC strategy over 8 real-world driving profiles representing commutes from **Bath Spa to Corsham**

	RPEC strategy		RBEC strategy	
Driving cycle	**Charge sustenance status**	**Efficiency rating (Assuming charge sustenance)**	**Charge sustenance status**	**Efficiency rating (Assuming charge sustenance)**
Driving profile 1	Near charge-sustaining	Less efficient	Near charge-sustaining	More efficient
Driving profile 2	Near charge-sustaining	Less efficient	Near charge-sustaining	More efficient
Driving profile 3	Near charge-sustaining	Less efficient	Near charge-sustaining	More efficient
Driving profile 4	Near charge-sustaining	Less efficient	Near charge-sustaining	More efficient
Driving profile 5	Near charge-sustaining	Less efficient	Near charge-sustaining	More efficient
Driving profile 6	Near charge-sustaining	Less efficient	Near charge-sustaining	More efficient
Driving profile 7	Near charge-sustaining	Less efficient	Near charge-sustaining	More efficient
Driving profile 8	Near charge-sustaining	Less efficient	Near charge-sustaining	More efficient

Key	Desired	Undesired

Table 6-4: Subjective performance comparison between the RBEC strategy and the RPEC strategy over 8 real-world driving profiles representing commutes from **Bath Spa to Corsham**

6.3 Fuel savings through vehicle speed control

6.3.1 Problem statement

In the previous section, a predictive control approach to applying route preview information was formulated. The resulting controller (RBEC) was simulated comparatively in real time against a controller of similar design but without access to route preview information (RPEC strategy). Simulation results show that, as a result of having access to route preview information, the RBEC strategy outperforms the RPEC strategy by yielding a more robust controller which is optimised for braking energy regeneration, fuel savings and charge sustenance.

In this section, variations to look-ahead HEV control involving the use of 2 novel vehicle speed control approaches are investigated. The speed control of conventional vehicles with look-ahead information is an emerging approach for achieving fuel savings and reduced emissions [232]. Studies according to Hellstrom *et al.* [196, 197] show that the predictive control of vehicle speed and gear shifting over a road terrain can reduce fuel consumption. Similarly, the acceleration of a vehicle along a fuel-optimal vehicle speed trajectory can lead to fuel savings. These fuel savings are mainly as a result of:

1. Reduced engine transients
2. Improved engine efficiency
3. Reduced engine idling
4. Optimised braking energy regeneration

The concept of vehicle speed control is relatively new and has only been investigated by a few researchers [194-197]. With the research area in its early

days, most of the proposed vehicle speed control models are overly simplified and often yield non-realisable fuel-optimal speed trajectories. For example, the author was unable to find any study that considered engine braking effects in the formulation of fuel-optimal vehicle speed trajectories. By ignoring these real-world effects, the resulting speed trajectory is only of academic interest.

In this section, two novel variations to vehicle speed control are proposed. The first approach is an optimal but non-causal vehicle speed control approach, which is formulated through the use of dynamic programming and accounts for real-world dynamic effects like engine braking. The second approach is a real-time vehicle speed control method, which is formulated using past speed trajectories of the vehicle immediately in front of the controlled vehicle (lead vehicle). Using different simulation studies, the fuel savings potential of both methods are investigated over different real-world driving profiles. The additional benefits of using a hybrid system alongside the proposed vehicle speed control methods are also investigated.

6.3.2 Optimal vehicle speed control (OPT-speed)

Fuel efficient driving can be achieved through the use of a predominantly steady and low-speed driving profile, assuming time is not a constraint. The problem becomes more complex when trying to achieve an efficient driving profile that maximises fuel savings without much penalty to trip time. This problem is tackled here through the use of easily available route preview information, to formulate a globally optimal vehicle speed profile. The problem is represented as an optimal control problem and solved using the dynamic programming algorithm. By definition, the optimal control problem formulated assumes ideal driving

conditions and no traffic disturbances. These assumptions are for simplification reasons. The formulations leading up to the optimal vehicle speed profile are elucidated in the succeeding sections.

6.3.2.1 Vehicle dynamics modelling

The tractive force and rotational speed needed to propel a vehicle along a route segment can be represented as shown in Equations 6-15 and 6-16 respectively.

$$F_{seg} = 0.5\rho A_f C_d (V_{v_{seg}} - V_a)^2 + mg\sin(\propto_{seg}) + \mu N_c\, cos(\propto_{seg}) + m\frac{dV_{v_{seg}}}{dt}_{seg} \quad 6\text{-}15$$

$$\omega_{wheel_{seg}} = \frac{V_{v_{seg}}}{R_w}\frac{60}{2\pi} \quad 6\text{-}16$$

Where:

$0.5\rho A_f C_d (V_{v_{seg}} - V_a)^2$	Represents the aerodynamic force acting across each route segment
$mg\sin(\propto_{seg})$	Represents the grade force acting across each route segment
$\mu N_c\, cos(\propto_{seg})$	Represents the rolling resistance acting across each route segment
$m\frac{dV_{v_{seg}}}{dt}_{seg}$	Represents the inertia force acting across each route segment

Table 6-5: Formula definition for the power required to move a vehicle along a route segment

Similarly, the engine torque and speed required can be expressed as shown in Equations 6-17 and 6-18 respectively.

$$T_{ICE_{seg}} = \frac{\left(0.5\rho A_f C_d (V_{v_{seg}} - V_a)^2 + mg\sin(\propto_{seg}) + \mu N_c \cos(\propto_{seg}) + m\frac{dV_{v_{seg}}}{dt}_{seg}\right)}{FDR\ G_E\ \eta_{drivetrain}} \quad 6\text{-}17$$

$$\omega_{ICE_{seg}} = \omega_{wheel_{seg}}\ FDR\ G_E \quad 6\text{-}18$$

Using the engine torque and speed values derived from Equations 6-17 and 6-18 respectively, the instantaneous fuel consumption rate from each engine torque-speed point (which is also the objective function to be minimised) can be estimated using the engine fuel consumption map detailed in Section 3.5.3 (Figure 3-4).

6.3.2.2 Optimal vehicle speed control problem formulation

The optimal vehicle speed control problem involves finding the sequence of vehicle acceleration values ($\frac{dV_{v_{seg}}}{dt}_{seg}$) that optimises the total fuel consumption cost of operating the vehicle over the defined driving horizon without violating any constraints. In this study, vehicle speed is considered as a vehicle state, resulting from integrating the control variables.

In more formal terms, the optimisation cost function can be expressed mathematically as follows:

$$C_{seg+1} = \sum_{seg=0}^{N_{seg}-1} L_{seg}\left(\omega_{ICE_{seg}}, \frac{dV_{v_{seg}}}{dt}_{seg}\right) + \emptyset_{seg}\left(V_{v_{seg}}(seg) - V_{v_{seg_f}}\right)^2 \quad 6\text{-}19$$

Where N_{seg} is the number of route segments (Equation 6-3), L_{seg} is the instantaneous fuel consumption rate for each route segment and C_{seg+1} is the cost function (fuel consumption) to be minimised. $\omega_{ICE_{seg}}$ is the engine speed, $\frac{dV_{v_{seg}}}{dt}_{seg}$ is the vector of control variables, $V_{v_{seg_f}}$ is the desired final vehicle speed at the end of the route and $\emptyset_{seg}$ is the terminal cost (cost due to the final value of the state).

The optimisation routine involves finding the optimal control variables $\frac{dV_{v_{seg}}}{dt}_{seg}$ (vehicle acceleration for each route segment) which minimises the total cost function "C_{seg+1}" (Equation 6-19) over the entire route as expressed in Equation 6-20, subject to the optimisation constraints in Section 6.3.2.2.1. These constraints are imposed as hard constraints [140], which implies that infringing control variables are simply discarded. Conversely, the terminal cost "$\emptyset_{seg}$" is imposed as a soft constraint that modifies the cost function as shown in Equation 6-19, such that the final values of the constrained variable (vehicle speed) are close but not necessarily identical to the desired target.

$$\frac{dV_{v_{seg}}}{dt}_{seg}^{*} = \arg\min\left[\sum_{seg=0}^{N_{seg}} L_{seg}\left(\omega_{ICE_{seg}}, \frac{dV_{v_{seg}}}{dt}_{seg}\right)\right] \quad 6\text{-}20$$

6.3.2.2.1 Optimisation constraints

6.3.2.2.1.1 State constraints

These are constraints that are imposed on state variables due to physical limitations.

Constraint	**Implication**
$V_{v_{seg}}{}_0 = V_{v_{seg}}{}_f = 0$	The vehicle speed at the beginning and the end of the route must be zero
$V_{v_{seg}} \geq 0$	Vehicle speed cannot be negative
$V_{v_{seg}} \leq V_{road\ limit_{seg}}$	Vehicle speed cannot exceed the allowed speed for each route segment (set by legislation). With no access to this information, a constant value of 30m/s was assumed for the entire route.
$P_{ICE_{seg}} \leq P_{ICE_{max_{seg}}}$	Instantaneous engine power must be lower or equal to the maximum permissible engine power at the current speed

Table 6-6: State constraints

6.3.2.2.1.2 Time-optimal constraints

These are constraints imposed to ensure a vehicle speed trajectory that is also optimised for time. Though it is not possible to simultaneously obtain the lowest trip time and lowest fuel consumption, these constraints ensure a good compromise among the competing but conflicting objectives. They also ensure that the route traffic flow patterns are not disturbed.

Constraint	Implication
$\text{If } (\propto_{seg} \geq 0) : \left(\frac{dV_{v_{seg}}}{dt}_{seg} \geq 0\right)$	Vehicle accelerates or continues at constant speed when the road grade is greater or equal to zero.
$\text{If } (\propto_{seg} < 0) : \left(\frac{dV_{v_{seg}}}{dt}_{seg} < 0\right)$	Vehicle braking is initiated on downhill route segments
$V_{v_{seg}} \geq V_{route_{seg_{min}}}$	Vehicle speed cannot be lower than the minimum speed estimated for each route segment. To make this estimation, a scaling factor of 0.3 was applied to the average route driving speed trajectory obtained via the Google API. This constraint is used to ensure that the resulting optimal vehicle speed trajectory is in harmony with the typical average driving trend along the specified route. It also ensures that the journey time does not differ much from what is typically obtained along the analysed route.

Table 6-7: Time-optimal constraints

6.3.2.2.1.3 Control constraints

These are constraints imposed to ensure feasible control variables.

Constraint	Implication
If $\frac{dV_{v_{seg}}}{dt}_{seg} > 0$: $\frac{dV_{v_{seg}}}{dt}_{seg} \leq \frac{dV_{v_{seg}}}{dt}_{seg_{max}}$	Vehicle acceleration does not exceed the maximum allowed acceleration for each vehicle speed (the maximum acceleration values shown in Figure 6-19, are estimated using the technique detailed in Figure 6-18)
If $\frac{dV_{v_{seg}}}{dt}_{seg} < 0$: $\frac{dV_{v_{seg}}}{dt}_{seg} \leq \frac{dV_{v_{seg}}}{dt}_{seg_{min}}$	Vehicle deceleration cannot be lower than the minimum deceleration estimated for each route segment. This estimation as shown in Section 6.3.2.2.1.4 takes into consideration factors like engine braking, rolling resistance and aerodynamic force that influences the deceleration trajectory of the vehicle.

Table 6-8: Control constraints

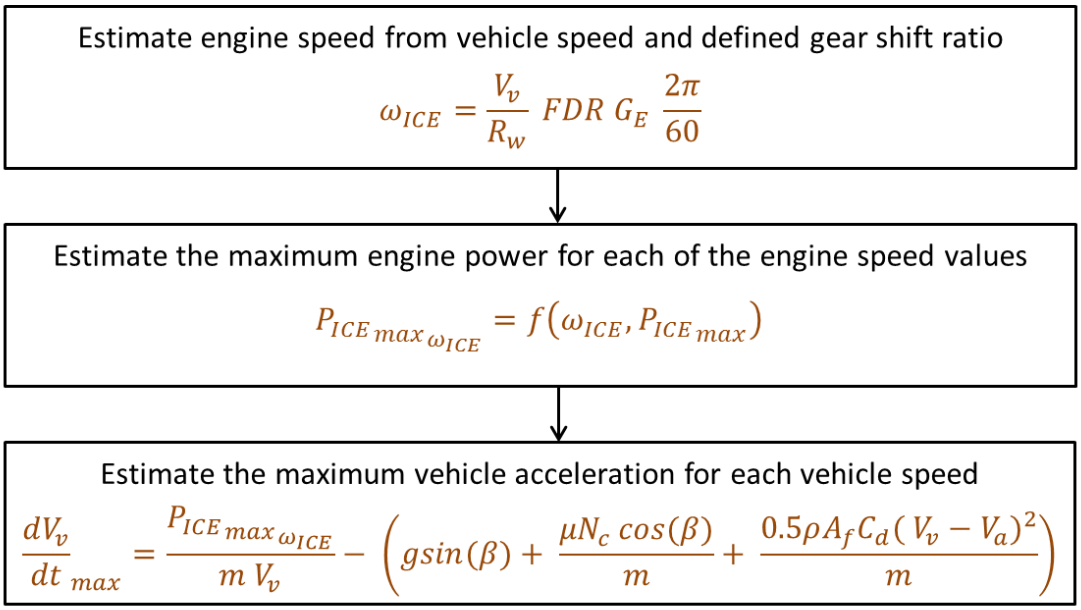

Figure 6-18: Flow chart showing a technique for estimating the maximum vehicle acceleration and allowable engine power for a given vehicle speed ($\beta = 0$)

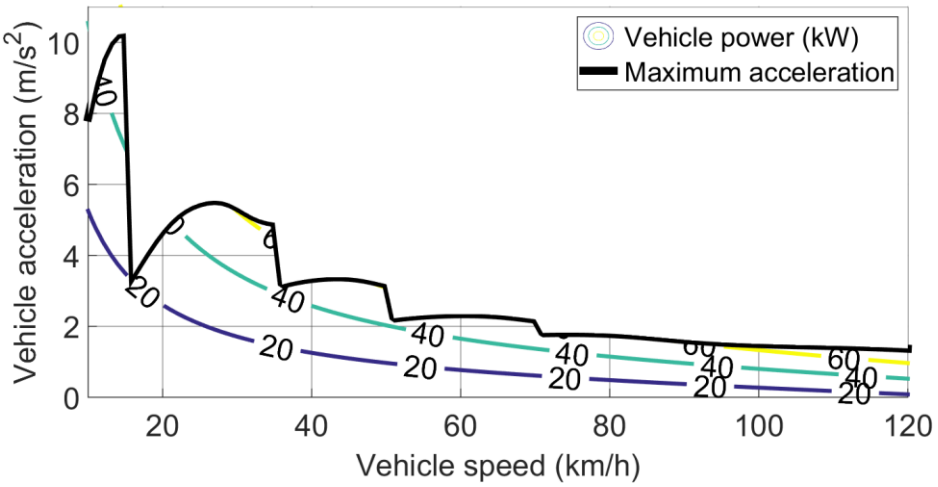

Figure 6-19: Plot of vehicle acceleration limits for each vehicle speed

6.3.2.2.1.4 Estimation of minimum vehicle deceleration

When driving on a downhill route segment, the vehicle deceleration is influenced by engine braking, rolling resistance and aerodynamic force. In this subsection, the mathematical or statistical relationship governing the effect of each force on vehicle braking is formulated.

1. **Braking force resulting from engine braking ($F_{ICE_{brake}}$)**

   When the vehicle throttle pedal is released and the transmission is not in neutral, fuel supply is immediately cut off and the engine is rotated by the vehicle through its wheels. Engine braking occurs because the retarding forces within the engine, such as compression resistance, internal friction, air intake and exhaust resistance, act on the driving wheel during the engine compression stroke to slow the vehicle down. The negative tractive (braking) effect of the engine on the wheels can be estimated by extrapolating to a zero line the relationship between the fuel energy input (wheel tractive force) and the engine output (fuel consumption) for each gear, as shown in Figure 6-20. The resulting relationships could be combined for different gears to create a relationship between the engine speed and the braking effect of the engine on the vehicle, as shown in Figure 6-21. As could be observed from this figure, the braking effect of the engine on the wheels are much higher in lower gears than higher gears.

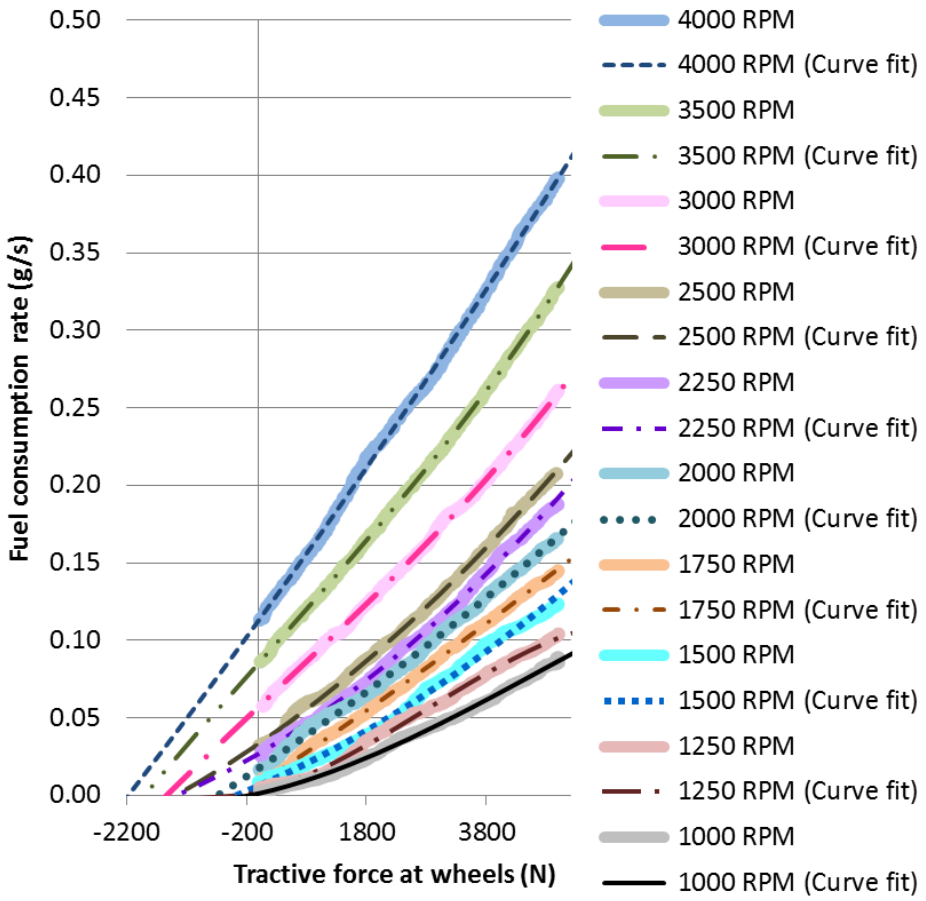

Figure 6-20: Relationship between wheel tractive force and instantaneous fuel consumption at **Gear 1**

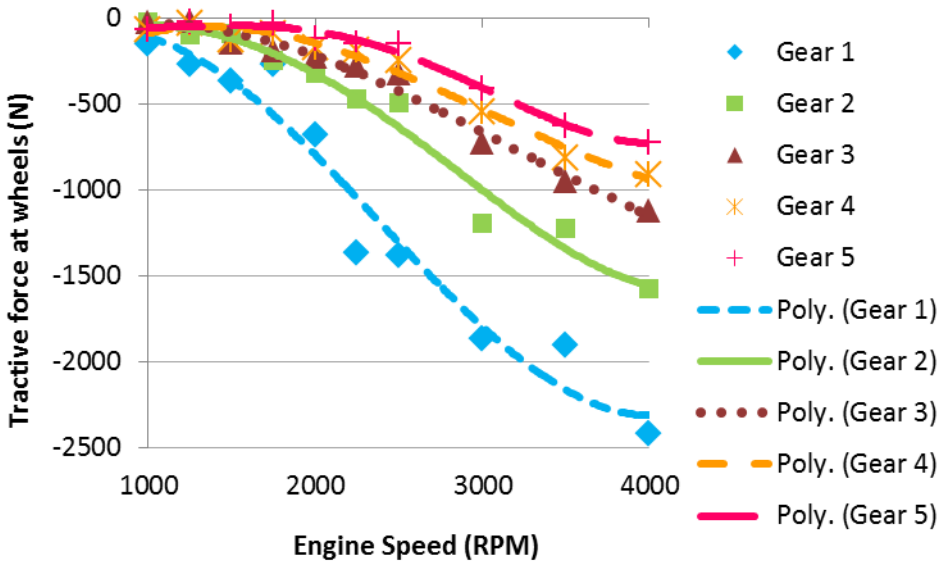

Figure 6-21: Relationship between engine speed and the braking effect of the engine on the vehicle

2. **<u>Braking force resulting from rolling resistance</u>** ($F_{rolling\ brake}$)

The vehicle braking force resulting from rolling resistance occurs mainly as a result of the deformation of the tyre material and the road surface. On road surfaces, the hysteresis due to deformation of the tyre material produces an uneven pressure distribution at the contact surface with the roadway. As such, the ground reaction force is shifted towards the direction of the vehicle movement from the wheel axle [205]. Mathematically, the braking force resulting from rolling resistance can be expressed in Equation 6-21.

$$F_{rolling_{brake}} = -\mu N_c \cos(\propto_{seg}) \qquad 6\text{-}21$$

3. **<u>Braking force resulting from aerodynamic drag</u> ($F_{aero\ brake}$)**

   The braking force resulting from aerodynamic drag occurs mainly as a result of shape drag and skin friction (Section 3.5.2). Mathematically, this force can be expressed in Equation 6-22.

$$F_{aero_{brake}} = -0.5\rho A_f C_d (V_{v_{seg}} - V_a)^2 \quad \text{6-22}$$

By combining the three forces formulated thus far, the minimum deceleration experienced by a braking vehicle can be expressed in Equation 6-23.

$$\frac{dV_{v_{seg}}}{dt}_{seg_{min}} = \frac{F_{ICE_{brake}}}{m} + \frac{\mu N_c \cos(\propto_{seg})}{m} + \frac{0.5\rho A_f C_d (V_{v_{seg}} - V_a)^2}{m} \quad \text{6-23}$$

Similarly, the total braking force experienced by a braking vehicle can be expressed in Equation 6-24.

$$F_{VEH_{brake}} = F_{ICE_{brake}} + \mu N_c \cos(\propto_{seg}) + 0.5\rho A_f C_d (V_{v_{seg}} - V_a)^2 + F_{mech\_brake} \quad \text{6-24}$$

Where "m" is the vehicle mass and "F_{mech_brake}" is the braking force from the mechanical brakes.

6.3.2.3 A dynamic programming solution approach to optimal vehicle speed control

Dynamic programming is a well suited approach for solving the optimal vehicle speed control problem, formulated in Equation 6-19. Considering the dynamic system introduced thus far, of which the control policies are:

$$\pi_{seg} = \left\{ \frac{dV_{v_{seg}}}{dt}_{0}, \frac{dV_{v_{seg}}}{dt}_{1} \dots\dots\dots, \frac{dV_{v_{seg}}}{dt}_{N_{seg}-1} \right\} \quad 6\text{-}25$$

The cost of the control policy π_{seg} starting at the beginning of the route seg_0 can be represented as:

$$C_{seg}{}_{\pi_{seg}}\left(V_{v_{seg}}{}_{0}\right) \quad 6\text{-}26$$

$$= L_{N_{seg}}\left(\omega_{ICE}{}_{N_{seg}}, \frac{dV_{v_{seg}}}{dt}_{N_{seg}}\right) + \sum_{seg=0}^{N_{seg}-1} L_{seg}\left(\omega_{ICE}{}_{seg}, \frac{dV_{v_{seg}}}{dt}_{seg}\right)$$

Where $L_{seg}\left(\omega_{ICE}{}_{seg}, \frac{dV_{v_{seg}}}{dt}_{seg}\right)$ is the transition cost at the state $V_{v_{seg}}$ with the control variable: $\frac{dV_{v_{seg}}}{dt}_{seg}$, and $L_{N_{seg}}\left(\omega_{ICE}{}_{N_{seg}}, \frac{dV_{v_{seg}}}{dt}_{N_{seg}}\right)$ is the terminal cost that represents the penalty cost for deviating from the final desired vehicle speed which is 0 (vehicle comes to a complete stop at the destination).

The optimal control policy defined in Equation 6-28 is the policy that minimises the cost function in Equation 6-26 as per the optimisation criterion in Equation 6-27.

$$C_{seg_{\pi_{seg}}}{}^{*}\left(V_{v_{seg_0}}\right) = \min_{\pi_{seg}} C_{seg_{\pi_{seg}}}\left(V_{v_{seg_0}}\right) \quad 6\text{-}27$$

$$\pi_{seg}{}^{*} = \left\{\frac{dV_{v_{seg}}}{dt}{}^{*}_{0}, \frac{dV_{v_{seg}}}{dt}{}^{*}_{1} \ldots\ldots\ldots, \frac{dV_{v_{seg}}}{dt}{}^{*}_{N_{seg}-1}\right\} \quad 6\text{-}28$$

Proceeding backwards in time, the cost $C_{seg}\left(V_{v_{seg_0}}\right)$ generated at the last time step, is equal to the optimum cost (minimum cost) $C_{seg}{}^{*}\left(V_{v_{seg_0}}\right)$. In other words, it is possible to determine the optimal sequence of control policies proceeding backwards from the final state, choosing at each step the path that minimises the cost-to-go (integral cost from that time step until the final state).

The foregoing recursive approach which can be expressed mathematically below, is implemented using the "generic dynamic programming tool" developed by Sundstrom *et al.* [212].

At step $N_{seg} - 1$

$$C_{seg_{N_{seg}-1}}{}^{*}\left(V_{v_{seg}}(N_{seg}-1)\right) = \min_{\frac{dV_{v_{seg}}}{dt}_{N_{seg}-1}} \left[L\left(V_{v_{seg}}(N_{seg}-1), P_{motor}(N_{seg}-1)\right) + \emptyset_{seg}\left(V_{v_{seg}}(seg) - V_{v_{seg_f}}\right)^2\right]$$

At step seg for $0 \leq seg \leq N_{seg} - 1$

$$C_{seg}{}^{*}\left(V_{v_{seg}}(seg)\right) = \overset{min}{\frac{dV_{v_{seg}}}{dt}(seg)} \left[L(V_{v_{seg}}(seg), P_{motor}(seg)) + C_{seg+1}{}^{*}(V_{v_{seg}}(seg+1))\right]$$

N_{seg} is the number of route segments. A discretisation resolution of 1m (0.01km) is used for the dynamic programming routine. This is to ensure that the variations in vehicle acceleration along the route segments are accurately captured.

The resulting route-optimised vehicle speed trajectories for the driving route from Bath Spa to Corsham and Corsham to Bath Spa are shown in Figure 6-22 and Figure 6-23 respectively. These trajectories physically translate to the vehicle speed path which optimises fuel consumption, time and braking energy regeneration along the specified route. On these plots, the "minimum driving speed on route" is an estimate that represents the minimum vehicle speed that will not lead to a distortion of the traffic flow on each route segment (Table 6-7). This constraint is used to ensure that the resulting optimal vehicle speed trajectory is in harmony with the typical average driving trends along the specified route. It also ensures that the journey time does not differ much from what is typically obtained along the chosen route. Distance is time variant and, as such, the optimal vehicle speed trajectory can also be expressed in real time simulations as a function of time.

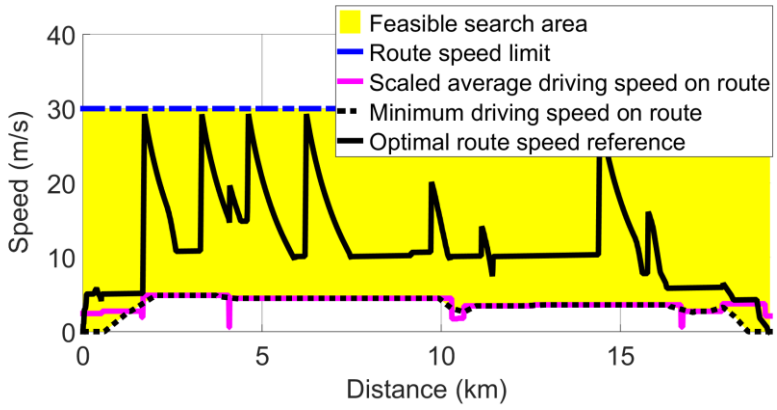

(a) Distance based optimal vehicle speed trajectory

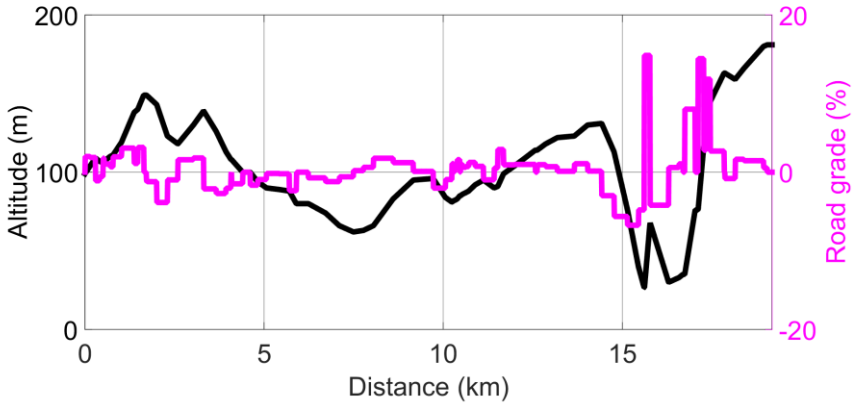

(b) Variation of altitude and road grade with distance

Figure 6-22: Distance-based optimal vehicle speed trajectory over a driving route from **Bath Spa to Corsham**

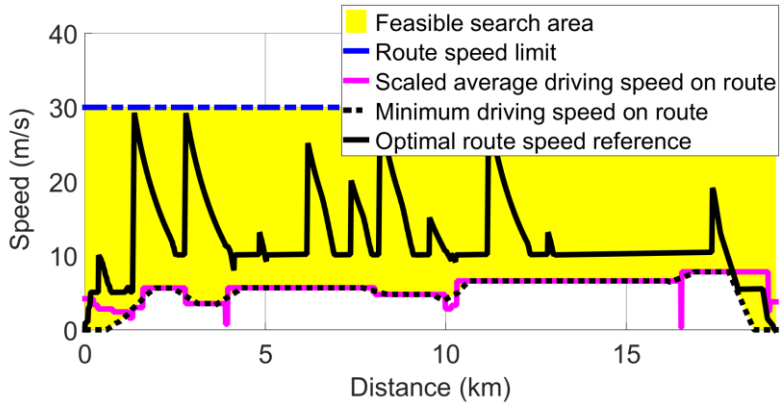

(a) Distance based optimal vehicle speed trajectory

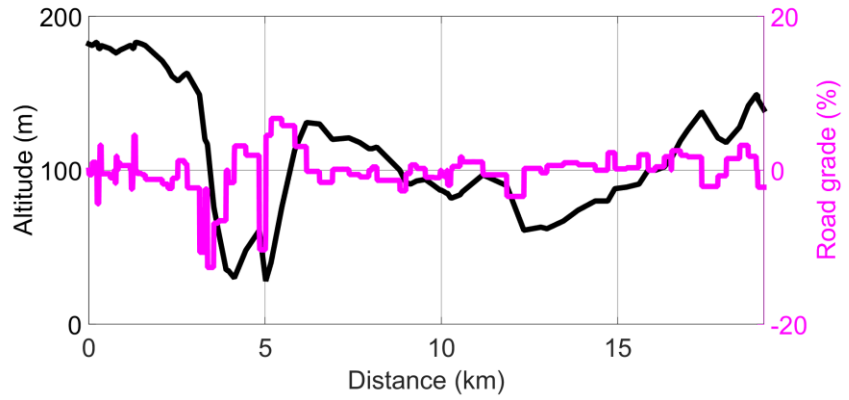

(b) Variation of altitude and road grade with distance

Figure 6-23: Distance-based optimal vehicle speed trajectory over a driving route from **Corsham to Bath Spa**

From the optimal vehicle speed trajectories shown in Figure 6-22 and Figure 6-23, the following trends are observed:

1. Hill climbing is mostly done at constant vehicle speeds.
2. Aggressive acceleration manoeuvres are minimised.
3. Mild acceleration manoeuvres are maximised.
4. Aggressive deceleration manoeuvres are minimised.

5. Mild deceleration manoeuvres are maximised. For conventional baseline vehicles, this increases the travelling distance being covered under fuel cut off. For HEVs, it translates to increased braking energy regeneration.
6. Constant vehicle speeds are maintained for most non-braking manoeuvres.

These trends could also be interpreted as fuel-efficient driving techniques for real-world driving.

6.3.2.4 Evaluation of the OPT-speed approach

In this section, a real-time simulation of the OPT-speed approach is undertaken. First, a time-based trajectory for the distance-based OPT-speed trajectory is estimated. Next, the resulting time-based trajectory for the route from Bath Spa to Corsham is simulated in real time and used to investigate:

1. The fuel savings potential of the OPT-speed approach on baseline vehicles
2. The fuel savings potential of the OPT-speed approach on HEVs

Results from the foregoing analyses are also compared to that of 8 driving profiles along the route from Bath Spa to Corsham. The RPEC strategy developed in Chapter 5 is used for the real-time HEV simulation.

6.3.2.4.1 Estimation of a time-based trajectory for the OPT-speed approach

In order to investigate the real-time fuel savings potential of the OPT-speed approach, a time-based trajectory is required. The estimation steps for the time-based trajectory are shown in Figure 6-24. The resulting trajectory for the route from Bath Spa to Corsham is simulated on an HEV, as shown in Figure 6-25.

From this figure, it could be inferred that a cumulative fuel savings of 22.74% with a near charge-sustaining performance of 59.11% is achieved through the use of the OPT-speed approach on an HEV. This near-optimal performance indicates that the proposed OPT-speed approach is beneficial to both baseline vehicles and HEVs. In HEVs, these benefits are realised through the use of gentle braking patterns which promote braking energy regeneration and thus a near-optimal HEV performance.

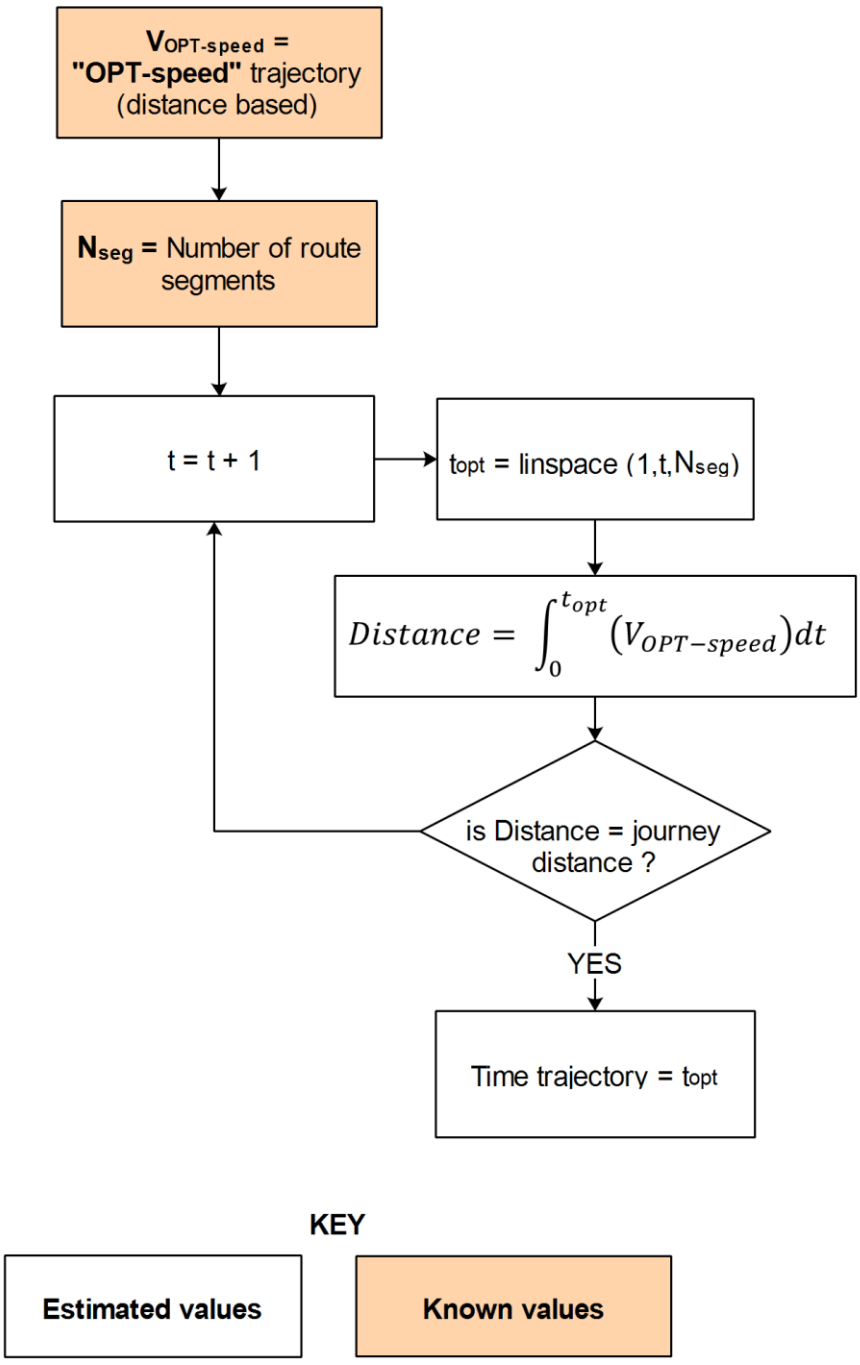

Figure 6-24: OPT-speed time trajectory estimation technique

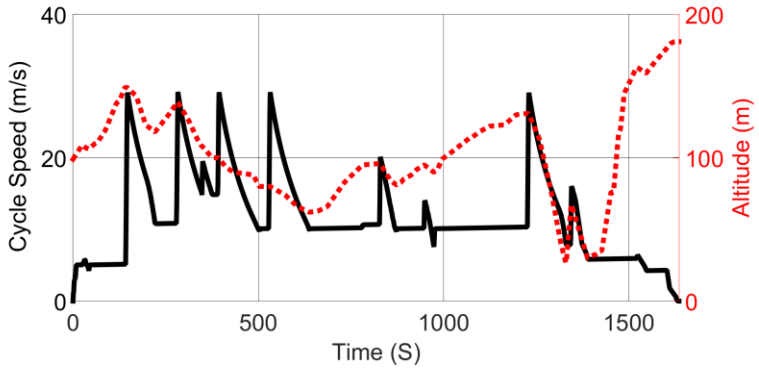

(a) Time-based optimal vehicle speed trajectory

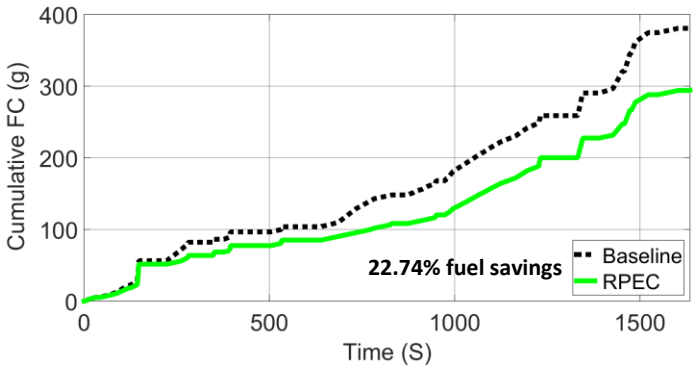

(b) Cumulative fuel consumption profile

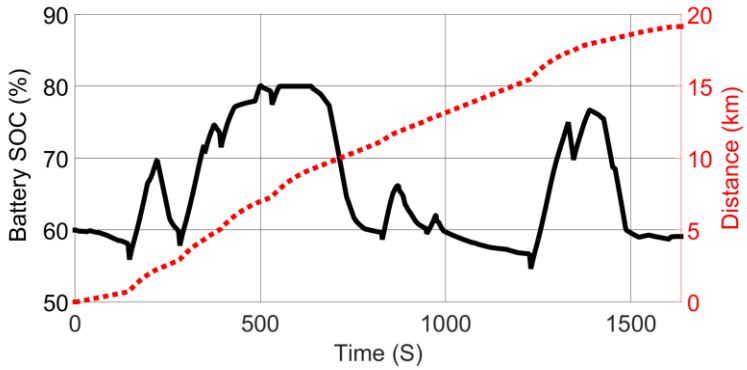

(c) Battery state of charge profile

Figure 6-25: RPEC strategy simulation results over a driving route from **Bath Spa to Corsham**

6.3.2.4.2 Comparative evaluations of the OPT-speed approach with normal vehicle speed profiles

In this section, the vehicle speed profile obtained from the OPT-speed approach is compared to 8 real-word driving profiles for the route from Bath Spa to Corsham. Fuel savings and journey time are the main evaluation criteria for this analysis.

Results from this analysis show that compared to normal driving profiles, fuel savings of up to 54.45% on conventional vehicles and 64.81% on HEVs can be realised through the use of the OPT-speed approach (Table 6-9). The predominant trend across all profiles indicates that a higher percentage of fuel savings is achieved through improved driving behaviour than through the hybrid system (Figure 6-26). This observation further highlights the importance of improved driving behaviour as a significant and cost effective approach to improving vehicular fuel economy.

A comparative analysis of journey time between the OPT-speed approach and 8 real-world driving profiles for the route from Bath Spa to Corsham is shown in Figure 6-27 and detailed in Table 6-10. Results from this analysis show that the simultaneous achievement of optimal fuel savings and optimal driving time is sometimes not feasible. Typically, a compromise is made between both competing objectives, although, the compromise must be such that the journey still gets completed in a reasonable driving time frame.

From this analysis, a compromise involving a maximum time penalty of -12.69% (208s or 3.47 minutes - Table 6-10) and fuel savings of 51.82% (Table 6-9) is observed for a conventional baseline vehicle. In comparison to driving profiles 2 (Figure 6-11), 4 (Figure 6-13) and 7 (Figure 6-16), the OPT-speed approach is found

to simultaneously achieve higher fuel savings and lower journey time. The latter trend is believed to be as a result of the high percentage of idling time that makes up these driving profiles, thus resulting in unnecessarily increased journey time.

	OPT-speed	Driving profile 1	Driving profile 2	Driving profile 3	Driving profile 4	Driving profile 5	Driving profile 6	Driving profile 7	Driving profile 8
Baseline fuel consumption (No hybrid)	380.90	792.64	786.03	790.58	754.6	836.3	755.65	735.43	712.83
Fuel savings gained by using OPT-speed with no hybrid (g)		411.74	405.13	409.68	373.70	455.40	374.75	354.53	331.93
Fuel savings gained by using OPT-speed with no hybrid (%)		51.95	51.54	51.82	49.52	54.45	49.59	48.21	46.57
Fuel savings gained by using OPT-speed with hybrid (g)		498.34	491.73	496.28	460.30	542.00	461.35	441.13	418.53
Fuel savings gained by using OPT-speed with hybrid (%)		62.87	62.56	62.77	61.00	64.81	61.05	59.98	58.71
Extra fuel savings gained by using OPT-speed with Hybrid (g)		86.60	86.60	86.60	86.60	86.60	86.60	86.60	86.60
Extra fuel savings gained by using OPT-speed with hybrid (%)		10.93	11.02	10.95	11.48	10.36	11.46	11.78	12.15

Table 6-9: A summary table evaluating the fuel savings potential of the OPT-speed approach over 8 real-world driving profiles representing commutes from **Bath Spa to Corsham**

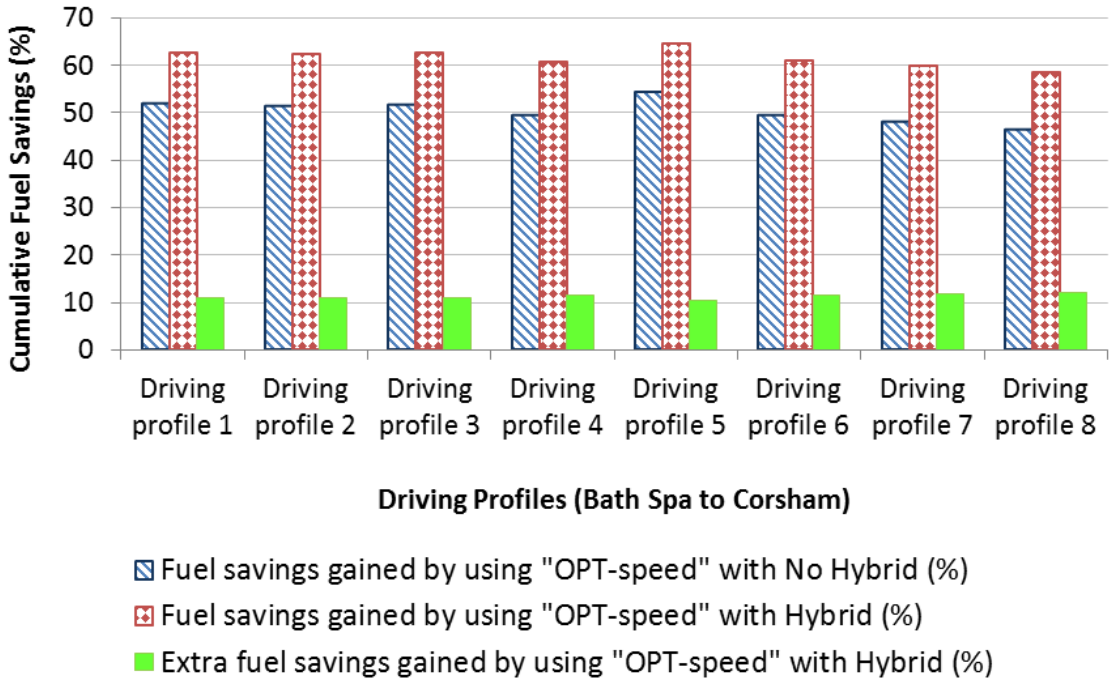

Figure 6-26: A plot showing the fuel savings potential of the OPT-speed approach over 8 real-world driving profiles representing commutes from **Bath Spa to Corsham**

	OPT-speed	Driving profile 1	Driving profile 2	Driving profile 3	Driving profile 4	Driving profile 5	Driving profile 6	Driving profile 7	Driving profile 8
Driving time (s)	1635.00	1532.97	1685.92	1427.45	1773.39	1567.95	1508.00	1668.94	1434.41
Driving time difference (s)	-	-102.03	50.92	-207.55	138.39	-67.05	-127.00	33.94	-200.59
Driving time difference (%)	-	-6.24	3.11	-12.69	8.46	-4.10	-7.77	2.08	-12.27

Table 6-10: A summary table comparing the journey time of the OPT-speed approach with that of driving profiles representing commutes from **Bath Spa to Corsham**

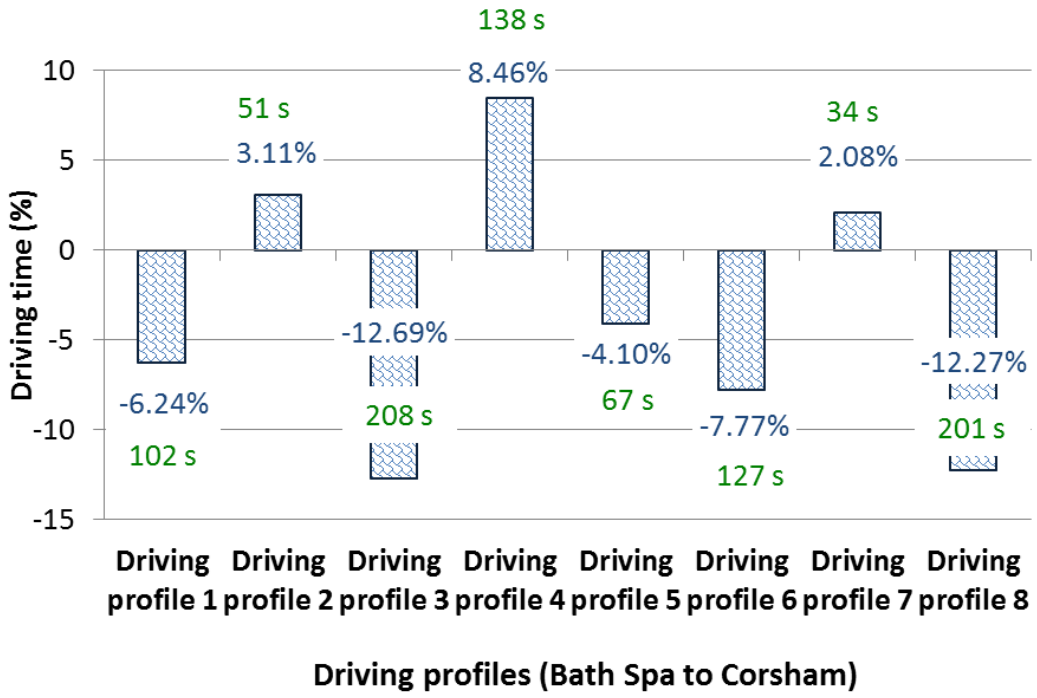

Figure 6-27: A plot comparing the journey time of the OPT-speed approach with that of driving profiles representing commutes from **Bath Spa to Corsham**

6.3.3 Real-time vehicle speed control (RTC-speed)

In Section 6.3.2, an optimal vehicle speed control approach that uses dynamic programming was formulated and simulated in real time. Although non-causal in nature (due to driveability concerns such as very harsh accelerations, safety concerns and route traffic congestion), results from the OPT-speed approach indicates the best fuel savings, which can be realised through vehicle speed control. In this section, a real-time control approach to vehicle speed control is formulated. This approach is based on averaging the speed trajectory of the vehicle immediately ahead (lead vehicle).

The disposition of this section is outlined as follows: first, the real-time vehicle speed control approach is theoretically formulated and simulated on a conventional vehicle, over different route preview horizons. The resulting fuel economies are then compared with that of normal driving profiles over a real-world driving route. Finally, the impact of the RTC-speed approach on hybrid electric vehicles are also investigated and appraised accordingly.

6.3.3.1 Real-time vehicle speed control problem formulation

Engine start and stop is a significant contributor to fuel use in an urban environment. Through the use of telematics in the form of inter-vehicle communication, a near-optimal online vehicle speed trajectory can be estimated such that fuel consumption and the frequency of engine start and stop is reduced without any compromise to trip distance.

In this section, a real-time vehicle speed control approach (RTC-speed), which is based on averaging the speed trajectory of the vehicle immediately ahead, is proposed. In literary terms, this approach uses the past speed trajectories of the vehicle immediately ahead of it, within a specified traffic preview window, to estimate the speed trajectory of the intelligent vehicle, such that fuel savings are optimised without any vehicle collision or violation to time or positional constraints. The speed trajectories of the vehicle immediately ahead (lead vehicle) can be obtained through inter-vehicle communication. In more formal terms, the proposed approach could be expressed mathematically as follows:

$$V_v = \frac{V_{lead_h} + V_{lead_{h-1}} + V_{lead_{h-2}} \cdots V_{lead_1}}{h} \quad 6\text{-}29$$

Where h is the length of the preview window considered.

The approach proposed in Equation 6-29 and shown in Figure 6-28 is subject to the constraint in Equation 6-30, which ensures that during the braking phase vehicle deceleration is not lower than the minimum deceleration estimated for each deceleration event. The mathematical function representing minimum deceleration, which was previously derived in Section 6.3.2.2.1.4, takes into consideration factors that influence the deceleration trajectory of the vehicle (engine braking, rolling resistance and aerodynamic force).

$$\frac{dV_v}{dt}_{min} \leq -\left(\frac{F_{ICE_{brake}}}{m} + \frac{\mu N_c \cos(\propto_{seg})}{m} + \frac{0.5\rho A_f C_d (V_v - V_a)^2}{m}\right) \quad 6\text{-}30$$

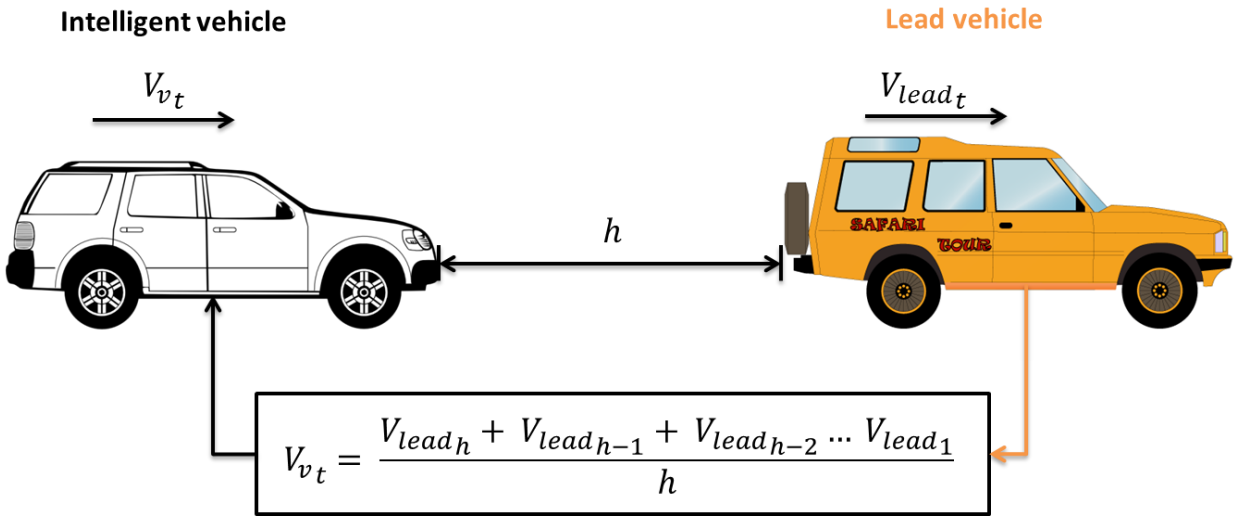

Figure 6-28: Real-time vehicle speed control approach

Building on the proposed real-time vehicle speed control approach, the following case studies are undertaken using 8 real world driving profiles (Figure 6-10 - Figure 6-17) representing commutes from Bath Spa to Corsham.

1. At first, the impact of traffic preview window on positional constraints, such as total driving distance and the instantaneous positional gap between both the lead vehicle and the intelligent vehicle are investigated. This analysis is important in determining a feasible range for the preview window, which does not violate any positional constraints.
2. Afterwards, the fuel savings potential of the proposed approach is analysed first on a conventional vehicle and then on an HEV.
3. Finally, the fuel savings potential of the different vehicular technologies are put into a comparative context, and used to determine the most cost-effective approach through which vehicular fuel economy could be maximised.

6.3.3.1.1 Impact of look-ahead preview window on positional constraints

In this section, the impact of traffic preview window on positional constraints, such as total driving distance and the instantaneous positional gap between the lead vehicle and the intelligent vehicle are investigated.

At first, a one-dimensional sensitivity analysis is undertaken to investigate the impact of look-ahead preview window on total driving distance (Figure 6-29). Results from this analysis (Figure 6-29) show an exponential decline in the total driving distance beyond a preview window of 45 seconds for most of the 8 driving profiles considered. At the beginning of the simulation, there is a lag in the vehicle speed information available to the intelligent vehicle. The size of this lag is equal in

length to the size of the traffic preview window. As the preview window increases beyond 45 seconds, the aforementioned lag results in an exponential decline in the total driving distance that can be covered by the intelligent vehicle based solely on modified speed information from the lead vehicle. This observation implies that in order not to violate positional constraints regarding the total driving distance that can be achieved using only modified speed information from the lead vehicle, the maximum preview window must not exceed 45 seconds.

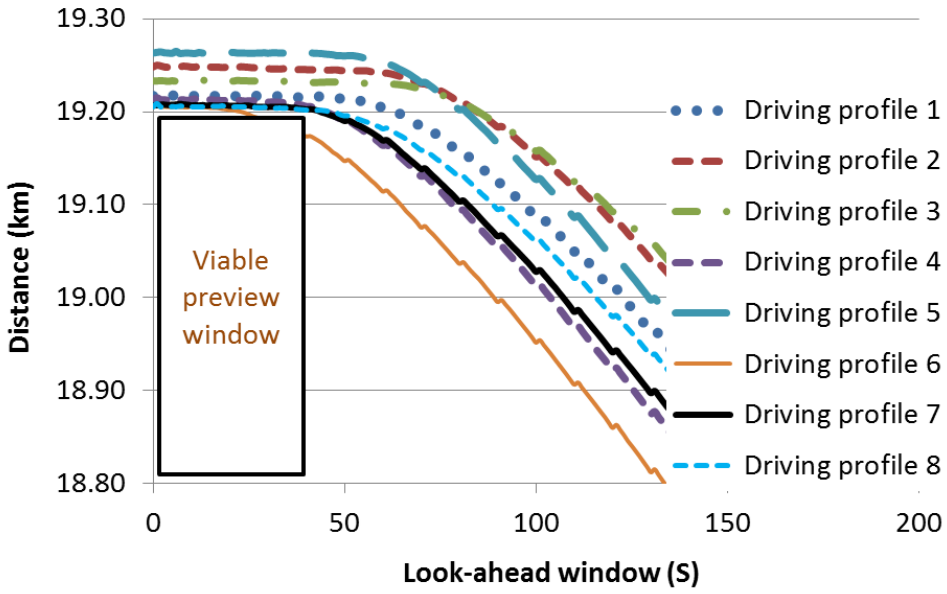

Figure 6-29: Impact of look-ahead preview window on total driving distance

In Figure 6-30, the impact of the traffic preview window on the instantaneous positional gap between the lead vehicle and the intelligent vehicle is investigated. From this analysis, the following observations are made:

1. The gap between the lead vehicle and the intelligent vehicle is positive, thus implying that overtaking is not allowed. This gap however increases with increasing preview window and peaks at maximum vehicle speeds.

2. The real-time speed control approach acts to smooth the speed trajectory of the lead vehicle, consequently reducing the acceleration and deceleration events that the intelligent vehicle will undergo.

Although not considered in this study, additional constraints may be applied to limit the maximum distance between the lead vehicle and the intelligent vehicle. However, these additional constraints are likely to result in some deterioration in achievable fuel economy.

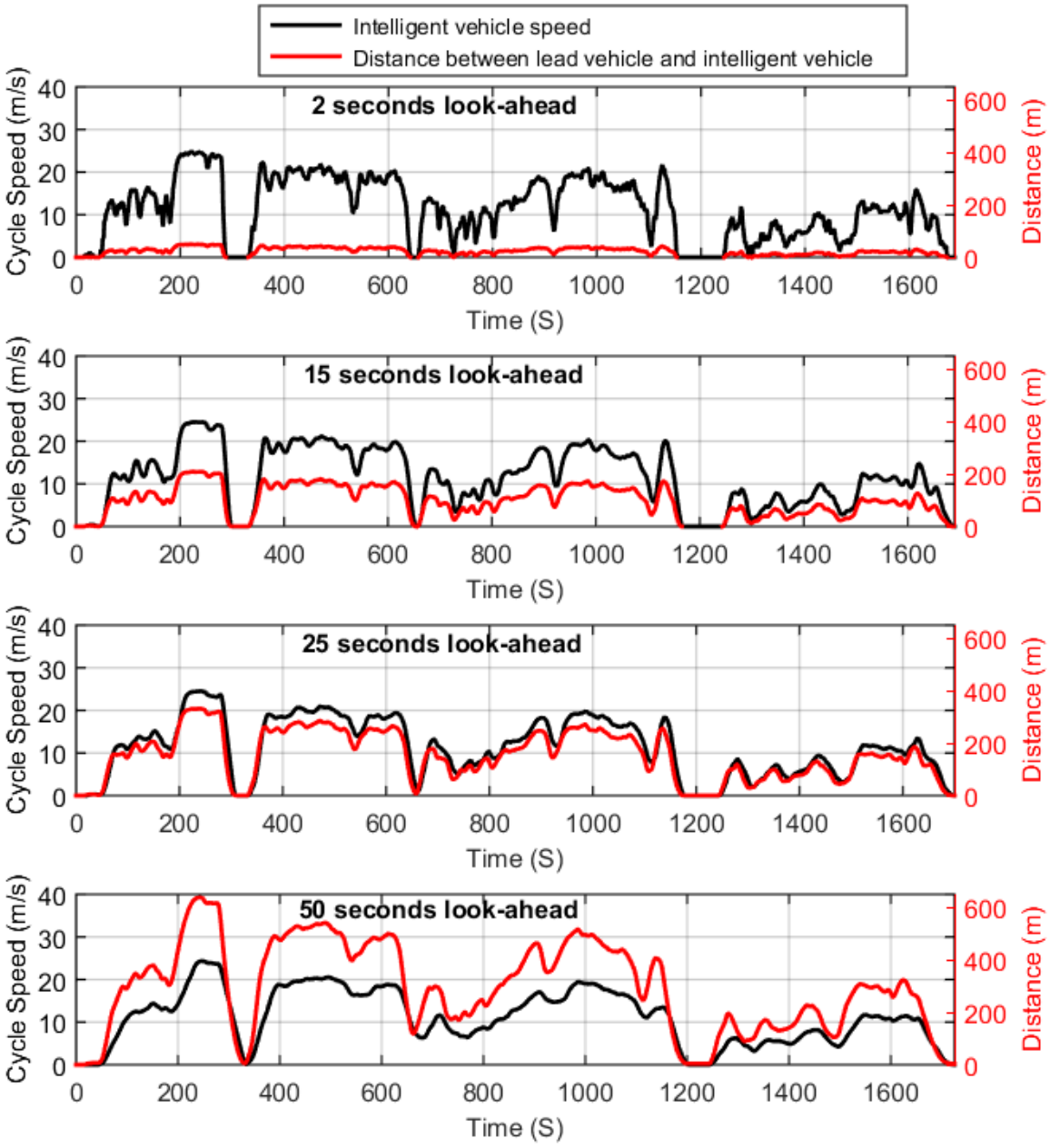

Figure 6-30: Plot showing the instantaneous positional gap between the lead vehicle and the intelligent vehicle for different traffic preview lengths

6.3.3.1.2 Evaluation of the RTC-speed approach for a conventional vehicle

In this section, the fuel savings potential of the RTC-speed approach is investigated over 8 real-world driving profiles of a conventional vehicle (driving profiles contained in Figure 6-33 to Figure 6-40). The fuel savings potential of the OPT-speed approach is also included for comparative reasons. For this analysis, a maximum preview window of 45 seconds is considered to ensure that no positional constraints are violated (see Section 6.3.3.1.1).

From Figure 6-31, it could be observed that cumulative fuel consumption decreases exponentially with increasing traffic preview window for all driving profiles analysed. By definition, the real-time speed control approach acts to smooth the speed trajectory of the lead vehicle, consequently reducing the acceleration and deceleration events that the intelligent vehicle will undergo (Figure 6-32). This smoothing effect translates into increased fuel economy, which tends to increase with increasing traffic preview window, as shown in Figure 6-31 and summarised quantitatively in Table 6-11. From Figure 6-31, significant improvements in fuel economy can also be observed for relatively short traffic previews (less than 20s), on all driving profiles analysed. Furthermore, there appears to be a knee-point at approximately 21s of traffic preview, beyond which the rate of improvement in fuel economy for extra preview information decreases.

From Figure 6-31, a significant gap is observed between the fuel savings potential of the OPT-speed approach (formulated in Section 6.3.2) and the fuel savings potential of the RTC-speed approach even at high traffic preview windows. This performance gap represents the fuel consumption cost introduced by real-world traffic conditions. Unlike the OPT-speed approach, which assumes perfect traffic conditions, the RTC-speed approach is formulated to ensure that real-time fuel

savings are realised without violating any traffic constraints, i.e. positional constraints. Consequently, the RTC-speed approach incorporates more real-world constraints and thus a higher fuel consumption penalty.

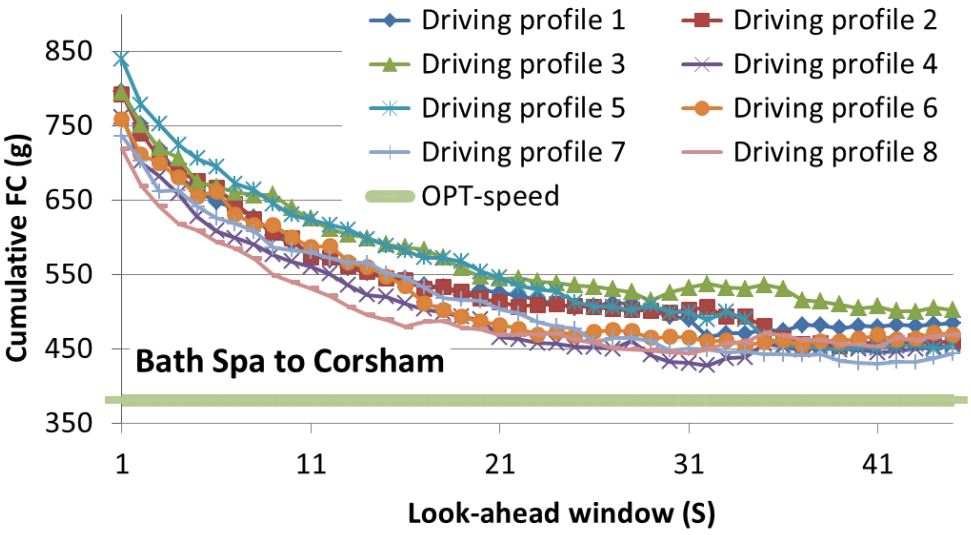

Figure 6-31: Impact of traffic preview window on cumulative fuel consumption for the RTC-speed approach and the OPT-speed approach

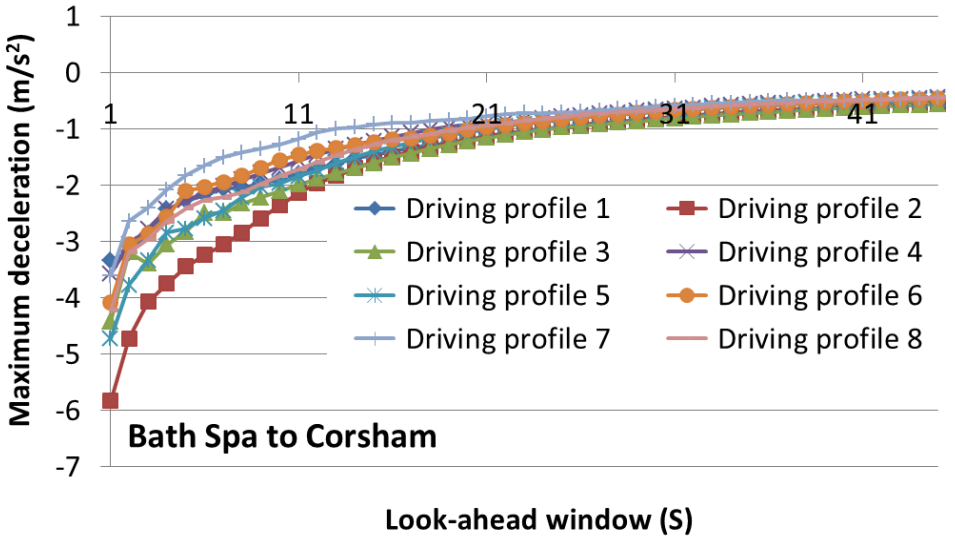

Figure 6-32: Impact of traffic preview window on maximum deceleration for the RTC-speed approach and the OPT-speed approach

Cumulative fuel consumption (g)								
Look-ahead Time (s)	**Driving profile 1**	**Driving profile 2**	**Driving profile 3**	**Driving profile 4**	**Driving profile 5**	**Driving profile 6**	**Driving profile 7**	**Driving profile 8**
0	792.64	786.03	790.58	754.6	836.3	755.65	735.43	712.83
5	661.55	675.40	673.75	627.10	705.50	654.68	640.89	608.72
10	592.24	597.70	639.02	566.94	630.03	600.02	582.79	539.37
15	545.68	544.47	590.05	520.08	588.64	547.58	551.22	488.85
20	529.59	517.37	546.42	489.04	553.87	486.30	514.16	476.38
25	504.86	507.11	535.05	452.20	512.61	467.79	476.86	461.90
30	493.31	498.02	525.22	432.37	498.93	465.63	448.00	445.63
35	470.57	492.56	530.96	438.58	488.96	453.91	445.77	458.90
40	480.82	455.70	504.50	449.38	451.93	463.65	431.00	455.55
45	484.20	460.06	502.05	455.79	453.50	468.82	443.40	469.43

Table 6-11: A summary table evaluating the impact of traffic preview window on cumulative fuel consumption using the RTC-speed approach on a **conventional vehicle**

6.3.3.1.3 Evaluation of the RTC-speed approach for an HEV

In the previous section, a real-time vehicle speed control approach, formulated in Section 6.3.3, is simulated on a conventional vehicle over 8 real-world driving profiles. In this section, the RTC-speed approach is simulated on an HEV to investigate the fuel savings that can be realised by integrating both the real-time speed modification technology and the hybrid technology into one vehicle. The RPEC strategy developed in Chapter 5 is used here for the real-time HEV simulations.

The resulting fuel savings potential from this analysis are shown in Figure 6-33 to Figure 6-40 and summarised in Table 6-12. From these plots it could be observed that the combination of the HEV technology with a real-time vehicle speed control technology does result in additional reduction in fuel consumption. From these plots, the resulting fuel savings can also been seen to decrease with increasing traffic preview window. By definition, the RTC-speed algorithm acts to increasingly smoothen the vehicle speed profile as traffic preview length increases. This smoothing effect leads to reduced deceleration events which impact the ability of the HEV to benefit from regenerative braking, thus resulting in reduced fuel savings for increasing traffic preview window.

The additional fuel savings potential of simulating the RTC-speed algorithm on an HEV is quantitatively summarised in Table 6-13. From this table, it could be inferred that as much as 25.69% extra fuel savings could be achieved through the collaborative application of both technologies. The impact of traffic preview window on the final battery state of charge of an HEV is investigated in Figure 6-41 and summarised in Table 6-14. Results from this plot do not show any conclusive trend with regards to the impact of preview window on the final battery SOC of an

HEV. However, a near-charge-sustaining performance is observed for all traffic preview windows. This trend is believed to be mainly as a result of the robust nature of the RPEC strategy.

In Figure 6-43, the maximum cumulative fuel savings that can be realised through different vehicle technologies (HEV, OPT-speed and RTC-speed) are assessed over 8 real-world driving profiles. A plot of minimum fuel consumption for each technology is also included in Figure 6-42 for emphasis. Results from these plots (summarised in Table 6-15) show that relative to an HEV technology which comes at a bigger cost, far higher fuel savings could be achieved through a simple real-time vehicle speed control approach. By definition, the speed trajectories derived from the OPT-speed approach are non-causal, and so can only be used to estimate the best fuel savings that can be realised along a route through vehicle speed control.

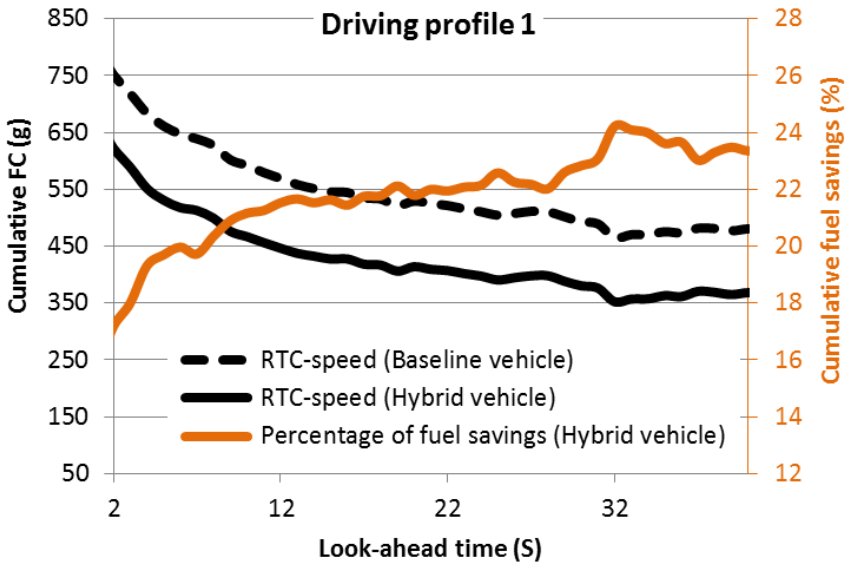

Figure 6-33: Impact of traffic preview window on the cumulative fuel savings and cumulative fuel consumption of an HEV, over **driving profile 1** for a route from Bath Spa to Corsham

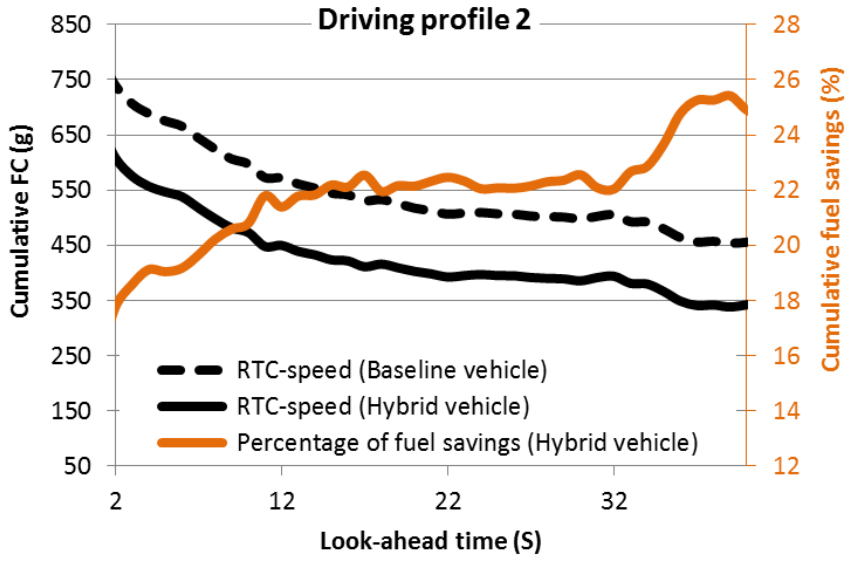

Figure 6-34: Impact of traffic preview window on the cumulative fuel savings and cumulative fuel consumption of an HEV, over **driving profile 2** for a route from Bath Spa to Corsham

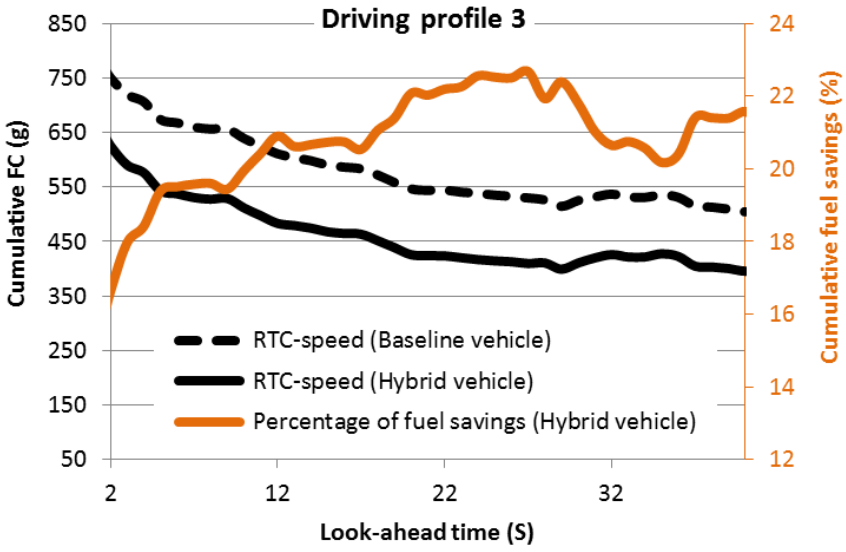

Figure 6-35: Impact of traffic preview window on the cumulative fuel savings and cumulative fuel consumption of an HEV, over **driving profile 3** for a route from Bath Spa to Corsham

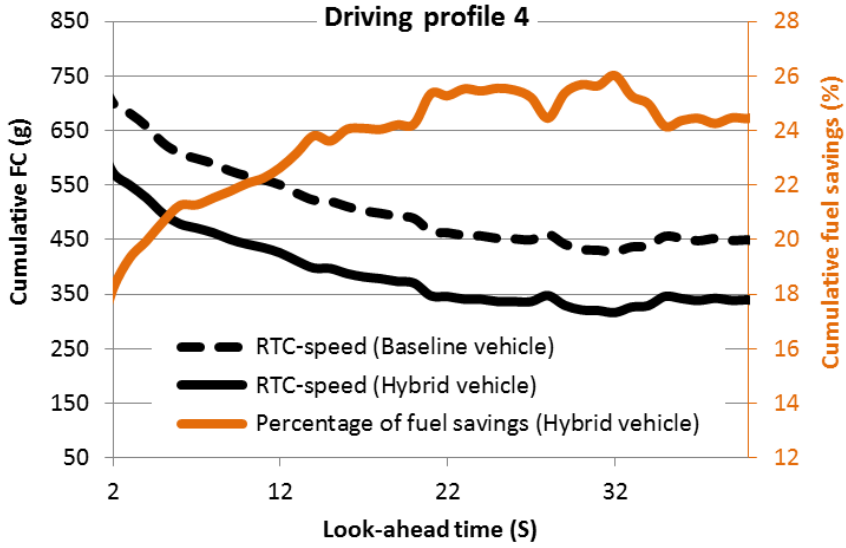

Figure 6-36: Impact of traffic preview window on the cumulative fuel savings and cumulative fuel consumption of an HEV, over **driving profile 4** for a route from Bath Spa to Corsham

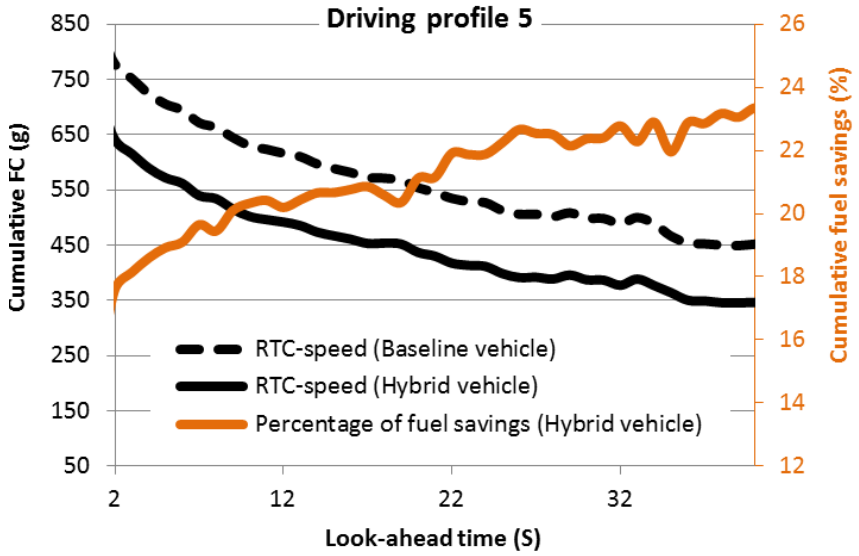

Figure 6-37: Impact of traffic preview window on the cumulative fuel savings and cumulative fuel consumption of an HEV, over **driving profile 5** for a route from Bath Spa to Corsham

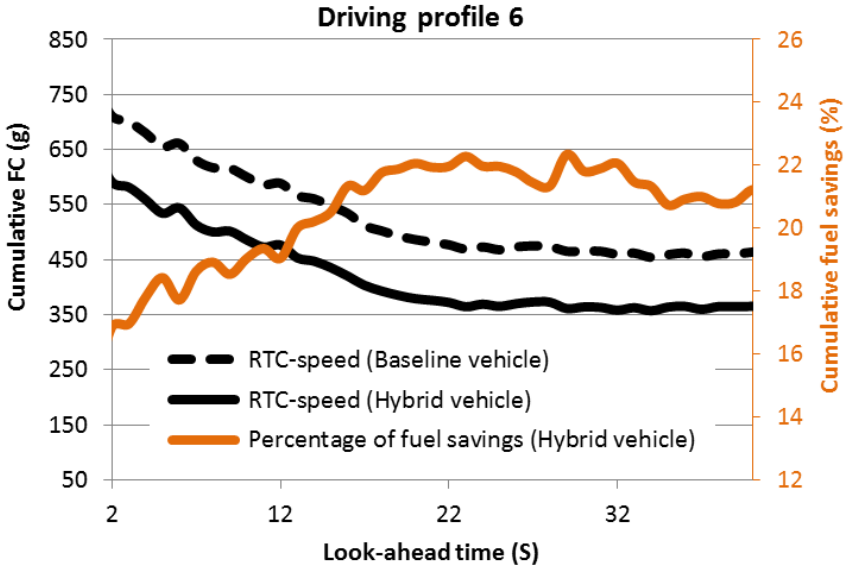

Figure 6-38: Impact of traffic preview window on the cumulative fuel savings and cumulative fuel consumption of an HEV, over **driving profile 6** for a route from Bath Spa to Corsham

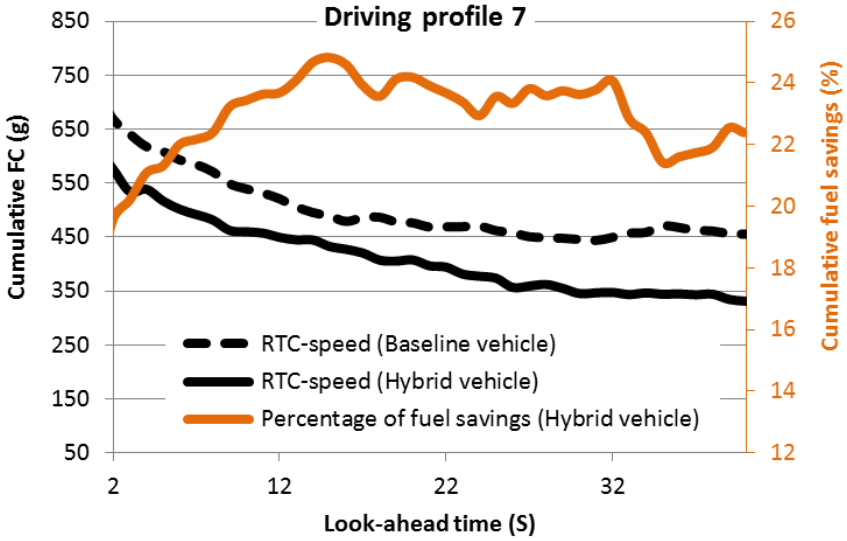

Figure 6-39: Impact of traffic preview window on the cumulative fuel savings and cumulative fuel consumption of an HEV, over **driving profile 7** for a route from Bath Spa to Corsham

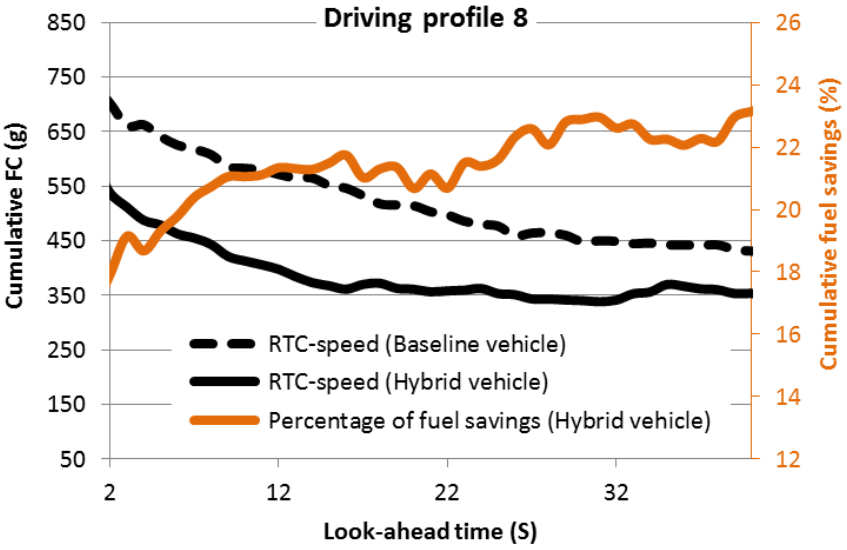

Figure 6-40: Impact of traffic preview window on the cumulative fuel savings and cumulative fuel consumption of an HEV, over **driving profile 8** for a route from Bath Spa to Corsham

Cumulative fuel consumption (g)								
Look-ahead time (s)	**Driving profile 1**	**Driving profile 2**	**Driving profile 3**	**Driving profile 4**	**Driving profile 5**	**Driving profile 6**	**Driving profile 7**	**Driving profile 8**
0	667.66	658.82	671.09	631.44	708.48	640.79	611.55	587.46
5	531.26	546.77	543.12	497.56	572.01	534.04	517.12	478.99
10	466.89	473.45	511.51	441.87	501.96	485.79	460.07	412.96
15	427.63	423.69	467.72	397.25	466.99	435.23	432.73	367.50
20	414.17	402.81	425.79	370.51	436.86	379.03	407.84	361.18
25	390.85	395.13	414.54	336.64	398.55	365.06	373.82	353.05
30	380.65	385.68	410.69	321.31	387.30	364.08	345.44	340.34
35	357.68	379.97	421.76	329.03	376.98	357.11	346.58	356.19
40	368.51	342.22	395.64	339.52	346.39	365.26	331.24	353.56
45	373.13	350.82	397.16	347.91	347.50	368.54	343.04	371.06

Table 6-12: A summary table evaluating the impact of traffic preview window on the cumulative fuel consumption obtained by simulating the RTC-speed approach on an **HEV**

Cumulative fuel consumption (%)								
Look-ahead Time (s)	**Driving profile 1**	**Driving profile 2**	**Driving profile 3**	**Driving profile 4**	**Driving profile 5**	**Driving profile 6**	**Driving profile 7**	**Driving profile 8**
0	15.78	16.20	15.13	16.33	15.29	15.21	16.86	17.60
5	19.70	19.04	19.39	20.66	18.92	18.43	19.31	21.31
10	21.17	20.79	19.95	22.06	20.33	19.04	21.06	23.44
15	21.63	22.18	20.73	23.62	20.67	20.52	21.50	24.82
20	21.79	22.14	22.08	24.24	21.13	22.06	20.68	24.18
25	22.58	22.08	22.52	25.55	22.25	21.96	21.61	23.57
30	22.84	22.56	21.81	25.69	22.37	21.81	22.89	23.63
35	23.99	22.86	20.57	24.98	22.90	21.33	22.25	22.38
40	23.36	24.90	21.58	24.45	23.35	21.22	23.15	22.39
45	22.94	23.75	20.89	23.67	23.37	21.39	22.63	20.96

Table 6-13: A summary table evaluating the additional fuel savings potential derived from simulating the RTC-speed approach on an **HEV**

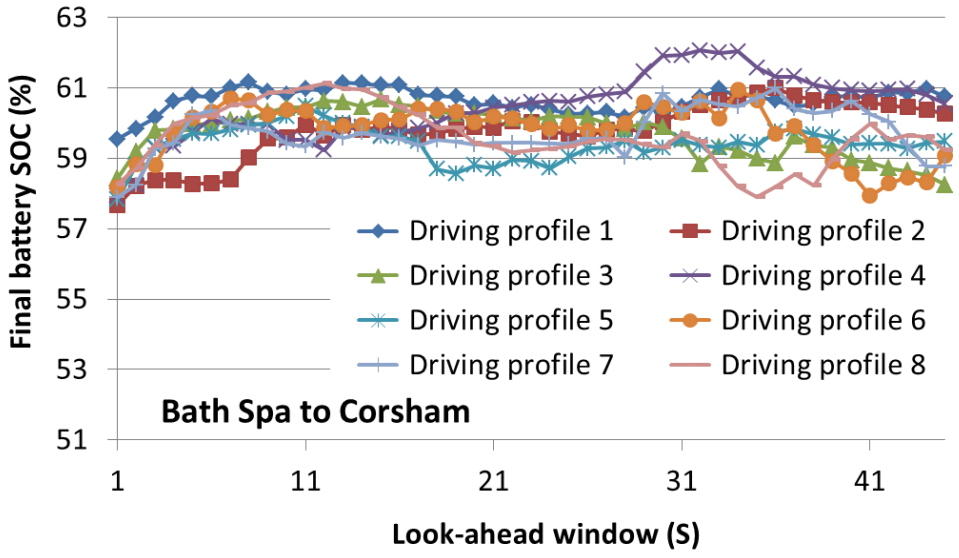

Figure 6-41: Impact of traffic preview window on the final battery SOC of an HEV

Final battery state of charge (%)								
Look-ahead Time (s)	**Driving profile 1**	**Driving profile 2**	**Driving profile 3**	**Driving profile 4**	**Driving profile 5**	**Driving profile 6**	**Driving profile 7**	**Driving profile 8**
0	59.54	57.72	58.44	57.83	57.86	58.15	57.90	58.29
5	60.78	58.27	59.98	59.75	59.71	60.17	60.24	60.16
10	60.83	59.59	60.44	59.52	60.19	60.37	59.42	60.91
15	61.08	59.91	60.68	59.65	59.62	60.09	59.64	60.75
20	60.51	59.90	60.29	60.29	58.81	60.02	59.39	59.43
25	60.26	59.71	60.19	60.61	59.05	59.94	59.41	59.34
30	60.28	60.03	59.88	61.92	59.30	60.45	60.85	59.32
35	60.78	60.75	59.22	62.04	59.46	60.96	60.47	58.21
40	60.78	60.60	58.96	60.95	59.40	58.57	60.63	59.55
45	60.76	60.26	58.24	60.56	59.48	59.08	58.78	59.24

Table 6-14: A summary table evaluating the impact of traffic preview window on the final battery state of charge obtained by simulating the RTC-speed approach on an **HEV**

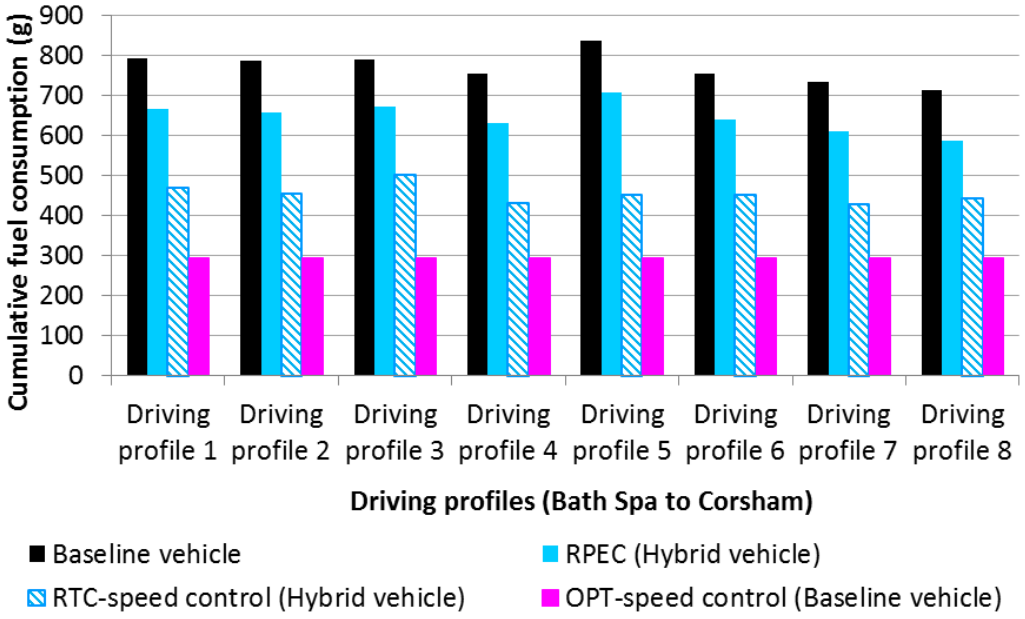

Figure 6-42: A plot showing the minimum cumulative fuel consumption that can be realised through different vehicle technologies

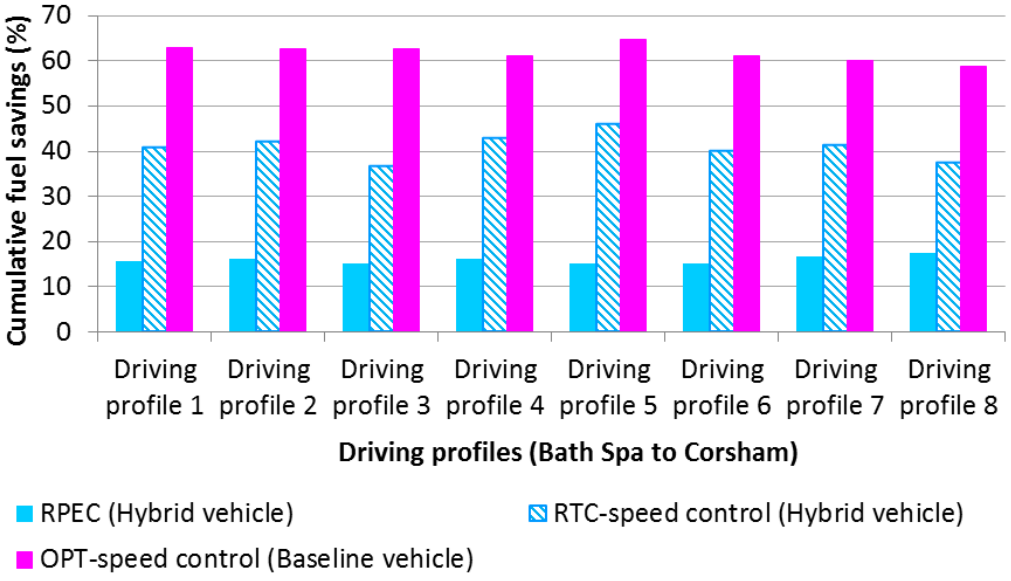

Figure 6-43: A plot showing the maximum cumulative fuel savings that can be realised through different vehicle technologies

(RTC-speed) – Baseline vehicle									
		Driving profile 1	**Driving profile 2**	**Driving profile 3**	**Driving profile 4**	**Driving profile 5**	**Driving profile 6**	**Driving profile 7**	**Driving profile 8**
Cumulative fuel consumption (g)	Baseline vehicle	792.64	786.03	790.58	754.6	836.3	755.65	735.43	712.83
	RPEC strategy **(Hybrid vehicle)**	667.66	658.82	671.09	631.44	708.48	640.79	611.55	587.46
	OPT-speed **(Baseline vehicle)**	380.90	380.90	380.90	380.90	380.90	380.90	380.90	380.90
	RTC-speed **(Baseline vehicle)**	470.57	455.70	502.05	432.37	451.93	453.91	431.00	445.63
Cumulative fuel savings (%)	RPEC strategy **(Hybrid vehicle)**	15.77	16.18	15.11	16.32	15.28	15.20	16.84	17.59
	OPT-speed **(Baseline vehicle)**	51.95	51.54	51.82	49.52	54.45	49.59	48.21	46.57
	RTC-speed **(Baseline vehicle)**	40.63	42.03	36.50	42.70	45.96	39.93	41.39	37.49

Table 6-15: A summary table detailing the minimum cumulative fuel consumption and maximum cumulative fuel savings that can be realised through different vehicle technologies

6.4 Chapter conclusions

In this chapter, three novel variations to the real-time predictive control of HEVs (RBEC, OPT-speed and RTC-speed) were formulated and simulated over a driving route from Bath Spa to Corsham. These novel contributions are summarised subsequently in Section 6.4.1 on a point by point basis.

6.4.1 Summary of the RBEC strategy development and simulation

The first variation is a novel route based ECMS control strategy which uses a route optimised battery SOC trajectory to adapt the predictive controller towards achieving an optimal performance in real time. The route-optimised battery SOC trajectory in this case was formulated from partial route preview information in the form of average route driving speed and altitude. First, the "least expendable or regenerable energy across the driving route segments" were calculated from the estimated route preview information (average route driving speed and altitude). Thereafter, the resulting energy profile was used to formulate a route-optimised battery state of charge reference trajectory. Finally, the route-optimised battery SOC trajectory was incorporated into the RPEC framework. The resulting controller dubbed RBEC (Route Based ECMS Control) was simulated in comparison with the RPEC strategy over different driving scenarios, with a view to investigating the additional benefits associated with incorporating route preview information into an HEV energy management control framework. Results from this analysis showed that as much as 2.44% extra fuel savings could be achieved over a real-world driving route, through the incorporation of route preview information into a real-time HEV controller.

Summarily, the benefits of the proposed novel RBEC strategy can be elucidated as follows:

1. The RBEC strategy is a pioneer of the novel concept of incorporating both an offline optimisation algorithm (dynamic programming) and an online optimisation algorithm (ECMS) for the near-optimal management of energy in HEVs.
2. It offers a coherent and logical approach towards route planning for optimisation of fuel economy and braking energy regeneration.
3. Converse to existing approaches which enforce the use of the electric motor and battery just before an energy recuperation segment (downhill), the RBEC strategy differs conceptually in the sense that it enforces electric motor and battery usage at the most efficient route segments where fuel economy and braking energy regeneration are maximised.

6.4.2 Summary of the OPT-speed development and simulation

In the second variation, an optimal but non-causal vehicle speed control approach, which accounts for real-time dynamic effects like engine braking, was formulated using deterministic dynamic programming. The optimisation objective was to maximise fuel savings without much penalty to trip time. Although idealistic in nature, the resulting optimal vehicle speed control approach proved useful in the following ways: first as a measure of the ultimate fuel savings that could be realised along a route through vehicle speed control, and then as an optimal benchmark for evaluating real-time vehicle speed control strategies. Finally, as a paradigm for the extraction of fuel efficient driving patterns, which include but are not limited to:

1. Hill climbing at constant vehicle speeds.
2. Minimised aggressive acceleration manoeuvres.
3. Maximised mild acceleration manoeuvres.
4. Minimised aggressive deceleration manoeuvres.
5. The utilisation of constant vehicle speeds for most non-braking manoeuvres.
6. Maximised mild deceleration manoeuvres. For conventional baseline vehicles, maximising mild deceleration manoeuvres increases the travelling distance being covered under fuel cut off. For HEVs, it translates to increased braking energy regeneration.

Using real-time simulation analysis, the fuel savings potential of the optimal vehicle speed control approach was investigated first on a conventional vehicle and then on an HEV over a driving route from Bath Spa to Corsham. Fuel savings and journey time were used as the main evaluation criteria for this analysis. Results from this analysis show that:

1. Compared to real-world driving profiles, fuel savings of up to 54.45% on conventional vehicles and 64.81% on HEVs can be realised through the use of the OPT-speed approach.
2. A higher percentage of fuel savings is achieved through improved driving behaviour than through the hybrid system. This observation further buttresses the importance of improved driving behaviour as a significant and cost effective approach to improving vehicle fuel economy.
3. The simultaneous achievement of optimal fuel savings and optimal driving time is sometimes not feasible. Typically, a compromise is made between

both competing objectives, although, the compromise must be such that the journey still gets completed in a reasonable time frame.

4. A compromise involving a maximum time penalty of -12.69% (208s or 3.47 minutes) and fuel savings of 51.82% was observed for the conventional baseline vehicle.

Although very hypothetical in nature (due to driveability concerns - very harsh accelerations, safety concerns and route traffic congestion), these results indicate the best fuel savings which can be realised through vehicle speed control.

The benefits of the OPT-speed approach can be summarised as follows:

1. The OPT-speed approach does not require the specification of a look-ahead horizon length for optimisation, consequently eliminating the question regarding the impact of look-ahead horizon length on the optimality of the obtained results. This approach also does not require an online prediction of any kind, as the predictive optimisation process is done offline and can be accomplished using the fully available “partial route preview” information.
2. The OPT-speed approach yields a vehicle speed trajectory, which is globally optimal (considering the optimisation process is carried out over the full driving horizon) and can be simulated on any vehicle without the need for any further tuning.
3. The OPT-speed approach yields a route-optimised vehicle speed profile which can be simulated in real time to obtain the ultimate fuel savings potential that can be realised through the control of vehicle speed along a specified route.

6.4.3 Summary of the RTC-speed development and simulation

In the final variation, a real-time vehicle speed control approach based on averaging the speed trajectory of the vehicle immediately ahead (lead vehicle) was theoretically formulated and simulated on a conventional vehicle, over different route preview horizons. The resulting fuel economies were then compared with that of 8 normal driving profiles over a real-world driving route. Finally, the RTC-speed approach was simulated along with the RPEC strategy on an HEV, with a view to investigating the fuel savings potential of using both technologies collaboratively.

Results from these analyses show:

1. An exponential decline in the achievable total driving distance beyond a preview window of 45s for most of the 8 real-world driving profiles analysed. As previously explained, at the beginning of the simulation, there is a lag in the vehicle speed information available to the intelligent vehicle. The size of this lag is equal in length to the size of the traffic preview window. As the preview window increases beyond 45s, the aforementioned lag results in an exponential decline in the total driving distance that can be covered by the intelligent vehicle based solely on modified speed information from the lead vehicle. This observation implies that in order not to violate positional constraints regarding the total driving distance that can be achieved using only modified speed information from the lead vehicle, the maximum preview window must not exceed 45s.
2. That the real-time vehicle speed control approach acts to smooth the speed trajectory of the lead vehicle, consequently reducing the acceleration and deceleration events that the intelligent vehicle will undergo. This smoothing

effect translates into increased fuel economy which tends to increase with increasing traffic preview window.

3. That the gap between the lead vehicle and the intelligent vehicle is positive, thus implying that overtaking is not allowed. This gap increases with increasing preview window and peaks at maximum vehicle speeds.
4. That significant improvements in fuel economy can realised for relatively short traffic previews (less than 20s).
5. That a combination of the HEV technology with a real-time vehicle speed control technology does result in additional reduction in fuel consumption (as much as 25.69% extra fuel savings), although the resulting fuel savings decreases with increasing traffic preview window. By definition, the RTC-speed algorithm acts to increasingly smoothen the vehicle speed profile as traffic preview length increases. This smoothing effect leads to reduced deceleration events which impact the ability of the HEV to benefit from regenerative braking, thus resulting in reduced fuel savings for increasing traffic preview window.
6. That compared to an HEV technology which comes at a bigger cost, far higher fuel savings as much as 45.96% could be achieved through a simple real-time vehicle speed control approach.

In summary, the RTC-speed approach presents an easily implementable approach towards achieving real-time fuel savings with very little computational effort. A further fuel economy benefit of incorporating route preview information, which is not accounted for in this study, is through a closer inter-vehicle spacing as in platooning, which results in reduced coefficient of drag for the follower vehicles in the platoon. In a study by Barth [233], the improvements in fuel economy

obtained solely through reduced drag coefficients in a platooning situation were estimated to be in the range of 5-15%, over highway driving cycles.

Thus far, several controllers which differ in structure, utility of route preview information and complexity, have been developed and preliminarily analysed on standard driving cycles. Considering that these controllers are intended for production vehicles, there is need for these simulations to also be performed over real-world driving profiles, which are typically very different in aggressivity and length, from standard driving cycles. Consequently, Chapter 7 investigates the performance and robustness of the three causal controllers (HST-modified, DP-HST and RPEC) proposed in this thesis over 1197 real-world driving profiles (representing real-world driving conditions). These three causal controllers are of particular interest because they do not require any access to route preview information, and as such are relatively easier to implement on vehicles.

7 COMPARATIVE EVALUATION OF REAL-TIME HEV CONTROL STRATEGIES OVER REAL-WORLD DRIVING PROFILES

7.1 Introduction

In Chapters 3 to 5, three causal HEV controllers (HST-modified, DP-HST and RPEC) were developed and simulated over different driving cycles, in order to investigate their fuel savings potential in real time. Simulation results showed that, on standard driving cycles, all 3 controllers performed near-optimally. Considering that these controllers are intended for production vehicles, there is a need for these simulations to also be performed over real-world driving profiles, which are typically very different in aggressivity and length, from standard driving cycles. Consequently, this chapter will investigate the performance and robustness of all three causal controllers over 1197 real-world driving profiles (representing real-world driving conditions), with a view to identifying the most robust, charge-sustaining and consistent causal controller suitable for implementation on production vehicles. The three causal controllers investigated in this chapter are of particular interest because they do not require any access to route preview information, and as such are more straightforward to implement on vehicles.

7.2 Definition and classification of real-world driving profiles

In order to ensure the capture of naturalistic driving data with no instructions, intrusions or driver aid, all 1197 randomly selected driving profiles were extracted from the blind trial data originally captured by Vagg *et al.* [234, 235], as part of the eco-drive study. The driving profiles extracted for this study represent a total of 28,903km and 667 hours of real-world driving patterns.

In order to put into perspective the classifications and degree of aggressivity of the real-world driving profiles considered, the novel two-class grouping system proposed in section 3.2 is applied. As detailed in Table 7-1, the 1197 driving profiles considered consist of: 206 calm neighbourhood driving profiles, 131 moderate neighbourhood driving profiles, 8 aggressive neighbourhood driving profiles, 51 calm urban driving profiles, 365 moderate urban driving profiles, 303 aggressive urban driving profiles, 1 calm highway driving profile, 19 moderate highway driving profiles and 113 aggressive highway driving profiles.

		Calm	Moderate	Aggressive
Neighbourhood driving	Number of driving profiles	206	131	8
	Total trip time (h)	63.285	37.697	2.107
	Total driving time (h)	46.361	27.907	1.626
	Average driving speed (km/h)	22.121	28.611	29.176
	Average trip speed (km/h)	16.187	21.342	22.731
	Total trip distance (km)	1023.563	802.886	48.456
	Average aggressivity (m^2/s^3)	3.076	4.611	7.482
Urban driving	Number of driving profiles	51	365	303
	Total trip time (h)	15.829	121.857	262.407
	Total driving time (h)	13.999	105.605	198.298
	Average driving speed (km/h)	39.130	44.423	56.400
	Average trip speed (km/h)	34.444	38.516	49.442
	Total trip distance (km)	556.699	4800.797	12423.384
	Average aggressivity (m^2/s^3)	3.610	5.059	8.287
Highway driving	Number of driving profiles	1	19	113
	Total trip time (h)	1.984	8.025	152.835
	Total driving time (h)	1.978	7.601	108.222
	Average driving speed (km/h)	101.248	79.195	78.340
	Average trip speed (km/h)	100.950	75.145	71.287
	Total trip distance (km)	200.274	603.106	8444.322
	Average aggressivity (m^2/s^3)	3.331	5.193	10.569

Table 7-1: A summary table detailing the properties of 1197 real-world driving profiles

7.3 Assessment of controllers over real-world driving profiles

In this section, the causal controllers (HST-modified, DP-HST and RPEC) developed in Chapters 3 to 5 are evaluated over the real-world driving profiles. These evaluations are broken down into nine categories to investigate the fuel savings potential of all 3 controllers under the following conditions: calm neighbourhood driving, moderate neighbourhood driving, aggressive neighbourhood driving, calm urban driving, moderate urban driving, aggressive urban driving, calm highway driving, moderate highway driving and aggressive highway driving. These controllers are of particular interest, because they are causal and do not require any form of route preview information.

7.3.1 Neighbourhood driving

Over calm neighbourhood driving profiles, it could be observed that all 3 controllers perform near-optimally with the final battery state of charge ranging between 59.06% and 62.37% (detailed in Table 7-2 and shown in Figure 7-1b) and fuel savings potential ranging between 0.08% and 24.66% (detailed in Table 7-3 and shown in Figure 7-1a). Although the reported fuel savings in Table 7-3 could be used to gain a general idea of the possible fuel savings expected from each controller in the different categories, it cannot be used to compare the controllers. In order to accurately compare the fuel savings potential of different HEV control strategies, they must yield a perfectly charge-sustaining performance ($SOC_{final} = 60$). In a case where the controller is not perfectly charge-sustaining, an SOC correction is required to account for the fuel lost or gained due to non-charge sustenance. To comparatively examine the fuel savings potential of each controller

over various driving categories, Table 7-4 estimates the average fuel savings for each controller, assuming charge sustenance. The values of the average fuel savings assuming charge sustenance are estimated from Equations 3-28 and 3-29 (Section 3.5.7). As could be inferred from Table 7-4, the DP-HST controller achieves the highest charge-sustaining average fuel savings (15.97%) over the calm neighbourhood driving profiles. A similar inference can also be drawn from the simulation results obtained over the moderate neighbourhood driving profiles. Although the fuel savings potential and battery charge sustenance of all 3 controllers are similar over the aggressive neighbourhood driving profiles (detailed in Table 7-3 and Table 7-2 respectively), on average, the HST-modified controller has a slight performance advantage over the other two controllers (Table 7-4).

7.3.2 Urban driving

Over calm urban driving profiles, it could be observed that all 3 controllers perform near-optimally with the final battery state of charge ranging between 59.09% and 62.97% (detailed in Table 7-2 and shown in Figure 7-2b), and fuel savings potential ranging between 10.24% and 24.13% (detailed in Table 7-3 and shown in Figure 7-2a). Although the fuel savings potential and battery charge sustenance of all 3 controllers are similar (Table 7-2 and Table 7-3), the RPEC strategy has a slight performance advantage over the other two controllers (Table 7-4). Over moderate urban driving profiles, a similar near-charge-sustaining performance could be observed for all controllers (detailed in Table 7-2 and Table 7-3). Over aggressive urban driving profiles, the RPEC and HST-modified controllers are observed to yield charge-depleting performances over some driving profiles (detailed in Table 7-2). These observations are further highlighted in the cumulative distribution function plot detailed in Figure 7-3. The double-hump shape observed in Figure 7-3a is as a result of the characteristics of the driving profiles analysed in this category. The data set under the aggressive urban driving category contains lots of repeat driving profiles with similar fuel savings. Consequently, the cumulative distribution function plot in Figure 7-3a could be interpreted as an integral of probability density functions representing a set of driving profiles that could be grouped into several widely-spaced classes of cumulative fuel savings. The same explanation also applies to the double-hump shape observed in Figure 7-8a, for the aggressive highway driving category.

To understand the cause of the charge-depleting performance observed in Figure 7-3 for the RPEC and HST-modified controllers, a probability density function of aggressivity and final battery state of charge is produced for all controllers as

shown in Figure 7-4 to Figure 7-6. The data points with peak probability density functions represent repeat driving profiles with similar values of final battery SOC and aggressivity. From these plots, it could be observed that the RPEC and HST-modified controllers are more charge-depleting, over highly aggressive urban driving profiles. The comparative advantage of the DP-HST controller over the RPEC and HST-modified controllers lies in the implicit estimation of its fuel equivalence weighting factors, and ability to estimate and compensate for future energy variations, using real-time driving information.

Fundamentally, all fuel-minimising control strategies estimate the value of battery charge in terms of fuel, and then formulate representative weighting factors. These weighting factors may be explicit as in the case of the RPEC strategy and HST-modified controller, or implicit as in the case of the DP-HST controller. Typically, all known information is incorporated into this weighting factor, including the vehicle dynamics and expected future driving patterns. The basic difference between all controllers lies in how their weighting factors are estimated. For the RPEC and HST-modified controllers, the weighting factors are assigned by the designer. For the DP-HST controller, this estimation is based on cycle statistics. Consequently, the DP-HST controller is able to better adapt the SOC profile in real time, such that charge sustenance is achieved. In addition, the DP-HST controller is able to estimate and compensate for future energy variations using real-time driving information (Section 4.6.2).

7.3.3 Highway driving

Only 1 calm highway driving profile was tested in this study and as such, there are not enough comparative bases to draw any conclusions. However, from the summary results detailed in Table 7-2, it could be inferred that the RPEC strategy was the least charge-sustaining (54.44%). As detailed in Table 7-3, over the calm highway driving profile, the fuel savings potential for all 3 controllers range between 3.33% to 3.61%. Over moderate highway driving profiles, it could be observed that all 3 controllers perform near-optimally with the final battery state of charge ranging between 59.42% and 62.77% (detailed in Table 7-2 and shown in Figure 7-7b) and fuel savings potential ranging between 8.32% and 13.47% (detailed in Table 7-3 and shown in Figure 7-7a). Although the fuel savings potential and battery charge sustenance of all 3 controllers are similar (Table 7-2 and Table 7-3), the HST-modified controller has a slight performance advantage over the other two controllers (Table 7-4). Over aggressive highway driving profiles, the RPEC and HST-modified controllers are the least charge-sustaining (Table 7-2). Over these driving profiles, a final battery state of charge value as low as 46.16% and 46.62% were observed for the RPEC and HST-modified controllers respectively. These observations are further highlighted in the cumulative distribution function plot shown in Figure 7-8. By comparing the probability density function of all controllers as shown in Figure 7-9 to Figure 7-11, it could be observed that the RPEC and HST-modified controllers are more charge-depleting over highly aggressive highway driving profiles. As previously explained in Section 7.3.2, the comparative advantage of the DP-HST controller over the RPEC and HST-modified controllers lies in the implicit estimation of its fuel equivalence weighting

factors, and ability to estimate and compensate for future energy variations, using real-time driving information.

Figure 7-9 to Figure 7-11 are also characterised by interesting performance outliers worth investigating further. For example, although the general trend suggests that the RPEC and HST-modified controllers are more charge-depleting over highly aggressive highway driving profiles, there are some notable variants (dubbed "A" in Figure 7-9 to Figure 7-11). Over the driving profiles being represented by the earmarked probability density functions, it could be observed that all 3 controllers are able to yield a near charge-sustaining performance, over a highly aggressive highway driving profile. The simulation plots for the driving profiles in question are shown in Figure 7-12. Observed trends show that although the driving profile in question is predominantly a highway driving profile, it is characterised towards the end by a significant urban driving phase with lots of regenerative braking opportunities. This implies that although for each controller the battery SOC is significantly depleted during the highway driving phase, the regenerative braking opportunities characterising the subsequent urban driving phase enables each controller to recover the battery state of charge in a near charge-sustaining manner. The same explanation applies to the other similar performance outlier in Figure 7-9, dubbed "A*".

Another trend worth noting in Figure 7-12 is that in comparison to the other controllers, the DP-HST controller has a lower depth of discharge, but differs in charge-sustaining fuel savings by 0.26% ($1.88\% - 1.62\%$: Table 7-5) from HST-modified, which is the most fuel efficient controller over the aggressive highway driving profile in question. Battery life directly depends on the total energy throughput that its active chemicals can tolerate. As already discussed in Section

4.3, regardless of other ageing effects, the total energy throughput is fixed, such that 1 cycle of 100% DOD (Depth Of Discharge) is roughly equivalent to 2 cycles at 50% DOD, 10 cycles at 10% DOD and 100 cycles at 1% DOD. This implies that a lower depth of discharge promotes improved battery durability. As such, the 0.26% performance trade-off for improved battery durability represents a good compromise. Also, with a lower depth of discharge, the battery SOC could be easily contrasted for charge sustenance. This advantage becomes even more significant when a predominantly highway driving profile with fewer regenerative braking opportunities after the highway phase is considered (Figure 7-13). From Figure 7-13, it could be observed that during the cruise phase, the RPEC and HST-modified controllers completely deplete the battery state of charge, and are unable to recover subsequently, due to not having significant breaking opportunities after the cruise phase. In contrast, the DP-HST controller operates within a narrow SOC range, which makes it easier for near-charge sustenance to be achieved through the addition of small amounts of regenerative braking energy. To understand why the HST-modified controller and the RPEC strategy are not able to near-optimally contrast battery SOC over the aggressive driving profile shown in Figure 7-13, it is pertinent to re-evaluate the structural definition of each controller. As previously explained in Section 7.3.2, the fuel equivalence weighting factors of fuel minimising controllers can either be implicitly estimated using cycle statistics and real-time driving information, or explicitly estimated by the designer. The fuel equivalence weighting factors of the HST-modified controller (power allocation factor – Section 3.7.2.4) and RPEC strategy (initial equivalence factor and proportional controller gain – Section 5.6) were estimated and tuned explicitly, based on intuition. In contrast, the fuel equivalence weighting factor of the DP-HST controller is estimated implicitly, based on real-time driving information and cycle

statistics. The performance of explicitly-tuned controllers are limited by the number and variety of driving profiles used for the estimation and tuning, as well as the estimation method applied. Consequently, explicitly tuned-controllers may not perform very well if simulated on a driving profile with very different characteristics from the driving profiles used during the estimation and tuning process. Conversely, implicitly-tuned controllers are able to better adapt the battery SOC profile based on real-time driving information and cycle statistics.

Other performance outliers worth investigating further are the driving profiles represented by the probability density functions dubbed “B” and “C” in Figure 7-9 for the DP-HST controller. Over these driving profiles, it could be observed that the DP-HST controller yields a charge-hoarding performance over lowly aggressive highway driving profiles. As shown in Figure 7-14, the earmarked driving profiles are characterised by a highway driving phase, which ends with a mild deceleration phase. As previously explained in Section 3.7.2.6, mild deceleration promotes braking energy regeneration. Consequently, a culmination of a low depth of discharge during the highway driving phase, and a significant amount of braking energy during the subsequent braking phase, results in the charge-hoarding trend observed in Figure 7-14 for the DP-HST controller.

Neighbourhood driving				
		Calm	Moderate	Aggressive
DP-HST	Minimum final battery SOC (%)	59.06	59.35	58.67
	Maximum final battery SOC (%)	61.71	61.85	61.75
RPEC	Minimum final battery SOC (%)	59.18	59.83	58.33
	Maximum final battery SOC (%)	61.46	61.61	61.11
HST-modified	Minimum final battery SOC (%)	60.01	60.61	59.41
	Maximum final battery SOC (%)	62.37	62.12	61.91
Urban driving				
DP-HST	Minimum final battery SOC (%)	59.09	58.95	57.90
	Maximum final battery SOC (%)	62.56	65.40	64.03
RPEC	Minimum final battery SOC (%)	59.75	57.93	47.97
	Maximum final battery SOC (%)	61.33	61.81	61.66
HST-modified	Minimum final battery SOC (%)	60.34	60.53	49.05
	Maximum final battery SOC (%)	62.97	63.86	63.31
Highway driving				
DP-HST	Minimum final battery SOC (%)	62.73	59.42	58.65
	Maximum final battery SOC (%)	62.73	62.54	67.85
RPEC	Minimum final battery SOC (%)	54.44	60.01	46.16
	Maximum final battery SOC (%)	54.44	62.53	62.24
HST-modified	Minimum final battery SOC (%)	63.54	61.07	46.62
	Maximum final battery SOC (%)	63.54	62.77	64.01

Table 7-2: A summary table detailing a comparative evaluation of the DP-HST controller, the RPEC strategy and the HST-modified controller on the basis of final battery state of charge, over calm, moderate and aggressive neighbourhood, urban and highway driving

Neighbourhood driving				
		Calm	Moderate	Aggressive
DP-HST	Minimum fuel savings (%)	0.19	10.64	3.78
	Maximum fuel savings (%)	24.66	24.13	20.66
RPEC	Minimum fuel savings (%)	0.10	10.29	3.34
	Maximum fuel savings (%)	23.67	22.94	18.44
HST-modified	Minimum fuel savings (%)	0.08	10.19	5.35
	Maximum fuel savings (%)	24.56	24.13	19.78
Fuel savings range for all controllers	Minimum fuel savings (%)	0.08	10.19	3.34
	Maximum fuel savings (%)	24.66	24.13	20.66
Urban driving				
DP-HST	Minimum fuel savings (%)	10.24	9.46	1.11
	Maximum fuel savings (%)	24.13	25.91	22.80
RPEC	Minimum fuel savings (%)	11.05	9.68	1.27
	Maximum fuel savings (%)	23.93	24.63	22.15
HST-modified	Minimum fuel savings (%)	10.44	9.43	1.22
	Maximum fuel savings (%)	24.09	24.93	22.71
Fuel savings range for all controllers	Minimum fuel savings (%)	10.24	9.43	1.11
	Maximum fuel savings (%)	24.13	25.91	22.80
Highway driving				
DP-HST	Minimum fuel savings (%)	3.33	8.33	0.91
	Maximum fuel savings (%)	3.33	13.08	12.81
RPEC	Minimum fuel savings (%)	3.61	8.55	1.20
	Maximum fuel savings (%)	3.61	13.47	12.70
HST-modified	Minimum fuel savings (%)	3.42	8.32	1.27
	Maximum fuel savings (%)	3.42	12.93	12.53
Fuel savings range for all controllers	Minimum fuel savings (%)	3.33	8.32	0.91
	Maximum fuel savings (%)	3.61	13.47	12.81

Table 7-3: A summary table detailing a comparative evaluation of the DP-HST controller, the RPEC strategy and the HST-modified controller on the basis of cumulative fuel savings, over calm, moderate and aggressive neighbourhood, urban and highway driving

Neighbourhood driving				
		Calm	**Moderate**	**Aggressive**
DP-HST	Average fuel savings assuming charge sustenance (%)	15.97	18.58	14.38
RPEC		15.32	17.42	13.43
HST-modified		15.90	18.11	14.53
Urban driving				
DP-HST	Average fuel savings assuming charge sustenance (%)	17.29	17.20	11.48
RPEC		17.77	16.98	11.06
HST-modified		17.53	17.07	11.28
Highway driving				
DP-HST	Average fuel savings assuming charge sustenance (%)	3.49	10.84	4.95
RPEC		2.65	11.08	4.53
HST-modified		3.63	10.76	4.56
Controllers	**Number of categories with highest average fuel savings assuming charge sustenance**			
DP-HST	**5**			
RPEC	**2**			
HST-modified	**2**			

Table 7-4: A summary table detailing a comparative evaluation of the DP-HST controller, the RPEC strategy and the HST-modified controller on the basis of average fuel savings assuming charge sustenance, over calm, moderate and aggressive neighbourhood, urban and highway driving

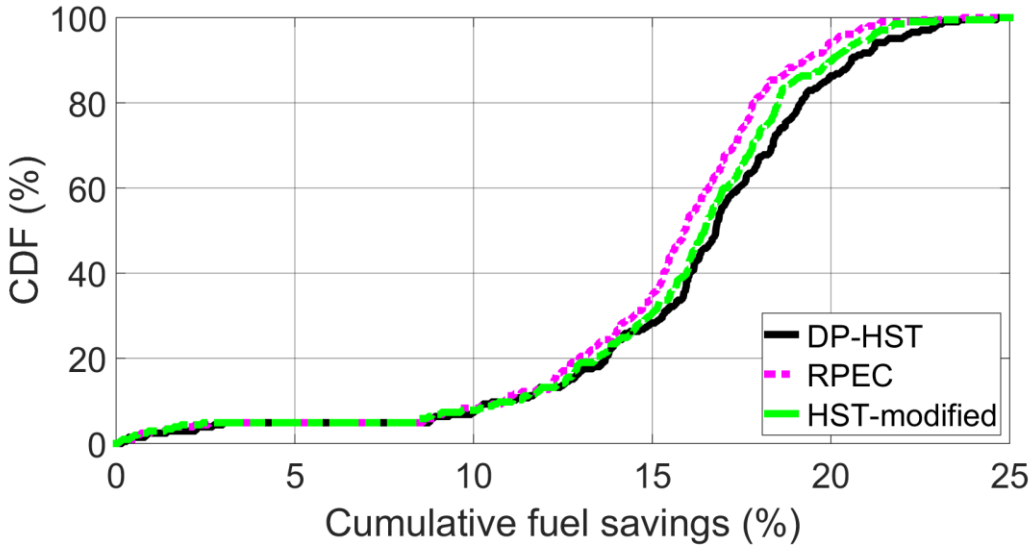

(a) The cumulative distribution function of cumulative fuel savings

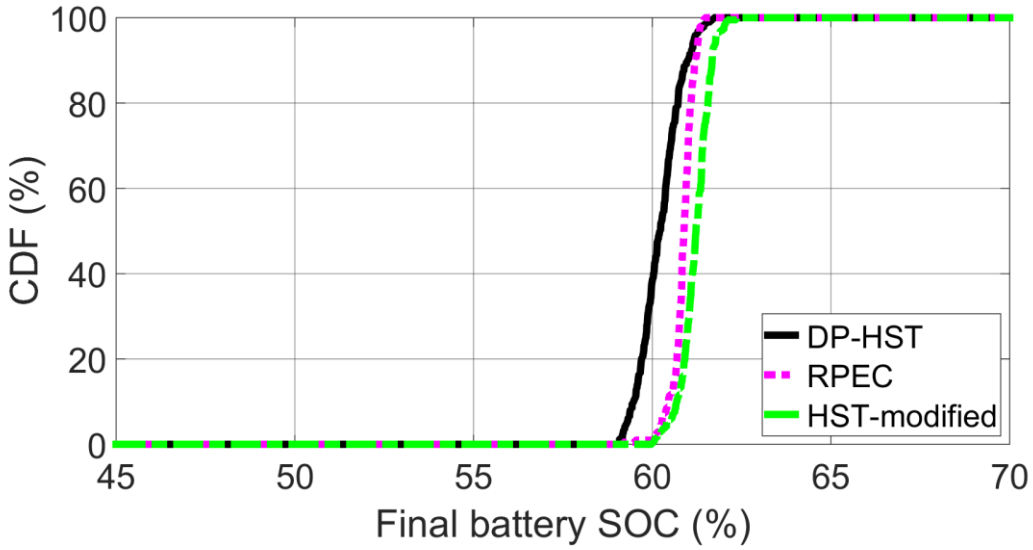

(b) The cumulative distribution function of final battery state of charge

Figure 7-1: Cumulative distribution function plots of cumulative fuel savings and final battery state of charge, over calm neighbourhood driving profiles

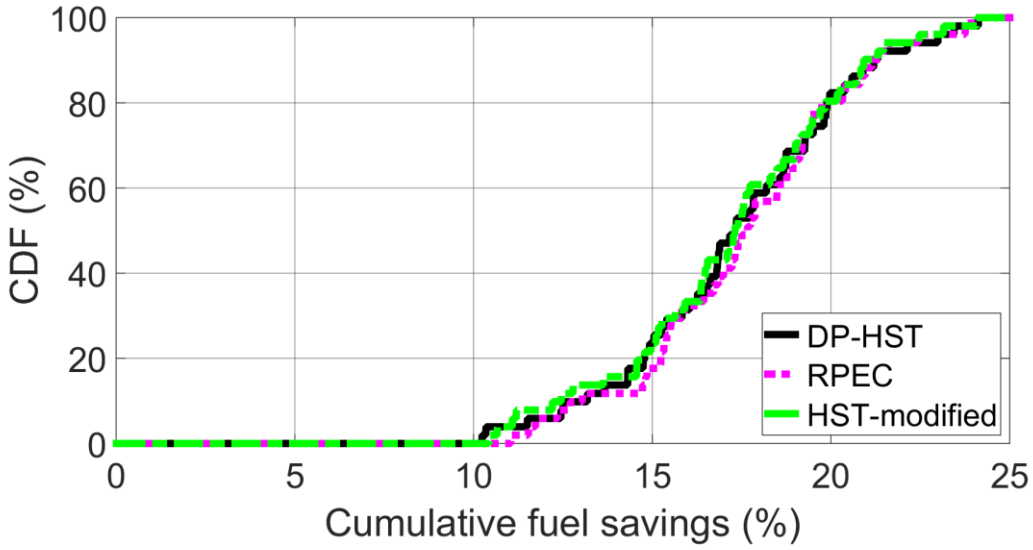

(a) The cumulative distribution function of cumulative fuel savings

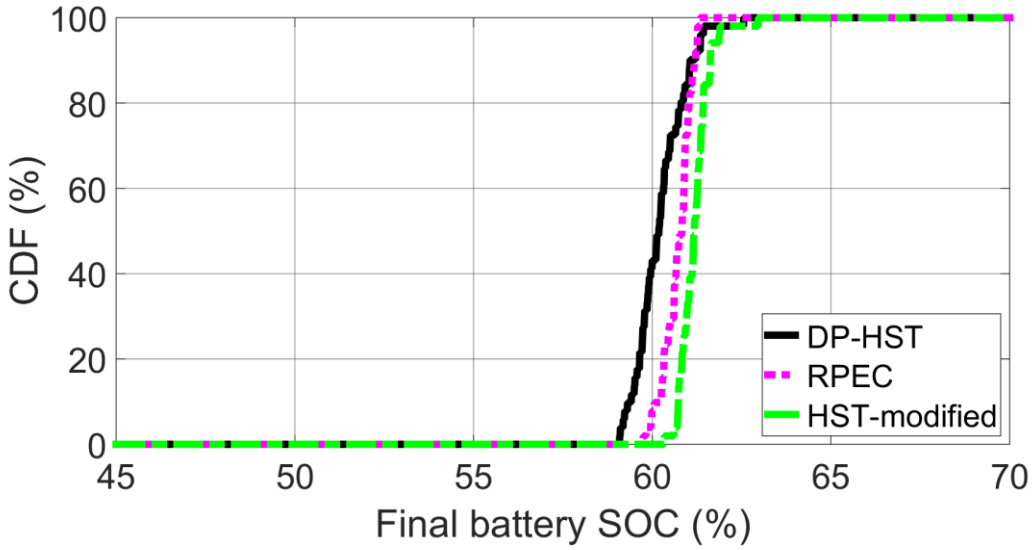

(b) The cumulative distribution function of final battery state of charge

Figure 7-2: Cumulative distribution function plots of cumulative fuel savings and final battery state of charge, over calm urban driving profiles

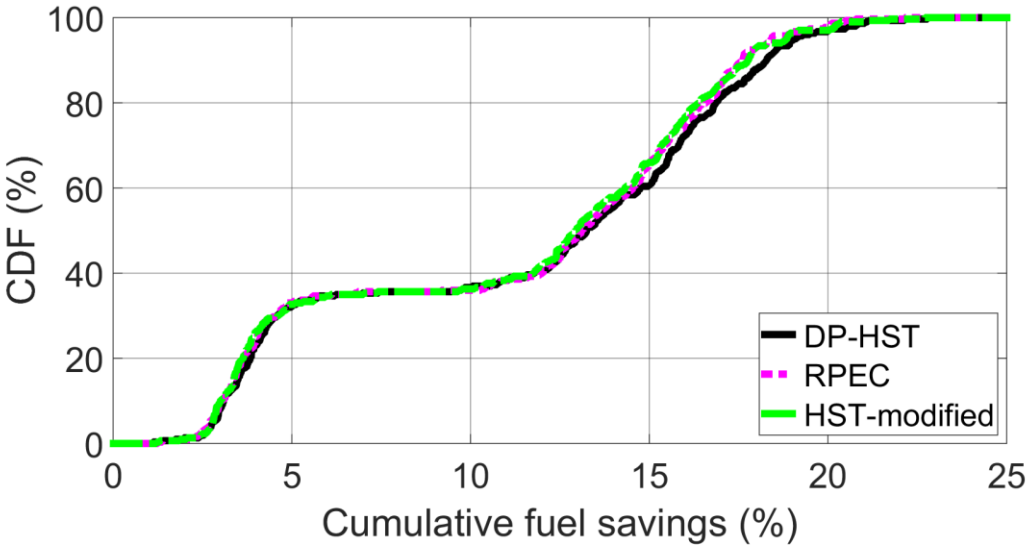

(a) The cumulative distribution function of cumulative fuel savings

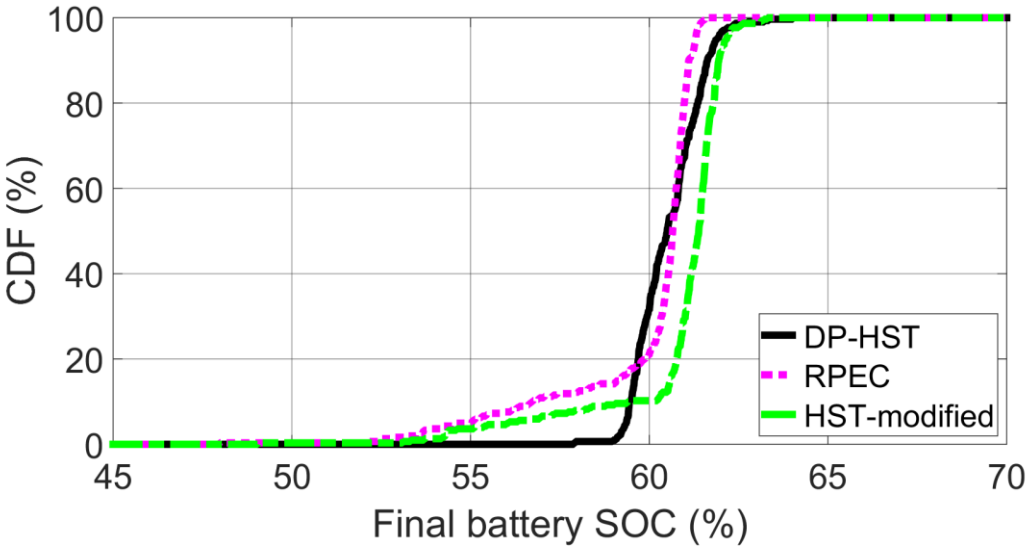

(b) The cumulative distribution function of final battery state of charge

Figure 7-3: Cumulative distribution function plots of cumulative fuel savings and final battery state of charge, over aggressive urban driving profiles

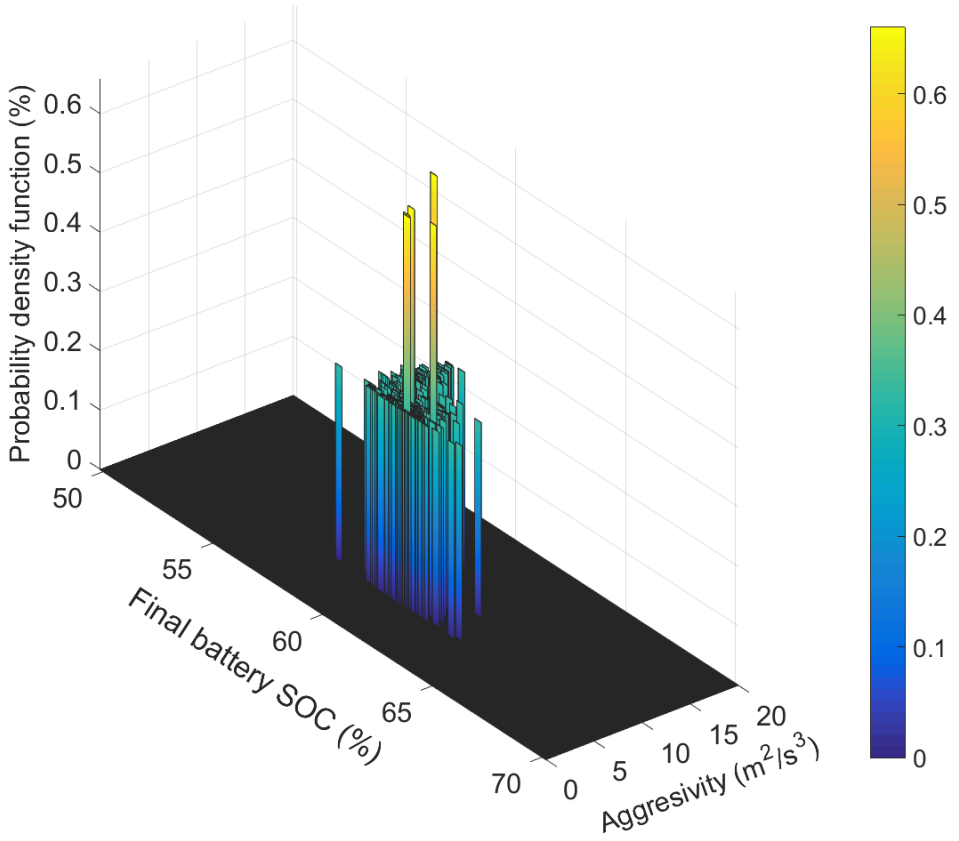

Figure 7-4: A probability density function of aggressivity and final battery state of charge for the DP-HST controller simulation, over aggressive urban driving profiles

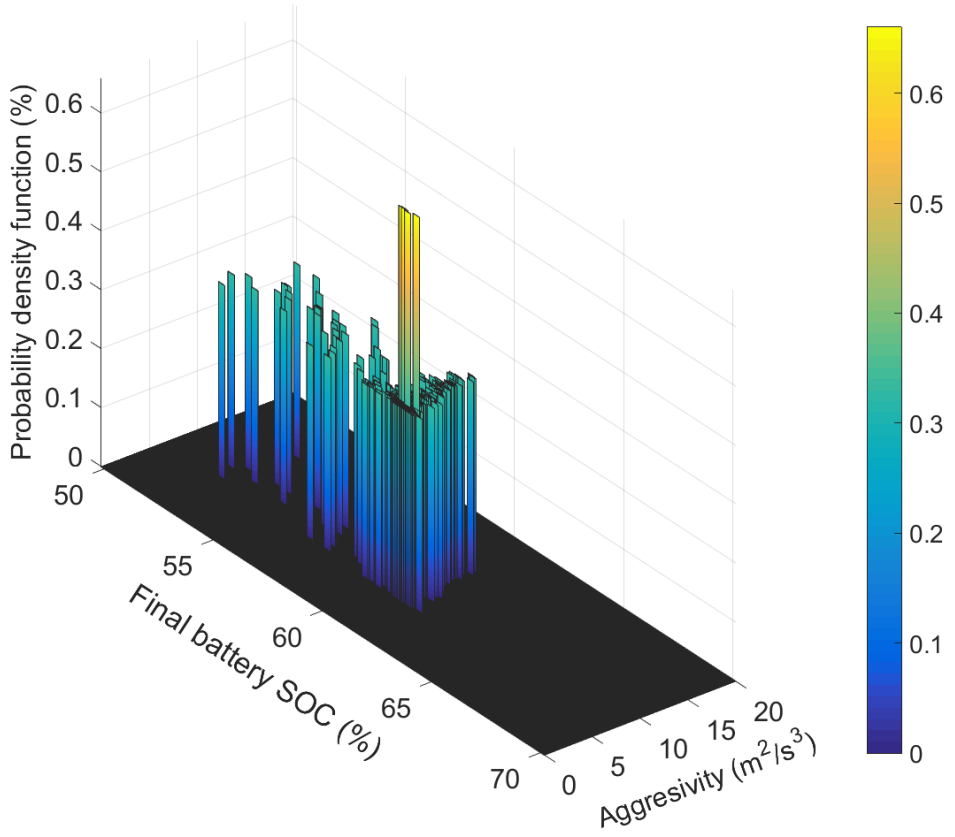

Figure 7-5: A probability density function of aggressivity and final battery state of charge for the RPEC strategy simulation, over aggressive urban driving profiles

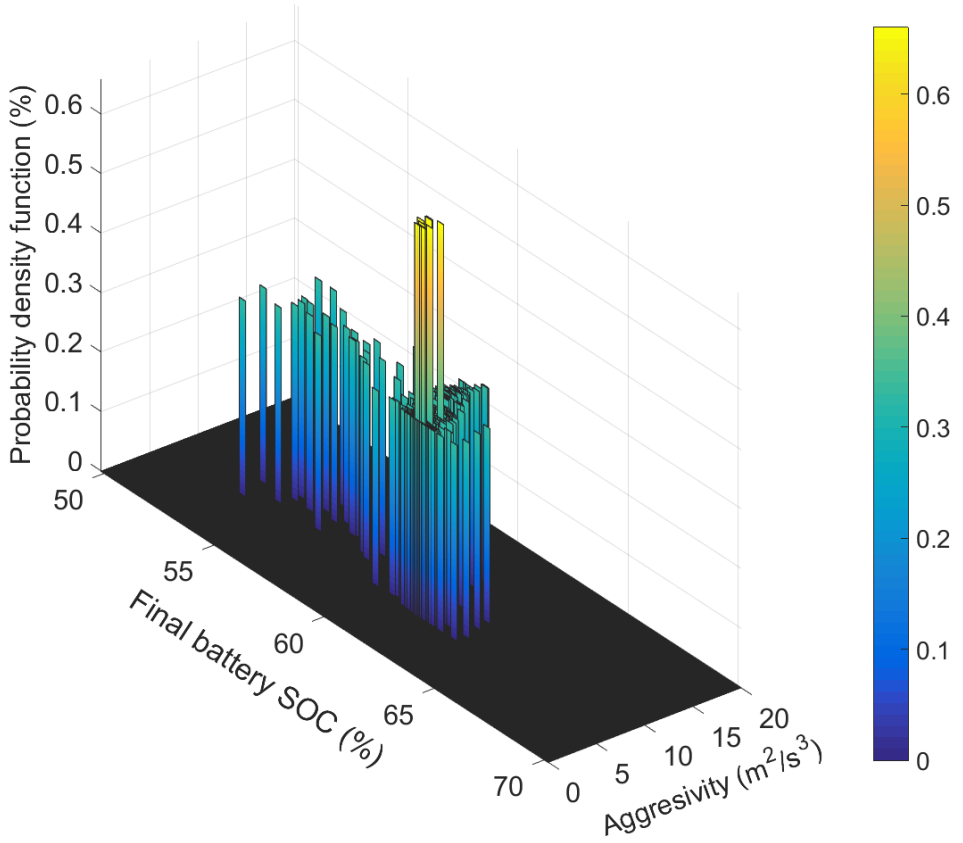

Figure 7-6: A probability density function of aggressivity and final battery state of charge for the HST-modified controller simulation, over aggressive urban driving profiles

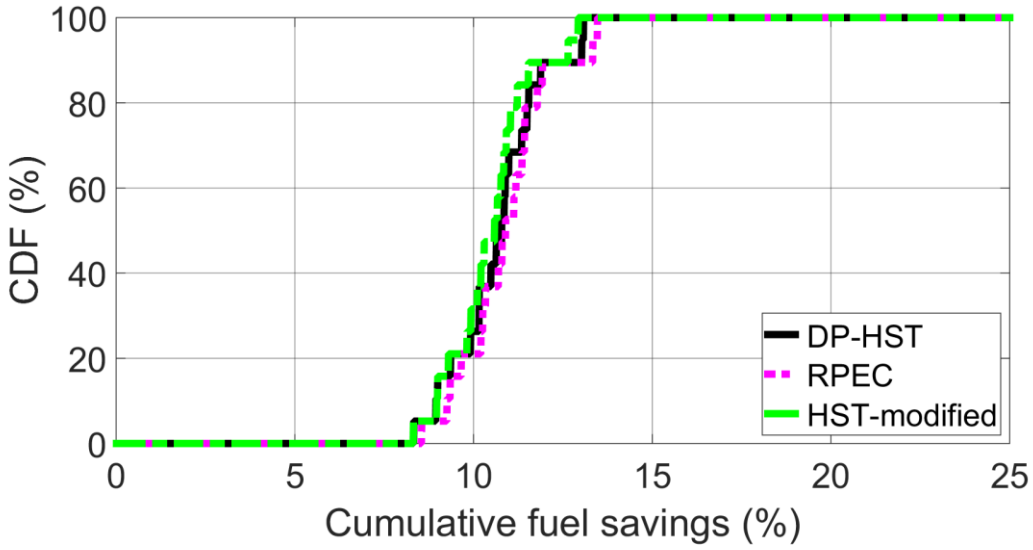

(a) The cumulative distribution function of cumulative fuel savings

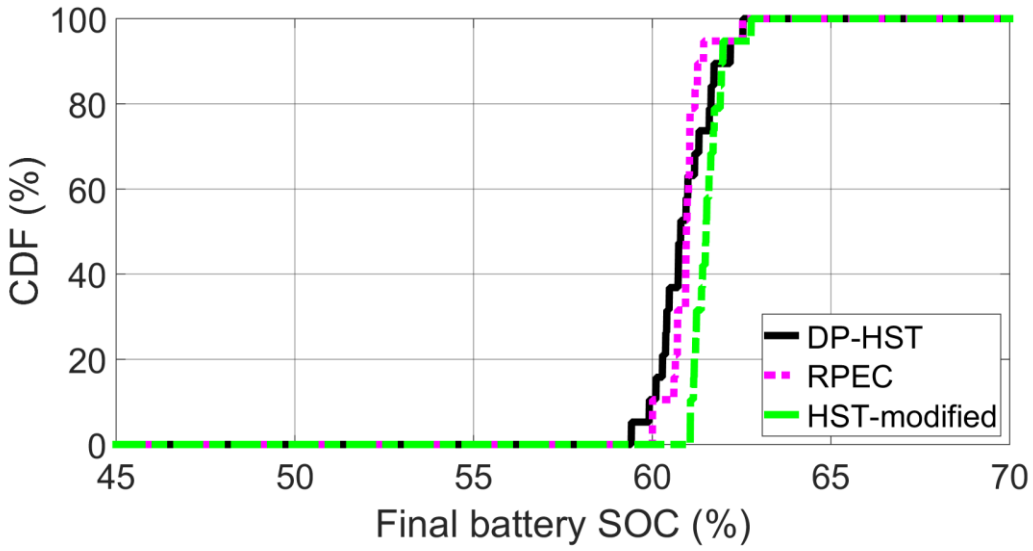

(b) The cumulative distribution function of final battery state of charge

Figure 7-7: Cumulative distribution function plots of cumulative fuel savings and final battery state of charge, over moderate highway driving profiles

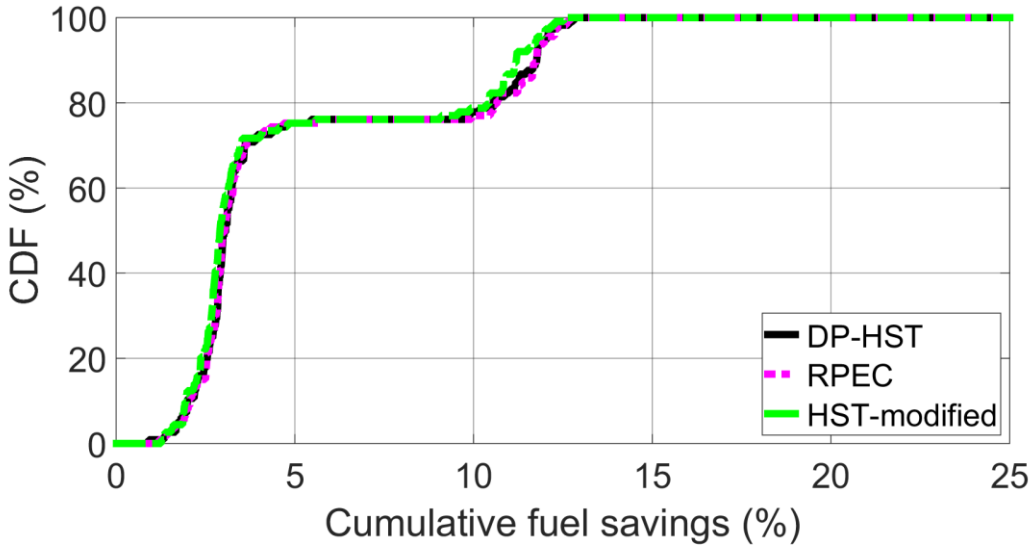

(a) The cumulative distribution function of cumulative fuel savings

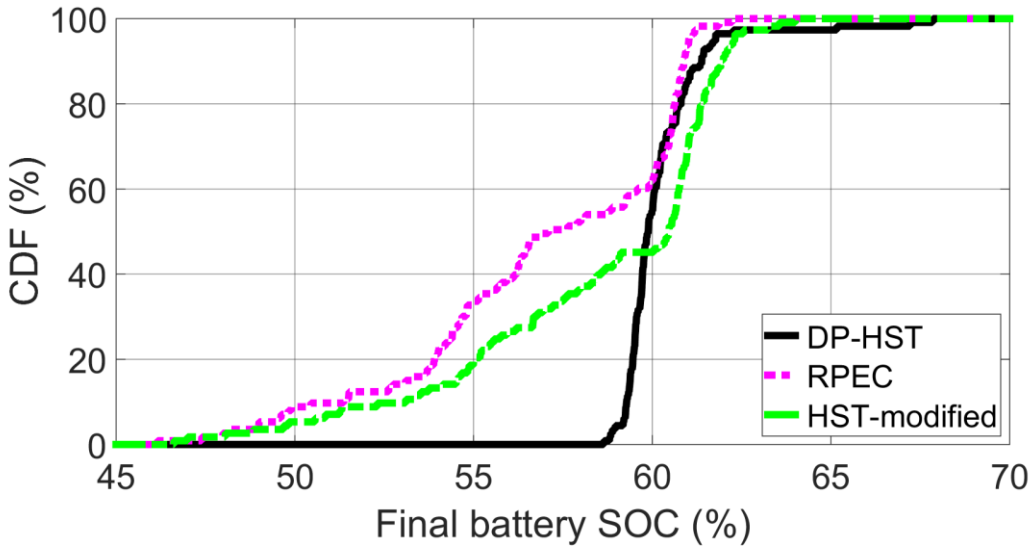

(b) The cumulative distribution function of final battery state of charge

Figure 7-8: Cumulative distribution function plots of cumulative fuel savings and final battery state of charge, over aggressive highway driving profiles

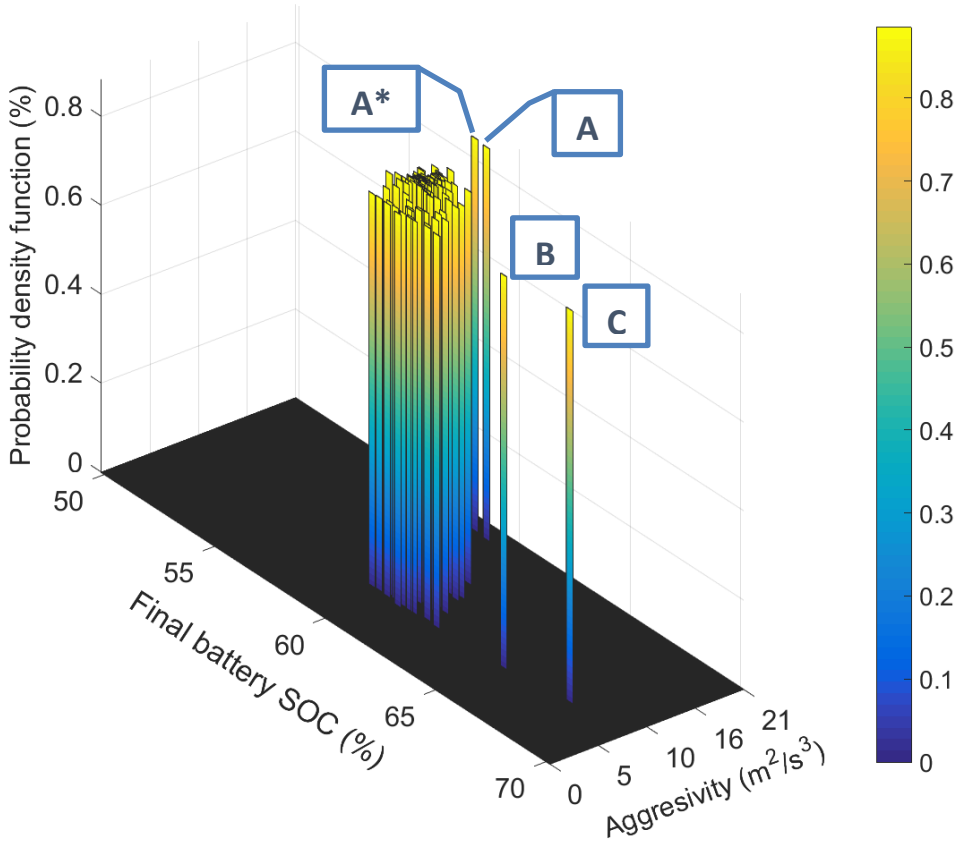

Figure 7-9: A probability density function of aggressivity and final battery state of charge for the DP-HST controller simulation, over aggressive highway driving profiles

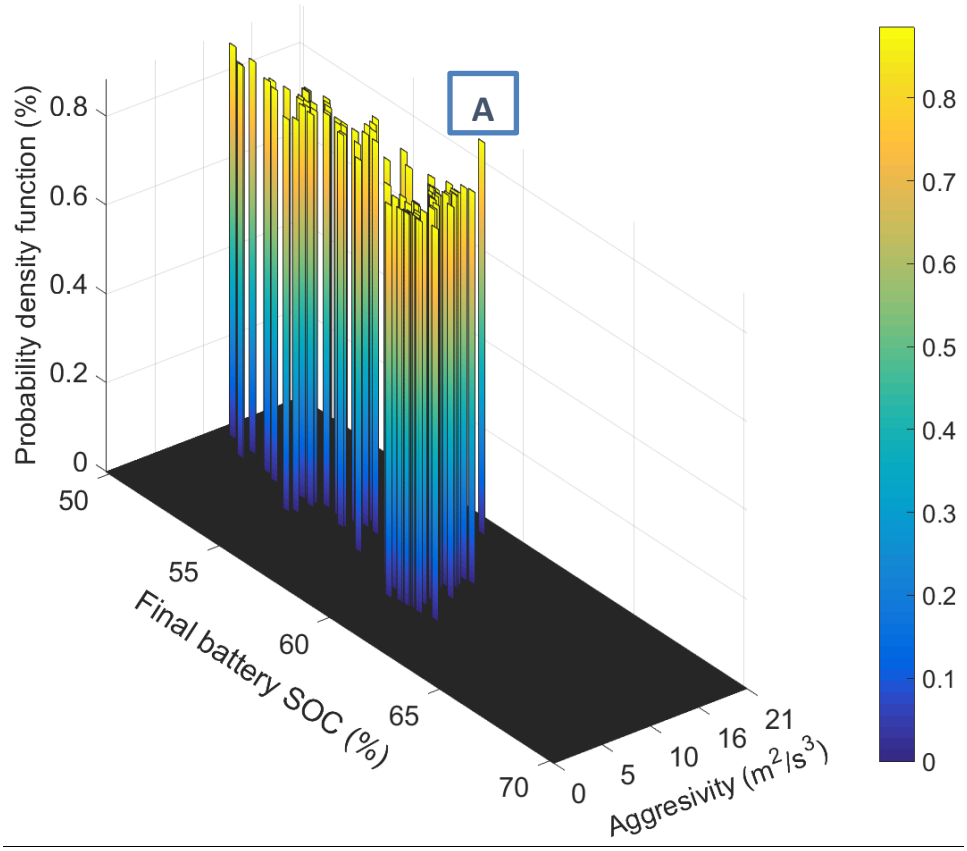

Figure 7-10: A probability density function of aggressivity and final battery state of charge for the RPEC strategy simulation, over aggressive highway driving profiles

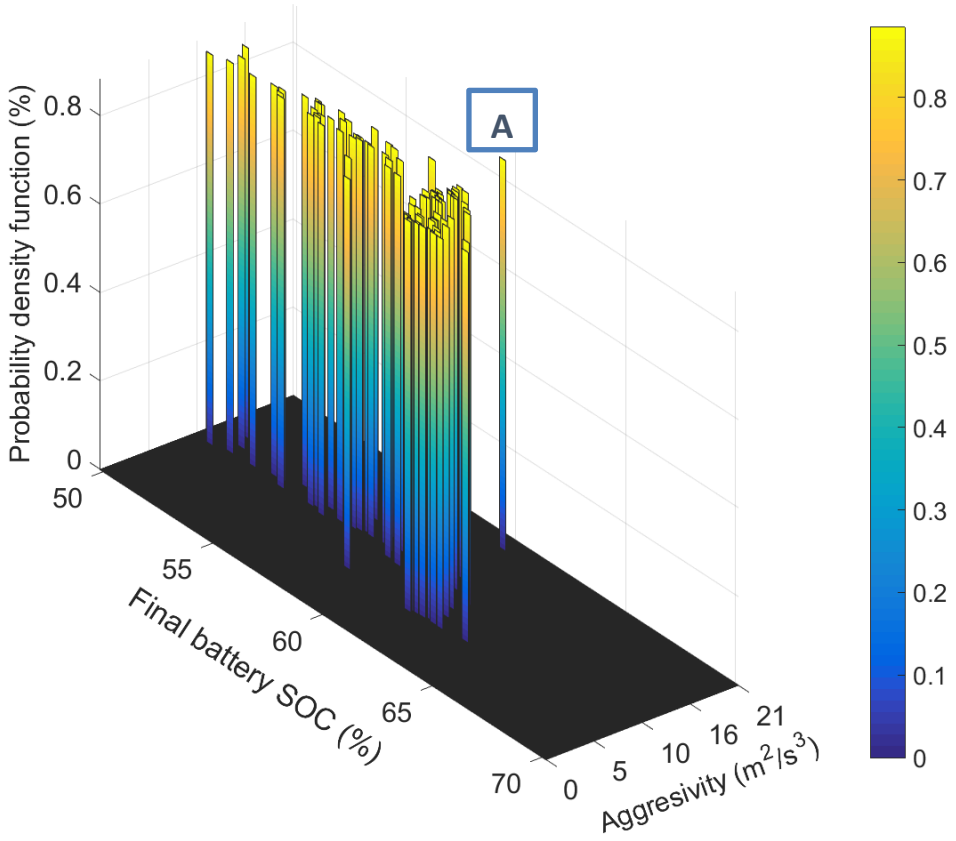

Figure 7-11: A probability density function of aggressivity and final battery state of charge for the HST-modified controller simulation, over aggressive highway driving profiles

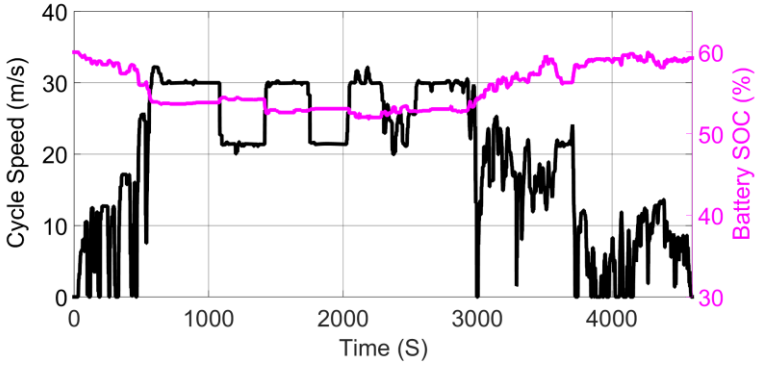

a. DP-HST controller

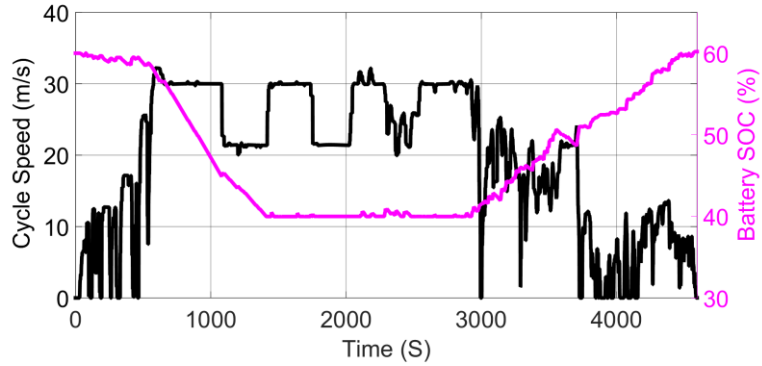

b. HST-modified

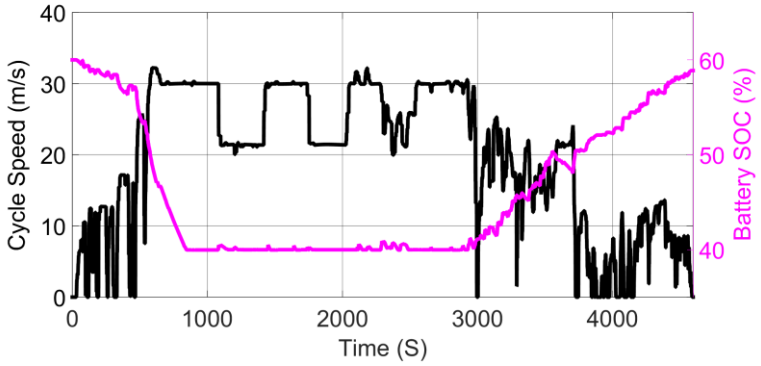

c. RPEC

Figure 7-12: Controller simulation results for the DP-HST, RPEC and HST-modified controllers over an aggressive highway driving profile (dubbed “A” in Figure 7-9 to Figure 7-11)

	Actual fuel savings (%)	Fuel savings assuming charge sustenance (%)	Final battery state of charge (%)
DP-HST controller	1.68	1.62	59.28
RPEC strategy	1.86	1.74	58.88
HST-modified controller	1.88	1.88	60.19

Table 7-5: A summary table detailing controller simulation results over an aggressive highway driving profile

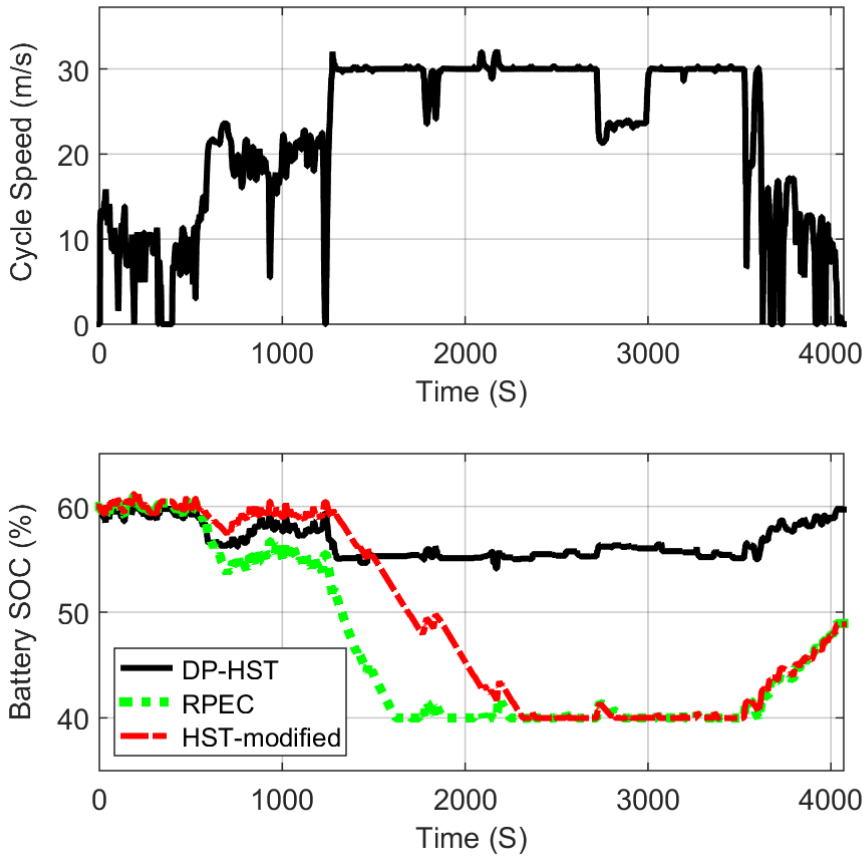

Figure 7-13: Comparative simulation results for the DP-HST, RPEC and HST-modified controllers over an aggressive real-world driving profile

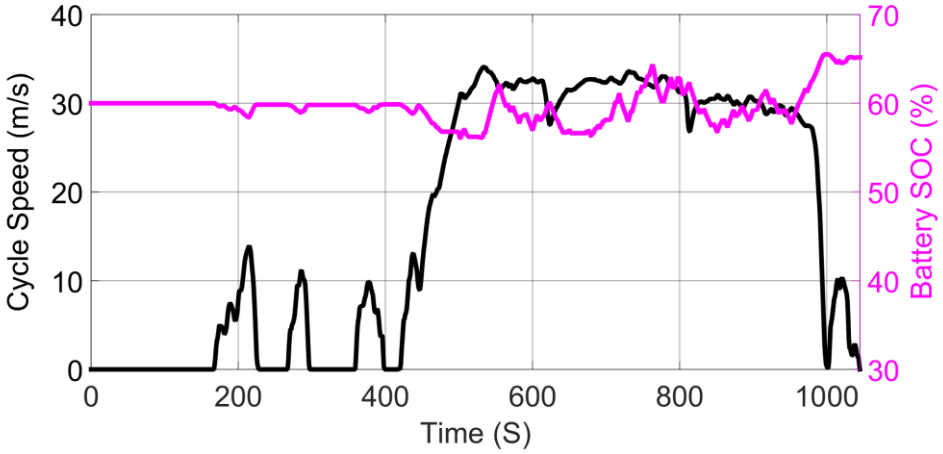

a. Highway driving profile (dubbed “B” in Figure 7-9 to Figure 7-11)

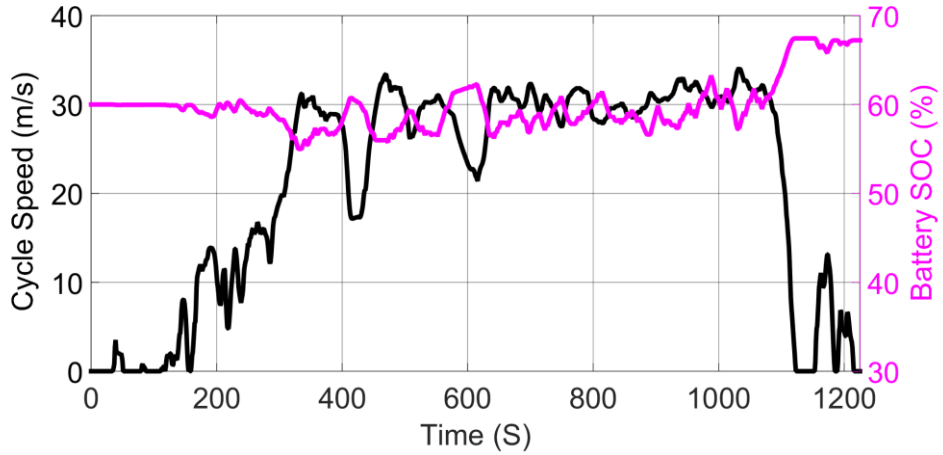

b. Highway driving profile (dubbed “C” in Figure 7-9 to Figure 7-11)

Figure 7-14: Controller simulation results for the DP-HST controller over an aggressive highway driving profile

In summary, the DP-HST controller performs consistently well over the nine categories of real-world driving profiles analysed. This performance is further highlighted in Table 7-6, which details the distribution of real-world driving profiles under different levels of charge sustenance for all 3 controllers. Results from this table show that, in comparison to the RPEC and HST-modified controllers, the DP-HST controller performed the best, by being near-perfectly charge-sustaining over 59 driving profiles and maintaining a near charge-sustaining performance over most of the 1197 driving profiles analysed. This assertion is further supported by Table 7-4, which partly investigates the best performing controllers for each of the defined driving categories, using average fuel savings assuming charge sustenance. From Table 7-4, it could be inferred that the DP-HST controller outperforms the other 2 controllers over 5 of the 9 categories analysed. As previously explained in Section 7.3.2, the comparative advantage of the DP-HST controller over the RPEC and HST-modified controllers lies in the implicit estimation of its fuel equivalence weighting factors, and ability to estimate and compensate for future energy variations, using real-time driving information.

	Charge-depleting	Near charge-sustaining	Near-perfectly charge-sustaining	Charge-hoarding
	$SOC_f < 55$	$55 < SOC_f < 59.95$ or $60.05 < SOC_f < 65$	$59.95 < SOC_f < 60.05$	$SOC_f > 65$
DP-HST	0	1134	59	4
RPEC	53	1128	16	0
HST-modified	32	1163	2	0

Table 7-6: A summary table detailing the distribution of real-world driving profiles under different levels of charge sustenance for the DP-HST, RPEC and HST-modified controllers

7.4 Chapter conclusions

This chapter examines the fuel savings potential of three causal controllers (HST-modified, DP-HST and RPEC) in real-world driving conditions, through the use of 1197 real-world driving profiles. Real-world driving profiles typically differ in length and aggressivity from standard driving cycles. Consequently, these simulation studies were necessary for ensuring that the causal controllers are ready for use on production vehicles.

In order to put into perspective the classifications and degree of aggressivity of the real-world driving profiles considered, the novel two-class grouping system proposed in Chapter 2 was applied. Using this classification method, the 1197 real-world driving profiles considered could be broken down into: 206 calm neighbourhood driving profiles, 131 moderate neighbourhood driving profiles, 8 aggressive neighbourhood driving profiles, 51 calm urban driving profiles, 365 moderate urban driving profiles, 303 aggressive urban driving profiles, 1 calm highway driving profile, 19 moderate highway driving profiles and 113 aggressive highway driving profiles.

Over calm neighbourhood driving profiles, the three causal controllers were found to perform near-optimally with a final battery state of charge ranging between 59.06% and 62.37%. A similar observation was made over moderate and aggressive neighbourhood driving profiles. These results generally indicate that all 3 controllers are well suited for neighbourhood driving and are able to offer near charge-sustaining performances.

Over calm and moderate urban driving profiles, all 3 controllers also performed near-optimally with the final battery state of charge ranging between 59.09% and

62.97%. A similar observation was made for calm and moderate highway driving profiles. Over aggressive urban and highway driving profiles however, the RPEC and HST-modified controllers were observed to be more charge-depleting. Conversely, the DP-HST controller performed consistently well over these profiles. The performance of explicitly tuned controllers (RPEC and HST-modified) are limited by the number and variety of driving profiles used for the estimation and tuning, as well as the estimation method applied. Consequently, explicitly-tuned controllers may not perform very well if simulated on a driving profile with very different characteristics from the driving profiles used during the estimation and tuning process. In summary, the comparative advantage of the DP-HST controller over the RPEC and HST-modified controllers lies in the implicit estimation of its fuel equivalence weighting factors, and ability to estimate and compensate for future energy variations, using real-time driving information. Although a culmination of the foregoing comparative advantage, as well as the results detailed in this treatise generally do suggest that implicitly-adapted controllers are superior in performance to explicitly-adapted controllers, this assertion and thus the results reported in this thesis remain to be validated in a more rigorous framework from an experimental standpoint.

8 CONCLUSIONS AND FURTHERWORK

8.1 Introduction

In this chapter, the main ideas and novelties proposed in the thesis are recapitulated. For improved clarity, the main ideas and findings are put into the context of the study objectives defined in Chapter 1, and existing research gaps. Recommendations for further research efforts are also provided subsequently.

8.2 Final conclusions

Objective 1 - Conducting a detailed review of existing literature

A detailed literature review was conducted to highlight the complexity of the HEV energy management problem, potential solutions, as well as existing exploitable research gaps which formed the main inspiration for the studies contained in this thesis. From the review, it was concluded that existing HEV control strategies were lacking primarily in the aspects of: optimisation of braking energy regeneration and charge-sustaining sub-optimal control using partial route preview information and no route preview information.

Rule-based control strategies, for example, were found to be sub-optimal by nature, and as such unable to guarantee the fulfilment of integral constraints, i.e. charge sustenance. They also require rigorous tuning to optimise the rules for specific driving scenarios. Dynamic programming, although known to yield global optimal solutions to HEV energy management problems, was found to produce non-causal results which are non-implementable in real time. Research studies

show that the equivalence factor of equivalent consumption minimisation strategies are highly sensitive and cycle dependent, i.e. the optimal equivalence factor for one driving cycle might lead to a poor performance on another driving cycle. It was also found that in most production vehicles today, model predictive controllers are formulated using heuristics, which decide when the battery should be charged or discharged accordingly. Consequently, the resulting controller contains no form of optimisation and is not defined to account for charge sustenance. Existing vehicle speed control models were found to be overly simplified, and in some cases unable to yield realisable fuel-optimal speed trajectories. For example, to date, the author could find no research study known to consider engine braking effects in the formulation of fuel-optimal vehicle speed trajectories. By ignoring these real-world effects, the resulting speed trajectory is only of academic interest.

Objective 2 - The development of a novel and simple grouping system useful for classifying standard driving cycles on the basis of aggressivity and road type

To emphasise the peculiarity of each selected driving cycle contained in this thesis, a novel two-class grouping system was proposed. In this grouping system, driving cycles are classed based on aggressivity (quantified as aggressivity factor (AGF)) and road type.

Objective 3 – Development and validation of a quasi-static vehicle model

In a control application where reduction in fuel consumption is the primary objective, it is important to develop vehicle models with a robust and accurate ability to predict fuel consumption even under rapid transients. Three typical

vehicle modelling approaches were reviewed. The review proved the quasi-static vehicle modelling approach to be a suitable modelling technique which yields a high level of accuracy for the evaluation of fuel consumption and NOx of a vehicle equipped with conventional powertrain. From this review it was concluded that, from a control development stand point, the quasi-static approach is preferred since it maintains the physical causality of the vehicle system, and allows for the possibility of using the same controller inputs/outputs in the simulator as well as on the real vehicle. On this basis, a quasi-static model was developed, validated and used for the studies detailed in this thesis. Validation results over the NEDC driving cycle showed that the simulated baseline cumulative fuel consumption profile of the vehicle compares very closely to that of the experimentally obtained profile (within a $\pm$ 3% error margin).

Objective 4 - Investigation of the impact of gear up-shift RPM on baseline fuel consumption

The impact of gear up-shift RPM on baseline fuel consumption was investigated in order to better understand how best to optimise fuel savings through gear shift control. This analysis, carried out over the NEDC, showed a decrease in cumulative fuel consumption, with decreasing up-shift engine RPM. From this analysis it was concluded that, whilst it is evident that a low upshift engine RPM will lead to lower fuel consumption, this advantage must be weighed against driveability constraints, such as meeting torque requirements and driver comfort. It was shown that compared to the NEDC standard shift strategy, a 2.5% fuel savings can be achieved using an early engine speed upshift.

Objective 5 - Investigation of the impact of braking patterns on kinetic energy recovery

Understanding the impact of driving manoeuvres on kinetic energy regeneration is a primary step towards the formulation of a real-time HEV control strategy which is able to optimise braking energy regeneration and fuel savings. Consequently, the impact of braking patterns on kinetic energy regeneration was quantitatively investigated. From this analysis, gentle braking patterns were found to promote kinetic energy regeneration by the electric motor. Vehicle deceleration less than $0.5m/s^2$ was also found to optimise braking energy regeneration.

Objective 6 - Development of a novel, simple and effective near-optimal heuristic control strategy with no access to route preview information

It was found through review that, rule-based control strategies are sub-optimal by nature, and as such unable to guarantee the fulfilment of integral constraints i.e. charge sustenance. They also require rigorous tuning to optimise the rules for specific driving scenarios. On this basis, the objective of formulating a near-optimal heuristic control strategy capable of performing with no access to route preview information became eminent. The proffered solution is a simple and effective heuristic strategy that optimises the ratio of fuel savings to battery SOC cost, thus ensuring the near-optimal use of battery energy at highly beneficial ICE operating points. Simulation results showed that the proposed controller (HST-modified) performed consistently well over all driving cycles analysed (battery state of charge ranges from 61.01% to 63.98%).

Objective 7 - Development of a dynamic programming-inspired real-time near-optimal control strategy with no access to route preview information

Through an in-depth review of existing literature, dynamic programming algorithm was found to produce non-causal results which are non-implementable in real time. Besides using the results from dynamic programming for benchmarking other controllers, a more useful application would be, to formulate a near-optimal controller for real-time application. A causal and novel control strategy was formulated using a "Markov chains" predictive model, which estimates future energy variations within a defined prediction horizon and then adjusts real-time control policies near-optimally, such that charge sustenance and optimisation of energy utilisation are achieved simultaneously. Simulation results showed that the proposed controller (DP-HST) performed consistently well over all driving cycles analysed (battery state of charge ranges from 60.21% to 63.54%). The fuel savings potential of the DP-HST controller was compared to that of the global optimal controller over standard driving cycles. Simulation results show that over all driving cycles analysed, the DP-HST controller maintains a near-optimal performance, which differs only slightly from the performance of the global optimal controller (maximum difference of 3.71% fuel savings, which occurs over the ARTEMIS U130 driving cycle). The significance of the DP-HST controller is further reinforced when considered in the context of its overall benefits, which include but are not limited to:

1. It proves useful as a "near-optimal" and "charge-sustaining" derivative of the global optimal dynamic programming controller.
2. It replaces the need for expensive telematics to estimate future vehicular energy variations.

3. Previously, the application of Markov chains to solve HEV energy management problems was only limited to the development of a stochastic dynamic programming controller, which is non-causal and commands a very high computational burden. A more practical and causal application of Markov chains to solving HEV energy management problems was proposed.

Objective 8 - Development of an ECMS-inspired real-time near-optimal control strategy with no access to route preview information

In comparison to the dynamic programming technique, online optimisation techniques have a more formalised rules extraction process involving the estimation and calibration of few control parameters, which represent fuel equivalence weighting factors. Although the ECMS is a promising online optimisation technique suitable for real-time application, it was shown that its equivalence factor of equivalent consumption minimisation strategies are highly sensitive and cycle dependent, i.e. the optimal equivalence factor for one driving cycle might lead to a poor performance on another driving cycle. This challenge was tackled through the use of an equivalence adaptation method which differs conceptually from existing SOC feedback adaptation strategies in that the proposed method simultaneously optimises and selects the adaptation factors (proportional controller gain and initial equivalence factor) as single parameters which can be applied in real time over any driving cycle. Unlike other existing SOC feedback methods, this approach solves a conflicting multi-objective optimisation control problem, thus ensuring that the obtained adaptation factors are optimised for robustness, charge sustenance and fuel reduction. Results from comparative studies showed that, in comparison to existing SOC feedback ECMS controllers, the

resulting controller (RPEC) was found to perform well, specifically in two key areas. The first being that the RPEC strategy appears robust and unaffected by the intuitive estimate of the initial equivalence factor, as in the case of the "SP (Static Prediction) controller" and the second being that the controller is highly efficient. Over the US06, LA92 and ARTEMIS U130 driving cycles, it was shown that the "AP (Adaptive Prediction) controller", in comparison to the RPEC strategy, depleted similar levels of battery energy but achieved less fuel savings.

Objective 9 - Development of an ECMS-inspired real-time near-optimal control strategy with access to partial route preview information

With wide availability of route preview information through the global positioning system (GPS), the geographic information system (GIS) and the intelligent transportation system (ITS), HEV energy management problems can be approached from a global perspective, with efficient utilisation of energy regeneration opportunities resulting from road grade. Through an in-depth review of existing literature, it was found that in most production vehicles today, the MPC framework is formulated using heuristics which decides when the battery should be charged or discharged accordingly. Consequently, the resulting controller contains no form of optimisation and is not defined to account for charge sustenance.

Up until the amalgamation of the studies contained in this thesis, no research study known to the author had been performed to develop a global route-optimal predictive control strategy for real-time application. Developing a predictive controller such as this is a non-trivial task, and involves the formulation of route preview information (predicted average route driving speed and altitude) into a

global optimal reference trajectory which can be implemented in an HEV control framework. Building on this research gap, an ECMS control strategy (RBEC), which uses a route optimised battery SOC trajectory to adapt the predictive controller towards achieving an optimal performance in real time, was proposed. Comparative simulation studies of the RBEC strategy and RPEC strategy showed that as much as 2.44% extra fuel savings could be achieved over a real-world driving route, through the incorporation of route preview information into a real-time HEV controller. The fuel savings potential of the RBEC strategy was also shown to be very close to that of the global optimal controller.

Objective 10 - Development of a dynamic programming-based route-optimal vehicle speed control strategy which accounts for real-time dynamic effects like engine braking, while solving an optimisation problem involving the maximisation of fuel savings with little or no penalty to trip time

The concept of vehicle speed control is relatively new and has only been investigated by a few researchers. With the research area only being in its early days, most of the proposed vehicle speed control models are overly simplified, and often yield non-realisable fuel-optimal speed trajectories. For example, the author was unable to find any study that considered engine braking effects in the formulation of fuel-optimal vehicle speed trajectories. In this study, an optimal vehicle speed control approach based on deterministic dynamic programming was proposed. Although idealistic in nature, the optimal vehicle speed control approach proved useful in the following ways: first as a measure of the ultimate fuel savings that could be realised along a route, through vehicle speed control, and then as an optimal benchmark for evaluating real-time vehicle speed control

strategies, and finally, as a paradigm for the extraction of fuel efficient driving patterns. Using real-time simulation analysis, the fuel savings potential of the OPT-speed approach was investigated first on a conventional vehicle and then on an HEV, over a driving route from Bath Spa to Corsham, in the UK. Results from these analyses showed that, compared to real-world driving profiles, fuel savings of up to 54.45% on conventional vehicles and 64.81% on HEVs can be realised through the use of an optimal vehicle speed control approach. A compromise involving a maximum time penalty of -12.69% (208s or 3.47 minutes) and fuel savings of 51.82% was observed for the conventional baseline vehicle. It was also observed that a higher percentage of fuel savings (as much as 49.53% extra fuel saving over a real-world driving route) could be achieved through improved driving behaviour than through the hybrid system. Although very hypothetical in nature (due to driveability concerns - very harsh accelerations, safety concerns and route traffic congestion), these results indicate the best fuel savings which can be realised through vehicle speed control.

Objective 11 - Development of a real-time vehicle speed control approach, which is based on smoothing the speed trajectory of the lead vehicle, consequently reducing the acceleration and deceleration events that the intelligent vehicle will undergo

To yield a causal vehicle speed control approach, the RTC-speed technique, which is based on averaging the speed trajectory of the vehicle immediately ahead, was proposed. The RTC-speed approach was simulated over 8 real-world driving profiles representing commutes from Bath Spa to Corsham in the UK. Results from these analyses showed an exponential decline in the achievable total driving

distance, beyond a preview window of 45s for most of the real-world driving profiles considered. As previously explained, at the beginning of the simulation, there is a lag in the vehicle speed information available to the intelligent vehicle. The size of this lag is equal in length to the size of the traffic preview window. As the preview window increases beyond 45s, the aforementioned lag results in an exponential decline in the total driving distance that can be covered by the intelligent vehicle based solely on modified speed information from the lead vehicle. This observation implies that in order not to violate positional constraints regarding the total driving distance that can be achieved using only modified speed information from the lead vehicle, the maximum preview window must not exceed 45s. It was also observed that significant improvements in fuel economy can be realised for relatively short traffic previews (less than 20s). A combination of the HEV technology with a real-time vehicle speed control technology was found to result in an additional reduction in fuel consumption (as much as 25.69% extra fuel savings over real-world driving profiles), although the resulting fuel savings were found to decrease with an increasing traffic preview window. By definition, the RTC-speed algorithm acts to increasingly smoothen the vehicle speed profile as traffic preview length increases. This smoothing effect leads to reduced deceleration events which impact the ability of the HEV to benefit from regenerative braking, thus resulting in reduced fuel savings for an increasing traffic preview window. In comparison to the HEV technology, which is more expensive, the real-time vehicle speed controller was found to yield as much as 45.96% fuel savings. This observation further highlights the importance of improved driving behaviour as a significant and cost-effective approach to improving vehicular fuel economy.

Objective 12 - Investigation of the fuel savings potential of the proposed controllers over real-world driving profiles

Considering that the controllers developed in this thesis are intended for production vehicles, they needed to be simulated over real-world driving profiles, which are typically very different in aggressivity and length, from standard driving cycles. This analysis was undertaken for three causal controllers (HST-modified, DP-HST and RPEC), over 1197 real-world driving profiles (representing real-world driving conditions), with a view to identifying the most robust, charge-sustaining and consistent causal controller suitable for implementation on production vehicles. In order to put into perspective the classifications and degree of aggressivity of the real-world driving profiles considered, the novel two-class grouping system proposed in this study was applied. Using this classification method, the 1197 real-world driving profiles considered were broken down into: 206 calm neighbourhood driving profiles, 131 moderate neighbourhood driving profiles, 8 aggressive neighbourhood driving profiles, 51 calm urban driving profiles, 365 moderate urban driving profiles, 303 aggressive urban driving profiles, 1 calm highway driving profile, 19 moderate highway driving profiles and 113 aggressive highway driving profiles.

Results from these simulation studies showed that the performances of all 3 controllers are similar and near-optimal over non-aggressive driving profiles, and aggressive neighbourhood driving profiles. Over aggressive urban and highway driving profiles however, the RPEC and HST-modified controllers were observed to be more charge-depleting. Conversely, the DP-HST controller performed consistently well over these profiles. The performance of explicitly tuned controllers (RPEC and HST-modified) are limited by the number and variety of

driving profiles used for the estimation and tuning, as well as the estimation method applied. Consequently, explicitly tuned controllers may not perform very well if simulated on a driving profile with very different characteristics from the driving profiles used during the estimation and tuning process. The comparative advantage of the DP-HST controller over the RPEC and HST-modified controllers lies in the implicit estimation of its fuel equivalence weighting factors, and ability to estimate and compensate for future energy variations, using real-time driving information.

8.3 Further research

There exist a few directions to further the research studies contained in this thesis. Examples of some exploitable research areas are analysed in this section.

8.3.1 Multi-objective HEV optimal control

The results presented in this thesis are based on fuel consumption as the sole optimisation objective. Optimising fuel consumption without accounting for emissions, vehicle performance and driveability means that more fuel consumption penalties are yet to be accounted for. Consequently, the fuel economy performance reported in this thesis will differ at least slightly from what can be obtained from the production vehicle.

This holds particularly true if reducing emissions is considered a minimisation objective, since fuel consumption and emissions minimisation are often conflicting objectives. Optimising fuel economy, emissions, vehicle performance and driveability simultaneously is an extremely challenging problem, recommended for further research work. This recommended further research work becomes even more interesting considering that the formulation of effective measures for explicitly representing driveability in an optimal control problem is an on-going task.

8.3.2 Integrated powertrain HEV control

To meet the Euro VI legislation (2013), diesel vehicles are equipped with a complex after treatment system involving a urea-based selective catalytic reduction (SCR) technology, exhaust gas recirculation (EGR) and a diesel particulate filter (DPF)

[236]. The performance of some of these after treatment systems relies on dynamic qualities such as the temperature of the catalyst.

The heat used in the catalyst is extracted from the exhaust; consequently, using the hybrid system temporarily to reduce engine load could result in a decrease in the after-treatment performance. Determining the optimal balance between these competing technologies involves solving an optimal integrated powertrain HEV control problem which is a non-trivial task that has never been solved before. Further research in this study area is recommended.

8.3.3 Vehicle platooning

In Chapter 6, two novel methods of achieving significant fuel savings through vehicle speed control were presented. Results from real-time simulation studies show that, in comparison to the HEV technology which is more expensive, as much as 45.96% fuel savings could be achieved through real-time vehicle speed control. Although not considered in this study, further fuel savings could be achieved through closer inter-vehicle spacing, as in platooning, which results in reduced coefficient of drag for the follower vehicles in the platoon. In a study by Barth [233], the improvements in fuel economy obtained solely through reduced drag coefficients in a platooning situation were estimated to be in the range of 5-15% over highway driving cycles. Further research work is recommended in this study area.

8.3.4 Adaptive vehicle speed control

The optimal vehicle speed trajectory derived in Chapter 6 could also be used as a reference input for a cruise control system. Theoretically, this trajectory could be

followed. However, in a real traffic situation it might not be possible to perfectly track the optimal vehicle speed reference. In that case, a controller capable of switching between optimal speed tracking and car following is required. The concept of integrating such adaptive cruise controllers into HEVs is relatively new, and still requires further work.

8.3.5 Driver behaviour modelling

Besides achieving an optimal power split between the power devices in an HEV, driver behaviour plays an important role in reducing vehicle fuel consumption (as shown in Chapter 6). Therefore, accurate modelling of human driver behaviour is an important step towards understanding and predicting its effect on vehicle fuel consumption and emissions. Research studies aimed at mathematically modelling the impact of driver behaviour on fuel consumption are in their early stages, and still require additional research effort. The resulting driver behaviour model is expected to ultimately lead to the development of optimal HEV controllers which, take into account driving patterns, in order to decide a suitable control action to be implemented on the controller in real time.

8.3.6 Experimental validation of the proposed causal controllers

In Chapter 7, the fuel savings potential of three causal HEV controllers (HST-modified, DP-HST and RPEC) were investigated over 1197 real-world driving profiles representing real-world driving conditions. Simulation results from this analysis showed that the performance of all 3 controllers were similar and near-optimal over non-aggressive driving profiles. Over aggressive urban and highway driving profiles however, the HST-modified and RPEC strategies yielded a

predominantly charge-depleting performance for highly aggressive driving profiles. Experimental testing of all 3 controllers is required for validation of the simulation results obtained for the non-aggressive driving profiles. The relevant aspects of this recommended research area requiring specific attention are: real-time controller implementation, integration with existing vehicle controllers and dealing with unreliable actuations. To ensure a more robust controller performance over aggressive urban and highway driving profiles, a driving pattern-inspired adaptation approach is recommended for estimation of the fuel equivalence weighting factors for the HST-modified and RPEC strategies.

REFERENCES

1 Mohr, S., Wang, J., Ellem, G., Ward, J., and Giurco, D.: 'Projection of World Fossil Fuels By Country', Fuel, 2015, vol. 141, pp. 120-135

2 Sorrell, S., Speirs, J., Bentley, R., Miller, R., and Thompson, E.: 'Shaping the Global Oil Peak: A Review of the Evidence On Field Sizes, Reserve Growth, Decline Rates And Depletion Rates', Energy Conversion and Management, 2012, 37, pp. 709–724

3 Sorrell, S., Speirs, J., Bentley, R., Brandt, A., and Miller, R.: 'Global Oil Depletion: A Review of the Evidence', Energy Policy, 2010, 38, pp. 5290–5295

4 Sorrell, S., Miller, R., Bentley, R., and Speirs, J.: 'Oil Futures: A Comparison of Global Supply Forecasts', Energy Policy, 2010, vol. 38, pp. 4990–5003

5 Owen, N., Inderwildi, O., and King, D.: 'The Status Of Conventional World Oil Reserves-Hype or Cause for Concern?', Energy Policy, 2010, 38, pp. 4743–4749

6 Yang, Z.: 'Improving the Conversions Between the Various Passenger Vehicle Fuel Economy/Co2 Emission Standards Around the World', The International Council On Clean Transportation, (http://www.theicct.org/blogs/staff/improving-conversions-between-passenger-vehicle-efficiency-standards), 03 December 2014

7 Plotkin, S.: 'Examining Fuel Economy And Carbon Standards For Light Vehicles', Energy Policy, 2009, vol. 37, (no. 10), pp. 3843-3853

8 Teratani, T., Kuramochi, K., Nakao, H., Tachibana, T., Yagi, K., and Abou, S.: 'Development of Toyota Mild Hybrid System (THS-M) with 42v Powernet', Electric Machines and Drives Conference, IEMDC'03. IEEE International, 2003, vol. 1, pp. 3-10

9 Assanis, D., Delagrammatikas, G., Fellini, R., Filipi, Z., Liedtke, J., Michelena, N., Papalambros, P., Reyes, D., Rosenbaum, D., Sales, A., and Sasena, M.: 'Optimization Approach To Hybrid Electric Propulsion System Design', Mechanics of Structures and Machines, 1999, vol. 27, (no. 4), pp. 393-421

10 Takaishi, T., Numata, A., Nakano, R., and Sakaguchi, K.: 'Approach to High Efficiency Diesel and Gas Engines', Mitsubishi Heavy Industries, Ltd. Technical Review, 2008, vol. 45, (no. 1)

11 Khan, M., and C. Kar, N.: 'Hybrid Electric Vehicles for Sustainable Transportation: A Canadian Perspective', World Electric Vehicle Journal, 2009, vol. 3

12 Duoba, M.: 'Engine Design, Sizing and Operation in Hybrid Electric Vehicles', Argonne National Laboratory, Presentation at University of Wisconsin – Madison, ERC 2011 Symposium, June 8, 2011

13 Cente for Advanced Automotive Technology: 'HEV Levels', (http://autocaat.org/Technologies/Hybrid_and_Battery_Electric_Vehicles/HEV_Levels/), 22 May 2016

14 Koichiro, M., Yamazaki, M., and Tokieda, J.: 'Development of New-Generation Hybrid System THS II - Drastic Improvement of Power, Performance and Fuel Economy', SAE Technical Paper 2004-01-0064, 2004, pp. 182-192

15 Chan, C.C.: 'The State of the Art of Electric and Hybrid Vehicles', in: Proceedings of the IEEE 90.2, 2002, pp. 247-275

16 Leduc, P., and Dubar, B.: 'Downsizing of Gasoline Engine: An Efficient Way to Reduce CO2 Emissions', Oil & Gas Science and Technology, 2003, vol. 58, (no. 1), pp. 115–127

17 Yeo, H., and Kim, H.: 'Hardware-In-The-Loop Simulation of Regenerative Braking for a Hybrid Electric Vehicle', in: Proceedings of the Institution of Mechanical Engineers, Part D: Journal of Automobile Engineering, 2002, vol. 216, (no. 11), pp. 855-864

18 Egbue, O., and Long, S.: 'Barriers to Widespread Adoption of Electric Vehicles: An Analysis of Consumer Attitudes and Perceptions', Energy Policy, 2012, vol. 48, pp. 717–729

19 Axsen, J., and Kurani, K.S.: 'Hybrid, Plug-In Hybrid, or Electric – What Do Car Buyers Want', Energy Policy, 2013, vol. 61, pp. 532–543

20 Bitsche, O., Gutmann, G., and 'Systems for Hybrid Cars', Journal of Power Sources, 2004, vol. 127, (no. 1-2), pp. 8-15

21 Mercier, C.: 'Advanced Powertrain Controls', Lecture at IFP School. PSA Peugeot Citroën, 2012

22 Kermani, S., Delprat, S., Guerra, T.M., and Trigui, R.: 'Predictive Control For HEV Energy Management: Experimental Results', in: Proceedings of the 5th IEEE Vehicle Power and Propulsion Conference (VPPC '09), Lille, France, September 2009, pp. 364–369

23 Perez, L., Bossio, G., Moitre, D., and Garcia, G.: 'Supervisory Control Of An HEV Using An Inventory Control Approach', Latin American Applied Research, 2006, vol. 36, (no. 2), pp. 93-100

24 Perez, L., and Pilotta, E.: 'Optimal Power Split in a Hybrid Electric Vehicle Using Diect Transcription of an Optimal Control Problem', Mathematics and Computers in Simulation, 2009, vol. 79, (no. 6), pp. 1959-1970

25 Johannesson, L., Asbogard, M., and Egardt, B.: 'Assessing The Potential of Predictive Control for Hybrid Vehicle Powertrains Using Stochastic Dynamic Programming', Intelligent Transportation Systems, 2005. Proceedings. 2005 IEEE, 13-15 September 2005, pp. 366-371

26 Gong, Q., Li, Y., and Peng, Z.-R.: 'Trip-Based Optimal Power Management of Plug-In Hybrid Electric Vehicles', IEEE Transactions on Vehicular Technology, November 2008, vol. 57, (no. 11), pp. 3393–3401

27 Chau, K.T., and Wong, Y.S.: 'Overview of Power Management in Hybrid Electric Vehicles', Energy Conversion and Management, October, 2002, vol. 43, (no. 15), pp. 1953-1968

28 Guzzella, L., and Sciarretta, A.: 'Vehicle Propulsion Systems: Introduction to Modelling and Optimization', Springer: 9783642094156, Berlin, 2007, 2nd Edition

29 Husain, I.: 'Electric and Hybrid Vehicles: Design Fundamentals', Florida: CRC Press, 2010, 2nd edition

30 Çağatay Bayindir, K., Gözüküçük, M., and Teke, A.: 'A Comprehensive Overview of Hybrid Electric Vehicle: Powertrain Configurations, Powertrain Control

Techniques and Electronic Control Units', Energy Conversion and Management, February 2011, 52, (no. 2), pp. 1305–1313

31 Liu, J., Peng, H., and Filipi, Z.: 'Modeling And Control Analysis Of Toyota Hybrid System', Advanced Intelligent Mechatronics. Proceedings, 2005 IEEE/ASME International Conference, 2005, pp. 134-139

32 Millo, F., Rolando, L., and Andreata, M.: 'Numerical Simulation for Vehicle Powertrain Development', in Book: Numerical Analysis - Theory and Application, 2011

33 Genta, G.: 'Motor Vehicle Dynamics: Modelling and Simulation', Series on Advances in Mathematics for Applied Sciences. World Scientific Pub Co. Inc. Singapore, 1997, vol. 43

34 Vassallo, A., Cipolla, G., and Mallamo, F.: 'Transient Correction of Diesel Engine Steady-State Emissions and Fuel Consumption Maps for Vehicle Performance Simulation', Aachener Kolloquim Fahrzeug und Motorentechnik, Aachen, Germany, 2007

35 Keribar, R., Ciesla, C., and Morel, T.: 'Engine/Powertrain/Vehicle Modeling Tool Applicable to all Stages of the Design Process', SAE Technical Paper 2000-01-0934, 2000

36 Morel, T., Keribar, R., and Leonard, A.: 'Virtual Engine/Powertrain/Vehicle Simulation Tool Solves Complex Interacting System Issues', SAE Technical Paper 2003-01-0372, 2003

37 Pettiti, M., Pilo, L., and Millo, F.: 'Developement of a New Mean Value Model for the Analysis of Turbolag Phenomena in Automotive Diesel Engines', SAE Technical paper; 2007-01-1301, 2007, pp. 14

38 Ehsani, M., Gao, Y., and Gay, S.E.: 'Modern Electric, Hybrid Electric, and Fuel Cell Vehicles Fundamentals, Theory, and Design', Taylor & Francis Group, 2005

39 Tate, E., and Boyd, S.: 'Finding Ultimate Limits of Performance for Hybrid Electric Vehicles', in: Proceedings of Society of Automotive Engineers 2000 Future Transportation Technology Conference, 2001, vol. No of paper 2000-01-3099

40 Kleimaier, A., and Schroeder, D.: 'Optimization Strategy for Design and Control of a Hybrid Vehicle', in: Proceedings of the 6th International Workshop on Advanced Motion Control, Nagoya,Japan, April 2000, pp. 459– 464

41 Pisu, P., Silani, E., Rizzoni, G., and Savaresi, S.M.: 'A LMI-based Supervisory Robust Control for Hybrid Vehicles', in: Proceedings of the American Control Conference, Denver, Colorado, USA, June 2003, pp. 4681–4686

42 Lewis, F., and Syrmos, V.: 'Optimal Control', Wiley-Interscience, 1995

43 Shen , C., and Chaoying, X.: 'Optimal Power Split in a Hybrid Electric Vehicle Using Improved Dynamic Programming', in: Proceedings of the Asia-Pacific Power and Energy Engineering Conference (APPEEC'10), Chengdu, China, March 2010, pp. 1–4

44 Brahma, A., Guezennec, Y., and Rizzoni, G.: 'Optimal Energy Management in Series Hybrid Electric Vehicles', in: Proceedings of the American Control Conference, October 2000, vol. 1, (no. 6), pp. 60 - 64

45 Back, M., Simons, M., Kirschaum, F., and Krebs, V.: 'Predictive Control of Drivetrains', in: Proceedings of IFAC 15th Triennial World Congress, Barcelona, Spain, 2002, vol. 35, (no. 1), pp. 241–246

46 Lin, C.C., Peng, H., Grizzle, J.W., and Kang, J.M.: 'Power Management Strategy for a Parallel Hybrid Electric Truck', IEEE Transactions on Control Systems Technology, 2003, vol. 11, (no. 6), pp. 839–849

47 Arsie, I., Graziosi, M., Pianese, C., Rizzo, G., and Sorrentino, M.: 'Optimization of Supervisory Control Strategy for Parallel Hybrid Vehicle With Provisional Load Estimate', in: Proceedings of the 7th International Symposium on Advanced Vehicle Control (AVEC), Arnhem, The Netherlands, August 2004, pp. 483-488

48 Lin, C.C., Kang, J.M., Grizzle, J.W., and Peng, H.: 'Energy Management Strategy for a Parallel Hybrid Electric Truck', in: Proceedings of the American Control Conference, Ann Arbor, Mich, USA, June 2001, pp. 2878–2883

49 O'Keefe, M.P., and Markel, T.: 'Dynamic Programming Applied to Investigate Energy Management Strategies for a Plug-In HEV1', in: Proceedings of the 22nd International Battery, Hybrid and Fuel Cell Electric Vehicle Symposium and Exposition (EVS '06), National Renewable Energy Laboratory, Golden, CO, October 2006, (Report No. NREL/CP- 540-40376), pp. 1035–1046

50 Zhou, Z., Mi, C., Chen, Z., Masrur, A., and Murphey, Y.L.: 'Power Management of Passive Multi-Source Hybrid Electric Vehicle', in: Proceedings of the IEEE Vehicle Power and Propulsion Conference (VPPC'11), Chicago, Ill, USA, September 2011, pp. 1–4

51 Van Keulen, T., DeJager, B., and Steinbuch, M.: 'An Adaptive Suboptimal Energy Management Strategy for Hybrid Drive-Trains', in: Proceedings of the 17th International Federation of Automatic Control World Congress (IFAC'08), July 2008, vol. 17, pp. 102–107

52 Tulpule, P., Stocker, S., Marano, V., and Rizzoni, G.: 'Optimality Assessment of Equivalent Consumption Minimization Strategy for PHEV Applications', in: Proceedings of the ASME Dynamic Systems and Control Conference, Hollywood, California, USA, October 2009, (Paper No. DSCC2009-2748), pp. 265–272

53 Tulpule, p., Marano, V., and Rizzoni, G.: 'Energy management for plug-in hybrid electric vehicles using equivalent consumption minimisation strategy', International Journal of Electric and Hybrid Vehicles, 2010, vol. 2, (no. 4), pp. 329–350

54 Shams-Zahraei, M., Kouzani, A.Z., Kutter, S., and Baker, B.: 'Integrated Thermal and Energy Management of Plug-in Hybrid Electric Vehicles', Journal of Power Sources, 2012, vol. 216, pp. 237-248

55 Ravey, A., Roche, R., Blunier, B., and Miraoui, A.: 'Combined optimal sizing and energy management of hybrid electric vehicles', in: Proceedings of the IEEE Transportation Electrification Conference and Exposition (ITEC'12), Dearborn, Mich, USA, June 2012, pp. 1–6

56 P´erez, L.V., Bossio, G.R., Moitre, D., and Garcia, G.O.: 'Optimization of Power Management in an Hybrid Electric Vehicle Using Dynamic Programming', Mathematics and Computers in Simulation, 2006, vol. 73, (no. 1–4), pp. 244–254

57 Oprean, M., Ionescu, V., Mocanu, N., Beloiu, S., and Stanciu, C.: 'Dynamic Programming Applied to Hybrid Vehicle Control', in: Proceedings of the International Conference on Electric Drives (ICED'88), 1988, vol. 4, pp. D2/10/11–D12/10/20

58 Ngo, D.V., Hofman, T., Steinbuch, M., and Serrarens, A.F.A.: 'An Optimal Control-Based Algorithm for Hybrid Electric Vehicle Using Preview Route Information', in: Proceedings of the American Control Conference (ACC '10), Baltimore, Md, USA, July 2010, pp. 5818–5823

59 Miaohua, H., and Houyu, Y.: 'Optimal Design of Control Strategy for Series Hybrid Electric Bus', Journal of Yuhan University of Technology, 2004, vol. 4

60 Li , Y., and Kar, N.C.: 'Advanced Design Approach of Power Split Device of Plug-In Hybrid Electric Vehicles Using Dynamic Programming', in: Proceedings of the 7th IEEE Vehicle Power and Propulsion Conference (VPPC '11), Chicago, Ill, USA, September 2011, pp. 1–6

61 Kum, D., Peng, H., and Bucknor, N.K.: 'Optimal Catalyst Temperature Management of Plug-In Hybrid Electric Vehicles', in: Proceedings of the American Control Conference (ACC '11), San Francisco, California, USA, June-July 2011, pp. 2732-2738

62 Koot, M., Kessels, A., Jager, B., Heemels, W., Bosch, P., and Steinbuch, M.: 'Energy Management Strategies for Vehicular Electric Power Systems', IEEE Transactions on Vehicular Technology, 2005, vol. 54, (no. 3), pp. 771–782

63 Jang, J.S.R., Sun, C.T., and Mizutani, E.: 'Neuro-Fuzzy and Soft Computing: A Computational Approach to Learning and Machine Intelligence', Prentice Hall, New York, NY, USA, 1997

64 Gong, Q., Li, Y., and Peng, Z.R.: 'Computationally Efficient Optimal Power Management For Plug-In Hybrid Electric Vehicles Based on Spatial-Domain Two-Scale Dynamic Programming', in: Proceedings of the IEEE International Conference on Vehicular Electronics and Safety (ICVES '08), Milwaukee, 22-24 September 2008, pp. 90–95

65 Lin, C.C., Peng, H., and Grizzle, J.W.: 'A Stochastic Control Strategy for Hybrid Electric Vehicles', in: Proceedings of the American Control Conference (AAC'04), Boston, Mass, USA, June-July 2004, pp. 4710–4715

66 Moura, J.S., Fathy, H.K., Callaway, D.S., and Stein, J.L.: 'A Stochastic Optimal Control Approach for Power Management in Plug-In Hybrid Electric Vehicles', IEEE Transactions on Control SystemsTechnology, 2011, vol. 19, (no. 3), pp. 545–555

67 Opila, D.F., Wang, X., McGee, R., and Grizzle, J.W.: 'Real-time Implementation and Hardware Testing Of A Hybrid Vehicle Energy Management Controller Based on Stochastic Dynamic Programming', Journal of Dynamic Systems, Measurement and Control, Transactions of the ASME, 2013, vol. 135, (no. 2), pp. 11

68 Liu, J., Hagena, J., Peng, H., and Filipi, Z.S.: 'Engine-In-The-Loop Study of the Stochastic Dynamic Programming Optimal Control Design for a Hybrid Electric HMMW', International Journal of Heavy Vehicle Systems, 2008, vol. 15, (no. 2–4), pp. 309–326

69 D, T.E., Grizzle, J.W., and Peng, H.: 'Shortest Path Stochastic Control for Hybrid Electric Vehicles', International Journalof Robust and Nonlinear Control, 2008, vol. 18, (no. 14), pp. 1409–1429

70 Tate, E.D., Grizzle, J.W., and Peng, H.: 'SP-SDP for Fuel Consumption and Tailpipe Emissions Minimization in an EVT Hybrid', IEEE Transactions on Control Systems Technology, 2010, vol. 18, (no. 3), pp. 673–687

71 Opila, D.F., Wang, X., McGee, R., Gillespie, R.B., Cook, J.A., and Grizzle, J.W.: 'An Energy Management Controller to Optimally Trade Off Fuel Economy and Drivability for Hybrid Vehicles', IEEE Transactions on Control Systems Technology, 2012, vol. 20, (no. 6), pp. 1490-1505

72 Wang, Y., and Sun, Z.: 'SDP-Based Extremum Seeking Energy Management Strategy for a Power-Split Hybrid Electric Vehicle', in: Proceedings of the American Control Conference (ACC'12), Fairmont Queen Elizabeth, Montr´eal, Canada, June 2012, pp. 553–558

73 Wenzhong , G., and Porandla, S.K.: 'Design Optimization of a Parallel Hybrid Electric Power Train', in: Proceedings of the IEEE Vehicle Power and Propulsion Conference (VPPC'05), Chicago, Ill, USA, 7-9 September 2005, pp. 530– 535

74 Montazeri-Gh, M., and Poursamad, A.: 'Optimization of Component Sizes in Parallel Hybrid Electric Vehicles via Genetic Algorithm', in: Proceedings of the ASME International Mechanical Engineering Congress and Exposition, Orlando, Fla, USA, November 2005, (Paper No. IMECE200582338), pp. 225–232

75 Song, P.G., Guan, E.Y., Zhao, L., and Liu, S.P.: 'Hybrid Electric Vehicles With Multi Level Cascaded Converter Using Genetic Algorithm', in: Proceedings of the

1st IEEE Conference on Industrial Electronics and Applications (ICIEA ’06), Singapore, 24-26 May 2006, pp. 1–6

76 Montazeri-Gh, M., and Poursamad, A.: ‘Application of Genetic Algorithm For Simultaneous Optimization of HEV Component Sizing And Control Strategy’, International Journal Alternative Propulsion, 2006, vol. 1, (no. 1), pp. 63–78

77 Liu, X., Wu, Y., and Duan, J.: ‘Optimal Sizing of a Series Hybrid Electric Vehicle Using A Hybrid Genetic Algorithm’, in: Proceedings of the IEEE International Conferenceon Automation and Logistics (ICAL’07), Jinan, Chin, 18-21 August 2007, pp. 1125–1129

78 Zhang, B., Chen, Z., Mi, C., and Murphey, Y.L.: ‘Multi-Objective Parameter Optimization of a Series Hybrid Electric Vehicle Using Evolutionary Algorithms’, in: Proceedings of the IEEE Vehicle Powerand Propulsion Conference, Dearborn, Mich, USA, 7-10 September 2009, pp. 921–925

79 Huang, B., Shi, X., and Xu, Y.: ‘Parameter Optimization of Power Control Strategy for Series Hybrid Electric Vehicle’, in: Proceedings of the IEEE Congress on Evolutionary Computation (CEC ’06), Vancouver, Canada, July 2006, pp. 1989–1994

80 Huang, B., Wang, Z., and Xu, Y.: ‘Multi-Objective Genetic Algorithm for Hybrid Electric Vehicle Parameter Optimization’, in: Proceedings of the IEEE/RSJ International Conference on Intelligent Robots and Systems (IROS ’06), October 2006, pp. 5177–5182

81 Fang, L.C., and Qin, S.Y.: ‘Concurrent Optimization For Parameters of Power Train and Control System of Hybrid Electric Vehicle Based on Multi-Objective

Genetic Algorithms', in: Proceedings of the SICE-ICASE International Joint Conference, Busan, Republic of Korea, October 2006, pp. 2424–2429

82 Piccolo, A., Ippolito, L., Galdi, V.Z., and Vaccaro, A.: 'Optimisation of Energy Flow Management in Hybrid Electric Vehicles via Genetic Algorithms', in: Proceedings of the IEEE/ASME International Conference on Advanced Intelligent Mechatronics, Como, Italy, July 2001, vol. 1, pp. 434–439

83 Ippolito, L., Loia, V., and Siano, P.: 'Extended Fuzzy C-Means and Genetic Algorithms to Optimize Power Flow Management in Hybrid Electric Vehicles', in: Proceedings of the IEEE Conference on Control Applications, Istanbul, Turkey, June 2003, vol. 1, pp. 115–119

84 Wang, A., and Yang, W.: 'Design of Energy Management Strategy in Hybrid Vehicles By Evolutionary Fuzzy System Part I: Fuzzy Logic Controller Development', in: Proceedings of the 6th World Congress on Intelligent Control and Automation (WCICA '06), Dalian, China, June 2006, vol. 2, pp. 8324-8328

85 Poursamad, A., and Montazeri, M.: 'Design of Genetic-Fuzzy Control Strategy For Parallel Hybrid Electric Vehicles', Control Engineering Practice, 2008, vol. 16, (no. 7), pp. 861-873

86 Yi, T., Xin, Z., and Liang, Z.: 'Fuzzy-Genetic Control Strategy of Hybrid Electric Vehicle', in: Proceedings of the 2nd International Conference on Intelligent Computing Technology and Automation (ICICTA '09), Zhangjiajie, China, October 2009, pp. 720–723

87 Desai, C., and Williamson, S.S.: 'Optimal Design of a Parallel Hybrid Electric Vehicle Using Multi-Objective Genetic Algorithms', in: Proceedings of the 5th IEEE

Vehicle Power and Propulsion Conference (VPPC ’09), Dearborn, Mich, USA, September 2009, pp. 871–876

88 Hu, X., Wang, Z., Liao, L., and Xiao, Z.: ‘Application of Multi Objective Evolutionary Algorithm In Hybrid Electric Vehicle Design and Control’, Journal of Wuhan University of Technology, 2004, vol. 28, (no. 3), pp. 384–387

89 Montazeri-Gh, M., Ahmadi, A., and Asadi, A.: ‘Driving Condition Recognition for Genetic-Fuzzy HEV Control’, in: Proceedings of the 3rd International Workshop on Genetic and Evolving Fuzzy Systems, Witten-Bommerholz, Germany, March 2008, pp. 65–70

90 Eberhart, R.C., and Kennedy, J.: ‘A New Optimizer Using Particle Swarm Theory’, in: Proceedings of the 6th International Symposium on MicroMachine and Human Science, Nagoya, Japan, October 1995, pp. 39–43

91 Shi , Y., and Eberhart, R.C.: ‘Parameter Selection in Particle Swarm Optimization’, in: Proceedings of the 7th Annual Conference on Evolutionary Programming, San Diego, California, USA, March 1998, pp. 591–600

92 Huang, M.: ‘Optimal Multilevel Hierarchical Control Strategy for Parallel Hybrid Electric Vehicle’, in: Proceedings of the IEEE Vehicle Power and Propulsion Conference (VPPC’06), Windsor, UK, 6-8 September 2006, pp. 1-4

93 Junhong, L.X.Z.: ‘Optimal Energy Management Strategy for a Plug-In Hybrid Electric Vehicle Based On Particle Swarm Arithmetic’, Journal Shanghai Auto, 2011, vol. 5, pp. 3

94 Huang, M., and Yu, H.: 'Optimal Control Strategy Based On PSO For Powertrain of Parallel Hybrid Electric Vehicle', in: Proceedings of the IEEE International Conference on Vehicular Electronics and Safety (ICVES'06), Beijing, China, 13-15 December 2006, pp. 352–355

95 Wang, Z., Huang, B., Li, W., and Xu, Y.: 'Particle Swarm Optimization for Operational Parameters of Series Hybrid Electric Vehicle', in: Proceedings of the IEEE International Conference on Robotics and Biomimetics (ROBIO '06), Kunming, China, 17-20 December 2006, pp. 682–688

96 Wu, J., Zhang, C.H., and Cui, N.X.: 'Fuzzy Energy Management Strategy of Parallel Hybrid Electric Vehicle Based on Particle Swarm Optimization', Control and Decision, 2008, vol. 23, (no. 1), pp. 46–50

97 Al-Aawar, N., Hijazi, T.M., and Arkadan, A.A.: 'EM-TFL Identification for Particle Swarm Optimization Of HEV Power Train', in: Proceedings of the IEEE International Electric Machines and Drives Conference (IEMDC'09), Miami, Fla, USA, 3-6 May 2009, pp. 109–112

98 Wu, L., Wang, Y., Yuan, X., and Chen, Z.: 'Multiobjective Optimization of HEV Fuel Economy and Emissions Using the Self-Adaptive Differential Evolution Algorithm', IEEE Transactions on Vehicular Technology, 2011, vol. 60, (no. 6), pp. 2458-2470

99 Al-Aawar, N., Hijazi, T.M., and Arkadan, A.A.: 'Particle Swarm Optimization of Coupled Electromechanical Systems', IEEE Transactions on Magnetics, 2011, vol. 47, (no. 5), pp. 1314–1317

100 Desai, C., and Williamson, S.S.: ‘Particle Swarm Optimization for Efficient Selection of Hybrid Electric Vehicle Design Parameters’, in: Proceedings of the 2nd IEEE Energy Conversion Congress and Exposition (ECCE ’10), Atlanta, Ga, USA, September 2010, pp. 1623–1628

101 Varesi, K., and Radan, A.: ‘A Novel PSO Based Technique For Optimizing The DOH In Hybrid Electric Vehicles to Improve Both the Fuel Economy and Vehicle Performance and Reduce the Emissions’, in: Proceedings of the 2nd Power Electronics, Drive Systems and Technologies Conference (PEDSTC ’11), Tehran, Iran, February 2011, pp. 342–349

102 Boyali, A., Demirci, M., Acarman, T., Guvenc, L., Tur, O., Ucarol, H., Kiray, B., Ozatay, E., and ‘Modeling and Control of a Four Wheel Drive Parallel hybrid Electric Vehicle’, in: Proceedings of the 2006 IEEE International Conference on Control Applications, Munich, Germany, October 4-6, 2006, (155 - 162)

103 Bowles, P., Peng, H., and Zhang, X.: ‘Energy Management in a Parallel Hybrid Electric Vehicle with a Continuously Variable Transmission’, in: Proceedings of the American Control Conference, Chicago, Illinois, June 2000 pp. 55-59

104 Jalil, N., Kheir, N.A., and Salman, M.: ‘A Rule-Based Energy Management Strategy for a Serie Shybrid Vehicle’, in: Proceedings of the American Control Conference, Albuquerque, NM, USA, June 1997, vol. 1, pp. 689–693

105 Mohebbi, M., Charkhgard, M., and Farrokhi, M.: ‘Optimal Neuro-Fuzzy Control of Parallel Hybrid Electric Vehicles’, in: Proceedings of the IEEE Vehicle Power and Propulsion Conference (VPPC’05), Tehran, Iran, 7-9 September 2005, pp. 26–30

106 Schouten, N.J., Salman, M.A., and Kheir, N.A.: 'Fuzzy Logic Control for Parallel Hybrid Vehicles', IEEE Transaction on Control Systems Technology, May 2002, vol. 10, (no. 3), pp. 460 - 468

107 Baumann, B.M., Washington, G., Glenn, B.C., and Rizzoni, G.: 'Mechatronic Design and Control of Hybrid Electric Vehicles', IEEE/ASME Trans. Mechatronics, March 2000, vol. 5, (no. 1), pp. 58–72

108 Powell, B.K., Bailey, K.E., and Cikanek, S.R.: 'Dynamic modeling and control of hybrid electric vehicle powertrain systems', IEEE Control Syst. Mag, October 1998, vol. 18, (no. 5), pp. 17–33

109 Rizoulis, D., Burl, J., and Beard, J.: 'Control Strategies for a Series-Parallel Hybrid Electric Vehicle', SAE, Warrendale, PA, 2001, Paper No. 2001-01-1354

110 Sharer, P.B., Rousseau, A., Karbowski, D., and Pagerit, S.: 'Plug-in Hybrid Electric Vehicle Control Strategy: Comparison Between EV and Charge-Depleting Options', SAE, Warrendale, PA, 2008, Paper No. 2008-01-0460

111 Rousseau, A., Pagerit, S., and Gao, D.: 'Plug-in Hybrid Electric Vehicle Control Strategy Parameter Optimization, Anaheim, California', Electric Vehicle Symposium and Exposition 2–5 December 2007

112 Sciarretta, A., and Guzzella, L.: 'Rule-Based and Optimal Control Strategies for Energy Management in Parallel Hybrid Vehicles', 6th International Conference on Engines for Automobile (ICE 2003), 2003

113 Opila, D.F., Wang, X., McGee, R., Cook, A., and Grizzle, J.W.: 'Fundamental Structural Limitations of an Industrial Energy Management Controller Architecture for Hybrid Vehicles', ASME Dynamic Systems and Control Conference, 2009

114 Shumei, C., Wei, Z., and Likun, T.: 'Control Strategy for Double Shaft Parallel Hybrid Electric Vehicle', in: Vehicle Power and Propulsion Conference, 2006, VPPC'06. IEEE, pp. 1-4

115 Kim, C., NamGoong, E., Lee, S., Kim, T., and Kim, H.: 'Fuel Economy Optimization for Parallel Hybrid Vehicles With CVT', SAE Technical Paper 1999-01-1148, 1999, pp. 9

116 Pisu, P., and Rizzoni, G.: 'A Comparative Study of Supervisory Control Strategies for Hybrid Electric Vehicles', IEEE Trans. on Control SystemsTechnology, 2007, vol. 15, (no. 3), pp. 506–518

117 Mohammadian, M., and Bathaee, M.: 'Motion Control for Hybrid Electric Vehicle', Power Electronics and Motion Control Conference. IPEMC 2004. The 4th International, 2004, pp. 1490-1494

118 Phillips, A.M., Jankovic, M, and Bailey, K.E.: 'Vehicle System Controller Design for a Hybrid Electric Vehicle', Control Applications. Proceedings of the IEEE International Conference, 2000, pp. 297-302

119 Zeng, Q., and Huang, J.: 'The Design And Simulation of Fuzzy Logic Controller for Parallel Hybrid Electric Vehicles', in: Proceedings of the IEEE International Conferenceon Automationand Logistics (ICAL '07), Jinan, China, August 2007, pp. 908–912

120 Khoucha, F., Benbouzid, M.E.H., and Kheloui, A.: 'An Optimal Fuzzy Logic Power Sharing Strategy for Parallel Hybrid Electric Vehicles', in: Proceedings of the IEEE Vehicle Power and Propulsion Conference (VPPC '10), Lille, France, September 2010, pp. 1–5

121 Liu, X., Wu, Y., and Duan, J.: 'Power Split Control Strategy for a Series Hybrid Electric Vehicle Using Fuzzy Logic', in: Proceedings of the IEEE International Conference on Automation and Logistics (ICAL'08), Qingdao,China, September2008, pp. 481–486

122 Rajagopalan, A., and Washington, G.: 'Intelligent Control of Hybrid Electric Vehicles Using GPS Information', SAE Technical Paper 2002-01-1936, Future Car Congress, 2002

123 Arsie, I., Pianese, C., Rizzo, G., and Santoro, M.: 'A Model For The Energy Management in a Parallel Hybrid Vehicle', in: Proceedings of the 3rd International Conference on Control and Diagnostics in Automotive Applications, Sestri Levante, Italy, July 2001, pp. Paper No. 01A3037

124 Lee, H.D., S, K.E., K, S.S., and Kim, J.S.: 'Torque Control Strategy for a Parallel-Hybrid Vehicle Using Fuzzy Logic', IEEE Industry Applications Magazine, 2000, vol. 6, (no. 6), pp. 33–38

125 Tao, C.W., and Taur, J.S.: 'Flexible Complexity Reduced Pidlike Fuzzy Controllers', IEEE Transactions on Systems, Man, and Cybernetics B: Cybernetics, 2000, vol. 30, (no. 4), pp. 510-516

126 Syed, F.U., Kuang, M.L., Smith, M., Okubo, S., and Ying, H.: 'Fuzzy Gain-Scheduling Proportional-Integral Control For Improving Engine Power and Speed

Behavior in a Hybrid Electric Vehicle', IEEE Transactions on Vehicular Technology, 2009, vol. 58, (no. 1), pp. 69–84

127 Patel, A.V., and Mohan, B.M.: 'Analytical Structures and Analysis of the Simplest fuzzy PI Controllers', Automatica, 2002, vol. 38, (no. 6), pp. 981–993

128 Galichet, S., and Foulloy, L.: 'Fuzzy Controllers: Synthesis and Equivalences', IEEE Transactions on Fuzzy Systems 1995, vol. 3, (no. 2), pp. 140-148

129 Jianlong, Z., Chengliang, Y., and Jianwu, Z.: 'Use Of Fuzzy Controller for Hybrid Traction Control System in Hybrid Electric Vehicles', in: Proceedings of the IEEE International Conference on Mechatronics and Automation (ICMA '06), Luoyang, China, June 2006, pp. 1351–1356

130 Zhou, M., Zhang, H., and Wang, X.: 'Research on Fuzzy Energy Management Strategy of Parallel Hybrid Electric Vehicle', in: Proceedings of the International Conference on Electronic and Mechanical Engineering and Information Technology (EMEIT '11), Heilongjiang, China, August 2011, pp. 967–971

131 Hajimiri, M.H., and Salmasi, F.R.: 'A Predictive and Battery Protective Control Strategy for Series HEV', Asian Electric Vehicle, December, 2008, vol. 6, (no. 2)

132 Langari, R., and Won, J.S.: 'Integrated Drive Cycle Analysis for Fuzzy Logic Based Energy Management in Hybrid Vehicles', in: Proceedings of the 12th IEEE International Conferenceon Fuzzy Systems (FUZZ '03), Missouri, 25-28 May 2003, pp. 290–295

133 Golkar , M.A., and Hajizadeh, A.: ‘Power Management Strategy for Parallel Hybrid Electric Vehicles’, in: Proceedings of the Joint International Conference on Sustainable Energy and Environment, Bangkok, Thailand, November 2006, pp. 1–6

134 Lu, D., Li, W., and Zhou, M.: ‘Fuzzy Logic Control Approach To The Energy Management Of Parallel Hybrid Electric Vehicles’, in: Proceedings of the IEEE International Conference on Information and Automation(ICIA’12), Shenyang, China, 6-8 June 2012, pp. 592–596

135 Zhumu, F., Junya, X., and Aiyun, G.: ‘Research on Energy Management and Optimization for PHEV’, Automation and Logistics (ICAL), 2012 IEEE International Conference, 15-17 August 2012, pp. 578-582

136 Brahma, A., Glenn, B., Guezennec, Y., Miller, T., Rizzoni, G., and Washington, G.: ‘Modeling, Performance Analysis and Control Design of a Hybrid Sport-Utility Vehicle’, in: Proceedings of the IEEE International Conference on Control Applications (CCA’99), Kohala Coast, Hawaii, USA, August 1999, pp. 448–453

137 Paganelli, G., Delprat, S., Guerra, T.M., Rimaux, J., and Santin, J.J.: ‘Equivalent Consumption Minimization Strategy for Parallel Hybrid Power Trains’, in: Proceedings of the 55th Vehicular Technology Conference, Vancouver, BC, Canada, May 2002, vol. 4, pp. 2076–2081

138 Kleimaier, A., and Schr¨oder, D.: ‘An Approach for the Online Optimized Control of a Hybrid Powertrain’, in: Proceedings of 7th International Workshop Advanced on Motion Control, 2002, pp. 215–220

139 Rizzoni, G., Pisu, P., and Calo, E.: 'Control Strategies for Parallel Hybrid Electric Vehicles', in: Proceedings of IFAC Symposium on Advanced Automotive Control, 2004, pp. 508–513

140 Sciarretta, A., Back, M., and Guzzella, L.: 'Optimal Control of Parallel Hybrid Electric Vehicles', IEEE Transactions On Control Systems Technology, 2004, vol. 12, (no. 3)

141 Delprat, S., Guerra, T.M., and Rimaux, J.: 'Optimal Control of a Parallel Powertrain: From Global Optimization to Real-time Control Strategy', in: Proceedings of the 55th VehicularTechnology Conference, Berlin, Germany, May 2002, pp. 2082–2088

142 Kim, N., Cha, S., and Peng, H.: 'Optimal Control of Hybrid Electric Vehicles Based on Pontryagin's Minimum Principle', IEEE Transactions on Control Systems Technology, September 2011, vol. 19, (no. 5), pp. 1279–1287

143 Serrao, L., Onori, S., and Rizzoni, G.: 'ECMS as a Realization of Pontryagin's Minimum Principle for HEV Control', in: American Control Conference, IEEE, 2009, pp. 3964-3969

144 Krotov, V.F.: 'Global Methods in Optimal Control Theory', Marcel Dekker, Incorporated. New York, USA, , 1995, pp. 74-121

145 Geering, H.: 'Optimal Control with Engineering Applications', Springer, New York, NY, USA, 2007

146 Serrao, L., and Rizzoni, G.: 'Optimal Control of Power Split for a Hybrid Electric Refuse Vehicle', in: Proceedings of the American Control Conference (ACC '08), Washington, D.C., USA, June 2008, pp. 4498–4503

147 Stockar, S., Marano, V., Rizzoni, G., and Guzzella, L.: 'Optimal Control for Plug-In Hybrid Electric Vehicle Applications', in: Proceedings of the American Control Conference (ACC '10), Baltimore, Md, USA, July 2010, pp. 5024–5030

148 Chasse, A., and Sciarretta, A.: 'Supervisory Control of Hybrid Powertrains: An Experimental Benchmark of Offline Optimization and Online Energy Management', Control Engineering Practice, 2011, vol. 19, (no. 11), pp. 1253-1265

149 Kim, N., Lee, D., Cha, S.W., and Peng, H.: 'Optimal Control of a Plug-In Hybrid Electric Vehicle (PHEV) Based on Driving Patterns', in: Proceedings of the 24th International Battery, Hybrid and Fuel Cell Electric Vehicle Symposium, Stavanger, Norway, 2009, pp. 1–9

150 Kim, N., Rousseau, A., and Lee, D.: 'A Jump Condition of Pmpbased Control for PHEVs', Journal of Power Sources, 2011, vol. 196, (no. 23), pp. 10380–10386

151 Stockar, S., Marano, V., Canova, M., Rizzoni, G., and Guzzella, L.: 'Energy-Optimal Control of Plug-In Hybrid Electric Vehicles for Real-World Driving Cycles', IEEE Transactions on Vehicular Technology, 2011, vol. 60, (no. 7), pp. 2949–2962

152 Musardo, C., Staccia, B., and Rizzoni, G.: 'A-ECMS: An Adaptive Algorithm for Hybrid Electric Vehicle Energy Management', in: Proceedings of the 44th IEEE Conference on Decision and Control,and the European Control Conference (CDC-ECC'05), Seville, Spain, December 2005, pp. 1816–1823

153 Paganelli, G., Tateno, M., Brahma, A., Rizzoni, G., and Guezennec, Y.: 'Control Development for a Hybrid-Electric Sport Utility Vehicle: Strategy, Implementation and Field Test Results', in: Proceedings of the American Control Conference, Columbus, Ohio, USA, June-July 2001, pp. 5064–5069

154 Won, J.S., Langari, R., and Ehsani, M.: 'An Energy Management and Charge Sustaining Strategy for a Parallel Hybrid Vehicle with CVT', IEEE Transactionson Control Systems Technology, 2005, vol. 13, (no. 2), pp. 313–320

155 Pisu, P., and Rizzoni, G.: 'A Supervisory Control Strategy for Series Hybrid Electric Vehicles With Two Energy Storage Systems', in: Proceedings of the IEEE Vehicle Power and Propulsion Conference (VPPC'05), Chicago, Ill, USA, September 2005, pp. 65–72

156 Xu, l., Cao, g., Li, J., Yang, F., Lu, L., and Ouyang, M.: 'Equivalent Consumption Minimization Strategies of Series Hybrid City Buses', Energy Management, 2010, pp. 133–146

157 Salmasi, F.R.: 'Control Strategies for Hybrid Electric Vehicles: Evolution, Classification, Comparison, and Future Trends', IEEE Transactions on Vehicular Technology, 2007, vol. 56, (no. 5), pp. 2393-2404

158 Paganelli, G., Ercole, G., Brahma, A., Guezennec, Y., and Rizzoni, G.: 'General Supervisory Control Policy for the Energy Optimization of Charge-Sustaining Hybrid Electric Vehicles', Society Automotive Engineers Review, 2001, vol. 22, (no. 4), pp. 511–518

159 Gu, B., and Rizzoni, G.: 'An Adaptive Algorithm for Hybrid Electric Vehicle Energy Management Based on Driving Pattern Recognition', in: Proceedings of the

ASME International Mechanical Engineering Congress and Exposition, Chicago, Illinois, USA, 2006, pp. 249–258

160 Onori, S., L, S., and Rizzo, G.: 'Adaptive Equivalent Consumption Minimization Strategy for HEVs, Cambridge, MA', in: 3rd Annual Dynamic Systems and Control Conference, September 2010

161 Sciarretta, A., Guzzella, L., and Back, M.: 'A Real-time Optimal Control Strategy for Parallel Hybrid Vehicles With On-Board Estimation of Control Parameters', in: Proceedings of IFAC Symposium on Advances Automotive Control, Salerno, Italy, 2004, pp. 502–507

162 Gao, J.P., Zhu, G.M.G., Strangas, E.G., and Sun, F.C.: 'Equivalent Fuel Consumption Optimal Control of a Series Hybrid Electric Vehicle', Journal of Automobile Engineering, 2009, vol. 223, (no. 8), pp. 1003–1018

163 Rousseau, G., Sinoquet, D., Sciarretta, A., and Milhau, Y.: 'Design Optimization and Optimal Control for Hybrid Vehicles', in: Proceedings of the International Conference Engineering Optimization, Riode Janeiro, Brazil, 2008, pp. 1–10

164 Marano, V., Tulpule, P., Stockar, S., and Rizzoni, G.: 'Comparative Study of Different Control Strategies for Plug-In Hybrid Electric Vehicles', in: Proceedings of the SAE International Conference on Engines and Vehicles, Naples, Italy, 2009, (Paperno. 2009-24-0071)

165 He, Y., Chowdhury, M., Pisu, P., and Ma, Y.: 'An Energy Optimization Strategy For Power-Split Drivetrain Plug-In Hybrid Electric Vehicles', Transportation Research Part C: Emerging Technologies, 2012, vol. 22, pp. 29–41

166 Tulpule, P., Marano, V., and Rizzoni, G.: 'Effects of Different PHEV Control Strategies on Vehicle Performance', in: Proceedings of the American Control Conference (ACC '09), St.Louis, Mo, USA, June 2009, pp. 3950– 3955

167 Salman, M., Chang, M.F., and Chen, J.S.: 'Predictive Energy Management Strategies for Hybrid Electric Vehicles', in: Proceedings of the IEEE Vehicle Power and Propulsion Conference (VPPC'05), Chicago, Illinois, September 2005, pp. 536-540

168 Cui, N., Fan, J., Zhang, C., and Wu, J.: 'Research on Predictive Control Based Energy Management Strategy for Hybrid Electric Vehicle', in: Proceedings of the 3rd IEEE International Symposium on Power Electronics for Distributed Generation Systems(PEDG '12), Aalborg, Denmark, June 2012, pp. 642–646

169 Serrao, L.: 'A Comparative Analysis of Energy Management Strategies for Hybrid Electric Vehicles (Phd. Dissertation)', The Ohio State University, 2009

170 Beck, R., and Richert, B., A. F: 'Model Predictive Control of a Parallel Hybrid Vehicle Drivetrain', in: Proceedings of the 44th IEEE Conference on Decision and Control, and the European Control Conference, Aachen, Germany, December 2005, pp. 2670–2675

171 Wang, Y., and Boyd, S.: 'Fast Model Predictive Control Using Online Optimization', in: Proceedings of the International Federation Automatic Control World Congress (IFAC '08), Seoul, Korea, July 2008, pp. 6974 – 6997

172 Sampathnarayanan, B., Serrao, L., Onori, S., Rizzoni, G., and Yurkovich, S.: 'Model Predictive Control as an Energymanagement Strategy for Hybrid Electric

Vehicles', in: Proceedings of the ASME Dynamic Systems and Control Conference (DSCC '09), October 2009, pp. 1161–1168

173 Ichikawa, S., Yokoi, Y., Doki, S., Okuma, S., Naitou, T., Shiimado, T., and Miki, N.: 'Novel Energy Management System for Hybrid Electric Vehicles Utilizing Car Navigation Over a Commuting Route', Intelligent Vehicles Symposium, 2004 IEEE, 2004, pp. 161-166

174 Yan, F., Wang, J., and Huang, K.: 'Hybrid Electric Vehicle Model Predictive Control Torque-Split Strategy Incorporating Engine Transient Characteristics', IEEE Transactionson VehicularTechnology, 2012, vol. 61, (no. 6), pp. 2458–2467

175 Won, J.S., and Langari, R.: 'Intelligent Energy Management Agent for a Parallel Hybrid Vehicle - Part II: Torque Distribution, Charge Sustenance Strategies, and Performance Results', in: Proceeding of the American Control Conference, Denver, Colo, USA, June 2003, (no. 54), pp. 935–956

176 Poramapojana , P., and Chen, B.: 'Minimizing HEV Fuel Consumption Using Model Predictive Control', in: Proceedings of the 8th IEEE/ASME International Conference on Mechatronic and Embedded Systems and Applications (MESA '12), Sozhou, China, 8-10 July 2012, pp. 148–153

177 Mahapatra, S.: 'Model-Based Design for Hybrid Electric Vehicle Systems', Auto Electronics. http://autoelectronics.com/powertrain/hybridelectricvehicles/model-based-design-forhybrid-electric-vehicles-081109/, 2009

178 Nuijten, E., Koot, M., and Kessels, J.: 'Advanced Energy Management Strategies for Vehicle Power Nets', in: Proceedings of EAEC 9th Int. Congress: European Automotive Industry, 2003

179 Vito, D.D., Miotti, A., and Scattolini, R.: 'Power Flow Management With Predictive Capabilities for a Hybrid Fuel Cell Vehicle', in: Proceedings of the 5th IFAC Symposium on Advances in Automotive Control, 2007, vol. 40, (no. 10), pp. 9-16

180 West, M.J., Bingham, C.M., and Schofield, N.: 'Predictive Control for Energy Management in All/More Electric Vehicles With Multiple Energy Storage Units', in: Proceedings of the IEEE International Electric Machines and Drives Conference, M. J. West, Ed, 1-4 June 2003, vol. 1, pp. 222–228

181 Borhan, H.A., Zhang, C., Vahidi, A., Phillips, A.M., Kuang, M.I., and Di Cairano, S.: 'Nonlinear Model Predictive Control for Power-Split Hybrid Electric Vehicles', in: Proceedings of the 49th IEEE Conference on Decisionand Control (CDC'10), Clemson, SC, USA, December 2010, pp. 4890– 4895

182 Ripaccioli, G., Bemporad, A., Assadian, F., Dextreit, C., Cairano, S.D., and Olmanovsky, I.: 'Hybrid Modeling, Identification, and Predictive Control: An Application to Hybrid Electric Vehicle Energy Management', Hybrid Systems: Computation and Control, Springer, Berlin, Germany, 2009, vol. 5469 of Lecture Notes in Computer Science, pp. 321– 335

183 Ripaccioli, G., Bernardini, D., Di Cairano, S., Bemporad, A., and Kolmanovsky, I.V.: 'A Stochastic Model Predictive Control Approach for Series Hybrid

Electricvehicle Power Management', in: Proceedings of the International Conference Mechatronics and Automation, Siena, Italy, 2011, pp. 4890–4895

184 Vogal, A., Ramchandran, D., Gupta, R., and Raux, A.: 'Improving Hybrid Vehicle Fuel Efficiency Using Inverse Reinforcement Learning', in: Proceedings of 26th AAAI Conference on Artificial Intelligence, 2012, pp. 384–390

185 Borhan, H., Vahidi, A., Phillips, A.M., Kolmanovsky, I.V., Kuang, M.I., and Di Cairano, S.: 'MPC-Based Energy Management of a Power-Split Hybrid Electric Vehicle', IEEE Transactions on Control Systems Technology, 2012, vol. 20, (no. 3), pp. 593–603

186 Hagan, M.T., Demuth, H.B., and Beale, M.H.: 'Neural Network Design', PWS Publishing Company, Boston, 1996, 1st edition

187 Baumann, B., Rizzoni, G., and Washington, G.: 'Intelligent Control of Hybrid Vehicles Using Neural Networks and Fuzzy Logic', SAE Technical Paper no. 981061, Society of Automotive Engineers, 1998, pp. 11

188 Suzuki, M., Yamaguchi, S., Araki, T., Raksincharoensak, P., Yoshizawa, M., and Nagai, M.: 'Fuel Economy Improvement Strategy for Light Duty Hybrid Truck Based on Fuel Consumption Computational Model Using Neural Network', in: Proceedings of the 7th World Congress, International Federation of Automatic Control, Seoul, Korea, July 2008, pp. 10719–10725

189 Prokhorov, D.: 'Toyota Prius HEV Neurocontrol', in: Proceedings of the International Joint Conference on Neural Networks (IJCNN'07), Orlando, Florida, USA, August 2007, pp. 2129–2134

190 Gong, Q., Li , Y., and Peng, H.: 'Power Management of Plugin Hybrid Electric Vehicles Using Neural Network Based Trip Modeling', in: Proceedings of the American Control Conference (ACC'09), St. Louis, Mo, USA, June 2009, pp. 4601–4606

191 Boyali, A., and G¨uvenc, L.: 'Real-time Controller Design for a Parallel Hybrid Electric Vehicle Using Neuro-Dynamic Programming Method', in: Proceedings of the IEEE International Conference on Systems, Man and Cybernetics (SMC '10), Istanbul, Turkey, 10-13 Oct. 2010, pp. 4318–4324

192 Liu, M.J.: 'A Fuzzy Neural Network Control System Based on Improved Learning Algorithms', in: Proceedings of the Chinese Society of Electrical Engineering, 2007, vol. 27, pp. 87–92

193 Sivertsson, M., Sundstrom, C., and Eriksson, L.: 'Adaptive Control of a Hybrid Powertrain with Map-based ECMS', IFAC World Congress, 2011

194 Manzie, C.: 'Relative Fuel Economy Potential of Intelligent, Hybrid and Intelligent–Hybrid Passenger Vehicles', Electric and Hybrid Vehicles, 2010, pp. 61-90

195 Adhikari, S.: 'Real-time Power Management of Parallel Full Hybrid Electric Vehicle', PhD Thesis, October, 2010

196 Hellstrom, E., Aslund, J., and Nielsen, L.: 'Horizon Length and Fuel Equivalents for Fuel-Optimal Look-Ahead Control', 6th IFAC Symposium Advances in Automatic Control, 2010

197 Hellstrom, E., Ivarsson, M., Aslund, J., and Nielsen, L.: 'Look-ahead Control for Heavy Trucks To Minimize Trip Time and Fuel Consumption', Control Engineering Practice, 2009, vol. 17, (no. 2), pp. 245-254

198 Watson, H.C.: 'Vehicle Driving Patterns and Measurement Methods for Energy and Emissions Assessment', University of Melbourne, Tech. Rep, Australia, 1978

199 Berry, I.: 'The Effect of Driving Style and Vehicle Performance on the Real-World Fuel Consumption of U.S. Light-Duty Vehicles', Mechanical Engineering Department, Master of Science in Mechanical Engineering, February 2010, pp. 140

200 Barlow, T., Latham, S., and McCrae, I.: 'A Reference Book of Driving Cycles For Use In The Measurement of Road Vehicles Emissions', Published Project Report 354. Department for Transport, Clearner Fuels & Vehicles. Transport Research Laboratory, 2009, version 3, pp. 284

201 Sundstrom, O., Guzzella, L., and Soltic, P.: 'Optimal Hybridization in Two Parallel Hybrid Electric Vehicle Susing Dynamic Programming', in: Proceedings of the 17th IFAC World Congress, Seoul, Republic of Korea, 2008, vol. 17, pp. 4642–4647

202 Maggetto, G., and Van Mierlo, J.: 'Electric and electric hybrid vehicle technology: a survey', Electric, Hybrid and Fuel Cell Vehicles (Ref. No. 2000/050), IEE Seminar, 2000, pp. 1-111

203 Maggetto, G., and Van Mierlo, J.: 'Electric Vehicles, Hybrid Electric Vehicles and Fuel Cell Electric Vehicles: State of the Art And Perspectives', Annales de Chimie Science des Materiaux, 31 August 2001, vol. 26, (no. 6), pp. 9-26

204 Cerofolini, A.: ‘Optimal Supervisory Control of Hybrid Vehicles’, ALMA (PhD Thesis), University of Bologna, 2016

205 Wong, J.Y.: ‘Theory of Ground Vehicles’, Third edition, United States of America, John Wiley & Sons. Inc, 2001

206 André, M., Hickman, J., and Hassel, D.: ‘Driving Cycles for Emission Measurements Under European Conditions’, SAE congress, Detroit, USA, SAE Technical Paper 950926, Warrendale, USA, Feb. 27 - March 2, 1995

207 Andre, J.M., lacour, S., and Hugot, M.: ‘Impact of the Gearshift Strategy on Emissions Measurement, Artemis 3142 report: Report n° LTE 0307’, 2003, pp. 63

208 Larminie, J., and Lowry, J.: ‘Electric Vehicle Technology Explained’, John Wiley and Sons Ltd. The Atrium, Southern Gate, Chichester, West Sussex PO19 8SQ, England, 2003, pp. 303

209 Van Mierlo, J., Van den Bossche, P., and Maggetto, G.: ‘Models Of Energy Sources For EV And HEV: Fuel Cells, Batteries, Ultracapacitors, Wheels and Engine-Generators’, Journal of Power Sources, 2004, vol. 128, (no. 1), pp. 76-89

210 Balch, R.C., Burke, A., and Frank, A.A.: ‘The Effect of Battery Pack Technolog and Size Choices on Hybrid Electric Vehicle Performance and Fuel Economy’, Applications and Advances, 2001. The Sixteenth Annual Battery Conference, January 2001, pp. 31-36

211 Lin, C.-C., Peng, H., and Grizzle, J.W.: ‘Control System Development for an Advanced-Technology Medium-Duty Hybrid Electric Truck’, International Truck & Bus Meeting & Exhibition, Fort Worth, TX, SAE International, November 2003

212 Sundstrom, O., and Guzzella, L.: 'A Generic Dynamic Programming Matlab Function', in: Proceedings of the IEEE International Conference on Control Applications & Intelligent Control (CCAISIC'09), Saint Petersburg, Russia, 8-10 July 2009, pp. 1625–1630

213 Yoon, H.-J., and Lee, S.-J.: 'An Optimized Control Strategy For Parallel Hybrid Electric Vehicle', SAE transactions, 2003, vol. 112, (no. 7), pp. 579–586

214 Bianchi, D., Rolando, L., and Serrao, L.: 'A Rule-Based Strategy For a Series/Parallel Hybrid Electric Vehicle: An Approach Based On Dynamic Programming', in: Proceedings of the ASME 2010 Dynamic Systems and Control Conference, Cambridge, Massachusetts, USA, September 12-15, 2010

215 Kim, B., Kim, Y.-g., Kim, T., Park, Y.-i., and Cha, S.W.: 'HEV Cruise Control Strategy on GPS (Navigation) Information', World Electric Vehicle Journal 2009, vol. 3

216 Cassebaum, O., Ba, X., and ker, B.: 'Predictive Supervisory Control Strategy for Parallel HEVs Using Former Velocity Trajectories', in: Vehicle Power and Propulsion Conference (VPPC), 2011 IEEE, 6-9 Sept. 2011, pp. 1-6

217 Chao, S., Xiaosong, H., Moura, S.J., and Fengchun, S.: 'Velocity Predictors for Predictive Energy Management in Hybrid Electric Vehicles', Control Systems Technology, IEEE Transactions on, 2015, vol. 23, (no. 3), pp. 1197-1204

218 Chao, S., Xiaosong, H., Scott, M., and Fengchun, S.: 'Comparison of Velocity Forecasting Strategies for Predictive Control in HEVs', in: Proceedings of the ASME 2014 Dynamic Systems and Control Conference, 2014, vol. 2 pp. 9

219 Fotouhi, A., Montazeri, M., and Jannatipour, M.: 'Vehicle's Velocity Time Series Prediction Using Neural Network', International Journal of Automotive Engineering, 2011, vol. 1, (no. 1), pp. 21-28

220 He, H., Sun, C., and Zhang, X.: 'A Method for Identification of Driving Patterns in Hybrid Electric Vehicles Based on a LVQ Neural Network', Energies, 2012, vol. 5, (no. 9), pp. 3363

221 Murphey, Y.L., Park, J., and Kiliaris et al, L.: 'Intelligent Hybrid Vehicle Power Control—Part II: Online Intelligent Energy Management', IEEE Transactions on Vehicular Technology, 2013, vol. 62, (no. 1), pp. 69–79

222 Murphey, Y.L., Jungme, P., Zhihang, C., Kuang, M.L., Masrur, M.A., and Phillips, A.M.: 'Intelligent Hybrid Vehicle Power Control ; Part I: Machine Learning of Optimal Vehicle Power', Vehicular Technology, IEEE Transactions, 2012, vol. 61, (no. 8), pp. 3519-3530

223 Jiao, X., and Shen, T.: 'SDP Policy Iteration-Based Energy Management Strategy Using Traffic Information for Commuter Hybrid Electric Vehicles', Energies: ISSN 1996-1073, 2014, vol. 7, pp. 4648-4675

224 Pontryagin, L., Boltyanskii, V., Gamkrelidze, R., and E., M.: 'Mathematical Theory Of Optimal Processes', New York: Interscience Publishers, 1962

225 Delprat, S., Guerra, T.M., Paganelli, G., Lauber, J., and Delhom, M.: 'Control Strategy Optimization for an Hybrid Parallel Powertrain', in: Proceedings of the American Control Conference, IEEE, Arlington, Va, USA, June 2001, vol. 2, pp. 1315–1320

226 Schouten, N.J., Salman, M.A., and Kheir, N.A.: 'Energy Management Strategies for Parallel Hybrid Vehicles Using Fuzzy Logic', Control Engineering Practice, 2003, vol. 11, (no. 2), pp. 171-177

227 Jeon, S., Jo, S., Park, Y., and Lee, J.: 'Multi-Mode Driving Control of a Parallel Hybrid Electric Vehicle Using Driving Pattern Recognition', ASME Journal of dynamic systems, measurement, and control, 2002, vol. 124, (no. 1), pp. 141–149

228 Ambuh, D., and Guzzella, L.: 'Predictive Reference Signal Generator for Hybrid Electric Vehicles', Vehicular Technology, IEEE Transactions, 2009, vol. 58, (no. 9), pp. 4730-4740

229 Zhang, C., Vahidi, A., Pisu, P., Li, X., and Tennant, K.: 'Role Of Terrain Preview in Energy Management of Hybrid Electric Vehicles', IEEE Trans. Veh. Technol., 2010, 59, pp. 1139–1147

230 Appelkvist, O., and Gebel, P.: 'Route Predictive Optimization of State-of-Charge Reference Signal', Master of Science Thesis in the Master Degree Programme's: Intelligent System Design and Systems, Control & Mechatronics, 2010

231 Nicolas, R.: 'Hybrid energy management of the new Mercedes C-Class', Car Engineer, (http://www.car-engineer.com/hybrid-energy-management-new-mercedes-c-class/), 14 December 2014

232 Lee, S., Walters, S., and Howlett, R.: 'Intelligent GPS-Based Vehicle Control For Improved Fuel Consumption and Reduced Emissions', in: Knowledge-Based Intelligent Information and Engineering Systems, ser. Lecture Notes in Computer

Science, I. Lovrek, R. Howlett, and L. Jain, Eds. Springer Berlin / Heidelberg, 2008, vol. 5179, pp. 701-708

233 Barth, M.: 'An Emissions and Energy Comparison Between a Simulated Automated Highway System and Current Traffic Conditions', Intelligent Transportation Systems, IEEE, 2000, pp. 358–363

234 Vagg, C., Brace, C., Hari, D., Akehurst, S., Poxon, J., and Ash, L.: 'Development and Field Trial of a Driver Assistance System to Encourage Eco-Driving In Light Commercial Vehicle Fleets', IEEE Transactions on Intelligent Transportation Systems, 2013, vol. 14, (no. 2), pp. 796-805

235 Vagg, C., Brace, C., Hari, D., and Akehurst, S.: 'A Driver Advisory Tool to Reduce Fuel Consumption', SAE Technical Paper 2012-01-2087, 2013, pp. 6

236 Willems, F., and Cloudt, R.: 'Experimental Demonstration of a New Model-Based SCR Control Strategy for Cleaner Heavy-Duty Diesel Engines', IEEE Transactions on Control Systems Technology, 2011, vol. 19, (no. 5), pp. 1305-1313

NOMENCLATURE

Abbreviations	Description	Units
A-ECMS	Adaptive Equivalent Consumption Minimisation Strategy	[-]
AGF	Aggresivity Factor	[-]
ANN	Artificial Neural Network	[-]
AP	Adaptive Prediction	[-]
API	Application Programming Interface	[-]
ARTEMIS	Assessment and Reliability of Transport Emission Models and Inventory Systems	[-]
BA	Bath	[-]
CDF	Cumulative Distribution Function	[-]
CIDI	Compression Ignition Direct Ignition	[-]
CPU	Central Processing Unit	[-]
CVT	Continuous Varying Transmission	[-]
DB	Data Base	[-]
DEV	Deviation in Percentile	[-]
DIP	Driver's Intention Predictor	[-]
DIRCOL	Direction Cosine Linkage	[-]
DOD	Depth of Discharge	[-]
DOH	Degree Of Hybridisation	[-]
DP	Dynamic Programming	[-]
DPF	Diesel Particulate Filter	[-]
DP-HST	Dynamic Programming Heuristic Controller	[-]
DP-LT	Dynamic Programming Lookup Table	[-]

DPR	Driving Pattern Recognition	[-]
ECMS	Equivalent Consumption Minimisation Strategy	[-]
EDR	Energy-to-Distance Ratio	[-]
EFCOCS	Equivalent Fuel Consumption Optimal Control Strategy	[-]
EGR	Exhaust Gas Recirculation	[-]
EHR	Electric Hybridisation Ratio	[-]
EIL	Engine in Loop	[-]
EM	Electric Motor	[-]
EM-TFL	Electromagnetic-Team Fuzzy Logic	[-]
ES	Extremum Seeking	[-]
EU	European Union	[-]
EV	Electric Vehicle	[-]
EVs	Electric Vehicles	[-]
EVT	Electric Variable Transmission	[-]
FC	Fuel Consumption	[-]
FDR	Final Drive Ratio	[-]
FE	Fuel Economy	[-]
FHDS	Federal Highway Driving Schedule	[-]
FLC	Fuzzy Logic Control	[-]
FNN	Fuzzy Neural Network	[-]
FPIDF	Flexible Complexity Reduced PID-like Fuzzy Controller	[-]
FTP	Federal Test Procedure	[-]

GA	Genetic Algorithm	[-]
GIS	Geographic Information System	[-]
GPS	Global Positioning System	[-]
HC	Hydro Carbons	[-]
HEV	Hybrid Electric Vehicle	[-]
HIL	Hardware in the Loop	[-]
HJB	Hamilton-Jacobi-Bellman	[-]
HR	Hybridisation Ratio	[-]
HST	Heuristic	[-]
HVAC	Heating Ventilation and Air Conditioning	[-]
HWFET	Highway Fuel Economy Test	[-]
ICE	Internal Combustion Engine	[-]
IEMA	Intelligent Energy Management Agent	[-]
IM	Inspection and Maintenance	[-]
ISG	Integrated Starter Generator	[-]
ITS	Intelligent Transportation System	[-]
JC	Japanese Cycle	[-]
JP	Japan	[-]
LA	Los Angeles	[-]
MATLAB	Matrix Laboratory	[-]
MOGA	Multi-objective Genetic Algorithm	[-]
MOS	Multi-objective solutions	[-]
MOSADE	Multi objective Self Adaptive Differential Evolution	[-]
MPC	Model Predictive Control	[-]

MPG	Miles per Gallon	[-]
NDP	Neuro-Dynamic Programming	[-]
NEDC	New European Driving Cycle	[-]
NSGA	Non-Dominated Sorting Genetic Algorithm	[-]
NYCC	New York City Cycle	[-]
OPT	Optimal	[-]
PBC	Power Balance Controller	[-]
PCA	Principal Component Analysis	[-]
PD	Proportional-Derivative	[-]
PFC	Power Follower Control Strategy	[-]
PHEV	Plug in Hybrid Electric Vehicle	[-]
PHEVs	Plug-in Hybrid Electric Vehicles	[-]
PI	Proportional-Integral	[-]
PID	Proportional-Integral-Derivative	[-]
PIDF	PID-like Fuzzy	[-]
PM	Particulate Matter	[-]
PMP	Pontryagin's Minimum Principle	[-]
PNGV	Partnership for a New Generation of Vehicles	[-]
PSAT	PNGV System Analysis Toolkit	[-]
PSO	Particle Swarm Optimisation	[-]
PSR	Power Split Ratio	[-]
RBEC	Route Based ECMS Control	[-]
RPEC	Robust Proportional ECMS Control	[-]
RPM	Revolutions per Minute	[-]

RTC	Real Time Control	[-]
SC	Supplementary Cycle	[-]
SCR	Selective Catalytic Reduction	[-]
SDP	Stochastic Dynamic Programming	[-]
SDP-ES	Stochastic Dynamic-Extremum Seeking Programming	[-]
SIL	Software in the Loop	[-]
SMPC	Stochastic Model Predictive Control	[-]
SOC	State of Charge	[%]
SOE	State of Energy	[-]
SOGA	Single Objective Genetic Algorithm	[-]
SP	Static Prediction	[-]
SP-SDP	Shortest Path Stochastic Dynamic Programming	[-]
TCS	Thermostat Control Strategy	[-]
TDNN	Time Delay Neural Network	[-]
THS	Toyota Hybrid System	[-]
UDDS	Urban Dynamometer Driving Schedule	[-]
UDDSHDV	Urban Dynamometer Driving Schedule for Heavy Duty Vehicles	[-]
UK	United Kingdom	[-]
US	United States	[-]
WLTC	Worldwide Harmonised Light Duty Driving Test Cycle	[-]

Symbols	Description	Units
A_f	Vehicle frontal area	[m^2]
Ah	Ampere hours	[-]
$Altitude_{seg}$	Altitude at current route segment	[-]
$Altitude_{seg\ -\ resolution}$	Altitude at previous route segment	[-]
C	Optimisation cost function	[g]
C^*	Optimal cost function	[g]
C_d	Aerodynamic drag coefficient	[-]
$C_{node\ (g\ to\ b)}$	Transition cost from node g to b	[g/s]
$C_{optimal\ cost-to-go}$	Optimal cost to go from node	[g/s]
C_{seg}	Optimisation cost function for route segment seg	[g]
$C_{seg\ +\ 1}$	Cost function for route segment $seg + 1$	[g]
$C_{seg}{}^*$	Optimal cost function for route segment seg	[g]
C_{t+1}	Cost function at time $t + 1$	[g]
CO	Carbon Monoxide	[-]
CO_2	Carbon Dioxide	[-]
$Distance_{route}$	Route distance	[km]
E_k	Kinetic Energy	[J]
FC	Fuel consumption	[g/s]
$FC_{baseline}$	Baseline vehicle fuel consumption	[g]
$FC_{savings}$	Mass of actual cumulative fuel savings	[g]
$FC_{savings\ deviation}$	Fuel lost or gained due to non-charge sustenance	[g]

$FC_{savings\ charge\ sustaining}$	Mass of anticipated cumulative fuel savings assuming charge sustenance	[g]
FDR	Final drive ratio	[-]
F_{aero}	Aerodynamic drag force	[N]
$F_{aero\ brake}$	Braking force resulting from aerodynamic drag	[N]
F_{extra}	Extra tractive force needed for the vehicle to achieve the requested vehicle speed	[N]
F_{grade}	Resistance force by grade	[N]
F_{inert}	Inertia force	[N]
$F_{ICE\,brake}$	Braking force resulting from engine braking	[N]
F_{mech_brake}	Braking force from mechanical brakes	[N]
$F_{rolling}$	Rolling resistance force	[N]
$F_{rolling\ brake}$	Braking force resulting from rolling resistance	[N]
F_{seg}	Tractive force needed to propel a vehicle along route segment	[N]
$F_{VEH\,brake}$	Total braking force experienced by a braking vehicle	[N]
g	Grams	[-]
g	Gravitational constant	m/s^2
G_E	Engine gear ratio	[-]
G_M	Motor gear ratio	[-]
h	Look-ahead horizon	[s]

H	Hamiltonian function	[-]
hp	Horsepower	[-]
I_{batt}	Battery current	[A]
I_{batt_t}	Battery current at time t	[A]
K_d	Derivative gain	[-]
K_i	Integral gain	[-]
K_p	Proportional gain	[-]
K_{ps}	Proportional controller gain	[-]
km	Kilometres	[-]
kW	Kilowatt	[-]
L	Instantaneous fuel consumption rate	[g/s]
L_{seg}	Instantaneous fuel consumption rate for route segment seg	[g/s]
LHV	Low Heating Value of fuel	[J/g]
m	Effective mass of vehicle	kg
$N_{P_{motor\{admissible\ set\}}}$	Number of admissible control variables	[-]
$N_{in_{1,1}}$	Input to neural network hidden layer neurons	[-]
$N_{in_{1,2}}$	Input to neural network hidden layer neurons	[-]
$N_{out_{1,1}}$	Output from neural network hidden layer neuron	[-]
$N_{out_{1,2}}$	Output from neural network hidden layer neuron	[-]
N_c	Normal load acting on the centre of the	[N]

	rolling wheel	
N_{seg}	Number of route segments	[-]
NOx	Oxides of Nitrogen	[-]
P_{batt}	Battery power	[W]
P_{demand}	Vehicle power demand	[W]
$P_{demand_{seg}}$	Vehicle power demand for route segment seg	[W]
P_{demand_t}	Vehicle power demand at time t	[W]
$P_{electric}$	Motor electrical power	[W]
P_{ICE}	Internal combustion engine power	[W]
$P_{ICE_{max}}$	Maximum internal combustion engine power	[W]
$P_{ICE_{max_{W_{ICE}}}}$	Maximum internal combustion engine power engine speed W_{ICE}	[W]
$P_{ICE_{max_{seg}}}$	Maximum internal combustion engine power for route segment seg	[W]
$P_{ICE_{max_t}}$	Maximum internal combustion engine power at time t	[W]
$P_{ICE_{seg}}$	Internal combustion engine power for route segment seg	[W]
P_{ICE_t}	Internal combustion engine power at time t	[W]
P_{max_regen}	Maximum power regenerated	[W]
P_{motor}	Motor mechanical power	[W]
$P_{motor_{max_{seg}}}$	Maximum motor tractive power for route segment seg	[W]

$P_{motor_{max_t}}$	Maximum motor tractive power at time t	[W]
$P_{motor_{\{admissible\ set\}}}$	Admissible set of control variables	[W]
$P_{motor_{max}}$	Maximum motor tractive power	[W]
$P_{motor_{min}}$	Minimum motor mechanical power	[W]
$P_{motor_{resolution}}$	Discretisation resolution for control variable	[W]
$P_{motor_{seg}}$	Motor mechanical power for route segment seg	[W]
$P_{motor_{seg}}^{*}$	Optimal motor tractive power for route segment seg	[W]
P_{motor_t}	Motor mechanical power at time t	[W]
$P_{motor_t}^{*}$	Optimal motor mechanical power at time t	[W]
P_{PSR_t}	Optimal power split ratio	[-]
P_{RSP}	Optimal distribution of power split ratios	[-]
$P_{seg_{min}}$	The least possible instantaneous energy consumption or recuperation along a route segment	[W]
$P_{SOC_{regulator_t}}$	Future energy variation compensator	[W]
$P(S_t \mid S_{t+1})$	Markov chain transition probability from state S_t to S_{t+1}	[-]
Q_{batt}	Battery capacity	[Ah]
R_{batt}	Battery resistance	[Ohm]
R_w	Radius of rolling wheels	[m]
seg_0	Initial route segment	[-]
seg_f	Final route segment	[-]

$SOC_{admissible\ set}$	Admissible set of state variables	[%]
SOC_f	Final battery state of charge	[%]
SOC_h	Expected future battery state of charge	[%]
SOC_{max}	Maximum battery state of charge	[%]
SOC_{min}	Minimum battery state of charge	[%]
SOC_0	Initial state of charge	[%]
SOC_{ref}	Charge-sustaining battery state of charge	[%]
$SOC_{route\ optimized}$	Route optimised battery state of charge	[%]
$SOC_{\ resolution}$	Discretisation resolution for state variables	[%]
SOC_{seg}	Battery state of charge for route segment $seg+1$	[%]
SOC_{seg_0}	Battery state of charge for route segment seg_0 (initial route segment)	[%]
SOC_{seg_f}	Battery state of charge for route segment seg_f*+1* (final route segment)	[%]
SOC_t	Battery state of charge at time t	[%]
$\dot{SOC}_t$	Battery state of charge evolution	[%]
SOC_t^*	Optimal battery state of charge	[W]
SOC_{t_0}	Battery state of charge at time t_0 (intial time step)	[%]
SOC_{t_f}	Battery state of charge at time t_f (final time step)	[%]
SOC_{t+1}	Battery state of charge at time t	[%]
S_t	Markov chains state at time t	[-]
S_{t+1}	Markov chains state at time $t+1$	[-]

t	Time	[s]
t_f	Driving cycle length	[s]
t+1	Future simulation time	[s]
t-1	Past simulation time	[s]
T_{ICE}	Tractive torque from internal combustion engine	[Nm]
$T_{ICE\,max}$	Maximum tractive torque from internal combustion engine	[Nm]
TPM	Transition matrix	[-]
TPM^k	Transition matrix at k-th time step	[-]
T_{extra}	Extra tractive torque needed for the vehicle to achieve the requested vehicle speed	[Nm]
T_{motor}	Motor Torque	[Nm]
$T_{rolling}$	Rolling resistance moment	[Nm]
V_a	Speed of air	[m/s]
$V_{v_{avg\ driving\ spd}}$	Average driving speed	[m/s]
$V_{avg_{seg}}$	Average route driving speed for route segment $seg+1$	$V_{avg_{seg}}$
V_{batt}	Battery voltage	[V]
V_c	Driving cycle speed	[m/s]
V_{lead_t}	Speed of lead vehicle at time $t+1$	[m/s]
V_{oc}	Battery open circuit voltage	[V]
$V_{road\ limit}$	Speed limit for route segment seg	[m/s]
$V_{route_{seg_{min}}}$	Recommended minimum speed for each route segment	[m/s]

$V_{v_{seg_0}}$	Vehicle speed at the beginning of the route	[m/s]
$V_{v_{seg_f}}$	Final vehicle speed at the end of the route	[m/s]
V_v	Vehicle speed	[m/s]
$V_{v_{seg}}$	Vehicle speed for route segment seg	[m/s]
V_{v_t}	Vehicle speed at time t	[m/s]
ω_{ICE}	Engine speed	[RPM]
$\omega_{ICE_{max}}$	Maximum engine speed	[RPM]
$\omega_{ICE_{min}}$	Minimum engine speed	[RPM]
$\omega_{ICE_{seg}}$	Engine speed for route segment seg	[RPM]
ω_{ICE_t}	Engine speed at time t	[RPM]
ω_{motor}	Motor speed	[RPM]
$\omega_{motor_{seg}}$	Motor speed for route segment seg	[RPM]
ω_{wheel}	Wheel speed	[RPM]
$\omega_{wheel_{seg}}$	Wheel speed for route segmentseg	[RPM]
$W_{x_{1,1}}$	Randomly generated neural network input weights	[-]
$W_{x_{1,2\ old}}$	Old randomly generated neural network input weights	[-]
$W_{x_{1,2\ new}}$	New randomly generated neural network input weights	[-]
$W_{x_{1,2}}$	Randomly generated neural network input weights	[-]
$W_{x_{2,1\ old}}$	Old randomly generated neural network input weights	[-]

$W_{x_{2,1}\,new}$	New randomly generated neural network input weights	[-]
$W_{x_{2,1}}$	Randomly generated neural network input weights	[-]
$W_{x_{2,2}\,old}$	Old randomly generated neural network input weights	[-]
$W_{x_{2,2}\,new}$	New randomly generated neural network input weights	[-]
$W_{x_{2,2}}$	Randomly generated neural network input weights	[-]
X_1	Input to neural network	[-]
X_2	Input to neural network	[-]
X_{pf}	Motor power allocation factor	[-]
Y_{actual}	Actual output	[-]
Y_{in}	Input to neural network output neuron	[-]
Y_p	Predicted neural network output	[-]
$\Delta_{SOC_{\overrightarrow{t\ h}_t}}$	Expected net change in battery state of charge over a preview horizon	[-]
$E_{\Delta_{SOC_{\overrightarrow{t\ h}}dischg_t}}$	Expected net change in battery energy for a discharge operation over a preview horizon	[W]
$E_{\Delta_{SOC_{\overrightarrow{t\ h}}rechg_t}}$	Expected net change in battery energy for a recharge operation over a preview horizon	[W]
$\frac{dV_{v_{seg}}}{dt}$	Vehicle acceleration for route segment $seg+1$	[m/s^2]

$\frac{dV_v}{dt}$	Vehicle acceleration	[m/s^2]
$\frac{dV_v}{dt}_{avg\ pos\ accel}$	Average positive vehicle acceleration	[m/s^2]
$\frac{dV_v}{dt}_{max}$	Maximum vehicle acceleration	[m/s^2]
$\dot{m}_{f\ engine}$	Engine fuel cost	[g/s]
$\dot{m}_{f\ eq}$	Equivalent fuel cost	[g/s]
$\propto_{seg}$	Road grade for each route segment	[%]
α_{sp}	Controller switch parameter	[-]
γ_t	ECMS controller costate	[-]
$\delta_{N_{1,1}}$	Neural network local gradient	[-]
$\delta_{N_{1,2}}$	Neural network local gradient	[-]
δ_y	Neural network local gradient	[-]
ε_0	Initial equivalence factor	[-]
ε_t	Equivalence factor at time t	[-]
η_{chg}	Battery charge efficiency	[-]
η_{dis}	Battery discharge efficiency	[-]
$\eta_{drivetrain}$	Drive train efficiency	[-]
$\eta_{faradaic}$	Faradaic efficiency	[-]
η_{motor}	Motor efficiency	[-]
π	Optimisation control policies	[W]
π^*	Optimal control policies	[W]
π_{seg}	Control policies for route segment seg	[W]
$\pi_{seg}{}^*$	Optimal control policies for route segment seg	[W]

τ_{acf}	Aggressivity compensation factor	[-]
μ	Coefficient of rolling resistance	[-]
Ø	Terminal optimisation cost	[g/s]
$Ø_{seg}$	Terminal optimisation for route segment seg	[g/s]
β	Inclined vehicle angle	[%]
μ	Coefficient of rolling resistance	[-]
ρ	Air density	[kg/m^3]
σ	Neural network learning rate	[-]

APPENDICES

Appendix 1: Vehicle modelling data

Vehicle type	Light commercial	
Fuel	Diesel	
Engine	1.6HDi 90hp	
Transmission	Gear 1	11/38
	Gear 2	15/28
	Gear 3	32/37
	Gear 4	45/37
	Gear 5	50/33

Vehicle parameters

Wheel radius	0.307 meters
Drag coefficient	0.35
Rolling resistance	0.001
Vehicle mass	1360 Kg
Final drive ratio	4.2941
Car frontal area	$2m^2$
Drive train efficiency	1
Maximum engine speed	6500 RPM

Battery parameters

Battery cell composition	Lithium ion phosphate
Battery capacity	16 Ampere hours
Battery resistance	0.024 Ohms
Minimum state of charge	40%
Maximum state of charge	80%
Battery open circuit Voltage	60V

Electric motor parameters

Motor manufacturer	Perm Motor Germany
Motor type	Brushless DC motor
Motor model	PMS 120
Max motor torque	42 Nm
Max motor speed	4500 RPM
Motor gear ratio	1.178